

Technische Universität München
Fakultät Wissenschaftszentrum Weihenstephan
für Ernährung, Landnutzung und Umwelt
Lehrstuhl für Ökologische Chemie und Umweltanalytik

Analysis Concepts Of Aerosols by On-Line Aerosol Mass Spectrometry

Stéphane Gallavardin

Vollständiger Abdruck der von der
Fakultät Wissenschaftszentrum Weihenstephan
für Ernährung, Landnutzung und Umwelt
der Technischen Universität München
zur Erlangung des akademischen Grades eines

Doktors der Naturwissenschaften

genehmigten Dissertation.

Vorsitzender: Univ.-Prof. Dr.-Ing. Roland Meyer-Pitroff

Prüfer der Dissertation:

- 1. Univ.-Prof. Dr.rer.nat., Dr.h.c.(RO) Antonius Kettrup, em.**
- 2. Univ.-Prof. Dr.rer.nat., Dr.agr.habil., Dr.h.c.(Zonguldak Univ/Turkei) Harun Parlar**
- 3. Univ.-Prof. Dr.rer.nat. Ralf Zimmermann (Universität Augsburg)**

Die Dissertation wurde am 27.4.2006 bei der Technischen Universität München eingereicht und durch die Fakultät Wissenschaftszentrum Weihenstephan für Ernährung, Landnutzung und Umwelt am 17.06.2006 angenommen.

Results? Why, man, I have gotten lots of results! If I find 10,000 ways something won't work, I haven't failed. I am not discouraged, because every wrong attempt discarded is often a step forward....

Thomas Edison

Why the best solution is always the last one to come ?

Daniel Jacob

Acknowledgments

The work conducted over the last 3 years and half was for me the occasion of being involved in a nice “pioneer” project: the design, birth, growth, care and use of an aerosol mass spectrometer. This project made me discover the exciting field that is aerosol science and technology: a multidisciplinary field where mechanic, thermodynamic, optic, electricity and chemistry are involved. The outcome of this project was for me a real motivation in contributing in making this technique more mature and a very good start for a carrier in aerosol sciences and atmospheric sciences.

The success of this work was possible due to the excellent technical equipment facilities in Prof. Zimmermann's group at the GSF-Forschungszentrum and the wide library resources of the GSF-Forschungszentrum.

I first thank Prof. Kettrup and Prof. Zimmermann for offering me a PhD student position with this research topic which satisfied my interests in miscellaneous science and technology topics and made me participate to the birth, growth and operation of a high-tech aerosol mass spectrometer. This position gave me the opportunity to get a solid experience with all the necessary techniques that are involved in analytical chemistry instrumentation such as vacuum engineering, optic, electronics and data processing engineering.

I wish to special thank Dr. Fabian Mühlberger for its availability and patience to help me fixing my technical problems, Stefan Mitschke for his help in computer problems, Jürgen Maguhn for his support in GSF-administrative questions, Mr. Dietz and his collaborators of the GSF-workshop for their availability and their diligence in producing the mechanical parts needed for the project, Mr. Jungbauer for his patience and electronic lectures, Mr. Karg for aerosol generation questions, Mr. Reznikov and Dr. Wenzel for the PIXE analysis and finally Dr. T. Ferge for his early help in my first year in making me stepping efficiently in this project and for choosing/ordering/assembling the first elements of the instrument and Matthias Bente for his help during his training on this project. Finally I warmly thank my other collaborators in the group for their punctual help and their availability.

I would like to address also warm thanks to my friends in Munich, in particular those of the group “Compagnie de Munich”, from the “CRFM – Club de Rhétorique Francophone de Munich” and my two roommates of our “Auberge Espagnole” of the years 2004-2005 who support my much too usual litany “my instrument does not want to work ...”. They all support me as they could, motivated me efficiently writing-up this work, helped me understanding in depth my scientific work by their simple novice questions and made my stay in Munich a very nice time by many hikes in the Bavarian mountains, dinners and endless discussions in “Biergartens”.

As special thank goes to my parents for the education they provided me and their occasional financial support and my sisters and brothers for their moral support.

Finally I would like finally to thank particularly here Prof. Lohmann for offering me the very interesting post-doc position at the ETH Zürich before the PhD defense and Dr. Cziczo for his encouragements, suggestions and partial corrections.

Summary (English)

The work presented here was carried out by Stéphane Gallavardin at the Institute for Ecological Chemistry at the GSF-National Research Center for Health and Environment (GSF-Forschungszentrum für Umwelt und Gesundheit) in Neuherberg near Munich in Germany for the obtention of the title, Dr. rer. nat., at the Technical University of Munich under the supervision of Prof. Kettrup and Prof. Zimmermann. The work has been carried out from December 2001 to June 2005 and written-up in January 2006. The work consisted in assisting and continuing the initial work of T. Ferge in the design and building-up of an aerosol mass spectrometer, hereafter denominated SPALMS, dedicated to the analysis of the organic fraction of aerosol single particles and to form M. Bente on the instrument.

The Single Particle Aerosol Laser Mass Spectrometer (SPALMS) developed in this study appears to be a powerful instrument that permits the physical and chemical analysis of aerosol particles. This instrument was designed based on the critical analysis of a bibliographic review of the current state of the technique. The SPALMS instrument samples the aerosol particles with a nozzle inlet unit, detects and sizes them respectively optically and aerodynamically. After the particle sizing step, the chemical analysis is operated by vaporizing and ionizing its chemical constituents by laser either in one or two steps before the resulting ions are transmitted to a bipolar mass spectrometer. The ion mass analysis provides then the chemical composition of the particle. The SPALMS instrument offers many data acquisition points (up to 12 channels) in order to record information at each measurement step and to merge them together. This should lead to additional properties of the single particle in comparison to the current usual use in aerosol mass spectrometry.

The nozzle inlet unit shows two interesting features that compensate the low chemical analysis rate of 7 Hz in the instrument current state. It permits first the sampling of particles by impaction on the last skimmer of the inlet and secondly, due to its higher carrier gas velocity, a better aerodynamic differentiation of the particles than can do an APS instrument or an aerodynamic lens inlet unit. The combination of the detection/sizing unit and the inlet unit permits the measurement of the aerosol particle size distribution in a reliable manner between 0,5 μm to 4 μm at a concentration of up to 800 particles per cm^3 . The detection/sizing unit permits in particular the measurement of the amount of scattered light as the particle crosses each sizing laser by four photomultipliers. With an adapted data analysis procedure, particles can not only be aerodynamically sized but also optically differentiated. Indeed, a data analysis method makes the interpretation of the scattered light possible by limiting the trajectory ambiguity effects. With a lower noise photomultiplier signal, one can potentially access to a shape index, defined as the deviation from sphericity, of the particle and to a method to treat coincidence events.

With a good quality particle detection signal, it is possible to evaluate how representative of the whole aerosol is the observed single particle chemical composition by comparing the aerodynamic-optical data set of the whole particle population to the similar data set of the only chemically analyzed particles. This permits in particular the evaluation of measurement errors due to the desorption/ionization laser trigger scheme or due to the size/composition of the particles.

Indeed, the desorption/ionization process that provides a “fingerprint” of the chemical composition of the particle does not always permit its detection if the laser power density is not high enough, the chemicals are difficult to ionize or chemical reactions proceed in the desorption plume. This is in particular illustrated by the case of the usual low occurrence of positive carbon clusters in mass

spectra or by the apparent impossibility to detect ions from silica particles. This justifies the need of different desorption/ionization methods and their related trigger schemes and the need of a bipolar mass spectrometer.

Soot particles from Palas GmbH were extensively studied in this work since they are very convenient to test the SPALMS instrument. These soot particles were easily detected and the speciation of the carbon as elemental carbon was established in negative mass spectra. Similarly, negative mass spectra showed the presence of organic hydrogenated molecules in soot particles from wood combustion by the presence of hydrogenated carbon clusters C_nH_m ions. Positive mass spectra were found however to bring less chemical information since the relative high content of sodium or potassium in the particle masks the signal due to other positive ions probably by either saturating the detector or by dramatically depleting the amount of positive ions by charge-transfer reactions because of the low ionization potential of sodium and potassium. The advantage of one-step desorption/ionization with a bipolar mass spectrometer is also fully demonstrated by the analysis of ash from the incineration in private fireplace of wood waste material. It suggests that the negative mass spectrometer brings a wealth of information about the speciation of some elements in the particle. Indeed, negative mass spectra indicate that iron, sodium, potassium, calcium and silicon are present in the ash particles respectively as oxides, sulfates and aluminosilicates. Moreover analyses confirmed that particles are to be considered individually.

Even if the one-step desorption/ionization is rich in information, the processes occurring in this step are complex and render difficult the mass spectra analysis because of the chemical ionization and fragmentation processes that take place. Indeed the two-step laser desorption/ionization analysis permitted the detection of PAHs in wood sample particles that were not detected before with a one-step approach. It points out that the better management and control of both the desorption and ionization steps lead to (i) limit the fragmentation of the molecules and (ii) to better resolve chemical mixtures. The chemical analyses presented here suggest that the comparison of mass spectra obtained in both conditions permits a better evaluation of the particle chemical composition by a better understanding the ionization processes.

These analyses lead particularly to develop other desorption/ionization schemes that should enhance the analytical potential of the SPALMS instrument. This is made possible by the unique feature of the mass spectrometer to perform either a simultaneous bipolar ion analysis or two successive cation mass analyses delayed by some microseconds. In this configuration, the same particle can be analyzed twice with different ionization methods and information about the radial composition can be accessible. In this case, each mass spectrometer tube is operated in pulse mode one after the other that permits the operation of a given ionization method for each mass analysis. For instance, possible schemes can address the analysis of initially present native cations in the particle and/or a better molecule identification capacity by first operating a soft photoionization followed by electron impact ionization to fragment the molecules. In addition, it exists the possibility to operate bipolar mass analysis with soft ionization methods producing cations (SPI, Single Photo Ionization) and anions (PERCI, Photo-Electron Resonance Capture Ionization).

Since the two or many steps laser desorption/ionization schemes are complex to operate, it is also important to better qualify the one-step approach. Indeed due to its simplicity, it should be in a next future commonly implemented in field instruments. The careful examination of the mass spectra signal obtained with a sufficiently good mass resolution should permit the evaluation of the extent of the particle ablation in certain circumstances by looking at the shape of the mass peaks at given low masses for usual ions observed in mass spectra such as the C_2 , C_2H and C_2H_2 negatively charged carbon clusters.

The operation of the SPALMS can be completed with the off-line analysis of particles sampled by impaction within the instrument in the inlet unit or after the desorption/ionization unit. Their analysis can address any low-volatile chemicals, confirm and lead to extrapolate the observed chemical composition of the single particles to the whole aerosol. In this work, an off-line analysis has been performed with PIXE (Proton Induced X-ray Emission) which gives the elemental composition even if it can also be easily operated by LMMS (Laser Microprobe Mass Spectrometry) or any conventional chromatographic methods. An Aerodynamic Particle Sizer (APS3321, TSI, Inc) was operated simultaneously in parallel to confirm the SPALMS measurements of the particle size distribution.

As a result, the SPALMS instrument design permits the analysis of single particle aerosol by providing the usual aerosol mass spectrometry information, “size and chemical fingerprint”, and offering additional data that complete the analysis. Indeed, its modular and flexible desorption/ionization methods and trigger scheme permit the adaptation of particle analysis to different aerosol types and to specific laboratory studies aimed at better understanding the desorption/ionization processes. These laboratory works would serve the aerosol mass spectrometry community by permitting a re-interpretation of the data and a better determination of the “real” chemical composition of the single particles.

As a result, from this study it appears that aerosol mass spectrometers will evolve to simple, robust, small and cheap instruments for their use in field measurement campaign and observation networks since their current basic features are well tested, rather mature, technically more reliable and sensitive than they were some years ago. On the other hand, these instruments will be further developed in a modular manner with the same inlet unit, detection/sizing unit but with different chemical analyzers that range from different mass spectrometers and different ionization methods to infrared, Raman spectroscopy and UV fluorescence. Finally various modules measuring, for example, the particle light scattering patterns or light depolarization should be inserted between the inlet unit and the chemical analyzer to complete the physical description of the single particle.

Summary (German)

Diese Arbeit zur Erlangung des Titels „Doktor der Naturwissenschaften“ (Dr. rer. nat.) der Technischen Universität München-Weihenstephan wurde von Stephane Gallavardin am Institut für Ökologische Chemie des GSF-Forschungszentrums für Umwelt und Gesundheit in Neuherberg, Deutschland, unter der Betreuung von Profs. Kettrup und Zimmermann von Dezember 2001 bis Juni 2005 durchgeführt. Ziel der Arbeit war der Aufbau eines Aerosolmassenspektrometers, SPALMS, zur chemischen Analyse von organischen Verbindungen in Aerosolpartikeln.

Das SPLAMS-Instrument (Single Particle Aerosol Laser Mass Spectrometer) ist ein vielfältiges Gerät, das die physikalische und chemische Analyse von Aerosol-Einzelpartikeln ermöglicht. Dieses Gerät wurde auf Basis einer kritischen Literaturrecherche konzipiert und gebaut. Die Funktionsweise ist im Folgenden beschrieben: Die luftgetragenen Partikel werden durch ein Einlaßsystem eingesaugt und dann optisch detektiert. Gleichzeitig wird ihre Größe aerodynamisch und optisch bestimmt. Nach der Detektion werden die Partikel mittels eines energiereichen, gepulsten Lasers fragmentiert und verdampft; die entstehenden Verbindungen werden ionisiert. Mit dem SPALMS-Gerät können Desorption und Ionisation der Partikelbestandteile entweder ein- oder zweistufig durchgeführt werden. Die entstehenden Ionen werden dann in einem bipolaren Flugzeitmassenspektrometer detektiert, das einen „Fingerprint“ der chemischen Zusammensetzung der Partikel liefert. Das Meßinstrument ist mit bis zu 12 Datenerfassungskanälen ausgerüstet. Hiermit können – verglichen mit dem aktuellen Stand der Aerosolmassenspektrometrie-Technik - verschiedene zusätzliche Informationen bezüglich der Einzelpartikel erhalten werden.

Das Einlaßsystem besteht aus einem „Nozzle“-System mit drei hintereinander angeordneten Skimmern. Durch das Einlaßsystem wird das Aerosol in einem Partikelstrahl umgewandelt um die Partikelanalyse durchführen zu können. Selbst wenn dieses Einlaßsystems aufgrund einer uneffizienten Fokussierung der Partikel eine niedrige „Hit Rate“ liefert, können Einzelpartikeln erst bei Impaktion auf dem letzten Skimmer des Einlaßsystems gesammelt werden. Außerdem können Partikel mit ähnlichen aerodynamischen Durchmessern durch die - im Vergleich zu anderen Einlaßsystemen - hohe Geschwindigkeit der Luft wie bei aerodynamischen Linsen wirksamer unterschieden werden. Die Kopplung des Einlaßsystems mit dem optischen Detektionssystem ermöglicht bei dem SPALMS die Messung der Größenverteilung der Aerosole. Deren Partikelgröße liegt zwischen 0,5 und 4 µm bei einer Konzentration von ca. 800 Partikeln pro Kubikzentimeter.

Die Detektionseinheit erfasst das vom Partikel gestreute Laserlicht und ermöglicht eine Größenbestimmung. So wird der aerodynamische Partikeldurchmesser bestimmt und die Partikel können optisch voneinander unterschieden werden. Eine spezielle Datenanalyseprozedur wurde entwickelt, um die Auswertung des Streulichtsignals insofern zu erleichtern, dass die Unsicherheit wegen des „trajectory ambiguity effects“ reduziert werden kann. Weitere Informationen zum Partikel wie Form oder Abweichung von Sphärizität können möglicherweise durch Abschätzung erhalten werden, wenn das Signal-Rausch-Verhältnis des Photomultiplier-Signals verbessert werden kann.

Die gute Qualität der Partikeldetektionseinheit ermöglicht es die Repräsentativität der chemischen Partikelanalyse zu beurteilen, in dem die aerodynamische-optische Eigenschaften der chemischen analysierten Partikeln mit denen der gesamten Partikelpopulation verglichen werden. Dank dieser Methode können Messfehler aufgrund der Desorptions- und Ionisationsmethode abgeschätzt werden.

In der Tat geben Desorption und Ionisierung der Partikelbestandteile nur einen „Fingerabdruck“ der chemischen Zusammensetzung der Aerosoleinzelpartikel, da die Ionenerzeugung von der Ionisierbarkeit der Partikel, der Energiedichte des Lasers und von chemischen Reaktionen in der Ablationswolke abhängt. Aus diesem Grund werden nur wenige positiv geladene Kohlenstoff-Cluster aus Rußpartikeln und keine Massenspektren von Silica-Partikeln beobachtet. Da das Gerät mit einem bipolaren Flugzeitmassenspektrometer ausgerüstet ist, ist es sehr gut geeignet zum Einsatz verschiedener Ionisationsmethoden und zur besseren Partikeldetektion und -analyse.

In dieser Arbeit wurde die Elementzusammensetzung von Russpartikeln in einer Probe der Firma Palas durch negative Massenspektren nachgewiesen. Organische Verbindungen wie Kohlenwasserstoff-Cluster der Form C_nH_m wurden in Aerosolen aus der Holzverbrennung in negativen Massenspektren detektiert. Positive Massenspektren liefern wenig Informationen für solche Partikel, da bevorzugt die leicht ionisierbaren Natrium- und Kalium-Moleküle nachgewiesen werden. Diese Ionen saturieren entweder den Detektor oder erniedrigen die Menge an positiven Ionen durch Ladungsaustausch in der Ablationswolke. Der Vorteil eines bipolaren Massenspektrometers wird deutlicher anhand der Untersuchung mineralischer Aerosole aus Feuerasche oder aus dem Boden. Positive Massenspektren geben Auskunft über die Element-Zusammensetzung der Partikel, negative Massenspektren über die Speziation der Elemente in den Partikeln. Zum Beispiel kommen Eisen und Silizium als Oxidverbindungen und Natrium, Kalium und Kalzium als Sulfate in Partikeln vor. Diese Arbeit zeigt auch, daß die chemische Analyse von Einzelpartikeln lehrreicher ist als eine Gesamtanalyse des Aerosols, da so der Mischungszustand des Aerosols, externes oder internes Gemisch, ermittelt werden kann.

Selbst wenn die einstufige Desorption/Ionisation der Partikel sehr lehrreich ist, macht die Komplexität des Ablationsprozesses und die Vielfältigkeit der Prozesse, wie z.B. der Ladungsaustausch und die chemische Ionisation, die Auswertung der Massenspektren schwierig. Die zweistufige Desorption/Ionisation ermöglicht eine bessere Kontrolle dieses Prozesses. Sie reduziert die Fragmentierung der Bestandteile und erleichtert die Analyse von komplexen Gemischen von Verbindungen in Partikeln. In dieser Arbeit werden z.B. PAKs in Holzverbrennungasche nur mit einer zweistufigen Desorption/Ionisation detektiert. Der Vergleich beider Analysemethoden mit unterschiedlichen und besser bekannten Ionisationsmechanismen führt zu einer besseren Kenntnis der Zusammensetzung der Aerosolpartikel.

Aus den oben genannten Gründen wurden verschiedene Desorptions/Ionisationsmethoden zu entwickeln, um das analytische Potenzial des SPALMS-Gerätes voll auszuschöpfen. Diese Methoden konnten mit dem in dieser Arbeit verwendeten Flugzeit-Masspektrometer durchgeführt werden. Insbesondere kann es im gepulsten Modus betreiben werden und ermöglicht entweder eine gleichzeitige bipolare Ionenanalyse oder eine zeitlich versetzte, doppelte Kationenanalyse. Darüberhinaus kann auch die radiale Komposition der Aerosolpartikel bestimmt werden. Zum Beispiel ist es prinzipiell möglich, prä-existierende Ionen in Partikeln nachzuweisen und anschließend zusätzlich die restlichen Moleküle zu ionisieren. Weiterhin ist eine Photoionisation der Verbindungen mit anschließender Elektronstoßionisation möglich. Zum Schluß bietet dieses Massenspektrometer die Möglichkeit weicher Ionisierungsmethoden für die getrennte Erzeugung von Kationen und Anionen.

Der zweistufige Desorptions/Ionisationsprozeß ist technisch und in der Praxis anspruchsvoll. Daher ist es besonders wichtig, diesen Prozess zunächst für einen einzelnen Laser besser zu verstehen. Zudem werden vermutlich alle Feld-Aerosol-Masspektrometer mit einem einstufigen Desorptions/Ionisationsverfahren ausgerüstet werden. Die Untersuchung der Massenspektren für kleine, häufig vorkommende Ionen wie z.B. C_2 , C_2H und C_2H_2 sowie negative Kohlenstoffcluster eines Partikels kann unter besonderen Umständen Auskunft über Partikelablation geben.

Das analytische Potenzial des SPLAMS-Gerätes kann durch verschiedene off line-Analysen ergänzt werden. In der Tat können Aerosole an der letzten Stufe des Einlaßsystems und nach der Ionisationseinheit beprobt werden. Die gesammelten Partikel können dann durch LMMS (Laser Microprobe Mass Spectrometry), PIXE (Proton Induced X-Ray Emission) oder konventionelle Chromatographie-Techniken weiter analysiert werden, um Informationen über die schwerflüchtigen oder refraktorischen Bestandteile der Partikel zu erhalten. Im Rahmen dieser Arbeit wurde eine PIXE-Analyse bezüglich der Elementzusammensetzung der Feuerasche durchgeführt. Solche off line-Analysen ermöglichen die Abschätzung einiger Meßfehler des SPALMS-Gerätes, was wiederum eine Deduktion der chemischen Zusammensetzung des Gesamtaerosols aus den Daten des Massenspektrometers ermöglicht. Darüberhinaus kann ein Instrument zur Messung der Partikelgrößenverteilung (wie z.B. ein APS-Gerät, TSI Inc.) weitere wertvolle Zusatzinformationen liefern.

Mit dem SPALMS-Gerät kann somit nicht nur die Partikelgröße und deren massenspektrometrische Signatur bestimmt werden, es bietet darüber hinaus die Möglichkeit, diese Informationen durch eine Reihe verschiedener zusätzlicher Datenaufnahmegерäte sowie einen flexiblen und modularen Desorptions/Ionisationsaufbau zu ergänzen. Das Gerät kann an die Anforderungen unterschiedlicher nachzuweisender Aerosoltypen und Experimente angepasst werden, um eine bessere Kenntnis der Partikeleigenschaften und eine bessere Charakterisierung des Desorptions/Ionisationsprozesses zu liefern.

Aus dieser Arbeit wird deutlich, daß sich Aerosol-Massenspektrometer in zwei Richtungen weiterentwickeln werden: Auf der einen Seite werden robuste, stabile und mobile Geräte, die bereits seit Jahren kommerziell angeboten werden (z.B. ATOFMS, TSI Inc. oder Aerodyne AMS, Aerodyne Inc.), immer mehr im Feldeinsatz betrieben. Auf der anderen Seite werden Aerosol-Massenspektrometer modular weiterentwickelt. Standardisierte Bauteile wie z.B. Einlaßsysteme, Detektoren, Ionisations- und Massenspektrometersysteme werden in beliebigen Kombinationen gekoppelt, um verschiedene Eigenschaften eines Aerosols zu erforschen. Zusätzlich zu den etablierten Lasersystemen können z.B. Ramanspektrometrie oder UV-Fluoreszenz eingesetzt werden. Weiterhin können die Polarisation und das Streulicht der verwendeten Laser untersucht werden, um Kenntnisse über weitere physikalischer Eigenschaften der Einzelpartikel zu erhalten.

Table of Contents

Acknowledgments.....	5
Summary (English).....	7
Summary (German).....	11
Table of Contents.....	15
Illustration Index.....	19
Index of Tables.....	21
List of abbreviations.....	23
List of symbols.....	25
1 Introduction.....	29
2 Aerosol analysis overview.....	33
2.1 Concept of aerosol analysis.....	33
2.2 Overview of the available techniques.....	35
2.3 Requirements for the on-line single particle approach.....	38
2.4 Aerosol mass spectrometry.....	40
2.5 Critical analysis of the different measurement steps.....	42
2.5.1 Important aerosol mass spectrometer characteristics.....	43
2.5.2 Aerosol inlet.....	45
2.5.3 Particle sizing.....	47
2.5.4 Particle desorption/ionization.....	50
2.5.4.1 Standard sampling techniques in mass spectrometry	50
2.5.4.2 One-step desorption/ionization (One-step DI).....	51
2.5.4.3 Two-step laser desorption/ionization: Particle vaporization.....	55
2.5.4.4 Two-step laser desorption/ionization: Ionization methods.....	57
2.5.5 Mass analysis.....	60
2.6 Technical choice justification for the aerosol mass spectrometer.....	62
3 Aerosol mass spectrometer at GSF-Forschungszentrum: General design.....	65
3.1 General design and scaling rules.....	65
3.2 Setup and dimensions.....	65
3.3 Short particle path.....	67
3.4 High flexibility.....	70
3.5 Data acquisition points.....	72

4 Inlet unit.....	75
4.1 Technical characteristics.....	75
4.2 Particle velocity.....	77
4.3 Beam quality.....	79
4.4 Particle sampling with the inlet unit.....	81
5 Detection / sizing unit.....	85
5.1 General design.....	85
5.1.1 Light source.....	85
5.1.2 Sizing laser distance.....	86
5.1.3 Optical setup for the collection of the scattered light.....	89
5.1.4 Photomultiplier signal processing.....	93
5.1.4.1 Photomultiplier response to a light pulse of different time lengths.....	93
5.1.4.2 Processing of the photomultiplier signal for the particle detection and sizing.....	94
5.1.4.3 Electronic processing of the photomultiplier signals.....	97
5.1.4.4 Data acquisition hardware of the photomultiplier signal.....	97
5.1.4.5 Software processing of the photomultiplier signals.....	99
5.2 Characteristics of the detection/sizing unit of the SPALMS instrument.....	103
5.2.1 Particle identification from PMT scans	103
5.2.2 Particle counting efficiency.....	104
5.2.3 Particle size detection limit.....	105
5.2.4 Counting rate.....	107
5.2.5 Inlet efficiency.....	107
5.2.6 Accuracy of the particle velocity measurement.....	109
5.2.7 Sizing unit calibration.....	113
5.2.8 Particle concentration variation.....	116
5.2.9 Particle coincidence.....	116
5.2.10 Particle sizing by light scattering.....	118
5.3 Improvement possibilities.....	119
5.3.1 Current nozzle inlet unit.....	119
5.3.2 Aerodynamic lens.....	120
5.3.3 Particle detection unit.....	121
5.3.4 Hardware solutions for the elimination of the “trajectory ambiguity effect”.....	122
6 Desorption/ionization unit.....	123
6.1 Choice of the laser based technique.....	123
6.2 Laser light characteristics.....	123
6.2.1 One-step desorption/ionization laser light characteristics.....	124
6.2.2 Two-step desorption/ionization laser light characteristics.....	124
6.2.2.1 Desorption laser light.....	126
6.2.2.2 Ionization laser light.....	126
6.3 Laser operation characteristics.....	128
6.4 Optics arrangement.....	129
6.4.1 Laser systems for one-step desorption/ionization.....	133
6.4.2 Laser systems for two-step desorption/ionization.....	134

7	Coupling of the detection/sizing unit with the desorption/ionization unit.....	137
7.1	Free-running mode.....	137
7.2	Static Mode.....	138
7.3	Dynamic mode.....	142
7.4	Summary	148
8	Mass spectrometer unit.....	149
8.1	General principle.....	149
8.2	Technical details of the bipolar mass spectrometer.....	152
8.3	Geometry of the extraction zone.....	156
8.4	Microchannel plates (MCP) behavior.....	157
8.5	Calibration procedure.....	158
9	Data acquisition unit.....	161
9.1	Inventory of the available information from the SPALMS instrument.....	161
9.2	Standard data acquisition scheme (DAQ Scheme Nr.1).....	161
9.3	Data processing program for the DAQ Scheme Nr.1.....	166
10	Standard aerosol particle mass spectrometric analysis	167
10.1	Gas phase analysis.....	167
10.2	One-step laser desorption/ionization particle analysis.....	168
10.2.1	Palas GmbH soot particles.....	168
10.2.2	Observation of PAHs in combustion soot particles from incineration plant.....	173
10.2.3	Wood combustion soot particles.....	174
10.2.4	Particle mass spectra from rich PAHs particles (Sample #10).....	175
10.2.5	Particle mass spectra of Ash particles from a private fireplace.....	176
10.2.6	Other investigated particles.....	181
10.3	Two-step laser desorption/ionization particle analysis.....	182
11	Particle measurement steps integration.....	185
12	Benefits of additional particle sampling devices.....	189
12.1	Impactor sampling (Improvement type 4 and 1).....	189
12.1.1	Impactor capabilities of the inlet unit.....	189
12.1.2	Ash particle composition inferred from the SPALMS and PIXE analysis.....	191
12.2	Parallel operation of the APS and the SPALMS instrument (Improvement of type 2).....	194
12.2.1	APS principle.....	195
12.2.2	Comparison of the detection/sizing units of the APS and SPALMS.....	195
12.2.3	Comparison of the particle sizing data from APS and SPALMS.....	197
12.2.4	Particle velocity in APS and SPALMS instrument.....	198

13 To a better characterization of the particle physical properties	201
13.1 Introduction based on the APS optical system.....	201
13.2 Reduction of the impact of the “trajectory ambiguity effects”.....	203
13.3 Particle optical properties.....	207
13.4 Coincidence events evaluation.....	211
13.5 Analysis representativity inferred from the aerodynamic-optical particle properties	213
13.6 Modification of the particle light scattering collection optics.....	214
14 To a better chemical characterization of the aerosol gas and particle phases.....	217
14.1 Simultaneous particle and gas-phase analysis.....	217
14.2 Toward a better single particle chemical characterization.....	221
14.2.1 Control of the laser desorption/ionization conditions.....	221
14.2.2 Surface and bulk particle analysis.....	224
14.2.2.1 Published attempts.....	224
14.2.2.2 Double desorption/ionization	225
14.2.2.3 Mass spectrum analysis.....	226
14.2.3 Comprehensive qualitative chemical analysis of the single particle.....	228
14.2.3.1 Qualitative chemical analysis with different desorption/ionization scheme.....	229
14.2.3.2 Qualitative analysis with an increased mass spectrum resolution.....	233
15 My opinion about the future of aerosol mass spectrometry.....	235
15.1 Directions for immediate technical improvements and work.....	235
15.2 Evolution of aerosol mass spectrometry over the next decades.....	235
Annex A.....	243
A-1 Influence of sonic shock waves on the particle beam quality within the inlet unit.....	243
A-2 Commercial inlet nozzle-skimmers unit.....	244
A-3 Home-made nozzle-skimmer unit.....	245
A-4 Home-made aerodynamic lens.....	246
Bibliography.....	247
Curriculum Vitae.....	255

Illustration Index

Figure. 1 : Example of an aerosol analysis sequence.....	34
Figure. 2 : Some aerosol analysis approaches.....	36
Figure. 3 : On-line single particle analysis problematics.....	40
Figure. 4 : Various aerosol mass spectrometer technical setups (modified after [Jimenez, 2005]).....	42
Figure. 5 : Aerosol mass spectrometer measurement steps.....	63
Figure. 6 : SPALMS Aerosol mass spectrometer setup.....	66
Figure. 7 : Location of the different measurement steps in the SPALMS instrument.....	67
Figure. 8 : Particle inlet / ion source arrangement of the SPALMS instrument.....	69
Figure. 9 : Dimension and arrangement of the sizing unit of the SPALMS instrument.....	70
Figure. 10 : Particle information sources from the SPALMS instrument.....	72
Figure. 11 : Schematic view of the inlet unit of the SPALMS instrument.....	75
Figure. 12 : PSL particle velocity distribution obtained with the SPALMS instrument.....	78
Figure. 13 : Particle velocities obtained with different aerosol mass spectrometers.....	80
Figure. 14 : Particle beam size and particle deposition in the inlet unit.....	81
Figure. 15 : Sampling of particles by impaction in the inlet unit on skimmer I and skimmer II.....	83
Figure. 16 : Setup of the sizing laser beams in the detection/sizing unit.....	88
Figure. 17 : Variation of the scattered light intensity as a function of the size parameter α	90
Figure. 18 : Single particle light scattering pattern.....	90
Figure. 19 : Schematic view of the detection/sizing unit located in the ion source.....	92
Figure. 20 : Typical time response of the photomultiplier of the detection/sizing unit.....	94
Figure. 21 : Photomultiplier signals for particle sizing.....	95
Figure. 22 : Inappropriate photomultiplier signals for particle sizing.....	96
Figure. 23 : Accuracy of the different types of peak detection time.....	101
Figure. 24 : Relative peak height at the peak detection time.....	101
Figure. 25 : Particle sensing volumes of the different sizing laser beams.....	105
Figure. 26 : Particle size detection limit of the SPALMS instrument.....	106
Figure. 27 : Influence of the trajectory ambiguity effects on the particle sizing.....	111
Figure. 28 : Particle velocity variations due to the drift of the sizing laser distance for PSL 1 μm particles.....	113
Figure. 29 : Detection/sizing unit calibration curve.....	114
Figure. 30 : Variation of ash particle concentration in air measured with the APS and SPALMS instrument.....	115
Figure. 31 : Coincidence principle.....	117
Figure. 32 : Optical particle sizing with the APS and the SPALMS instrument.....	118
Figure. 33 : Aerodynamic lens principle.....	120
Figure. 34 : Aerodynamic lens built at GSF-Forschungszentrum.....	120
Figure. 35 : REMPI and SPI ionization process principle.....	127
Figure. 36 : Number of ionizable chemical species for a given photon energy ([NIST, Weekbook]).....	128
Figure. 37 : Laser desorption/ionization optical setup of the SPALMS instrument.....	131
Figure. 38 : Relative positions of the desorption and ionization laser beams (view from above).....	132
Figure. 39 : Desorption/ionization unit (side view).....	132
Figure. 40 : Desorption/ionization laser static trigger mode flow chart.....	139
Figure. 41 : Desorption/ionization laser static trigger mode with coincidence test flow chart.....	141
Figure. 42 : Desorption/ionization laser dynamic trigger mode flow chart.....	143
Figure. 43 : Dynamic Sizing Trigger Unit (DSTU) time diagram.....	144
Figure. 44 : Influence of 2 parameters of the Dynamic Sizing Trigger Unit.....	146
Figure. 45 : Typical geometric design of the time-of-flight mass spectrometer.....	150
Figure. 46 : Details of the bipolar time-of-flight mass spectrometer of the SPALMS instrument.....	154
Figure. 47 : Desorption plume in the Matrix-Assisted Laser Desorption process.....	156
Figure. 48 : Extraction electrode design.....	157
Figure. 49 : Variability of the ion time-of-flight for given m/z value from particle to particle.....	159
Figure. 50 : Setup of the SPALMS data acquisition unit (scheme Nr.1).....	163
Figure. 51 : Chart flow of the data acquisition scheme Nr.1.....	165
Figure. 52 : Gas-phase mass spectrum of aromatic compounds (Nd:YAG laser, $\lambda = 266 \text{ nm}$).....	168
Figure. 53 : Positive and negative mass spectra of Palas soot single particles (at $\lambda = 337,1 \text{ nm}$ and at $\lambda = 248 \text{ nm}$).....	169
Figure. 54 : Carbon cluster anions C_n peak intensity.....	171
Figure. 55 : Carbon cluster anions C_n peak intensity at $\lambda = 337,1 \text{ nm}$ and $\lambda = 248 \text{ nm}$	171
Figure. 56 : Thermochemical data of carbon clusters.....	172
Figure. 57 : Biomass soot single particle positive mass spectra at $\lambda = 266 \text{ nm}$ and $\lambda = 337,1 \text{ nm}$	173

Figure. 58 : Positive and negative mass spectra of soot single particles from wood combustion at $\lambda = 337,1$ nm.....	174
Figure. 59 : Summed mass spectra of ash single particles at $\lambda = 337$ nm and $\lambda = 248$ nm.....	177
Figure. 60 : Typical classes of negative mass spectra of ash single particles at $\lambda = 248$ nm.....	179
Figure. 61 : Wood soot particles processed with a one- and two-step laser desorption/ionization.....	182
Figure. 62 : Low mass carbon ions detected with a two-step and one-step laser desorption/ionization.....	183
Figure. 63 : SPALMS - APS information balance (weight and relationships).....	185
Figure. 64 : Particle sampling by impaction in the inlet unit.....	190
Figure. 65 : Light scattering signals of the SPALMS and APS for PSL and SiO ₂ particles.....	196
Figure. 66 : Particle velocity distribution measured for PSL and SiO ₂ particles by the SPALMS and the APS.....	197
Figure. 67 : Computed and measured particle velocity for the APS and the SPALMS instruments	199
Figure. 68 : Photomultiplier signal pattern of the APS3321.....	202
Figure. 69 : Particle time-of-flight and photomultiplier peak width equivalence for the APS.....	202
Figure. 70 : Characteristics of the “trajectory ambiguity effect”.....	204
Figure. 71 : Photomultiplier peak rising time distribution for PMT2a and PMT2b for different particle types.....	205
Figure. 72 : Particle relative residence time distribution for different particle types.....	206
Figure. 73 : Particle distribution of given relative residence time.....	207
Figure. 74 : Optical particle properties behavior for a given particle velocity and relative residence time.....	208
Figure. 75 : PMT2a signal amplitude for particles with similar velocity and relative residence time (1).....	209
Figure. 76 : PMT2a signal amplitude for particles with similar velocity and relative residence time (2).....	209
Figure. 77 : Photomultiplier peak amplitude correlation between PMT2a and PMT2b.....	210
Figure. 78 : Treatment of the coincidence using particle velocity (type 1 & 2).....	212
Figure. 79 : Particle scattered light versus particle time-of-flight at low photomultiplier noise level.....	214
Figure. 80 : Simultaneous gas & particle analysis SPALMS setup.....	218
Figure. 81 : Simultaneous gas and particle phase aerosol analysis data acquisition scheme.....	219
Figure. 82 : Usual gas inlet unit for laser time-of-flight mass spectrometers.....	220
Figure. 83 : Particle location in the desorption/ionization laser inferred from the mass spectra.....	222
Figure. 84 : Double peak at a given m/z in negative mass spectra.....	223
Figure. 85 : Influence of the ion cloud shape on mass spectra.....	227
Figure. 86 : Multi-directional ion capture by the mass spectrometer extraction electrodes.....	228
Figure. 87 : Principle of the 3-step desorption-ionization method for single particle analysis.....	232
Figure. 88 : Data acquisition scheme for the 3-step desorption – two ionizations method.....	232
Figure. 89 : Sonic barrel shock after a nozzle.....	243

Index of Tables

Table 1 : Aerosol properties according to different points of view.....	30
Table 2 : Characteristics of particles of different sizes (water droplets, 1000 kg/m ³).....	38
Table 3 : Aerosol mass spectrometer measurement step description.....	43
Table 4 : Examples of molecule ionization pathways.....	52
Table 5 : Thermochemical quantities of gas-phase ions (after [NIST, Weekbook]).....	54
Table 6 : Usual ionization methods in aerosol mass spectrometry.....	59
Table 7 : Size of different laser based aerosol bipolar mass spectrometers.....	67
Table 8 : Relative distance between the SPALMS laser beams.....	69
Table 9 : Available laser systems for the aerosol mass spectrometer.....	71
Table 10 : List of the particle information sources and their related acquisition hardwares.....	73
Table 11 : Geometrical characteristics of the current inlet units of the SPALMS instrument.....	76
Table 12 : Inlet unit operating conditions.....	76
Table 13 : PSL particle velocities in the SPALMS instrument.....	79
Table 14 : Effect of the nozzle downstream pressure on the PSL particle velocity.....	79
Table 15 : Particle beam diameter at different locations in the inlet unit.....	80
Table 16 : Characteristics of the particles sampled by impaction within the inlet unit.....	82
Table 17 : Sizing laser systems used in different aerosol mass spectrometers.....	86
Table 18 : Parameters to consider to set the distance between both sizing laser beams.....	87
Table 19 : Light scattering characteristics as a function of the particle size parameter α	89
Table 20 : Photomultiplier signal data acquisition device characteristics.....	98
Table 21 : Filter characteristics for the PMT scans.....	102
Table 22 : Typical photomultiplier signal classification characteristics.....	104
Table 23 : Inlet transmission for different PSL particle sizes.....	108
Table 24 : Inlet unit efficiency for different nozzle systems.....	108
Table 25 : Accuracy of the measured particle time-of-flight between both sizing lasers for PSL particles.....	112
Table 26 : Contribution of different parameters to the accuracy of the particle velocity measurement.....	112
Table 27 : Typical characteristics of commonly used lasers in aerosol mass spectrometers.....	125
Table 28 : Laser wavelengths used in two-step desorption/ionization in aerosol mass spectrometry.....	125
Table 29 : Laser trigger time delays for selected laser systems.....	130
Table 30 : Typical time delays encountered in the desorption/ionization laser static trigger mode scheme.....	139
Table 31 : Typical time delays encountered in the desorption/ionization laser static trigger mode (coincidence test) ..	141
Table 32 : Time delays to be accounted for the desorption/ionization laser trigger with the DSTU unit.....	146
Table 33 : Current technical problems of the Dynamic Sizing Trigger Units (DSTU).....	147
Table 34 : Overview of the characteristics of the different desorption/ionization laser trigger modes of the SPALMS.....	147
Table 35 : Bipolar time-of-flight mass spectrometer geometrical dimensions.....	153
Table 36 : Bipolar time-of-flight mass spectrometer voltage settings used in this work.....	153
Table 37 : Measurement steps and their related accessible information.....	162
Table 38 : List of primary information accessible with the different digitizer channels.....	163
Table 39 : Natural abundance (>1%) of some usual isotopes.....	178
Table 40 : Tentative ion identification of the negative mass spectra peaks of ash single particles at $\lambda = 248$ nm.....	180
Table 41 : Main characteristics of the negative mass spectra of ash single particles at $\lambda = 337,1$ nm.....	180
Table 42 : Particle number balance for the {SPALMS+APS} measurement setup.....	186
Table 43 : Ash sample analysis by PIXE and SPALMS.....	193
Table 44 : Operating conditions of the sizing unit of the APS and SPALMS instrument.....	196
Table 45 : Computed and measured particle velocities with the APS and SPALMS instrument.....	199
Table 46 : Laser system combinations for on-line single particle depth profiling.....	226
Table 47 : Chemical analysis scheme nomenclature.....	229
Table 48 : Parameters for the calculation of the sonic barrel shock dimensions.....	244
Table 49 : Relative position of the nozzle-skimmer orifices in the home-made and commercial inlet unit.....	244
Table 50 : Pressure levels in the commercial nozzle system.....	244
Table 51 : Characteristic dimensions of the home-made inlet unit.....	245

List of abbreviations

AMS	Aerosol Mass Spectrometry / Aerosol Mass Spectrometer
AOI	Angle Of Incidence
APS	Aerodynamic Particle Sizer (refers in this work to APS3321)
APS 3321	Aerodynamic Particle Sizer 3321, TSI Inc.
ART-2a	Adaptive Resonance Theory based algorithm for the mass spectra classification
ATOFMS	Aerosol time-of-flight Mass Spectrometer
BNC	BNC connector for coaxial cable used with standard oscilloscope
CA	Chemical Analysis
Ch.	Channel of a data acquisition device (oscilloscope or digitizer)
DAQ	Data AcQuisition system
DE	Delayed Extraction
DI	Desorption Ionization
DMA	Differential Mobility Analyzer
DSTU	Dynamic Sizing and Trigger Unit
DG1	Delay Generator DG535, Stanford Research System, Inc. (1)
DG2	Delay Generator DG535, Stanford Research System, Inc. (2)
DG3	Delay Generator DG535, Stanford Research System, Inc. (3)
DP210	Acqiris Digitizer, Model DP210
EC	Elemental carbon
EI	Electron Impact
F	Function transfer from primary information to secondary information
FIDI	Field Induced Droplet Ionization
GC-MS	Coupled Gas Chromatography Mass Spectrometry
GCxGC-TOFMS	Two-Dimensional Gas Chromatography Time-of-Flight Mass Spectrometry
GSF	GSF-Forschungszentrum für Umwelt und Gesundheit
ID	Inner diameter
IR	Infra-Red
LAMPAS	LAser Mass analyzer for Particle in Airborne State
LIBS	Laser Induced Breakdown Spectroscopy
LDI	Laser Desorption Ionization
LMMS	Laser Microprobe Mass Spectrometry
LT374	LeCroy Oscilloscope, Model LT374
MALD	Matrix-assisted Laser Desorption
MALDI	Matrix-Assisted Laser Desorption Ionization
MCP	Micro Channel Plate
MSⁿ	Tandem Mass spectrometry
MSN / MS(-)	Mass spectrum/Spectrometer of/for negative ions
MSP / MS(+)	Mass spectrum/Spectrometer of/for positive ions
NIST	National Institute of Standards and Technology
O_{1,2}	Inverted skimmer orifice between the inlet Chamber I and Chamber II
O_{2,ion source}	Plane skimmer orifice between the inlet Chamber II and the ion source
OC	Organic Carbon
OD	Outer Diameter
OPC	Optical Particle Counter
O_{atm,1}	Nozzle orifice between the ambient air and the chamber I
oaTOFMS	orthogonal acceleration Time-Of-Flight Mass Spectrometer/Spectrometry
PAH	PolyAromatic Hydrocarbons
PALMS	Particle Analysis by Laser Mass Spectrometry
PC	Personal Computer
PC1	Computer driving the digitizers
PC2	Computer dedicated to drive the APS3321
PERCI	Photo-Electron Resonance Capture Ionization
PIXE	Proton-Induced X-Ray Emission

PMT	Photomultiplier
PMT1a	Photomultiplier 1a
PMT2a	Photomultiplier 2a
PMT2b	Photomultiplier 2b
PSL	PolyStyrene Latex particle
QMS	Quadrupole Mass Spectrometry / Quadrupole Mass Spectrometry
REMPI	Resonance Enhanced Multi Photon Ionization
ReTOFMS	Reflectron Time-Of-Flight Mass Spectrometer
RS	Raman Spectroscopy
RS232	Serial port RS232
SEM	Scanning Electron Microscopy
SiO₂	Silica (particles)
SPALMS	Single Particle Aerosol Laser Mass Spectrometer (developed at GSF-Forschungszentrum)
SMPS	Scanning Mobility Particle Sizer
SPI	Single Photon Ionization
TEM	Transmission Electron Microscopy
TD-GCMS	(particle) ThermoDesorption-Coupled Gas Chromatography Mass Spectrometry
TIC	Total Ion Current
TOF	Time-Of-Flight / particle Time-Of-Flight
TOFMS	Time-Of-Flight Mass Spectrometer / time-Of-Flight Mass Spectrometry
TTL	Square shaped electric pulse with an amplitude of 4V and a few μ s length
USB	Universal Serial Bus (connector for rapid data exchange with an USB-stick)
UV	Ultra Violet
UV-FS	Ultra Violet Fused Silica
VUV	Vacuum Ultra Violet
WR6050a	LeCroy Oscilloscope, Model WR6050a

List of symbols

A*	Cross-section area of the gas flow in the nozzle orifice
A	Intercept of the calibration curve of the mass spectrometer
AE	Analysis Efficiency of the aerosol mass spectrometer
A_L	Surface area of the desorption ionization laser on the particle beam path
A_P	Surface area of the particle beam cross-section at its intersection with the desorption/ionization laser
B	Coefficient for the term $(m/z)^{0.5}$ of the calibration curve of the mass spectrometer
C	Coefficient for the term $(m/z)^{1.5}$ of the calibration curve of the mass spectrometer
C_c	Cunningham factor
C_D	Drag coefficient
CAE	Chemical Analysis Efficiency
CR	Chemical analysis Rate
E_{ablation}	Particle ablation efficiency of the aerosol mass spectrometer
E_{inlet,dp}	Inlet transmission efficiency for particle of diameter d_p
E_{photon}	Photon Energy
E_{stat,trig,mode}	Hit efficiency of the aerosol mass spectrometer in static trigger mode
F₁	Ion focal point in linear mode
F₂	Ion focal point in reflectron mode
HE	Hit efficiency of the aerosol mass spectrometer
HR	Hit rate of the aerosol mass spectrometer
IEF	Inlet efficiency
I_{scatt}	Intensity of the light scattered by a particle as it crosses a laser beam
L	Laser duty factor (product of the laser pulse duration by the laser firing frequency)
L_c	Characteristic length of the studied system
L_{flight,sizing}	Distance flown by the particle between its detection times by both sizing lasers
L_{flight,detection}	Distance flown by the particle during the time it is detected by a sizing laser
L_{drift zone}	Length of the drift region of the mass spectrometer
P₁	Gas pressure in the inlet chamber 1
P₂	Gas pressure in the inlet chamber 2
PCE	Particle Counting Efficiency
PCR	Particle Counting Rate
P_{ionsource}	Gas pressure in the ion source of the aerosol mass spectrometer
P_{upstream}	Gas pressure upstream of the inlet nozzle
P_{TOFMS Tube}	Pressure in the drift region of the TOFMS tube
Q_m	Sampling mass flow rate
Q_v	Sampling volumic flow rate
Q_{v,ionsource}	Volumic gas flow rate entering the ion source
R	Perfect gas constant ($8,31 \text{ J}\cdot\text{mol}^{-1}\cdot\text{K}^{-1}$)
SAE	Sizing Analysis Efficiency
SCAE	Sizing Chemical Analysis Efficiency
SCR	Sizing Chemical analysis Rate
SE	Sizing Efficiency
SR	Sizing Rate
S_d	Particle stopping distance
Stk	Stokes Number
Stk₅₀	Size Cut Stokes Number at 50% particle transmission
T	Inlet system transmission efficiency
TOF_{ion}	ion Time-Of-Flight between the ionization source and the detector
TOF_{sizing}	particle Time-Of-Flight measured between the two sizing lasers
T_{upstream}	Gas temperature upstream of the inlet nozzle
U_{ext,TOFMS}	Voltage between the extraction electrodes of the mass spectrometer
U_{gas}	Gas velocity
V_{ion}	Ion velocity
V_{ion source}	Effective volume of the ion source

$V_{ion,0}$	Initial ion velocity in at the laser desorption ionization time
$V_{ion,ext}$	Ion velocity at the exit of extraction zone of the mass spectrometer
$V_{ionization}$	Volume where the molecules are really ionized
V_p	Particle velocity
$V_{p,1}$	Particle velocity calculated from its time-of-flight between both sizing lasers
$V_{p,2}$	Particle velocity calculated from its detection/residence time in a sizing laser
$V_{peak\ bottom}$	Voltage level measured at the bottom of a PMT pulse peak
$V_{peak\ detection}$	Voltage level measured at the detection of a PMT pulse peak
$V_{peak\ top}$	Voltage level measured at the top of a PMT pulse peak
$V_{sizing,trig}$	Voltage level at which the PMT signal is considered
a_i	linear Coefficient of a variable to the power i of a polynomial equation
c	Light velocity (299792458 m/s)
$C_{app,max}$	Maximum apparent particle concentration obtained by the aerosol mass spectrometer
$C_{corr,max}$	Maximum real particle concentration measurable by the aerosol mass spectrometer
$C_{particle, C_o}$	Particle concentration in the aerosol at the sampling place
$d(TOF_{ion})$	Arrival time difference at detector of an ion m/z for particles at different location in the DI laser beam
$d_{desorp,ion}$	Distance between the desorption and ionization lasers as they cross the particle beam
$d_{ext,TOFMS}$	Distance between both extraction plates of the mass spectrometer
d_{lens}	Aerodynamic lens inner diameter
$d_{lens\ aperture}$	Aerodynamic lens aperture diameter
d_{nozzle}	Nozzle orifice diameter
d_p	Particle diameter
$d_{p,a}$	Particle aerodynamic diameter
$d_{p,av}$	Vacuum aerodynamic diameter
$d_{p,av,50}$	Particle size-cut vacuum aerodynamic diameter at 50% particle transmission
$d_{p,g}$	Geometric particle diameter
$d_{sizing\ laser}$	Distance between each both sizing lasers
dN/dt	Particle counting rate
dt_1	Time delay set by Delay Generator 1
dt_2	Time delay set by Delay Generator 2
e	Charge of electron ($1,602 \cdot 10^{-19}$ C)
f_{DAQ}	Data acquisition rate for the data acquisition device considered
$f_{DAQ,max}$	Maximum data acquisition rate for the data acquisition device considered
f_{DSTU}	Multiplication factor of TOF_{sizing} used by the DSTU
$f_{laser, firing}$	Laser firing frequency
h	Planck Constant ($6,626176 \cdot 10^{-34}$ J.s)
m/z	Ion mass to charge ratio
m_{ion}	Ion mass
$t_{L,DI,trigger}$	Calculated time of the trigger of the desorption/ionization laser
$t_{a,anal}$	Duration of analysis of the aerosol
$t_{a,i,lifetime}$	Duration during which the aerosol properties are considered constant
$t_{a,rig,anal}$	Duration of rigorous aerosol analysis
$t_{corr,start}$	Time correction for the particle time detection at the sizing laser 1
$t_{corr,stop}$	Time correction for the particle time detection at the sizing laser 2
$t_{corr,total}$	Total time correction required to calculate rigorously $t_{L,DI,trigger}$
$t_{dead,cycle}$	Waiting time beyond which the DSTU is reinitialized
$t_{delay\ electronic}$	Cumulated time delay due to the PMT signal processing by all electronic devices
$t_{ion,acc}$	Ion time-of-flight in the extraction zone of the mass spectrometer
$t_{ion,drift}$	Ion time-of-flight in the drift region of the mass spectrometer
$t_{laser,pulse}$	Duration of the laser light pulse
$t_{min,period}$	Minimum time interval between two laser pulses
$t_{ms,analysis}$	Duration of the ion mass analysis with the TOFMS
$t_{particle\ detection1}$	Time at which the particle is detected by the detection system in sizing laser 1
$t_{particle\ detection2}$	Time at which the particle is detected by the detection system in sizing laser 2
$t_{peak\ bottom}$	Time measured at the bottom of a PMT pulse
$t_{peak\ detection}$	Time measured at the detection time of a PMT pulse
$t_{peak\ top}$	Time measured at the top of a PMT pulse
$t_{rising\ time}$	Time needed for the PMT pulse to reach its maximum amplitude

$t_{\text{trig, scale}}$	Trigger system characteristic time scale (of the DSTU for example)
$t_{\text{trig, delay, laser}}$	Laser trigger time delay
$x_{\text{ion, 0}}$	Initial ion position in the ion source
$x_{\text{ion, ext}}$	Ion position at the extraction electrode
z	Electric charge number

Greek variables

α	optical Size parameter
γ	Gas specific heat ratio (for air $\gamma = 1.4$)
λ	Light wavelength
η	Gas viscosity
ν	Light frequency
ρ_p	Particle bulk density
$\tau_{\text{arbitrary}}$	Arbitrary calculated particle residence time in laser beam
$\tau_{\text{gas, ion source}}$	Residence time of the gas in the ion source
τ_{particle}	Particle residence time in laser beam
τ_{relative}	Relative particle residence time in laser beam [-]

1 Introduction

Aerosols can be considered, from a certain point of view, as a special state of the matter that consists of a suspension of a condensed phase, solid or liquid, in a gas phase. They are, as a result, as diverse as the gas phase and the condensed phase can be. Indeed the particulate phase distributed in the air in small entities, such as droplets, crystals, grains, etc, of any size, can be liquid or solid and composed of any combination of chemicals existing on Earth. Furthermore, the diversity of aerosols is even wider due to the variety of the gas phase chemical composition which can be simply air, pure nitrogen, pure argon or any, cold or hot, gas rich in organics from ambient air or combustion exhaust gases.

Aerosols are not a laboratory curiosity since they are ubiquitous at the surface of the Earth, in the air, in public buildings, in private houses, industrial facilities, mines, animals or human lungs. Therefore all these systems on Earth, humans, animals, plants, crops, mountains and oceans are exposed to them. According to different points of view, aerosols can have positive or negative effects on their environment. From an anthropic point of view, aerosols might affect negatively or positively the health ([Davidson et al., 2005]), the air chemistry and quality ([Ravishankara, 2003]), the Earth climate ([Lohmann et Feichter, 2005], ([Sokolik et Toon, 1999]), the oceanic biological production ([Walsh et Steidinger, 2001]), vegetation life ([Grantz et al., 2003]), industrial corrosion (cf. current project at GSF-Forschungszentrum in Prof. Zimmermann's group) or the fabrication of electronic chips ([Reents et al., 1995]). On the other hand, aerosols are not only natural elements that mankind has to deal with since they can also be "domesticated" for the production of high-tech materials with specific properties such as light fibers ([Friedlander, 2000]) or for the treatment of diseases such as asthma.

In any case, better knowing the aerosol effects on the environment or attempting to domesticate them for specific purposes require to understand how they can act and what are their most relevant properties to be looked at.

The most evident properties of aerosols are their particle size and concentration. Indeed, the size of the particles determines their transport properties whereas their concentration quantifies the amount of material that is to be considered. It determines in particular how and where the aerosol can be transported, how long it can travel and how much material can be transported. A recent French TV-program on mineral dust simply noted that the biggest exported good from Australia is its red sand which makes the system {aerosol+wind} being the best, most economic aerial good transporter of the world in terms of quantity but also of network. Indeed practically any places of the world, from a vast ocean surface area to microchips or lung alveoli, can be concerned. The only reproach for such an air transporter could be its rapidity, punctuality and reliability. For example, dusts from Sahara crosses the Atlantic ocean in a week.

Once at a given place, particles can affect their surroundings as they contact it directly. Indeed particles carry and bring chemicals that can be hazardous and easily liberated to their surroundings and offer surfaces on which chemical and physical processes can take place. Since many particles are present in an aerosol, there is no reasons why particles should be identical so that they have to be considered physically and chemically different from each other. In these conditions, considering a group of particle rather than individual particles is a mistake. To handle the large amount of particles in an aerosol and the single particle specificity, the aerosol characteristics are to be expressed in terms of property distributions.

As a result, the description of an aerosol requires to have access to all its properties listed in Table 1 i.e. and their distribution over the total number of particles.

<i>Gas Phase</i>	<i>Single Particle</i>	<i>Particle Population</i>
Temperature	Shape	Total number of particles
Pressure	Size	Concentration of particles
Composition	Mass	The property range
Homogeneity	Composition	Distribution of the property
	Homogeneity	Internal/External mixture
	in <i>Surface & Volume</i>	
	Porosity	

Table 1 : Aerosol properties according to different points of view

The chemical particle analysis leads to the definition of the notion of external/internal mixture. An internal mixture qualifies situations where particles contain many different compounds in the same particle. On the opposite an external mixture refers to particles that each contains a pure material which can differ from particle to particle. At the particle population scale, the chemicals are considered to be mixed in the aerosol so that no distinctions can be made between an internal or an external mixture.

An aerosol is also a quickly evolving system. For example, atmospheric and combustion aerosols have a typical lifetime of respectively one week and few seconds to some hours. Since the aerosol properties are time and place dependent, their analysis should be carried out accordingly, i.e. at the time and the location where the aerosol effects are to be studied. If the knowledge of all the aerosol properties at any time at the place of interest is the “ultimate” goal to be able to precisely describe the behavior of an aerosol in any situation, the methods and equipments for this task are currently not existing. This motivated a lot of work in aerosol analytical science up to now as reviewed by [Baron and Willeke, 2001].

In 1977, Davis ([Davis, 1977a]) introduced the concept of aerosol mass spectrometry that approaches the best the analytical requirement reported by Friedlander formalized by the size-composition probability density function ([Friedlander, 2000]). Since then the technique has quickly evolved over the last decades as described in [Noble et Prather, 2000] but it is still considered to be at its infancy by [Jimenez, 2005] who reviews the current state of aerosol mass spectrometry and its different configurations. This technique is the only one currently permitting the measurement of the particle size and the chemical composition on a single particle and real-time basis providing thereby a statistical significant number of analyzed particles. Moreover under certain circumstances, surface composition only and particle optical properties can also be obtained to answer the analytical needs of atmospheric chemists, climate modelers or/and remote sensing scientists as reported in [Jacob, 2000] and in [Sokolik et Toon, 1999]. Such an attractive technique should also contribute to address public health questions such as the impact of aerosol particles on the health whose mechanisms are not yet fully understood since their properties used in such studies were mainly their size distribution or load in the air.

These scientific questions motivated the construction of a new generation aerosol mass spectrometer permitting a comprehensive physical and chemical analysis of aerosol single particles which is presented in the following work.

The present manuscript presents the development of the aerosol mass spectrometer (named hereafter Single Particle Aerosol Laser Mass Spectrometer, SPALMS) developed at the GSF-Forschungszentrum für Umwelt und Gesundheit (Neuherberg, Germany) from December 2001 to June 2005. The aerosol mass spectrometer SPALMS is designed for its use in field measurement campaigns, in particular in industrial incineration plants, for a better description of the organic chemical composition of single particles in ambient air and combustion aerosols. Since the principle of this technique is fairly well established by the work of many aerosol mass spectrometer groups ([Jimenez, 2005]), the frame philosophy of this work is to operate different particle desorption/ionization methods and to consider all measurement events as a potential source of information that are to be compiled together. The objective of this work was first to build up the instrument, to operate and to characterize it in its standard base version and secondly to propose different operating modes and analysis strategies compatible with the SPALMS instrument current setup to make this technique more mature.

After a critical analysis in Chapter 2. on the usual on-line aerosol analysis techniques and the different aerosol mass spectrometer configurations, it was decided that the SPALMS instrument would be operated with a nozzle inlet unit, an optical detection/sizing unit, a laser based desorption/ionization unit and a bipolar time-of-flight mass spectrometer. The coupling of each unit was made very modular and flexible so that one- or two-step laser desorption/ionization can be operated as well as double cation analysis of the single particle. These technical choices should lead to a better description of the organic content of single particles and to investigate the particle homogeneity.

Chapter 3. presents the scaling rules followed to design the SPALMS instrument while the following ones, Chapter 3. to Chapter 9. present the characteristics and performances of the different units of the working SPALMS instrument version. In particular the inlet, detection/sizing, desorption/ionization, trigger, mass spectrometer and data acquisition units are successively presented. On its side, Chapter 10. presents the first particle chemical analysis measurements with the SPALMS instrument with one- and two-step laser desorption/ionization of different particle samples such as soot (from Palas GmbH for example), ash particles from biomass burning and soil materials.

Chapter 11. to Chapter 14. present different tested and proposed directions to improve the particle characterization. Indeed Chapter 12. illustrates the benefits of sampling particles by impaction within the inlet unit for off-line analysis by PIXE and in parallel with an APS instrument. Chapter 13. describes how single particles can be better aerodynamically and optically differentiated with the current detection/sizing unit by addressing the “trajectory ambiguity effects”. Finally Chapter 14. reports different ways to operate the mass spectrometric analysis and the desorption/ionization in order to respectively better characterize the desorption/ionization process and to obtain a better mixture resolution of the aerosol particle composition.

Finally Chapter 15. presents a possible future evolution of aerosol mass spectrometry before concluding that the SPALMS instrument developed in this study has a great potential to characterize single particles both physically and chemically.

2 Aerosol analysis overview

This section proposes an illustration and a summary of usual questions that rise when one wish to perform the analysis of an aerosol. Indeed an aerosol is a two-phase system consisting of a gas and a particle phase that is solid or liquid. According to the purpose of the analysis of the aerosol, which can be the investigation of health effects or of its impact on the earth radiative budget, different specific properties of the aerosol need to be measured so that a choice has to be made.

Different ways of classifying aerosol analysis methods can be categorized in terms of extractive or remote sensing methods, of single particle or integrated/bulk basis or of real-time or off-line basis. The best method would ideally permit the analysis in practice of every single particle of a given aerosol volume in a time smaller than the aerosol lifetime for every property.

The most promising technique until now in this regard has been recognized to be aerosol mass spectrometry. Depending on its technical design, aerosol mass spectrometry permits the sizing of single particles and the chemical analysis of their constituents by mass spectrometry, a usual technique in analytical chemistry.

Once the choice of the aerosol mass spectrometry technique has been justified, this section discusses the different steps of the aerosol particle analysis with this technique by proposing to the reader a critical analysis of the different measurement steps and their usual corresponding technical approaches. This will give the possibility to evaluate which technical solutions give access to which particle property or information and which technical choices are compatible together.

From this study, guidelines for the design of the aerosol mass spectrometer built at the GSF-Forschungszentrum will be defined.

2.1 Concept of aerosol analysis

The analysis of an aerosol is a real challenge for physicists and analytical chemists. A rigorous aerosol analysis requires to access to all properties presented in Table 1 at the different observation scales of the aerosol at the time and place where it is to be analyzed.

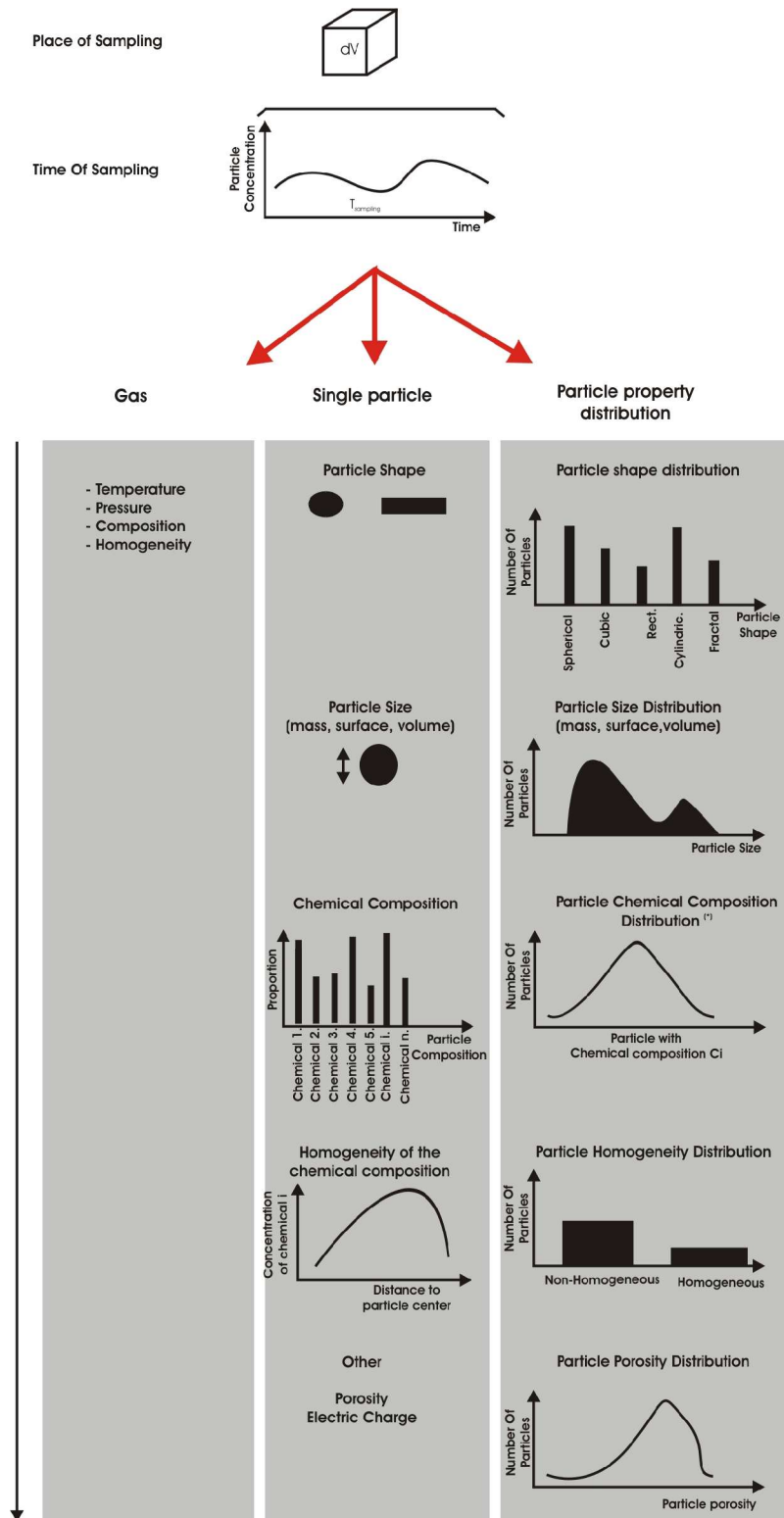
Considering the practical point of view, the problem is:

- to perform a representative, instantaneous and artefact-free sampling of the aerosol
- to evaluate all single particle properties and their corresponding distribution

Considering the physical analysis point of view, the objective is to get access to:

- pressure and temperature of the gas-phase
- shape, size, surface, volume, mass, porosity, electric charge and homogeneity of the single particle

2. Aerosol analysis overview



^(*) The particle chemical composition distribution stands for the proportion of particles containing a given amount of a given chemical in the aerosol

Figure. 1 : Example of an aerosol analysis sequence

Considering the chemical analysis point of view, the practical technical problems to solve are:

- to perform the chemical analysis of the gas phase only
- to perform the chemical analysis of each single particle
- to perform an extensive, complete chemical analysis on a very small probe, the single particle
- to evaluate the single particle homogeneity

Figure. 1 proposes an overview of the different analytical steps proposed to perform a rigorous aerosol analysis. In the rest of this work, one will focus only the particulate phase.

A rigorous aerosol analysis represents an enormous number of different parameters to measure simultaneously for a great number of samples, each single particle. In practice a given aerosol property is measured with a technique which is specific of it ([Baron and Willeke, 2001]). Obtaining different properties for the same aerosol requires then the simultaneous use of different instruments that permit the measurement of each property needed to elucidate the effects of the aerosol on its surroundings. For this purpose, instruments based on aerosol extraction are usually operated in parallel connected to the same sampling line if the aerosol is homogeneous while remote sensing instruments can analyze the same aerosol sample if their respective sensing volumes overlap each other. In the former case, any instrument considers different particles from a supposed homogeneous aerosol while in the latter case, the same particle can be analyzed by the different instruments. In the former case, one can not be sure that the same particles are “seen” by the different instruments. The comprehensive aerosol analysis is potentially biased in the first case by the homogeneity of the aerosol and the sampling quality of the instruments while in the second case biases are mainly due to possible interferences between the different sensing techniques. From this it appears that a single particle analyzed successively through different remote sensing sensors mounted in serie or tandem followed, if necessary, by a destructive method for every particle should be considered to be the most promising approach for an exhaustive rigorous aerosol analysis.

Towards this goal, it is necessary to list the available techniques and to evaluate how they can be connected together.

2.2 Overview of the available techniques

A tremendous amount of work has been done to approach an “as exhaustive as possible” aerosol particle analysis as presented in the book of [Baron and Willeke, 2001]. Up to now, no techniques offer the ultimate solution. Any chosen technique corresponds to a compromise between a good aerosol representativity, a good time resolution or a good particle properties description of the aerosol at the place and time of interest.

One can classify aerosol analysis techniques in different manners. Single-particle and ensemble/integrative techniques respectively consider each particle as a unique probe or all the particles in a given sensing volume as the probe. One can also differentiate extractive and in situ aerosol measurement techniques. In the first case, the aerosol is taken from its environment and transported into the instrument. This leads to a bias in the measurement since particles are lost in a given extent during its transport to the instrument. One can by-pass the problem by analyzing the aerosol where it is to be analyzed i.e. *in situ* what often involves “remote sensing” techniques. In the rest of this work, only the case of extractive measurements will be treated.

Examples of extractive techniques, as presented in Figure. 2, are presented below and briefly discussed to illustrate some aerosol analysis approaches.

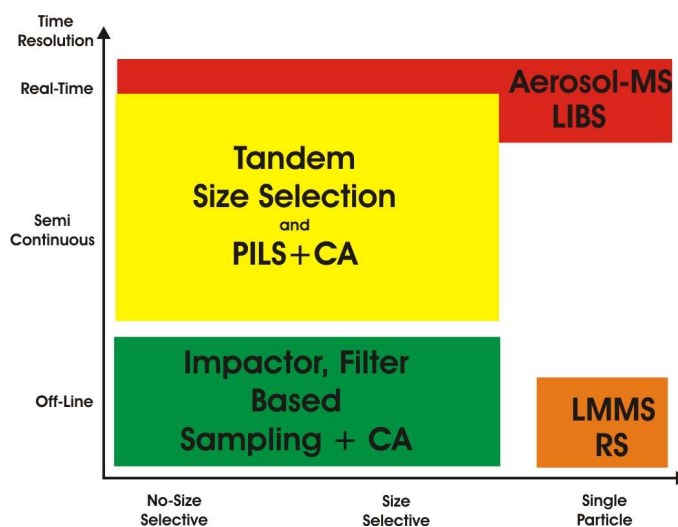


Figure. 2 : Some aerosol analysis approaches

Aerosol-MS (Aerosol Mass Spectrometry), LIBS (Laser Induced Breakdown Spectroscopy), CA (Chemical Analysis), PILS (Particle Into Liquid Sampling), LMMS (Laser Microprobe Mass Spectrometry), RS (Raman Spectroscopy)

The most simple way to analyze aerosols is to collect particles on filters by filtering particle-laden air or by impacting them on a plate. Particles can be either all collected on the same medium (Teflon filter, Quartz filter, aluminium foils for example) or can be collected after being classified according to their size by a size selector such as a cascade impactor. Once particles are collected, they can be analyzed by any conventional chemical analytical technique which permits diverse and complementary analyses since no time constraints nor probe quantity limit theoretically its quality. However, by their sampling itself, particles can be modified. For example, volatile and semi-volatile compounds contained in the particle can evaporate if particles are sampled or stored under vacuum or the gas phase products can interact with the particles if the time between the sampling and the analysis is important. This will lead to an error in the measurement of the aerosol composition since only a part of the chemicals originally present at the sampling time can be detected and quantified. One usually speak of “positive biases” (detection of material not originally present in the aerosol particles) or “negative biases” (missing material).

To overcome the effect of time, particles can be sampled and analyzed on-line, i.e. in a “short” time after their sampling. The work of [Sullivan et Prather, 2005] summarizes the diversity of aerosol on-line chemical instrumentation dedicated to atmospheric aerosols. In spite of its better “suitability” for a “rigorous” aerosol analysis, the on-line analysis of aerosol has some constraints as illustrated in the following sections.

On-line aerosol analysis limits the sample probe quantity to be analyzed and requires the analysis to be performed quickly without (most of the time) offering possibility to test the reproducibility of the measurement unless another identical or/and complementary instrument is operated in parallel. It requires then a rapid technique able to process a small amount of sample and that is “universal”. Indeed the same sample can not be analyzed successively by different complementary techniques unless successive non-destructive different analyses take place like in “production-line work” until the particle gets lost or gets significantly modified. The sensitivity of the chosen chemical analysis method, the available sampling flow rate and the aerosol load determine the time resolution of the

aerosol analysis method. The less sensitive the chemical analysis method is, the lower the aerosol particle concentration is, the worse the time resolution is.

To by-pass these hard technical requirements, many semi-continuous methods were developed to analyze aerosols on-line. For example, the aerosol is collected and brought into a liquid phase (Particle Into Liquid Sampling, PILS) which can then be analyzed on-line by a conventional technique such as ion chromatography. This method is used for the analysis of inorganic ions such as sulfates and other ionic species (See [Simon et Dasgupta, 1995] for example). In another approach, particles can also be collected by a humidified impaction process and flashed vaporized. The resulting gas can be analyzed with a conventional gas phase analyzer. This method is used for the analysis of the nitrate content of particles (See [Stolzenburg et Hering, 2000] for example).

Even if the sensitivity of these approaches can be as low as 100-200 ng/m³ for collected aerosol for given chemicals species (here inorganic ions such as sulfates, nitrates, chlorides, ammonium) and they are continuous with a time resolution in the order of 10 to 30 minutes, the sample concerns a group of many particles. In these conditions, it is not possible to discriminate whether the aerosol is externally or internally mixed. The only way to answer the question is to perform the analysis on a single particle basis.

Single particle chemical analysis can be performed by off-line techniques such as with Laser Microprobe Mass Spectrometry (LMMS), Scanning Electron Microscopy (SEM), Transmission Electron Microscopy (TEM) combined with X-ray analysis, Secondary Ion Mass Spectrometry (SIMS), Raman Spectroscopy (RS) or Infra-red microscopy for example. The reader is oriented to the Chapter 12 of [Baron and Willeke, 2001] for an overview about these techniques. Only the LMMS technique is here shortly described since on-line aerosol mass spectrometry is an adaptation of the Laser Microprobe Mass Spectrometry (LMMS) technique with a particle beam as a sample. In LMMS, particles are sampled on a plate which is disposed at the center of the ion source of a mass spectrometer. The particle is volatilized and ionized by a pulsed laser and the resulting ions are then analyzed by mass spectrometry. Different laser combinations can be used to analyze the aerosol particles according to targeted chemicals ([Hauler et al., 2004], [Ferge et al., 2005]). In this case, particles must first be first collected by an usual aerosol particle sampling technique such as a filter or an impactor and then moved into the LMMS analyzer. For these techniques, the probe is exposed to the high-vacuum required to operate the mass spectrometer what modifies *de facto* the composition of the aerosol. Indeed volatiles chemicals can be lost by the sample preparation.

To reduce this kind of sampling artefact, the ideal aerosol chemical analysis approach is to sample all particles one by one, analyze them comprehensively instantaneously (here before the particle has changed significantly) in a contact-free manner. Aerosol Mass Spectrometry (Aerosol-MS) and Laser Induced Breakdown Spectroscopy (LIBS) are techniques that allow the chemical analysis of aerosols on a on-line and single particle basis.

With the LIBS technique, the laser energy is high enough to initiate a microplasma that vaporizes, dissociates the molecules and excites the atoms contained in the particle. By analyzing the wavelengths and the corresponding intensities of the emitted light by the different atoms, one can have access to the elemental composition and the amount of the particle constituent elements. [Carranza et al., 2001] precises that LIBS can be considered quantitative so that the particle size can even be inferred from the particle composition. LIBS is, nevertheless, known to be less sensitive than aerosol mass spectrometry. Indeed the optical scheme and the light emission/absorption of the carrier gas affect the sensitivity of LIBS.

On the other hand, aerosol mass spectrometry can give access to the molecular composition of the particle. This technique was chosen for our purposes because of its sensitivity and its ability to

detect/characterize the particle constituents at the molecular level. This technique and the developed instrument will be thoroughly described in this work along with its capabilities. Before this, the next section precises the challenges specific to on-line single particle analysis instruments.

2.3 Requirements for the on-line single particle approach

The characterization of an aerosol by an on-line single particle approach has to be universal and very sensitive since the probe is the single particle itself and very rapid to analyze enough particles in order to obtain a statistically representative description of the aerosol.

Aerosols are rarely chemically homogeneous. They are usually both an internal mixture and an external mixture, in particular, for atmospheric aerosols. In spite of the work described by [Van Wuijckhuijse et al., 2005], [Stowers et al., 2004] and the special inlet described by [Kane et al., 2001], it is not possible to sort the particle according to their chemical composition or electrical charge before the analysis in order to orient the particle to a specific chemical analysis method. The chemical analysis method has then to be universal, i.e., it must react, ideally qualitatively and quantitatively, to each chemical specie that is contained in the particle.

Since the amount of material in a particle is small, the chemical analysis method must be very sensitive as well. Indeed the chemical analysis has to react to a low amount of material. Table 2 presents orders of magnitude of the number of molecules of water in particles of different sizes.

<i>Size [μm]</i>	<i>Surface [μm^2]</i>	<i>Volume [μm^3]</i>	<i>Mass [ng]</i>	<i>Nb. Molecules</i>
10	314	523	$5,23 \cdot 10^{-1}$ (530 pg)	$1,75 \cdot 10^{13}$
1	3.14	0.52	$5,23 \cdot 10^{-4}$ (530 femtog)	$1,75 \cdot 10^{10}$
0.1	$3,14 \cdot 10^{-2}$	$5,23 \cdot 10^{-4}$	$5,23 \cdot 10^{-7}$ (530 attog)	$1,75 \cdot 10^7$
0.01	$3,14 \cdot 10^{-4}$	$5,23 \cdot 10^{-7}$	$5,23 \cdot 10^{-10}$ (530 zeptog)	$1,75 \cdot 10^4$
0.001	$3,14 \cdot 10^{-6}$	$5,23 \cdot 10^{-10}$	$5,23 \cdot 10^{-13}$ (530 yoctog)	17.5

Table 2 : Characteristics of particles of different sizes (water droplets, 1000 kg/m³)

In the case of a mixture of different chemical species, the amount of each specie is even lower than for pure particles what requires the analysis method to be sensitive to the low amount of each present chemical species in the particle.

The need of a universal and sensitive chemical analysis method is determined by the fact that the sample is very small and by the fact that the analysis might be destructive and therefore operated during the particle flight only once. This requires that the chemical analysis can not be performed again on the same particle because there is not enough material left (if any), because the particle has been altered or its rest is no longer in the sensing volume. Since all single particles must be considered to be different from each other, one can theoretically not test the reproducibility of the analysis on another similar particle.

Once the analysis of the single particle can be made appropriately by a universal and sensitive method, the analysis of the single particle must be performed in a rapid manner to (i) limit the artefacts due to the sampling as explained in the previous paragraphs and (ii) to process as many particles as possible per time unit in order to get a representative description of the aerosol.

2. Aerosol analysis overview

To precise explicitly the need of a rapid analytical method, let us consider the analysis of a monodisperse aerosol with a concentration of 250 particle per cm^3 whose geometric diameter is 1 μm . Let us consider the analysis of one liter of aerosol. A rigorous analysis of the aerosol means that any single particle of the aerosol contained in the volume of 1 L should be analyzed, i.e. 250 000 particles. If the analysis rate of the aerosol mass spectrometer is of 20 Hz, the rigorous analysis would last around 3h25. This time is be called *aerosol rigorous analysis time* $t_{a,\text{rig},\text{anal}}$. If the aerosol is likely to be modified significantly within 3h25, one can not speak any more of rigorous real-time analysis of the aerosol. If in 5 minutes, the aerosol has not changed, one can say that 6000 particles were analyzed rigorously and that 244000 were not analyzed rigorously. In this case only 2,4% of the particles were analyzed rigorously.

Let us define by *aerosol identity lifetime* $t_{a,i,\text{lifetime}}$ the time during which the studied aerosol does not undergo any significant modification in terms of size distribution, shape and chemical composition. One can then speak of real-time analysis of aerosols only if the *aerosol analysis time* $t_{a,\text{anal}}$ required to perform the analysis is smaller or equal to the aerosol identity lifetime $t_{a,i,\text{lifetime}}$.

This leads to examine two cases:

- $t_{a,\text{rig},\text{anal}} < t_{a,i,\text{lifetime}}$

The chosen setup of the aerosol analyzer suits very well to the aerosol to be analyzed in the present circumstances since the aerosol particles can be analyzed before they are about to change.

- $t_{a,\text{rig},\text{anal}} > t_{a,i,\text{lifetime}}$

Here one can not speak anymore of real-time analysis. Only a fraction $f_{a,\text{rig},\text{anal}}$ of the aerosol is then analyzed rigorously. All the difficulty here is then to evaluate the size of the fraction $f_{a,\text{rig},\text{anal}}$ of rigorously analyzed aerosol particles and how to extrapolate, if it is possible, the observed properties or composition to the whole particle population. Usual aerosol analysis methods are often, if not always, in this case.

Figure. 3 illustrates the problematic that on-line single particle analysis has to face by the arrow from the right to the left and the question mark. Only a fraction of the particles is sampled and chemically analyzed. Due to the small number of analyzed particles and due to the limitation of the chemical analysis method, the observed chemical composition of the aerosol might not match its real chemical composition as it is when it is sampled. Similarly it can not allow the characterization of the mixing state of the aerosol over the whole particle population.

The problematic of the on-line single particle chemical analysis can be summarized as follows:

- How is it possible to extrapolate the results from the on-line single particle analysis to obtain a representative description of the aerosol as it is at its sampling place and time ?
- How can the physical and chemical analysis of the particle be made more certain and accurate ?

It should be noted that this problematic is also the same for the measurement of other properties than the chemical composition on a on-line single particle basis.

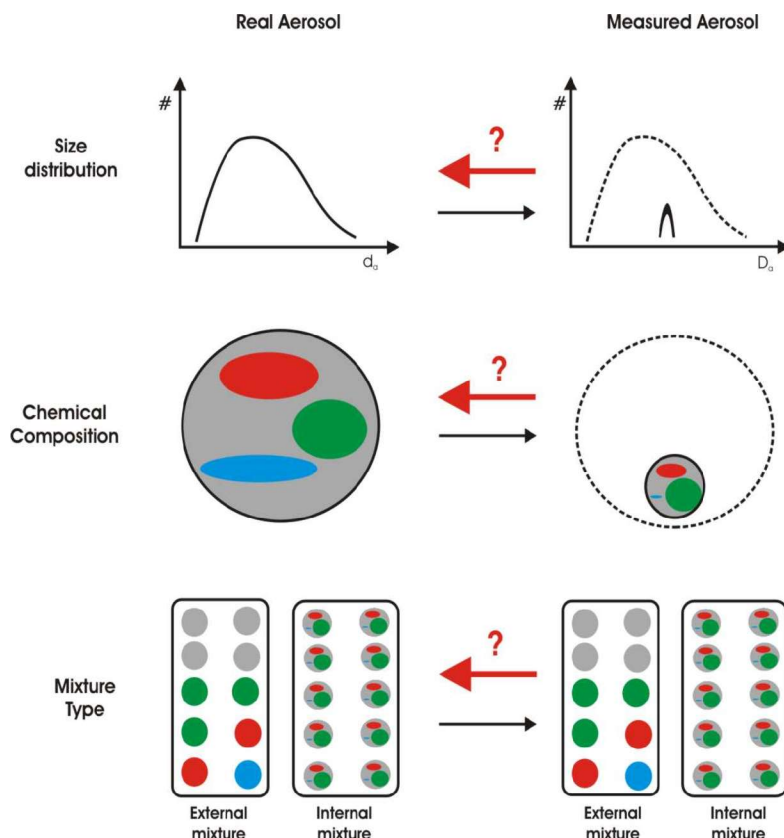


Figure. 3 : On-line single particle analysis problematics

The thin arrow pointing to the right illustrates the limitations due to the analysis method. The thick arrow pointing to the left and the question mark illustrate the problematic of on-line single particle analysis methods to be addressed.

If the rigorous on-line single particle analysis of an aerosol can not yet be performed by a unique stand-alone instrument, the current alternative is the parallel use of on-line single particle analyzer (s) in parallel with integrative techniques such as the aerosol particle collection by a cascade impactor with an off-line analysis as, for example, during the measurement campaign at Atlanta Supersite Experiment in 1999 as presented in [Middlebrook et al., 2003].

Aerosol mass spectrometry, as presented in Figure. 2, has the potential to answer the problematic to a given extent. This will be discussed in the rest of this work.

2.4 Aerosol mass spectrometry

Aerosol mass spectrometry refers to the analysis of the aerosol particle composition by mass spectrometry. Selected milestones about this technique are presented below.

Aerosol mass spectrometry is a technique that combines many processes one after the other. The particle is first taken into the instrument (by an inlet unit) where particles are focused into a beam that facilitates their analysis afterwards (sampling, concentration and focusing process). The particle can be then at the same time size-dependently accelerated, detected and sized as well (detection

and/or sizing process). It then reaches at a given time a region where the particle constituents are vaporized (desorption process) and its constituents ionized (ionization process) before being analyzed by mass spectrometry where the measurement of the mass-to-charge ratio m/z indicates the nature of the ion produced and therefore the particle composition (mass analysis process).

The first analysis of aerosol particles by mass spectrometry was demonstrated by Davis in the 1970s. Particles were sampled through a capillary and impacted on a heated wire that volatilized the particles and ionized the chemicals by surface ionization. The resulting ions were then analyzed by a magnetic sector mass spectrometer ([Davis, 1977a], [Davis, 1977b]). Single particle information was obtained by operating the heating wire at high temperatures that quickly vaporized the particle before the next particle arrived. [Sinha, 1984] introduced the first the coupling of the aerodynamic particle sizing with the laser desorption/ionization of the particle. [Marijnissen et al., 1988] proposed in 1988 the first the analysis of particles by laser desorption/ionization and the analysis of the ions by time-of-flight mass spectrometry what was first performed in practice by [McKeown et al., 1991]. To obtain more information about the single particle composition, [Hinz et al., 1996] operated the ion analysis by analyzing simultaneously cations and anions with a bipolar time-of-flight mass spectrometer. Finally [Morrical et al., 1998] demonstrated the feasibility and the advantages of a two-step laser desorption/ionization scheme on a on-line single particle mass spectrometer to reduce the molecule fragmentation. This leads to a better sensitivity and a lower detection limit compared to the usual one-step desorption/ionization approach. Recently a two-step desorption/ionization (thermodesorption/electron impact) aerosol mass spectrometer has been equipped with an orthogonal time-of-flight mass spectrometer (oaTOFMS) in C- and W-shape ([Drewnick et al., 2005]) permitting thereby a high mass resolution (up to 15000) of the ion analysis. This makes possible the use of the mass deficiency to infer the molecular elemental composition for high mass compounds. This setup significantly improves the chemical analysis resolution in the field of aerosol mass spectrometry.

For more details, the reviews of [Suess et Prather, 1999], [Noble et Prather, 2000], [Wexler et Prather, 2000] (special Aerosol Science and Technology issue), [Sullivan et Prather, 2005] and [Jimenez, 2005] give a rich recent overview of the field of aerosol mass spectrometry from the technical, historical and state of art point of view.

Since its invention, this technique has considerably evolved and reached nowadays a certain degree of maturity. Indeed two commercial instruments are currently available (ATOFMS from TSI. Inc., St. Paul, MN, USA and AMS, Aerodyne, Billerica, MA, USA) and over 45 groups are currently operating this technique for different purposes ranging from the analysis of atmospheric aerosols ([Sullivan et Prather, 2005] and references therein), of combustion aerosols ([Zimmermann et al., 2003]), theoretical study of atmospheric processes and aerosols of relevant importance for the industry ([Reents et al., 1995], [Mahadevan et al., 2002], [Park et al., 2005]). Most of the recent publications about this technique are related to results from measurement campaigns in field and laboratory rather than further technical developments. This indicates a certain degree of maturity of the technique even if it is still to be (and can be) improved as will be discussed later.

As mentioned before, real-time analysis of aerosol by mass spectrometry can be performed with different technical setups. The various available successful setups are presented in Figure. 4 and well presented in [Jimenez, 2005]. All the configurations consist of an aerosol interface whose aim is to sample the aerosol into the instrument (and eventually size the particle if possible) and to prepare it for the chemical analysis with conventional techniques and the mass spectrometry part which performs the chemical analysis of the aerosol constituents.

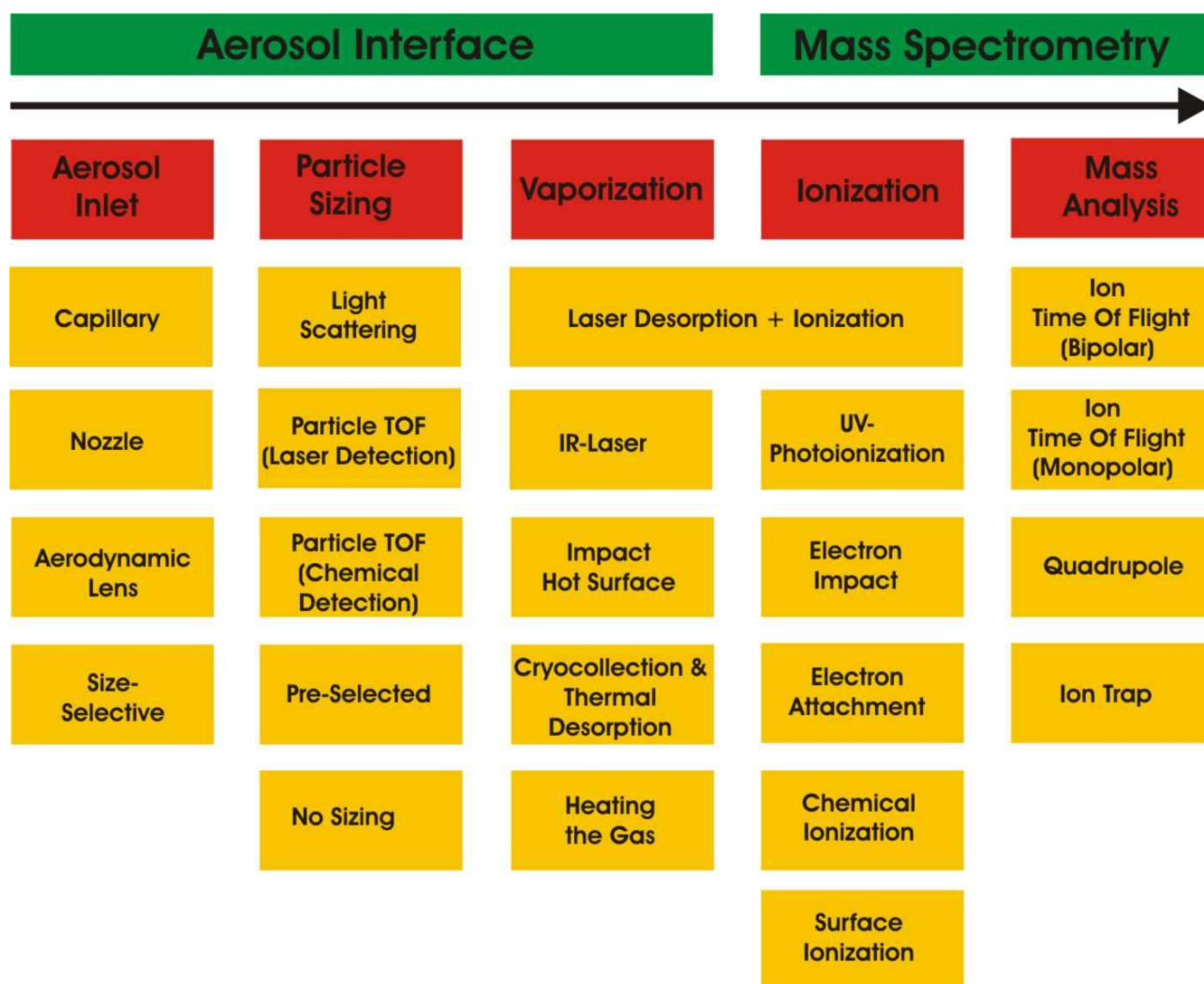


Figure. 4 : Various aerosol mass spectrometer technical setups (modified after [Jimenez, 2005])

The precise role of each aerosol processing operation is detailed in Table 3 below.

Up to now, many technical options have been demonstrated to be successful. The choice of an aerosol mass spectrometer or the construction of a unique one is determined by its application and the targeted aerosol particles to be analyzed. A short critical analysis of the different steps is presented below to orient the choice of the technical setup of the aerosol mass spectrometer at the GSF-Forschungszentrum.

2.5 Critical analysis of the different measurement steps

The next sections present advantages and drawbacks of some of the technical solutions for each measurement steps presented in Figure. 4 in order to orient the choice for the development of an innovative and highly capable aerosol mass spectrometer.

2. Aerosol analysis overview

<i>Measurement step</i>	<i>Aerosol analysis roles</i>	<i>Technical roles</i>
Aerosol inlet	Samples representatively the aerosol from the atmosphere in terms of quantity and size distribution	Reduces the pressure step by step to allow the mass spectrometer operation Concentrates and focuses the aerosol particles along an axis into a thin beam to facilitate their analysis Separates the particle phase from the gas phase in order to avoid interferences due to the gas phase composition Imparts to the particle a size-dependent velocity
Particle sizing	Performs the measurement of the size of the individual particle.	Detects the particle once it entered the instrument. Measures the particle velocity to calculate the time at which the particle will be in the center of the ion source of the mass spectrometer
Vaporization	Volatilizes the constituents of the aerosol	Turns the condensed phase of the particle into a gas phase to perform the ionization of all the particle constituents
Ionization	Eventually targets specific chemical species	Ionizes the gas phase molecules
Mass Spectrometry	Gives a “fingerprint” of the composition of the aerosol particle from the nature of the observed ions.	Measures the ratio m/z of the ions issued from the vaporization and ionization of the particle.

Table 3 : Aerosol mass spectrometer measurement step description

2.5.1 Important aerosol mass spectrometer characteristics

The review of [Johnston, 2000] defines the main characteristic parameters of a laser-based aerosol mass spectrometer.

The performance of aerosol mass spectrometers in terms of aerosol representativity is defined by its analysis efficiency AE, denominated as normalized hit rate by [Kane et Johnston, 2000]. The analysis efficiency AE is here the number of particles that are sized and chemically analyzed per time unit divided by the number of particle entering the instrument.

The analysis efficiency can be split in four categories: Particle Counting Efficiency (PCE), Sizing-Chemical Analysis Efficiency (SCAE), Sizing Analysis Efficiency (SAE) and Chemical Analysis Efficiency (CAE). PCE represents the proportion of particles entering the instrument that are detected. SCAE represents the proportion of particles entering the instrument that are sized and chemically analyzed, SAE the proportion of particles entering the instrument whose size and other physical properties are evaluated (refractive index, morphology, specific surface, etc) and CAE the proportion of particles entering the instrument that are only chemically analyzed. The different quantities can be calculated as follow in Eq. 1 , Eq. 2 and Eq. 3:

$$SCAE = T \cdot SE \cdot HE \cdot E_{ablation}$$

Eq. 1

$$SAE = T \cdot SE$$

Eq. 2

$$CAE = T \cdot HE \cdot E_{ablation}$$

Eq. 3

The different quantities SCAE, SAE and CAE are the products, according to the quantity described, of the inlet transmission T, the sizing efficiency SE, the hit efficiency HE and the ablation efficiency $E_{ablation}$. The inlet unit transmission efficiency T is the ratio of the number of particles that exit the inlet unit to the number of particles entering it. The sizing efficiency SE is the proportion of particles sized (physically analyzed) correctly compared to those entering the sizing unit. In practice, the inlet unit transmission T can not be measured directly since particles have to be detected at its exit. The measured inlet transmission is in reality the inlet efficiency, IEF, which is the product of T and DEF the particle Detection Efficiency which quantifies the ability of the instrument to detect particles. DEF is always larger than SE. The ablation efficiency $E_{ablation}$ is the fraction of particles hit by the desorption/ionization laser light that give a mass spectrum. The hit efficiency HE is the fraction of particles that have passed the inlet and the sizing devices and that are irradiated by the laser light in the center of the mass spectrometer. In case a particle can not be practically sized (as for fine particles with diameters smaller than 200 nm for an optical detection scheme), the sizing efficiency is set to SE=1 for practical reasons. This implies that the chemical analysis of the particles does not require the particle to be sized. The hit efficiency can be expressed as follow in Eq. 4:

$$HE = \frac{A_L}{A_P} \cdot L$$

Eq. 4

where A_L/A_P is the ratio of the desorption/ionization laser beam cross-section area A_L that intersects the particle beam to the particle beam area perpendicular the laser beam axis A_P (the ratio is set to unity if A_L is greater than A_P). This ratio represents the overlap degree of the particle beam and laser beam. L stands for the laser duty factor which corresponds to the time fraction of a time unit during which a particle is in the desorption/ionization laser beam as the laser is firing.

The product of the different analysis efficiencies PCE, SCAE, SAE and CAE by the number of particles entering the instrument, here given by $c_{particle}$. Q_v gives the respective particle counting rate (PCR), hit rate (HR), analysis rate (SCR, Sizing Chemical analysis Rate), SR (Sizing Rate) and CR (Chemical analysis Rate). These numbers are defined by Eq. 5.

$$(PCR, HR, SCR, SR, CR) = (PCE, HE, SCAE, SAE, CE) \cdot Q_v \cdot c_{particle}$$

Eq. 5

where $c_{particle}$ the particle concentration in the aerosol and Q_v the sampling volume flow rate.

The design of the aerosol mass spectrometer must make the different analysis efficiency SCAE, SAE and CAE the greatest possible in order to have enough single particle information that can be considered as statistically significant for a representative aerosol analysis.

To compare the different components of an aerosol mass spectrometer to other or similar aerosol

mass spectrometer configurations, the following quantities are to be considered:

- the inlet unit transmission T (or more precisely the inlet efficiency IEF)
- the sizing efficiency SE
- the hit efficiency HE
- the ablation efficiency E_{ablation} (for a given particle type)

The notions of hit efficiency HE and ablation efficiency E_{ablation} are quantities that are closely linked to laser based aerosol mass spectrometer since this work focuses this type of instruments. These quantities can, however, easily be translated for other aerosol mass spectrometers as follow. The hit efficiency HE means here the efficiency of the capture of the particles to make them ready for a chemical analysis and the ablation efficiency E_{ablation} is defined in terms of proportion of captured particles that give an “observable” signal that can be used to infer the particle chemical composition (here, a mass spectrum). In this regard, thermodesorption followed by electron ionization of refractory mineral particles would yield $HE \sim 0$ and $E_{\text{ablation}} \sim 0$ if 70eV electron can not create ions from this particle.

The different analysis efficiencies SCAE, SAE and CAE give a measure in which extent the obtained particle information can be considered to be representative of the aerosol. If these parameters can simply qualify how representative of the aerosol are the sizing information, it is difficult to qualify the quality and representativity of the chemical analysis since it strongly depends on the particle composition and size as well.

The evaluation of the quality of the chemical analysis can be performed by the analysis of a standard model aerosol (PSL particles, oleic acid particles, NaCl salt particles, ammonium nitrate, ammonium sulfate or soot particles for example) or by inter-comparison measurement campaigns for given chemicals either with collocated similar instruments (as described in [Middlebrook et al., 2003] for example) or with reference analytical techniques for given chemicals such as sulfates (as described in [Drewnick et al., 2003] for example) or NIST standard powders.

2.5.2 Aerosol inlet

Aerosol particles can be brought into the aerosol mass spectrometer by different devices which appeared historically successively such as capillary, nozzle system assembly, aerodynamic lenses and more recently slot aerodynamic lenses.

Recently introduced, aerodynamic lenses as described by [Liu et al., 1995a] and [Liu et al., 1995b] and recently further characterized by [Zhang et al., 2002] and [Zhang et al., 2004] can be considered as the most efficient inlet system up to now since aerodynamic lenses tend currently to be the standard inlet system in aerosol mass spectrometry. Indeed if new build aerosol mass spectrometers have aerodynamic lenses, capillary or nozzle inlet systems are progressively replaced in older instruments as for example for the PALMS instrument ([Cziczo et al, 2003]), the ATOFMS from TSI Inc. (St. Paul MN, USA), ATOFMS from Prather’s group ([Whiteaker et Prather, 2003]) or the mass spectrometer of Marijnissen's group in Delft ([Van Wuijckhuijse, 2003]).

Aerodynamic lenses can sample efficiently particles (with a transmission efficiency T up to 1) of size down to tens of nanometers over a wide size range from tens of nm to some micrometers and focus them in a particle beam of small divergence. As an example, the PALMS instrument lens

focuses particles from 300 nm to 3 micrometers ([Cziczo, 2005]). The particle size range that can be focused is defined by the dimensions of the lens (aperture diameter of each lens, diameter of the tube, the space between the lenses and the pressure level across the whole aerodynamic lens). The smallest size of the particle beam after the nozzle exit is limited by the Brownian motion of the particle ([Liu et al., 1995b], [Zhang et al., 2004]) and lift force effects for non-spherical particles ([Liu et al., 1995b], [Jayne et al., 2000], [Schreiner et al., 1998])

An interesting feature of aerodynamic lenses is their ability to permit the evaluation of the deviation of the particle shape from sphericity by considering the particle beam divergence compared to a particle beam of spherical particles ([Jayne et al., 2000], [Schreiner et al., 1998]).

However the major interests of aerodynamic lenses remain its unity particle transmission over a wide particle size range (an order of magnitude) and its ability to focus efficiently fine particles.

Before aerodynamic lenses became usual, nozzle-skimmers systems were usual ([Kievit, 1995], [Hinz et al., 1994], [Prather et al., 1994]). They consist of an assembly of a nozzle and skimmers or a capillary and skimmers mounted successively one after the other that transmit particles efficiently only for a narrow given particle size range. The divergence of the resulting particle beam is high and particles are distributed over a wider beam cross-section compared to the aerosol beam generated by an aerodynamic lens particularly for fine particles ($< 1\ \mu\text{m}$). If nozzle-skimmers systems are of low interest for sampling fine particles ($< 1\ \mu\text{m}$), they transmit enough big particles ($> 1\ \mu\text{m}$) that can be analyzed so that even if the principle of the aerodynamic lens is known since almost 10 years, nozzle systems are still operated as by [Hinz et al., 2005] and in this work.

Aerodynamic lenses are operated in a vacuum at some millibars which is much more than required for operating a mass spectrometer. Aerodynamic lens assemblies are in any case followed by some skimmers in order to reduce further the pressure level down to 10^{-6} mbar to operate a mass spectrometer. The added skimmers do not influence the particle beam quality since the skimmer aperture is wide enough compared to the particle beam and since particles are already focused in a beam if they are well centered.

The interest of aerodynamic lens might be limited in laser based aerosol mass spectrometer by the fact that all particles transmitted can not be chemically analyzed usually due to the low laser firing frequency (of 20 to 200 Hz) of the desorption/ionization laser and, if not, due to the data acquisition speed which appears to be more and more a relevant problem. Indeed a recent improved version of the Aerodyne mass spectrometer ([Drewnick et al., 2005]) whose quadrupole mass spectrometer has been replaced by an orthogonal time-of-flight mass spectrometer operates a continuous electron impact ionization step permitting thereby single particles to be chemically analyzed as they come. The authors precise in this case that the bottleneck for the single particle analysis is the data acquisition scheme and hardware. This is one reason that may delay aerosol mass spectrometry groups to use aerodynamic lenses.

The use of nozzle systems, if not appropriated for the production of a nice particle beam, permits nevertheless a better resolution in particle aerodynamic sizing because the particles are much more accelerated by nozzle systems than by aerodynamic lenses. Indeed the particle accelerating gas flow reaches 350 m/s at the nozzle system exit.

Aerosol inlet systems consisted from the early development of aerosol mass spectrometer until recently ([Murphy et Thomson, 1995], [Bläsner et al., 2000] for example) of capillaries which focus well particles. This advantage is counterbalanced by the sampling flow rate that is generally low compared to nozzle-skimmers systems and aerodynamic lenses-skimmer systems and by the high risk of clogging of the capillary. This makes, as a result, nozzles and aerodynamic lens far better

operational inlet systems than capillaries. As in aerodynamic lens setups, skimmers are usually mounted after in order to reduce further the pressure to operate a mass spectrometer.

Even if aerodynamic lenses appear to be an acceptable and more and more standard solution for aerosol mass spectrometer inlet systems, the tendency is to develop further inlet systems oriented to a better focusing of even smaller particles and to increase the sampling flow rate while maintaining a good particle focusing over a wide range of particle sizes. [Kane et al., 2001] explored electrostatic focusing of small particles after they exit an usual aerodynamic lens and showed the possibility with an unoptimized setup (but simple to build in principle) to enhance the chemical analysis efficiency CAE by a factor of 2 to 6 for particles as small as 25 nm. The additional interest is its possibility to select particles according to their electrical charge (unfortunately not their chemical composition yet) and to get access to the particle mass for a given particle aerodynamic diameter. This system has also the potential to let go or not, on application of a voltage, a particle to a given location in the instrument. This potentially allows the orientation of a particle according to different criteria as its fluorescence level for example ([Stowers et al., 2004]) to an appropriate chemical analysis method.

On their side [Middha et Wexler, 2005] propose to increase the sampling flow rate by replacing the circular apertures of the usual lenses by slots successively perpendicularly oriented to each other and a combination of V-shaped capped slot as presented in [Middha et Wexler, 2003] to increase the particle collection over the whole the sampling tube cross-section. Indeed, particles flying close the wall of the sampling tube may not be sampled due to their impactation on the lenses. The capped slot, in its V-geometry, permits the quantitative sampling of all the particles entering the sampling tube.

Aerodynamic lenses and nozzle skimmer systems appear to be the most tested and used inlets system approaches up to now and are currently best choices for this study.

2.5.3 Particle sizing

The particle sizing step in aerosol mass spectrometry is not a necessary step. Indeed the particle size information can be obtained in different manners and technical contexts. It was first obtained or inferred as a by-product of the mass spectrum information only or from the desorption/ionization laser trigger scheme that detects the particle before its ablation. The particle sizing step has been introduced first by [Prather et al., 1994] as a step to specifically get the particle size and to trigger the desorption/ionization laser.

Belonging to the by-products category, the particle size can be inferred from the mass spectrometer signals if the vaporization and ionization of the particle can be considered to be quantitative. Here the total ion signal measured by the mass spectrometer is to be related to the particle volume, and therefore its size. This approach is used by surface ionization techniques (early developments of aerosol mass spectrometer in the 1970s, [Noble et Prather, 2000]) and more recently by [Svane et al., 2004]) and by laser based approaches ([Reents et Ge, 2000], [Lee et al., 2005]) usually for sub-micron particles and light/hard ionizable species (alkali, polystyrene or silica). The obtained results agree well with other particle sizing techniques (SMPS, SEM) and provide an even better size resolution in some cases ([Reents et Ge, 2000]). This method depends on the particle composition and the extent of the desorption/ionization process. It is nevertheless generally used only for similar particle composition.

To avoid biases due to an incomplete desorption/ionization of the particle constituents leading to a bias in the particle size determination, particles can also be sized aerodynamically by measuring their time-of-flight between two points in a steady carrier gas flow. The inferred particle velocity is

then related to a particle diameter according to an appropriate calibration whose principle was first described by [Wilson et Liu, 1980] (see [Baron and Willeke, 2001] for further references). To measure the particle time-of-flight, and therefore the particle velocity in a given gas flow, different methods are used to detect the particle at their passage time at two locations. The related methods are either integrated in the inlet system, the chemical analysis system or simply extra designed/built/implemented for particle sizing purposes.

The Aerodyne AMS ([Jayne et al., 2000]) evaluates the particle size by measuring the particle time-of-flight between the time when the particle is let in the chamber (as it passes through a slit of a rotating wheel, named chopper) and its time detection by the ion detector of the mass spectrometer ([Jayne et al., 2000]). The particle detection (and therefore its size and size distribution) depends on the particle ability to be vaporized and to produce an ion signal only. The rotating wheel limits the number of sampled particles mechanically as they impact on the wheel.

In order to take advantageously of all the sampled particles by the inlet system, they are all let into the instrument and detected as they come. Particles are first detected optically as they scatter light as they cross a “sizing laser beam” (such laser can also be named “detection laser”) and then secondly detected as ions from the particle are detected in the mass spectrometer ([Hinz et al., 1994], [Weiss et al., 1997], [Murphy et Thomson, 1995]). In this case, the detection of the particle depends not only on the particle composition but also on the particle size. It means that optically detected particles are detected even if they do not give any mass spectrum. It suggests that particles from mixtures of chemically detectable and not chemically detectable particles can then be detected. If they can here all be optically sized, only the chemically detectable aerosol particle fraction can be aerodynamically sized.

The optical particle detection followed by a chemical detection was firstly intended to trigger the desorption/ionization laser in order to obtain a particle mass spectra and to obtain a high chemical analysis rate (CR). If this approach permits the detection of practically any particle of any composition, smart data acquisition setups permit their optical and/or aerodynamic sizing in addition to the trigger of the desorption/ionization laser. The works of [Murphy et Thomson, 1997a], [Murphy et Thomson, 1997b], [Hinz et al., 1994] and [Weiss et al., 1997] illustrate this.

Up to now, these particle detection methods depend on the particle ability to be vaporized and produce an ion signal. The chemical analysis step determines here then the quality of the particle size distribution measurements.

To fully eliminate the composition dependency in the detection and the sizing of the particle and to base it on particle physical properties only, particles can be either only detected optically and sized aerodynamically or only detected and sized optically.

In this regard, the second particle detection step is replaced by an optical detection of the particle as performed in commercial particle sizing instruments such as the APS3321 (APS3321 TSI, Inc., St Paul, MN, USA), the Aerosizer (API, Amherst, MA, USA) and the ATOFMS instrument from TSI Inc. (ATOFMS Model 38000, TSI Inc., St. Paul, MN, USA) and research aerosol mass spectrometers ([Prather et al., 1994], [Reilly et al., 1997] for example). The particle is detected at the two locations on its fly as it scatters light from a detection/sizing laser. For these instruments, the amount of scattered light is not relevant what makes the optical detection and light signal processing setup robust and easy to handle: is there one or no particle detected ? According to the acceleration gas flow (subsonic or sonic flow regime), the geometry of the nozzle and the detection system, the measured particle velocity can be considered to be the terminal velocity or a given particle velocity at a given location of its acceleration phase. The latter situation offers a potential for the obtention of additional information to the particle size such as shape or density.

The recent work of [Oskouie et al., 2002] mentioned the possibility of evaluating the further acceleration of the particle after its acceleration in a sonic nozzle in order to infer the particle diameter and a lumped density/shape factor. Their work provides the calculation method but its application, possible, requires a possible necessary rearrangement of the sizing laser beams just after the first nozzle and to use the desorption/ionization laser as a third sizing laser, what is possible in the case of an ATOFMS aerosol mass spectrometer or similar instruments.

An alternative to the aerodynamic sizing of the particle by detecting it optically which requires a steady particle carrier gas flow is to use the scattered light signal only. The particle is sized according to the amount of scattered light by the particle as it crosses the unique detection/sizing laser at one single location as by commercial instruments (see [Baron and Willeke, 2001] for further references). In this case, only a single sizing laser is necessary. However many groups in aerosol mass spectrometry prefer to size particles aerodynamically since the particle size inferred from the scattering light signal shows a larger variability ([Kievit et al., 1996], [Salt et al., 1996]). This is mainly due to the difficulty to process the light signal and to the fact that the light scattering patterns of a single particle are strongly, and not monotonically, dependent on the particle optical properties (size, shape, refraction index), on the optical setup quality and on the trajectory ambiguity effects. However, the optical particle sizing appears to be consistent in trends with the obtained aerodynamic diameter.

Surprisingly only few works have been published that use the light signal of two sizing lasers to size aerodynamically the particle and to infer an optical diameter in order to better determine the particle diameter, refractive index or density ([Murphy et al., 2004], [Moffet et Prather, 2005]).

Particles can also be sized by the inlet system itself so that no specific sizing devices nor data acquisition strategy have to be designed. Indeed particles can be sized in a discrete manner by simply adapting the inlet system operating conditions to a particle size range of interest as described in [Mallina et al., 2000]. This method does have interest only if one wish to analyze monodisperse particles of small size, typically below 200 μm where particles can not be sized optically nor aerodynamically.

The particle size can also be determined before leading the particles into the aerosol mass spectrometer. For example, [Slowik et al., 2004] performed the analysis of fine single particles by operating an AMS Aerodyne and a DMA (Differential Mobility Analyzer) in tandem. This has the advantages to precise more the measured equivalent particle diameter by comparing its mobility diameter (from the SMPS measurement which involves a DMA) and the vacuum aerodynamic diameter (from the Aerodyne AMS) and to use usual inlet systems. From such an experimental setup, information about the particle density and shape can be inferred. If the combination appears to be powerful, it still requires two instruments whereas one involving both methods would be preferable and more convenient.

Technical options for the particle sizing depend strongly on the particle size, composition and optical properties. The sizing of fine particles are more easily done by either a size-selective device (DMA or size-selective inlet) mounted upstream or inferred from the mass spectrometer signal under specific conditions since fine particles can not be sized optically nor aerodynamically. Indeed fines particles (diameter smaller than 200 nm) do not scatter enough light to be detected and their velocity in a gas flow is not size-dependent. For bigger particles (diameter typically exceeding 200 nm) both optical and aerodynamic sizing can be performed.

Sizing particles aerodynamically and optically is interesting since the obtained physical properties can be then confirmed by the particle chemical analysis and vice versa. This can also potentially permit a cross-check of the measurements.

2.5.4 Particle desorption/ionization

Once the particle is at the center of the mass spectrometer, its constituents have to be prepared, vaporized and ionized, for their mass analysis. It exists two ways to proceed. Either both steps are operated simultaneously with the same equipment (one-step desorption/ionization, later referred as 1-step DI) or successively with different equipments (two-step desorption/ionization, later referred as 2-step DI). This step is critical and determines the quality of the chemical analysis. Technical solutions used in aerosol mass spectrometry are presented here after an overview on usual sampling techniques used in classical mass spectrometry.

2.5.4.1 Standard sampling techniques in mass spectrometry

The analysis of compounds by mass spectrometry requires the sample to be ionized. The ionization technique to use depends on the state of the sample whether it is in gas, liquid or solid state. Gas phase samples are easy to handle since they can be easily transported into the mass spectrometer and its ionization device. This concerns only species which are either gaseous or which have a high vapor pressure and which are thermally stable if the sample need to be heated. For non-volatile or thermally labile compounds, the mass spectrometry technique to be used has to include a step to sample or/and create ions from liquid or solid samples ([De Hoffmann et Stroobant, 2003], [Gross, 2004]).

For the later techniques, many people use the nebulization of the sample, dissolved in a liquid with eventually additives, in the form of a spray to carry the sample into the mass spectrometer. Once introduced in the mass spectrometer, the solvent phase is evaporated by heating the spray radiatively or with a warm gas. The ionization requires specific processing of the sample or simply take advantage of “native ions” as listed hereafter. The charge of the ions can originate from the initial state of the compounds in the sample (such as basic compounds in basic media, salt solution for example), from the charge surface of the spray (like in electrospray ionization (ESI)) or from a specific ionization process such as chemical ionization (CI), photoionization (PI) or electron impact (EI), atmospheric pressure chemical ionization (APCI), atmospheric pressure photoionization (APPI) for example.

It exists setups for which the heating of the spray is not necessary to sample the already existing ions in the solution. A strong electric field operates the extraction of the ions from the liquid phase as done with thermospray (TSP).

The liquid sample can also be deposited on a surface which is then handled according to usual techniques as described below. The sample is first taken from the bulk, ionized and then sent to the mass spectrometer.

The deposited sample on a surface can be heated what simply desorbs and ionizes the chemicals (surface ionization/thermo-ionization). Other methods exist and require the exposition of the surface sample to different kinds of energy sources. Indeed the sample surface can be exposed either to a high voltage (up to 10^8 V.cm^{-1}) (Field Desorption, FD), to a beam of atoms or ions (Fast Atoms Bombardment, FAB, Secondary Ions Mass Spectrometry, SIMS), to a laser light (Laser Ablation, LA, Matrix Assisted Laser Desorption Ionization, MALDI), to a plasma (Plasma Desorption, PD, Desorption Chemical Ionization DCI) or to an electric discharge (such as a spark or a glow discharge). In these cases, ions are usually produced during the sampling process, i.e. the chemicals to be analyzed are quasi simultaneously desorbed from the bulk and ionized.

This later approach suits for the analysis of chemicals dissolved in a liquid phase, for chemicals embedded in a given selected matrix or simply for bulk materials.

Aerosol mass spectrometry can be considered as a special adaptation of the previously described sample preparation techniques. Nebulization techniques permit the analysis of aerosol particles (or spray) which are all considered to be representative of its mother bulk solution whereas the direct treatment of the sample surface needs to be applied to each single particle surface only. The specific features of aerosol mass spectrometry concern the fact that each studied sample, either a single particle of the generated spray or a tiny fraction of the bulk of the sample, is to be individually analyzed. It requires to use a specific interface that bring particles one by one to the desorption/ionization zone while operating the usual desorption/ionization techniques in mass spectrometry.

From [Noble et Prather, 2000] and [Jimenez, 2005], some of the techniques presented above have been adapted to aerosol mass spectrometers by considering the sample to be a particle solid particle, even if the particle is in liquid state as it is sampled. Both combined desorption/ionization techniques (one-step) and separated desorption/ionization (two-step) are used. Both options are discussed in the next paragraphs.

2.5.4.2 One-step desorption/ionization (One-step DI)

As seen in the previous section, many one-step desorption/ionization options do exist. The most current ones used in aerosol mass spectrometry are surface ionization (or thermoionization as denominated in [De Hoffmann et Stroobant, 2003]) or laser desorption/ionization.

If the former one was intensively used at the birth of aerosol mass spectrometry and recently used for the investigation of the content of alkali metals in particles ([Svane et al., 2004]), laser based desorption/ionization is now currently by far the most common method used. Since surface ionization is mainly restricted to chemicals with a low ionization potential such as alkali metals, the surface desorption/ionization will not be addressed in this section.

The one-step desorption/ionization process limits considerably the potential of on-line aerosol mass spectrometry in terms of “real chemical analysis” of the aerosol constituents. Current one-step laser desorption/ionization provides rather a “fingerprint” of the aerosol chemical composition that can be different from laser pulse to laser pulse for exactly the same particle as illustrated in the work of [Wenzel et Prather, 2004] and [Phares et al., 2001]. In these studies, the mass spectra classification with the ART-2a algorithm produces many different classes for a given particle type which are not specific of the particle type. This illustrates that one-step laser desorption/ionization does not lead to reproducible results.

Desorption and ionization processes are very complex since they take place in many different manners. Desorption processes depend on the laser pulse characteristics and the particle composition and homogeneity ([Zhigilei et al., 2003]). Ions identified in mass spectra result from the contribution of many ion sources which can be classified as “primary” ion sources and “secondary” ion sources. Primary ions correspond to ions that are initially present in the sample before and/or that are produced directly during the laser light irradiation of the particle. Ions can be pre-existent in the sample if the matrix is acidic or contains a high amount of salts ([Karas et Krüger, 2003]) or produced by photoionization of neutrals. The “secondary” ion source groups ions resulting from many ion-molecules or ion-ions reactions in the ejected material plume ([Karas et Krüger, 2003], [Knochenmuss et Zenobi, 2003]). Ions are in particular produced by chemical ionization whose ion production depends on the properties of the reacting materials (see Table 4).

2. Aerosol analysis overview

<i>Reaction name</i>	<i>Reaction type</i>	<i>Comments</i>
Positive ion production		
Electron ionization	$M + e \rightarrow M^+ + 2e$	For high electron energy such as 70 eV electrons
	$M^+ \rightarrow EE^+ + R^{\cdot}$	EE: even ion, R: radical
	$M^+ \rightarrow OE^{++} + N$	OE: odd ion, N: molecule
Protonation	$M + H^+ \rightarrow [MH]^+$	
Proton abstraction	$M + A \rightarrow [M-H]^{\cdot} + [AH]^+$	
Proton exchange	$MH^+ + A \rightarrow M + AH^+$	
Adduct formation	$MH^+ + N \rightarrow [MN+H]^+$	
	$M + F^+ \rightarrow [MF]^+$	
Charge transfer	$X^+ + M \rightarrow X + M^+$	Usually X has a higher ionization potential than M (case of rare and air gases)
Photoionization	$M + \text{photon (SPI)} \rightarrow M^+ \text{ (or fragments)}$	Typically $\lambda = 118 \text{ nm}$
	$M + \text{photon (REMPI)} \rightarrow M^+ \text{ (or fragments)}$	Typically $\lambda = 266 \text{ nm}$ for PAHs
Negative ion production		
Associative resonance capture	$M + e \rightarrow M^{\cdot-}$	For low electron energy 0-2 eV
Dissociative resonance capture	$AB + e \rightarrow A^{\cdot-} + B^{\cdot-}$	For electron energy 0-15 eV
Ion pair production	$AB \rightarrow A^+ + B^- + e$	For electron energy above 15 eV
Negative ion dissociation	$AB^{\cdot-} \rightarrow A + B^{\cdot-}$	
Proton abstraction	$X^{\cdot-} + MH \rightarrow M^{\cdot-} + XH$	

Table 4 : Examples of molecule ionization pathways

From Table 4 it is easy to understand that the obtained mass spectrum after the particle desorption/ionization is difficult to relate to the particle composition. Indeed fragmentation processes of the initially present molecules in the particle during the desorption/ionization processes and reactions occurring in the material plume that can produce new chemical species make the interpretation of the mass spectra difficult. Initially existing species are rearranged and fragmented by the reactions in the ablation plume.

The chemical ionization processes which take place in the plume can be used as a complementary technique to photoionization as the laser light pulse is over and as the molecules have a too high ionization potentials to be ionized by the current used laser wavelength. The occurrence of a “natural chemical ionization” by the aerosol particle constituents itself is particularly obvious when long laser wavelengths are used, such as nitrogen laser light at 337 nm for example. At this wavelength, very few chemicals only can be photoionized. Many works in aerosol mass spectrometry have pointed out the occurrence and interest of this type of chemical ionization as will be illustrated below.

Chemical ionization by sodium or potassium, a frequent element, was reported and used by [Lazar, 2000] in order to quantify tributylphosphate molecules at the surface of ambient particles. Indeed, tributylphosphate is electrically positively charged by formation of a molecule adduct a potassium atom ($[K^+$ -tributyl phosphate]). [Silva et Prather, 2000] reports the existence of chemical ionization of organic molecules M with sodium (Na) by the formation of an adduct $[Na^+$ -M] or the protonation of molecules. These authors take the example of phthalic acid as a proton source whose proton binds to an oxy-PAH such as perinaphtenone.

Chemical ionization also explains the occurrence of negative species in mass spectra. Indeed if negative ions can be produced by ion pair dissociation, negative ions are also produced by electron attachment. Indeed, irradiation of semiconductors by UV light is known to liberate electrons that can be then used to produce negative ions by electron capture. The work of [Thomson et al., 1997] and [Knochenmuss, 2004] show that the emission of free electrons during the laser desorption processes is real what was many time observed during this work. The possibility of obtaining a negative and positive mass spectrum enhances the chemical resolution of the chemical analysis of the particle.

Even if the chemical processes occurring in the desorption and ionization steps permit the enhancement of the detection of many chemicals initially present in the particle, different ion-molecule and charge transfers reactions affect the resulting mass spectra in "hiding" some species by fragmenting, rearranging them and/or neutralizing them electrically so that the mass spectrometer can not detect them.

Indeed one can reasonably understand that the diversity of ions detected by the mass spectrometer is reduced with time to a limited number of ionized species after a given time. Considering the plume lifetime of 0 to some microseconds with a rather high chemicals density at the beginning, [Knochenmuss et Zenobi, 2003] report the possibility of observing mainly products from the sample constituents resulting from the most thermodynamically favored reaction pathways. It has for consequence that some species initially present in the particle can not be observed in the mass spectrum since they do not exist any more.

Together with a charge exchange mechanism, this can explain the difficulty to detect sulfate in particles ([Thomson et al., 1997]) and explain why organic impurities or alkali metals appear to be present in significant amount from the mass spectra analysis even if they do not represent the major fraction of the particle constituents ([Middlebrook et al., 1997]). This effect motivated the development of correction factors, named relative sensitivity factor (RSF factor) that takes into account the relative behavior of different elements toward ionization in mass spectra for the right quantification of alkali metals in particles as presented by [Gross et al., 2000].

Charge transfers might not always occur with the particle constituents only but can also occur with the particle carrier gas, even at low pressure (at some Torr). Indeed, [Reents et Schabel, 2001] explain and demonstrate that the measured elemental composition of NaCl particles is biased by a charge transfer between the chlorine cation and the carrier gas, here argon as follow $Cl^+ + Ar \rightarrow Cl + Ar^+$. As argon is replaced by helium which has a higher ionization potential than argon, the measurement bias disappears. Even if no publications report chemical ionization of the particle constituents with the carrier gas constituents such as nitrogen or oxygen, such processes can reasonably not be excluded.

It rises in particular the question of the influence of the nitrogen and oxygen of the air on the final mass spectra, in particular when oxides are observed. Due to the low absolute pressure of carrier gas in the ionization zone (10^{-5} - 10^{-6} mbar), oxidation of the particle constituents with the oxygen can be reasonably estimated to be insignificant. Observed oxides in mass spectra can be considered to be

2. Aerosol analysis overview

either initially present in the particle or resulting from oxidation reactions between the aerosol constituents itself.

Some work was done to model the contribution of the different reactions occurring in the laser plume in order to attempt to relate the observed mass spectra to the initial sample composition for simple system in MALDI experiments ([Knochenmuss, 2003]). More simply the consideration of basic ion thermochemical data such as those presented in Table 5 can help to interpret the mass spectra as done by [Knochenmuss et Zenobi, 2003] or [Reents et Schabel, 2001] for example.

It is particularly interesting to list and compare the different ionization energies IE (improperly commonly named ionization potential IP), appearance energies (AE), proton affinities (PA, also named gas phase basicity), electron affinities (EA) and gas phase acidities (GPA, also named relative acidity) of the observed chemicals in the mass spectra and/or their supposed precursors. These quantities provide a help to guess which species would be the more probable to observe and to get a “feeling” of the preponderant processes during the volatilization and ionization of the particle constituents.

<i>Name</i>	<i>Definition</i>	<i>Reactions</i>
Ionization energy	Energy necessary to remove an electron from a parent molecule	$M + h\nu \rightarrow M^+ + e^-$
Appearance energy	Energy necessary to produce given fragments from a parent molecule	$AB \rightarrow A^+ + B + e^-$
Proton affinity	Opposite of the enthalpy (energy at constant pressure) of the reaction of formation of a cation MH^+ by protonation of a molecule M	$M + H^+ \rightarrow MH^+$
Electron affinity	Opposite of the enthalpy (energy at constant pressure) of the reaction of formation of an anion M^- by electron capture by the molecule M	$M + e^- \rightarrow M^-$
Gas phase acidity	Gibbs energy of the reaction of a molecule that liberates a proton and that gets negatively charged	$MH \rightarrow M^- + H^+$

Table 5 : Thermochemical quantities of gas-phase ions (after [NIST, Weekbook])

It can be here concluded, that one-step desorption/ionization can be considered as a “pseudo-universal”, “combined” or “multiple” ionization process that permits the ionization of a large variety of chemicals. The limitation of the one-step desorption/ionization process can be attributed to (i) mainly the charge transfer/fragmentation mechanisms that degrade the advantage of its “pseudo-universal” ionization ability, (ii) the impossibility to isolate ions once they are produced and (iv) the high efficiency in molecule fragmentation and rearrangement, (iii) the uncontrolled use of the laser energy to volatilize the particle only.

A way to by-pass this limitation is to avoid matrix-effects, i.e. the interaction of the neutrals, ions, and clusters within the laser plume and to better control the energy needed for each molecule to be softly vaporized and ionized. Using a laser whose photon energy does not ionize nor fragment the particle chemicals would permit a soft particle vaporization that conserves the original chemical nature of particle. A quick look at the ionization potential data base of the NIST (National Institute of Standards and Technology, [NIST, Weekbook]) and the work of [Thomson et Murphy, 1993], [Knochenmuss et Zenobi, 2003] and [Vestal, 2001] indicate infrared lasers to be good candidate for this task. A closer look in the MALDI field should help as well.

The work of [Grimm et Beauchamp, 2003] propose an other interesting approach named FIDI (Field-induced droplet ionization) and referred as Field Desorption (FD) in [De Hoffmann et Stroobant, 2003] that would ideally suit to the investigation of the composition of small liquid

droplets, such as cloud water droplets, without losing molecular information since the method seems to be soft. Indeed the authors report the observation in both polarities of analyte ions (tetraheptylammonium bromide and 1,2,4,5-benzen tetracarboxylic acid) contained in methanol droplets produced from a vibrating orifice aerosol generator (VOAG) (particles size of order of magnitude of some 10s of μm). The technique is actually not an ionization method *stricto sensu* but can be in the present problematic considered as to be a one-step desorption/ionization since the “native” ions (already existing ions in the particle) only have to be extracted from the water bulk so that they can be mass analyzed. The authors mentioned an electrostatic field to perform the ion desorption from the droplet of $\sim 2 \cdot 10^6 \text{ V}\cdot\text{m}^{-1}$, what is only an order of magnitude bigger than the current extraction field condition of the used for the SPALMS instrument.

2.5.4.3 Two-step laser desorption/ionization: Particle vaporization

Since performing the desorption and ionization of the particle in one-step makes the identification of its constituents difficult due to the complex ion-molecules reactions occurring in the ablation plume, the separation of both the desorption and the ionization step should give better results.

Indeed, the particle vaporization or desorption is the critical step of the aerosol mass spectrometry technique. It determines the quality of the chemical analysis of the particle constituents in terms of sensitivity, accuracy, universality and limit of detection. This step can be operated in a contact free manner or assisted by a hot surface. The energy needed is either brought by radiative heating with a laser, by conduction with a heated plate or by convection as the particle is heated by a warm gas flow. The objective is to put in gas phase all the constituents without molecular fragmentation whether they are refractive or not.

Laser based or gas-based methods are very interesting volatilization techniques since they are contact-free. The particle is irradiated by the laser on its flight what eliminates any contamination problem from previous analyzed particles or from the heating plate as it can be in the case of flash vaporized particle of a hot surface.

In laser based vaporization, all constituents of the particle can be brought into a gas phase whether they are volatile or refractory what is not the case for particle thermodesorption on heated surfaces or by a warm gas. Indeed lasers do not process the desorption of the constituents by simple heating but also by fragmenting the particle as a result of a sudden heating that induces pressure shock waves which help fragmenting the particle as explained in [Paltauf et Dyer, 2003] and [Zhigilei et al., 2003] depending on the ablation regime.

Refractory materials from deposited particles on thermodesorption surfaces can, for example, induce parasite reactions which may react with the constituents of the incoming particle. The resulting gas phase will not represent any more the composition of the particle to be analyzed what biases the interpretation of the resulting mass spectrum.

From the single particle analysis point of view, the laser based technique is more likely to perform really the single particle analysis since particles or their rests do not accumulate in the sensing volume formed by the mass spectrometer ion extraction region and the desorption/ionization laser beam. Indeed particles are flying so that new particles are always coming. Operating a pulsed laser with a pulse duration of 8 to 150 ns makes therefore more probable to hit a flying single particle rather than a group. However, if the aerosol is concentrated, it might happen to volatilize a group of particles simultaneously. Such events are difficult to identify as such. Nevertheless the single particle analysis is much more probable than in case of a desorption on a heated surface.

Indeed a heated surface, in the aerosol sampling point of view, is an impactor that collects all impacting particles if they not bounce off. The shape of such a surface, as a V- or C-shape, can favor the particle accumulation and therefore accentuate the contamination phenomenon. If the vaporization does not occurs before the next particle arrives, the analysis which will take place will not correspond to a single particle. This depends in particular on the sampling rate of the instruments, on the particle concentration of the aerosol being sampled and on the volatilization timescale of the particle. Single particle analysis becomes in this case more probable by low particle sampling rate, low aerosol concentration and small particle sizes.

If thermodesorption on a heated surface can not allow the vaporization of refractory material and the analysis of single particles, it is technically much more practical since it can be operated in a continuous manner and does not require a complex laser trigger scheme. Indeed, particles are vaporized as they arrive on the heater. The next step, ionization and mass spectrometry analysis, can be operated in a continuous manner since the measurement event (particle sizing and chemical analysis) is simply triggered “automatically” as the particle is vaporized or arbitrarily periodically.

The ionization and mass analysis steps can be triggered as well for thermodesorption but the scheme quickly catches up the complexity of the trigger scheme of the laser based approach since it requires the particle to be detected to trigger the different ionization devices and ion mass analyzers. This is of major concern if the ionization method can not be continuous as is the electron impact (EI) or chemical ionization (CI) is. For the example of the ionization with a laser light, a trigger scheme is necessary since most of usual ionization lasers are pulsed. However, complex laser trigger schemes for laser based instruments may disappear due the always better particle sampling efficiency of the inlet systems and for instruments focusing on the analysis of particles smaller than 200 nm. In these cases, the laser is simply arbitrarily periodically triggered, usually at its highest firing rate or data acquisition frequency.

The vaporization of particles on a hot surface can be considered more quantitative, at least for volatile compounds, than the laser based method since many authors report evidences of incomplete particle ablation by detecting optically the rest of particles ([Weiss et al., 1997]) and evidences of particle surface chemical analysis [Carson et al., 1997], [Lazar et al., 1999], [Woods et al., 2002] by laser based particle vaporization.

If the energy transferred to the particle for the vaporization process can be rather well quantified for the particle thermodesorption on a hot surface by determining the surface temperature of the surface, it is not the case for the laser based approach. Even if a particle of diameter 5 μm (a usual upper range of sampled particle size) in a focused laser beam of beam diameter of 30 μm can maybe be considered to be irradiated by a uniform energy density, the real irradiated energy on the particle surface is unknown. Indeed the laser beam energy distribution within the laser beam is never uniform. One usually assumes the energy density across the laser beam to be distributed according to a Gaussian law but one can not exclude hot spots, zone of high energy density, at different places. As a result, it is not possible to have reproducible particle vaporization conditions nor to quantify them with a laser unless the laser energy distribution in the laser beam is made uniform as attempted by [Wenzel et Prather, 2004] with an optical fiber or by [Franck et al., 2005] where only a fraction of the laser beam is directed to the ionization source of the mass spectrometer.

The uncertainty of the measurement of the laser light power density coming on the particle does not permit its precise adjustment to obtain a soft and reproducible particle desorption. Selecting appropriate laser wavelengths can compensate the uncertainty of the power density applied to the particle and allow the soft vaporization of the particle. Usually long wavelengths such as infrared light (IR-light) are preferred over ultraviolet light (UV-light) ([Thomson et Murphy, 1993]) and

appear to be quite efficient for vaporizing “large” quantity of material over a wider depth compared to ultraviolet wavelengths ([Vestal, 2001]). [Morrical et al., 1998] and [Cabalo et al., 2000] report particle vaporization with infrared laser whereas [Lazar et al., 1999] used an excimer laser at low power .

Operating laser desorption in a continuous manner without any trigger scheme could be possible since it does exist continuous infra-red laser of high power used in the industry for cutting applications. The particle irradiation for the desorption could then be better controlled by the size of the laser beam and the particle velocity. The single particle analysis ability is kept due to the fact that particles are flying through the laser. The major problems with such lasers are to find the best power characteristics for a reasonable laser size and the safety aspects.

Thermodesorption has other interesting features compared to the laser desorption if single particle chemical analysis is not any more a priority. Thermodesorption permits a rough first separation of the particle constituents according to their boiling point ([Tobias et Ziemann, 1999]) and the measurement of the vapor pressure of low volatility organic aerosol compounds ([Chattopadhyay et al., 2001]) before their mass analysis for a group of particles. Indeed particles “have time” to progressively liberate their chemicals to the ionization place what is not possible in the case of laser desorption.

The major technical drawback of the thermodesorption is that the particle constituents must be vaporized close to the ion source in the extraction electrodes of the mass spectrometer. The thermodesorption element has therefore to be positioned or designed such that the mass spectrometer extraction electric fields are not perturbed. Usually, the thermodesorption element is located outside of the extraction electrodes to avoid the distortion of the extraction electrostatic field (that usually affects negatively the ion sampling in the mass spectrometer) what requires the gas constituents to diffuse back to the ionization zone. This dilutes the gas species what leads to a loss of sensitivity. Moreover, it reduces the room around the extraction electrodes and makes the exchange of the vaporization method/ionization method less easy than for laser based desorption whose wavelength is just to be changed as well as the optics. Furthermore the distance between the thermodesorption element and the ionization zone might be considered advantageously to estimate the temperature of the desorbed molecules at the ionization time since the molecules velocities can be inferred by a Maxwell-Boltzmann gas velocity distribution which depends on the molecule mass and the temperature ([Sykes et al., 2002]). No practical use of this temperature has been found yet.

Aerosol particles can also be vaporized by mixing them into a warm carrier gas. The resulting gas {hot carrier gas + gaseous components of the particle} is then injected in the mass spectrometer. The chemical composition of the particle can then be inferred after subtraction of the carrier gas mass spectrometer signal. Such an approach does not permit the analysis of single and/or refractory material containing particles but stands for a contact-free volatilization technique ([Kückelmann et al., 2000]).

As a result, the laser based vaporization is the vaporization technique that performs the best single particle vaporization and that is the most universal in spite of its low degree of control of the energy density on the aerosol particle and the associated complex laser trigger scheme.

2.5.4.4 Two-step laser desorption/ionization: Ionization methods

The ionization step role is to confer to the gaseous molecule a positive or negative electric charge depending on the mass spectrometer characteristics. Eventually ionization can fragment the molecules in order to identify the molecules from their fragmentation patterns.

The choice of the ionization method is to be put in perspective of the ability of a mass spectrometer to identify the detected chemical species. If the ionization method confers softly to all molecules an electrical charge so that the molecule is not fragmented (later referred as “soft” ionization), only molecular ion can then be detected. If for small masses the resulting ions can be easily identified, the identification become more difficult as the molecular ion size increases. At high masses, it is still possible to determine the elemental composition of molecular ions of high masses by using the mass defect (as illustrated in [Hughey et al., 2001]) but a high resolution mass spectrometer of high resolution $R_{ms} = m/\Delta m$ is then required.

On the other hand, the fragmentation of the molecular ion can help to elucidate the nature of the ions but this will be unpractical in case of a complex mixture of compounds as it is always the case in ambient air aerosol particles. Induced ion fragmentation only makes sense if one ion is selected and its fragments are unambiguously identified as aimed in tandem mass spectrometry, usually abbreviated MSⁿ.

In order to resolve mixtures, the usual approaches are either to separate the different constituents according to different properties and then to analyze each resulting fraction as performed for example by a GC-MS (gas chromatography coupled with mass spectrometry), GCxGC-TOFMS (two dimensional gas chromatography coupled with time-of-flight mass spectrometry) or to operate a selective analysis for each suspected constituents in the mixture, which is *in fine* equivalent to a constituent separation. The former method is called “classical separation” whereas the latter will be named “virtual separation”.

Up to now, in aerosol mass spectrometry, except the work of [Reilly et al., 1997] who identified ions with tandem mass spectrometry with an ion trap mass spectrometer and [Tobias et Ziemann, 1999] who first sorted the particle constituents according to their boiling point by volatilizing the particle on a heated surface, no separation method of the constituents before the ionization nor the mass analysis has been attempted. This makes the chemical analysis of the aerosol particle constituents not straightforward.

In case of the particle analysis on its flight, the possibility to perform a “classical separation” of the constituent is even more inaccessible whereas a “virtual separation” remains possible.

At this stage, the ionization method is to be adapted to the chemical species that are wished to be examined in the particle. Some of the used ionization methods in aerosol mass spectrometry are briefly presented below in Table 6, at the exception the one-step laser desorption ionization which is treated in a previous section, most of the ionization methods require the chemicals to be analyzed in gas phase.

[Sullivan et Prather, 2005] reviewed recent progresses in aerosol mass spectrometry and mentioned three novel ionization methods that can be very promising since they can perform soft ionization in a continuous manner, unlike laser based ionization technique, and they require a rather simple equipment. These ionization techniques are respectively named direct electrospray ionization ([Takats et al., 2004]), glow discharge ionization ([Dalton et al., 2005]) and direct analysis in real time (DART) ion source ([Cody, 2005]).

To overcome the mixture resolution and the identification of high mass ions by an “ionization technique only”, the combination of different on-line ionization methods for the “quasi-identical” sample as realized by [Mühlberger et al., 2004] for the analysis of gaseous compounds which involves quasi simultaneously electron impact, REMPI and SPI ionization by laser appears to be a quite attracting approach. Indeed the combination of electron impact ionization (EI), REMPI and SPI laser ionization gives the possibility to obtain mass spectra of non-fragmented molecules (via

2. Aerosol analysis overview

<i>Ionization method</i>	<i>Suitable for species</i>	<i>Comments</i>	<i>Example of aerosol mass spectrometer</i>
Electron Impact (EI)	Low to middle polar species up to molecular weight 1000	<ul style="list-style-type: none"> • Standard ionization method with electron at 70eV • Wide mass spectra data base • Cheap, easy to build, continuous • Not fragment free 	[Jayne et al., 2000]
Electron Attachment (EA)	electron-acceptor species	<ul style="list-style-type: none"> • Fragment free • Low energy electron are to be produced 	[LaFranchi et al., 2004]
Chemical Ionization (CI)	H ₂ proton-acceptor species electron-acceptor species	<ul style="list-style-type: none"> • Soft ionization method • Need to produce the initial ions 	[Voisin et al., 2003]
Surface Ionization (SI)	Alkali metals	<ul style="list-style-type: none"> • Cheap, easy to build, continuous • Selective for light ionizable species 	[Svane et al., 2004]
Photoionization (PI)	SPI all if laser light wavelength is above the ionization potential. Well suited for aliphatics	<ul style="list-style-type: none"> • Low laser energy required but small wavelengths (typically $\lambda = 118$ nm) • Soft ionization for many compounds 	[Öktem et al., 2004] [Nash et al., 2005]
	REMPI Well suited for PAHs	<ul style="list-style-type: none"> • Low laser energy required but small wavelengths (typically $\lambda = 266$ nm) • Soft ionization for many compounds 	[Morrical et al., 1998] [Prather et al., 1994]

Table 6 : Usual ionization methods in aerosol mass spectrometry

REMPI, SPI) and fragments of “practically” the same chemicals (via EI), to resolve a mixture and to identify molecules through their fragmentation pattern.

If the method appears to be quite powerful by practically ionizing all constituents of the sample, the problematic is here to handle the same probe, here the single particle, successively on its flight for the different ionization processes and to relate the obtained mass spectra to the corresponding ionization event. Such approach should be quite accessible with a thermodesorption step since the sampled is emitted as a gas from the thermodesorption element.

If the quantity is too small to operate successive ionizations and mass analysis of the same sample, one could orient the particle to a given ionization method according to a pre-analysis. This approach seems to be possible since combined ionization methods are available ([Mühlberger et al., 2004]) and since particles can be classified according to different properties during their flight. [Kane et al., 2001] indicate the possibility to modify the trajectory of a particle on the flight to lead it, for example, to the appropriate ionization method. [Kane et al., 2001], [Stowers et al., 2004] and [Van Wuijckhuijse et al., 2005] report the possibility of modifying the particle trajectory or the possibility to trigger the desorption/ionization laser respectively according to the particle charge or its content of fluorescing material.

Such fore-selecting tests are yet not pertinent enough in the chemical point of view to orient on-line, the particle to a given ionization method, except maybe for PAHs which fluoresce easily and that can be nicely analyzed via a REMPI ionization at $\lambda = 266$ nm. This later approach, if powerful, requires a very complex technical setup what makes the combination of ionization methods (an “apparent/hybrid” universal ionization method) to analyze the same sample after [Mühlberger et al., 2004] appear to be the most successful.

As mentioned previously soft ionization methods must be either selective or combined with a high resolution mass spectrometer or with other ionization methods. At the present time, a combined ionization technique approach seems to be the more practical solution to be used in the case of two-step desorption/ionization for the chemical analysis of single particle.

2.5.5 Mass analysis

The role of the mass spectrometer is here to measure the ratio m/z of the ions resulting from the ionization of the particle constituents. The aim is to capture as much ions as possible of different m/z at once (if not all) anytime a particle is vaporized and ionized.

The need of capturing all ions is intended to infer the particle composition both qualitatively and quantitatively from the ion current signal as a function of the ion m/z . From this, under specific assumptions, the particle size can also be inferred in case of a complete desorption ionization of the particle. [Reents et Ge, 2000] explicit the requirements of both the mass spectrometer and the detector that should have a wide dynamical range in order to measure the total quantity of ion produced. On their side, [Lee et al., 2005] investigated the effects of ion loss in the mass spectrometer on the inferred particle size from the mass spectrometric analysis and found that the ion loss on the wall of the mass spectrometer biases the determination of the particle size inferred from the mass spectrum.

Attempting to capture all ions might be a real problem for the mass spectra resolution for time-of-flight mass spectrometer since the high quantity of ions can saturate the detector and produce coulomb space charge effects that will tend to increase the ion time-of-flight distribution of a given m/z . As a result, capturing all emitted ions must not be always an aim. It is in particularly important to sample the ions in a manner that is representative of the particle composition: the m/z ratio and the relative proportion of each representative ion of the particle composition have to be recorded at once for each particle.

Many types of mass spectrometers can be practically used for aerosol mass spectrometry. Quadrupole, sector, ion trap and time-of-flight mass spectrometers are still used at the exception of sector mass spectrometers that were used in the first days of this technique.

Time-of-flight mass spectrometers are very well adapted for this since they can practically analyze any ion of any m/z ratio without any theoretical limitation in m/z with a high transmission. This makes time-of-flight mass spectrometers now very commonly used in aerosol mass spectrometry. Furthermore, generally speaking, the combination of laser ionization with time-of-flight mass spectrometry is very powerful and convenient to operate as described by [Boesl et al., 1994], [Mamyryn, 1994].

One the drawback of this mass spectrometer is the loss of mass resolution as the ion mass increases due to the low variation of the ion time-of-flight as its mass increases and its calibration which need to be adjusted for each mass analysis in case of a one-step laser desorption/ionization. Indeed the produced ion cloud from the laser desorption/ionization event contains ions with a wide variety of

ions with many different initial positions and velocities that affect the arrival time of the ions on the detector. This affects negatively the resolution of mass spectrometer. Such problem can be reduced by using a reflectron time-of-flight mass spectrometer instead of a linear time-of-flight mass spectrometer.

A recent work proposed a mass spectrometer design that correct some drawbacks of usual time-of-flight mass spectrometer. Indeed, the negative effect of the initial ion position and velocity can be negated by using an orthogonal time-of-flight mass spectrometer (oa-TOFMS) in C-, V-, or W-design as recently presented in [Drewnick et al., 2005] for the C-design. Ions are first accelerated and focused in a beam. Once focused in beam, the ions are orthogonally extracted what eliminate the negative effect of the initial ion and particle velocity on the mass spectrometer resolution.

To capture more different ions of different m/z but also of different polarities, a bipolar time-of-flight mass spectrometer has been introduced by [Hinz et al., 1996] what allows the simultaneous analysis of cations and anions. Ions of both polarities are analyzed in two specific collinear drift tubes mounted at the opposite of each other around the same extraction electrodes.

The bipolar time-of-flight mass spectrometer potential is well presented in [Hinz et al., 1996] and [Silva et Prather, 2000]. Since the ionization pathways of molecules are different for cations and anions, the chemical species can be better identified. Indeed it can provide information about the chemical groups of molecules and the element speciation in the particle. For example, [Silva et Prather, 2000] report the detection of the group CNO^- to identify amide groups, of the group CN^- to detect the presence of carbon nitrogen bonds. Furthermore, it permits the differentiation of isobaric ions in one polarity if related ions can be detected in the other polarity and do not appear to be isobaric. In addition, it permits the detection of species that might be detectable in one polarity and not detectable for the other polarity.

However, the use of bipolar mass spectrometer might is pertinent only with a ionization method that produce simultaneously cations and anions. In other words, it must be used only with simultaneous different ionization processes producing ions of both polarities as it is the case with the one-step desorption/ionization. The interest of operating a bipolar time-of-flight mass spectrometer is therefore limited with a two-step laser desorption/ionization where the ionization produces only ions of the same polarity. Laser based ionization and electron impact are not appropriated ionization source for bipolar mass spectrometer. In this respect, chemical ionization and thermoionization might be more appropriated since it can produce simultaneously cations and anions ([De Hoffmann et Stroobant, 2003]). Combining artificially two soft ionization methods as presented before such as photoionization for cation production and electron attachment ([LaFranchi et al., 2004]) for anions production would fully exploit the potential of a bipolar mass spectrometer.

Bipolar mass spectrometers can also be advantageously used to perform twice the mass analysis of a sample within a short time of a few μs . The first analysis can take place in a tube while the second analysis can take place some microseconds later in the other tube for the same ion polarity. This is of particular interests if the sample is a small flying particle as in single particle mass spectrometry allowing thereby potentially the determination of the particle surface and core composition.

A combined linear-reflectron time-of-flight mass spectrometer could theoretically give the possibility to detect ions and neutrals resulting from the ion dissociation in the drift path of the mass spectrometer. Indeed, if the detector of the linear mode can be operated simultaneously with the reflectron mode, the detector of the linear mode can practically detect only neutral compounds whereas the detector of the reflectron mode will capture only ionic species. This setup can be considered as a pseudo-tandem mass spectrometer instrument. Such setup has not yet been reported in the literature probably due to the difficulty of operating a ion detector in the vicinity of a

reflectron but work in this direction was published by [Neubauer et al., 1995]

If time-of flight mass spectrometers appear to be practical to use and modular, other mass spectrometer were also recently used.

Ion trap mass spectrometers were used by [Lazar et al., 1999] and [Reilly et al., 1997] for aerosol mass spectrometry permitting them ion identification by tandem mass spectrometry. If, in practice, many m/z ions can be analyzed for the same particle, the analysis time of a particle is longer than with time-of-flight mass spectrometer. Quadrupole mass spectrometers were used in the early development of aerosol mass spectrometry and are still used by the Aerodyne AMS ([Jayne et al., 2000]) because of its robustness, compactness and low-price. The major drawback of the quadrupole mass spectrometer for aerosol analysis is its limitation to analyze ions of a given m/z ratio at one time. It requires to sample many aerosol particles to obtain a mass spectra over the whole range of m/z of interests. Sector magnetic mass spectrometers were also used in the early development of aerosol mass spectrometry. One of its limitation in the aerosol analysis problematic is the same as for quadrupole mass spectrometers, i.e., the ability to analyze only one m/z at a time.

The use of bipolar time-of-flight mass spectrometer with a reflectron mode appears to be the most promising tool for the mass analysis of the ionized particle constituents.

2.6 Technical choice justification for the aerosol mass spectrometer

The aerosol mass spectrometer developed at the GSF-Forschungszentrum, the SPALMS instrument, is dedicated to focus on the analysis of the organic fraction of aerosol particles in the environment and in incineration plants on a on-line and single particle basis in order to better identify aerosol sources and to better characterize the aerosol properties that may cause adverse health effects.

As mentioned previously, laser based aerosol mass spectrometers are the only instruments that allow a contact-free single particle analysis and that permit the analysis of both volatile and refractory chemicals. Considering the previous paragraphs, the final standard setup of the SPALMS instrument is expected to be operated in its standard setup with an aerodynamic lens to sample efficiently combustion aerosol and atmospheric aerosol particles ($< 1 \mu\text{m}$), with a two-step laser desorption/ionization approach for a comprehensive characterization of the organic fraction of the aerosol particles and with a modular ionization source.

The SPALMS instrument is inspired by the ATOFMS from [Gard et al., 1997] and the LAMPAS from [Trimborn et al., 2000] principle and design. In a first step, a nozzle inlet system and a one-step laser desorption/ionization approach were developed and operated in order to check the validity of its initial design and to test the equipment before implementing a dynamic trigger mode, a two-step laser desorption/ionization and an aerodynamic lens.

Its design permits the implementation of additional features that can contribute, with minimal extra-hardwares, to better characterize, physically and eventually chemically, the aerosol particles as illustrated in the work of [Murphy et al., 2004], [Franck et al., 2005] and [Moffet et Prather, 2005].

Figure. 5 presents as a flow chart the succession of the measurement steps that are operated by the SPALMS instrument.

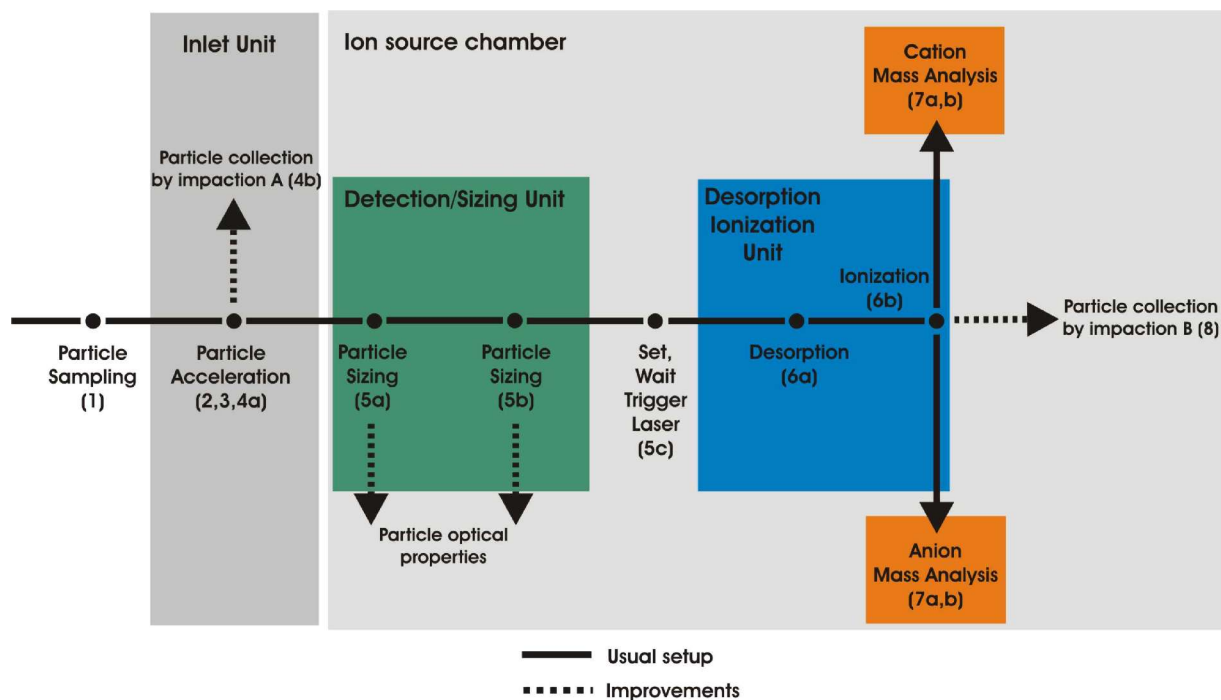


Figure. 5 : Aerosol mass spectrometer measurement steps

The plain lines indicate the usual operation of laser based aerosol mass spectrometers as performed by the ATOFMS ([Gard et al., 1997]) and LAMPAS ([Trimborn et al., 2000]) whereas the dashed lines indicate the planned improvements and extension of the SPALMS instrument.

The development of the SPALMS instrument is conducted with the permanent worry of improvements in the following four directions:

- aerosol representativity (Improvement of type 1)
- better characterization of the chemical composition of the single particle (Improvement of type 2)
- better description of the physical properties of the single particle (Improvement of type 3)
- better certainty of the obtained results (Improvement of type 4).

Improvements of type 1 attempt to find methodologies to extrapolate the data obtained from single particle to the particle population in order to describe as accurately as possible the real aerosol. Improvements of type 2 attempt to better process the single particle so that the chemical analysis biases from the laser desorption/ionization can be reduced. Improvements of type 3 attempt to better characterize physically the aerosol single particle in terms of size, shape, density and refractive index. Finally improvements of type 4 concern any method that permits the reduction of the uncertainty on the obtained information about the single particle.

3 Aerosol mass spectrometer at GSF-Forschungszentrum: General design

The following section presents the main design rules that were followed to build the aerosol mass spectrometer SPALMS (Single Particle Aerosol Laser Mass Spectrometer) at the GSF-Forschungszentrum. A special care was given to build the instrument with a small ground occupation surface to operate it in industrial plants and to have a short particle path between the inlet unit and the mass spectrometer unit to obtain a good particle analysis rate (SCR). In addition, the ionization source is planned to be modular to adapt it, when necessary, to the type of particles to study. Finally, the instrument was equipped with many data acquisition devices in order to obtain the most complete particle description possible as it is analyzed.

3.1 General design and scaling rules

From the critical analysis of the current state-of-art in aerosol mass spectrometry presented the Chapter 2, design rules have been identified. The aerosol mass spectrometer SPALMS has been designed at the GSF-Forschungszentrum such that:

- it has the smallest possible surface ground occupation (in order to be operated in field, industrial plants and small rooms with a narrow access corridor) and possibly the smallest volume possible
- the particle path in the instrument is the smallest possible
- the inlet system and the desorption/ionization method should be very modular
- it has many data acquisition points
- it can analyze aerosols as stand-alone instrument

3.2 Setup and dimensions

The aerosol mass spectrometer SPALMS is initially designed to be operated in field for the analysis of atmospheric aerosols, indoor aerosols and industrial aerosols, in particular from coal and waste incineration plants. In industrial plants, place is usually restricted what requires the instrument to have a small surface ground occupation. To limit its ground surface, all the voluminous equipments are set vertically stacked in two independent racks which are, once in field, connected together.

The SPALMS instrument consists of two racks, Rack I and Rack II, as presented in Figure. 6. The racks are mounted on air wheels which contribute to limit the vibrations from the rotary and membrane pumps being transmitted to the instrument racks.

The rack I contains all the analyzer parts including:

- the inlet unit
- rotary pumps
- the sizing unit (lasers, mirrors, optical fibers and photomultipliers)
- the desorption/ionization unit (laser, mirrors, lenses) and laser energy sensors
- bipolar time-of-flight mass spectrometer
- fore-vacuum membrane pumps, turbomolecular pumps, pressure gauges

3. Aerosol mass spectrometer at GSF-Forschungszentrum: General design

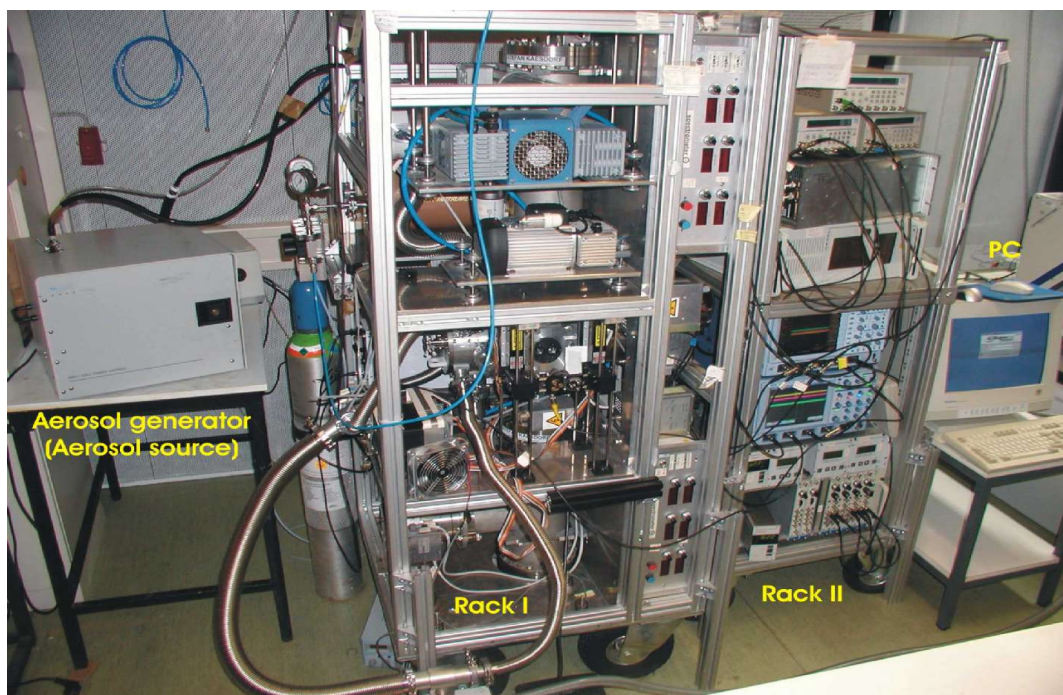


Figure. 6 : SPALMS Aerosol mass spectrometer setup

Left: Aerosol generator (here a Small Scale Particle Dispenser, SSPD). **Middle:** Rack I: Measurement hardwares (inlet unit, ion source, photomultipliers, bipolar mass spectrometer, lasers, vacuum pumps, high-voltage supply units). **Right:** Rack II: Control unit of the aerosol mass spectrometer (data acquisition and control unit and computers)

The rack II contains the steering electronics of the pump systems, the electronic devices for the processing of the photomultiplier signals, the analog-to-digital conversion devices (digitizers and oscilloscopes), computers and oscilloscopes.

Since the pumps are mounted in the rack I, the vibrations from the pumps have to be efficiently absorbed by spring suspensions because the optical lines (from the sizing unit and desorption/ionization unit) must not undergo vibrations. The optical mountings are arranged in a way that they are as firmly as possible fixed to the whole body of the ion source and the mass spectrometer in order to reduce the relative motion between the laser beams and the ion source. In spite of these precautions, vibrations are still problematic. The rack I must be in the future reinforced and the pumps better isolated from the rest of the Rack 1.

The dimension of the SPALMS instrument are presented in Table 7 and compared with similar laser based bipolar aerosol mass spectrometer instruments. The small ground surface occupation of the SPALMS instrument compared to the other instruments must be noted. This feature is particularly important when the aerosol mass spectrometer will be used in places with a narrow corridor access.

The different elements/units of the aerosol mass spectrometer are arranged as depicted in Figure. 7 which locates the different measurement steps within the Rack I of the instrument. From this arrangement, it is easy to keep a small the distance between the inlet unit and the ion source.

3. Aerosol mass spectrometer at GSF-Forschungszentrum: General design

<i>Instrument</i>	<i>Dimension [m] (Length x Width x Height)</i>	<i>Ground surface [m²]</i>	<i>Weight [kg]</i>	<i>Power</i>
This work	Rack I : 0,70 x 0,80 x 1,85 Rack II : 0,70 x 0,60 x 1,80	~ 0,56 + 0,42 Total : 0,98	~ 400	7,5 kW
[Gard et al., 1997]	1,84 x 0,72 x 1,54	~ 1,3	~ 250	30A x 110/220 V
AToFMS TSI.	1,7 x 0,74 x 1,3	~ 1,3	~ 360	Max. 4 kW
[Trimborn et al., 2000]	1,70 x 0,80 x 1,20	~ 1,4	~ 250	9A x 230 V
[Bläsner et al., 2000]	1,20 x 0,9 x 0,7	~ 1,1	~ 250	NA

Table 7 : Size of different laser based aerosol bipolar mass spectrometers

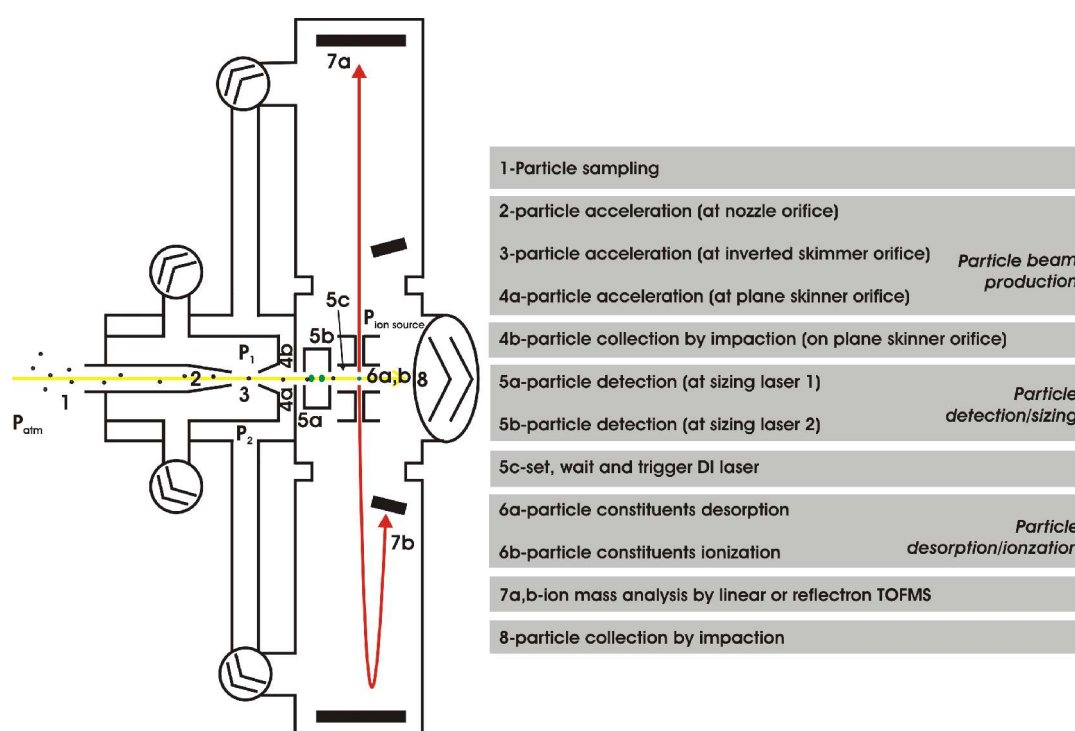


Figure. 7 : Location of the different measurement steps in the SPALMS instrument

3.3 Short particle path

The path of the particles in the instrument from the entrance of the inlet unit to the ion source has to be the smallest possible in order to (i) minimize the residence time of the particle in vacuum, (ii) minimize the final size of the particle beam and (iii) minimize the global volume of the instrument. Indeed a long path of the particle in vacuum between the inlet system and the ionization will favor the loss of volatile chemicals and will increase the particle beam diameter in the ionization source what leads to a decreased sizing chemical analysis rate (SCR).

3. Aerosol mass spectrometer at GSF-Forschungszentrum: General design

The length of the path of the particle in the instrument is determined by the inlet unit design, the geometry and size of the ion source unit. The ion source unit, as presented in Figure. 8, is a hollow aluminium cube (17 x 17 x 19 cm) whose center corresponds to the central point of the bipolar mass spectrometer where the ions are to be produced/extracted. The left and right faces (face (1) and face (2)) are connected respectively to the inlet unit and the ion source turbomolecular pump. The fore and behind faces (face (3) and face (4)) have two roles: the face (3) transmits the sizing laser light in the sizing unit whereas the face (4) transmits the desorption/ionization laser light to the ion source in the middle of the mass spectrometer. The top and bottom face (face (5) and face (6)) of the ion source are connected respectively to the cation and anion mass spectrometers. In order to spare place, the sizing unit (7) is inserted between the center of the ion source (8) and the face (1) which correspond roughly to the exit of the inlet unit (see the lower right inset of Figure. 8). The apertures in the faces (3), (4), (5) and (6) of the ion source are closed with flanges CF100 and CF160.

The sizing unit (7) could have been inserted between the extraction electrodes (8) of the mass spectrometer to make the distance between the exit of the inlet unit and the center of the ion source smaller (see the lower right insert of Figure. 8). In this case, it can not be possible to insert practically the scattering light collecting optics because both extraction electrodes are too close to each other (14 mm). It would have forced to design specific extraction electrodes as in the case of the PALMS instrument ([Murphy et Thomson, 1995]) for example. It was rather decided to use standard equipment from our time-of-flight mass spectrometer manufacturer (Stefan Kaesdorf, Geräte für Forschung und Industrie, Munich, Germany) and to place the sizing unit between the inlet unit exit and the extraction electrodes of the mass spectrometer. The sizing unit is located one 1 cm after the inlet unit and 2 mm before the extraction electrodes (8) (see Figure. 9).

The current dimensions of the ion source permit visits and interventions (such as cleaning) in its inside or/and to add additional devices, such as an arm to hold an impactor that can be exchanged during the measurement and/or light collection optics for an eventual light spectroscopic analysis. Moreover the particle time-of-flight between its detection by the first sizing laser and the ionization laser is long enough so that the electronic devices that detect particles and trigger the ionization laser have enough time to react and to fire the laser at the right time. The order of magnitude of the time required by the electronics to react was found to be, after experience, greater than 15-20 μ s and would have been set to at least several microseconds anyways. Indeed electronic signal processing need some time to proceed (from nanoseconds to hundreds of nanoseconds). Due to this typical electronic processing time, the particle velocity for such inlet unit which ranges from 100 to 600 m/s (after [Johnston, 2000]) requires a minimum distance of 1,5 mm between the first sizing laser and the ionization laser.

Considering these elements, the position and the arrangement of the sizing unit has been set as depicted in Figure. 9 and presented in Table 8. This sets in particular the distance between each sizing laser and the desorption/ionization laser.

The standard manufacturing of the opening of the different faces of the ion sources and the large room near the face (3) and face (4) permits the addition of many laser systems or detection devices what makes the SPALMS be a modular instrument.

3. Aerosol mass spectrometer at GSF-Forschungszentrum: General design

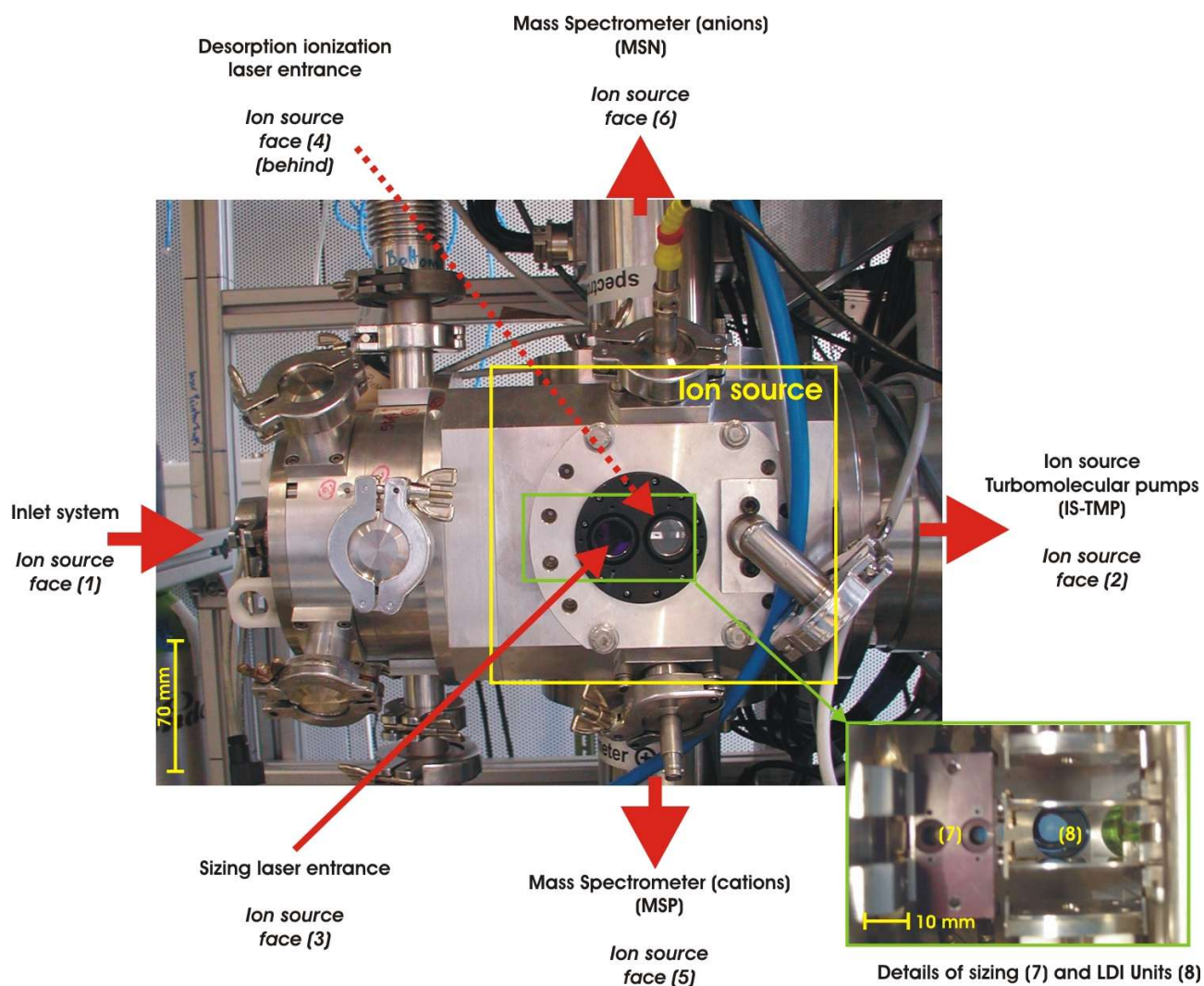


Figure. 8 : Particle inlet / ion source arrangement of the SPALMS instrument

The ion source is a hollow aluminum cube that contains the extraction electrodes of the bipolar mass spectrometer. It has six apertures which hold different devices. **Face (1)**: inlet unit. **Face (2)**: ion source turbomolecular pump. **Face (3)**: sizing laser windows. **Face (4)**: desorption/ionization laser windows. **Face (5)**: cation mass spectrometer. **Face (6)**: anion mass spectrometer.

The inset on the right bottom corner presents the inside of the ion source viewed from the face (3) in which the sizing unit (7) and the laser desorption/ionization unit (LDI unit) (8) are arranged together.

<i>Distance (Current Inlet Unit)</i>	<i>Distance [mm]</i>
exit inlet unit – sizing laser 1	14
sizing laser 1 – sizing 2	12
sizing 2 – desorption/ionization laser	28
Exit inlet system – desorption/ionization laser	54

Table 8 : Relative distance between the SPALMS laser beams

3. Aerosol mass spectrometer at GSF-Forschungszentrum: General design

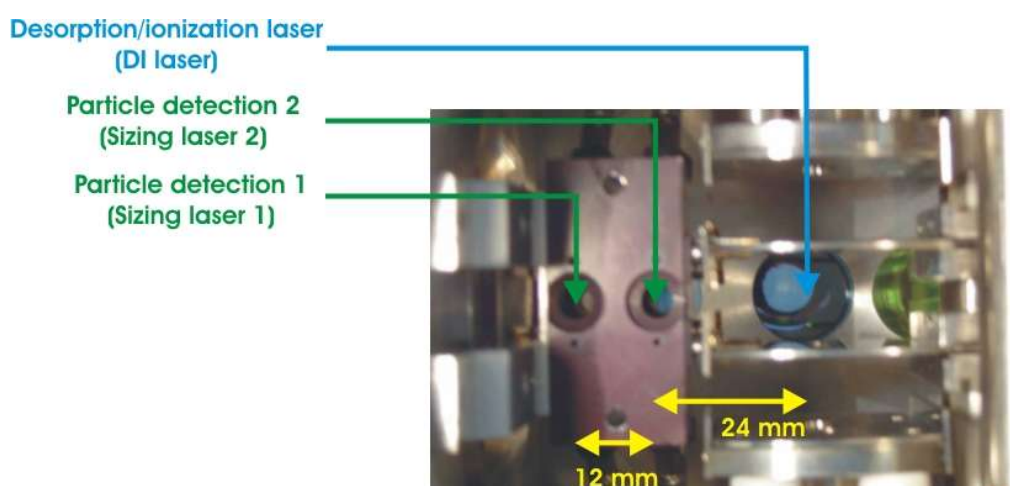


Figure. 9 : Dimension and arrangement of the sizing unit of the SPALMS instrument

The black rectangle on the left corresponds to the sizing unit, which holds the scattering light collection optics and sets the distance between both sizing lasers (1 and 2) to 12 mm. The two horizontal parallel plates on the right correspond to the extraction electrodes of the mass spectrometer.

3.4 High flexibility

The instrument should be able to be modified in a short time to different hardware configurations and operation mode according to the measurements to be performed. In particular it is of interest to have exchangeable ionization sources as explained in Chapter 2. The SPALMS instrument has a high modularity for the operation of different inlet unit, of different ionization methods and can be operated with different trigger modes as well as with a large choice of data acquisition possibilities.

- Hardware modularity

The SPALMS instrument can be operated with a commercial nozzle-skimmers inlet unit (from Bernhard Spengler and Klaus-Peter Hinz Scientific Instrument, Linden, Germany) or a home-made inlet unit (nozzle-skimmers assembly) if micron size particles have to be investigated and precisely sized aerodynamically. The latter permits moreover the implementation of a home-made aerodynamic lens (still to be tested) to focus on the analysis of submicron particles.

The desorption/ionization process can be also operated with different laser systems in one-step or two-step approach which are summarized in Table 9. Some of the systems and their related operation modes will be later precisely described. In the future, a thermodesorption mode and an ionization step with a VUV lamp (Vacuum Ultra Violet) that produces an energetic light at $\lambda = 118$ nm ([Mühlberger et al., 2002]) will be implemented in addition to the current laser desorption/ionization optical setup. Since the entrance point of the laser beams in the ion source from the the face (4) is made invariant, only optics have to be exchanged if the transmission grade of the optics needs them to be adapted to the laser wavelength.

Currently, four laser systems (LDI systems) listed in Table 9. have been operated either for gas or/and particle analysis.

3. Aerosol mass spectrometer at GSF-Forschungszentrum: General design

<i>LDI System</i>	<i>Operation Mode</i>	<i>State</i>
Nitrogen Laser (337.1 nm)	<ul style="list-style-type: none"> one-step laser desorption/ionization trigger mode : free running, static mode, dynamic mode 	Current
Nd:YAG Laser (266 nm)	<ul style="list-style-type: none"> one-step / two-step laser desorption/ionization (ionization only) after desorption either with CO₂-laser or thermodesorption) trigger mode : free running mode only 	Current
Excimer Laser (248 nm)	<ul style="list-style-type: none"> one-step / two-step laser desorption/ionization (ionization only) after desorption either with CO₂-laser or thermodesorption) trigger mode : free running, static mode, dynamic mode 	Current
CO ₂ -Laser (10.6 μm)	<ul style="list-style-type: none"> two-step laser desorption/ionization only (desorption only) trigger mode : free running, static mode, dynamic mode 	Current
Thermo-desorption	<ul style="list-style-type: none"> two-step laser desorption/ionization only (desorption only) trigger mode : free running 	Future
VUV-Lamp (118 nm)	<ul style="list-style-type: none"> two-step laser desorption/ionization (ionization only) after desorption either with CO₂-laser or thermodesorption) trigger mode : free running 	Future

Table 9 : Available laser systems for the aerosol mass spectrometer

The “operation mode” precises in which conditions, for which purpose and how the lasers should be used. These conditions are defined by the laser wavelength, its ability to ionize chemicals and the trigger features of the laser systems.

- Laser trigger modes

The trigger of the desorption/ionization laser is a purely technical necessity associated with the laser system which has no impact on the single particle analysis itself. Indeed, lasers can be periodically fired or externally triggered. In the first case, the chemical analysis rate (CR) might be low. To increase it, different methods to trigger a given laser system have to be used. The laser trigger mode depends on the ability of the SPALMS instrument to detect a particle whose detection permits the firing of the desorption/ionization laser at the right time and on the trigger features of the laser itself. Three modes are possible and named free-running mode, static mode and dynamic mode. They are presented in details in Chapter 7. The use of different laser systems requires to be able to perform different triggering methods.

- Conversion to gas analysis.

The instrument can also be equipped with a gas inlet system (capillary) mounted on the face (1) of the ion source in place of the aerosol inlet unit for gas phase analysis. Gas phase analysis are from time to time necessary to perform to test the good operation of the mass spectrometers, to calibrate them and if necessary to perform specific gas analysis studies. The instrument will be in this work quasi exclusively operated for the particle analysis even if gas phase analyses are possible simultaneously with the current particle inlet unit.

3. Aerosol mass spectrometer at GSF-Forschungszentrum: General design

3.5 Data acquisition points

Since the SPALMS instrument involves many different physical measurement principles, it is possible to increase its potential by recording all the information at the different measurement points. Figure. 10 lists and locates the different sources of information. The expected information concern either the aerosol population or the single particle itself.

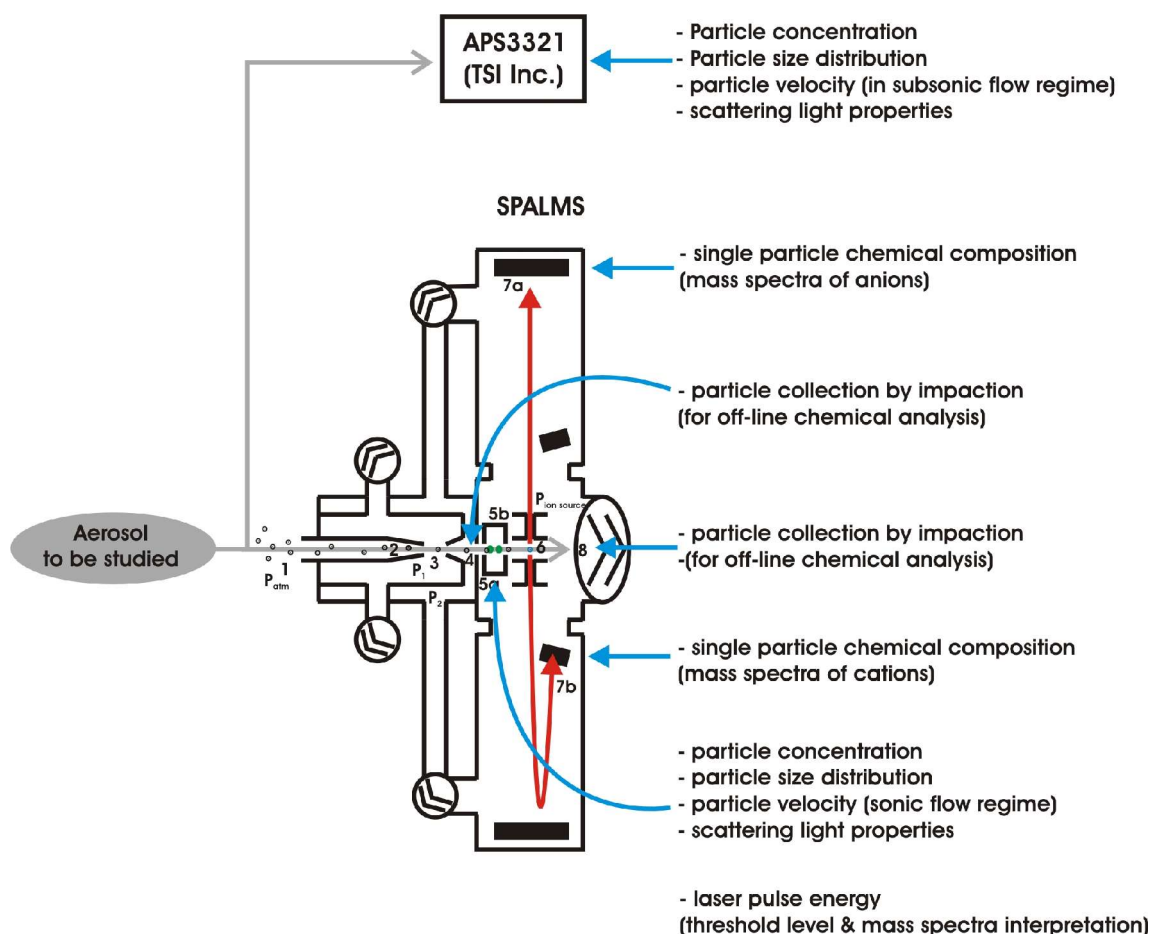


Figure. 10 : Particle information sources from the SPALMS instrument

This figure presents and locates the different information sources that can be used to better describe physically and chemically the aerosol. Indeed any measurements steps of this instrument are considered as an information source.

The data acquisition equipment of the SPALMS instrument consists of two oscilloscopes (LeCroy LT374 and LeCroy WR6050A, LeCroy, Chestnut Ridge, New York, USA), 4 PCI Digitizers Cards, Single Channel, DP210, (Acqiris, Geneva, Switzerland) and two laser energy sensors (Laser Star Dual, Ophir, Jerusalem, Israel). The PCI digitizers and the laser energy sensors are driven by different home-made Labview programs (Labview 6.i, Austin, Texas, USA) that permit the acquisition and the storage of the data on two computers PC1 (AMD XP1600, 1,8 GHz, 256 Mb, 40 Gb, Windows 2000) and PC2 (Pentium III, 500Mhz, 128Mb, Hard disk 16,2 Gb, Windows XP).

3. Aerosol mass spectrometer at GSF-Forschungszentrum: General design

<i>Information</i>	<i>Measuring hardware</i>	<i>Data acquisition device</i>
Particle size distribution (for consistency test)	APS	Computer download via RS-232
Particle count (access to particle concentration)	4 photomultipliers	Oscilloscope/Digitizer
Particle detection time at two locations (access to particle size)	4 photomultipliers	Oscilloscope/Digitizer
Particle scattered light amount (access to particle size)	4 photomultipliers	Oscilloscope/Digitizer
Mass spectrum (access to the particle chemical composition)	2 Time-of-flight mass spectrometers (2 microchannels plates, (MCPs))	Oscilloscope/Digitizer
Desorption laser pulse intensity (for consistency test)	Laser energy sensor	Sensor Display (or Computer via RS-232)
Ionization laser pulse intensity (for consistency test)	Laser energy sensor	Sensor Display (or Computer via RS-232)
Time desorption/ionization laser pulse (for consistency test)	4 photomultipliers photodiode Integrated optical sensor in Laser	Oscilloscope/Digitizer
Bulk particle composition for non volatile compounds (for consistency test)	Last inlet unit skimmer Impaction plate after the ion source	Off-line analysis with conventional chemical analysis methods (LMMS, GC x GC-MS, PIXE)

Table 10 : List of the particle information sources and their related acquisition hardwares

Table 10 presents the accessible information with their sensors and their related data acquisition devices. Some of the obtained information are directly related to different particle properties but can be also used to test if the obtained data are consistent together. They permit a good knowledge of the real operating conditions of the aerosol mass spectrometer and eventually the access to additional particle properties.

If particles are analyzed on a on-line single particle basis, this instrument offers also the possibility to analyze aerosols off-line in the classical manner. This feature is a by-product of the standard operation of the SPALMS aerosol mass spectrometer. Indeed particles can be collected by impaction in the last plane skimmer of the inlet unit and on the turbomolecular pump protection grid. The collected particles can be further off-line analyzed by conventional techniques available at the GSF-Forschungszentrum (such as LMMS, PIXE, TD-GCMS, GCxGC-TOFMS) if enough particles can be collected. LMMS permits the operation of the laser desorption/ionization in one or two steps with different ionization laser wavelengths as performed with the aerosol mass spectrometer but off-line and on bulk samples. PIXE provides the elemental composition for any element heavier than sodium (Na, $m/z = 23$). TD-GCMS and GCxGC-TOFMS are used to better characterize complex mixtures of organic compounds. The particle size distribution is monitored on-line in parallel to the SPALMS instrument with an Aerodynamic Particle Sizer (APS3321, TSI Inc., St. Paul, MN, USA).

4 Inlet unit

Chapter 4. presents the inlet unit currently used in the SPALMS instrument. The operating conditions will be here presented as well as the characteristics of the produced particle beam. The concentration and focusing of the particles into a beam by the inlet unit permits the easy sampling of the aerosol for its physical and chemical analysis. The inlet unit first reduces step by step by a factor of 100 to 1000 the pressure in the different chambers of the instrument down to 10^{-6} mbar in order to operate the mass spectrometer. Secondly it focuses the particles into a beam of a given divergence that should be small to obtain a high sizing and chemical analysis rate (SCR) and it accelerates them to a velocity that is specific of their size. Thirdly, due to the large divergence of the beam, particles can also simultaneously be sampled by impaction in the inlet unit for an eventual further off-line analysis.

4.1 Technical characteristics

The inlet unit currently operated was purchased from Bernhard Spengler & Klaus-Peter Hinz Scientific Instruments GBR, Linden, Germany, which is based on the work of Marijnissen at the Technical University of Delft ([Hinz et al., 1994], [Hinz et al., 1996] and references therein). The inlet consists of an assembly of a nozzle, an inverted skimmer and a plane skimmer as presented in Figure. 11. The different characteristic dimensions of the inlet are listed in Table 11.

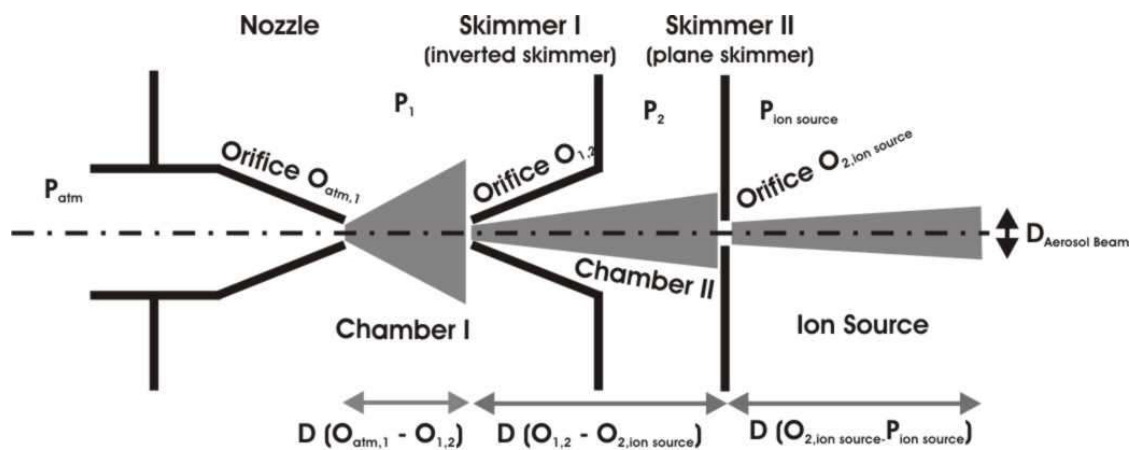


Figure. 11 : Schematic view of the inlet unit of the SPALMS instrument

The nozzle focuses and accelerates the particles. A fraction of the particles is transmitted to the Skimmer II while the rest is collected by impaction on the skimmer I (inverted skimmer). The fraction of the particles that exit the skimmer II is transmitted to the ion source center in the center of the mass spectrometer and the focusing point of the desorption/ionization laser while the rest is collected on the last skimmer II (plane skimmer).

4. Inlet unit

<i>Geometric dimension</i>	<i>Commercial inlet</i>	<i>Home-made inlet</i>
$\varnothing O_{\text{atm},1}$	0,5 mm	0,4 mm
$\varnothing O_{1,2}$	0,4 mm	0,3 mm
$\varnothing O_{2,\text{ion source}}$	0,3 mm	0,5 mm
$D(O_{\text{atm},1} - O_{1,2})$	3 mm	10 mm
$D(O_{1,2} - O_{2,\text{ion source}})$	12 mm (+/-0.5 mm)	10 mm
Opening angle of the nozzle (Half-angle)	$\sim 40^\circ$	17.5°
Angle of the inverted skimmer	$\sim 25^\circ$	$\sim 45^\circ$

Table 11 : Geometrical characteristics of the current inlet units of the SPALMS instrument

This inlet unit creates an aerosol beam by focusing aerodynamically the particles with a given Stokes number at the nozzle orifice. Particles that are not properly focused are, according to their inertia, either pumped out or impacted on the walls of the inlet unit. In addition, the inlet unit allows the pressure in the SPALMS instrument to be reduced step by step. Indeed each orifice reduces the pressure by a factor 100 to 1000. Over the three orifices the pressure drops from the atmospheric pressure down to 10^{-6} mbar where the mass spectrometer can be operated.

From the operational point of view, the commercial inlet unit (the inlet unit presented here and currently used) is very convenient for its maintenance. Indeed it can be taken apart, cleaned and reassembled within one hour and a half and insures a very easy, quick and reproducible alignment of the different orifices of the nozzle and skimmers. These alignments are extremely important for having a nice particle beam and a good particle transmission efficiency T. This characteristic made the purchased inlet unit be used.

The pressure level reached with the current inlet unit are listed in Table 12 where the term “open” indicates that the instrument samples air while the term “closed” means that it is closed.

<i>Location</i>	<i>Pressure[mbar] ⁽¹⁾</i>	<i>Pumps system ⁽³⁾</i>	<i>Pressure gauge ⁽³⁾</i>
Chamber I P_1	11 (open) $4 \cdot 10^{-3}$ (closed)	Rotary pump DUO20, 21 m ³ /h, final pressure $<5 \cdot 10^{-3}$ mbar	Compact Pirani gauge TPR265 (1000 - $<10^{-4}$ mbar)
Chamber II P_2	$5 \cdot 10^{-2}$ (open) $<10^{-4}$ (closed)	2 Turbomolecular pumps TMH-261-010 Split flow connection 10l/s	Pirani gauge TPR265 (1000 - $<10^{-4}$ mbar)
Ion Source $P_{\text{ion source}}$	$2 \cdot 10^{-6}$ (open) $<10^{-6}$ (closed)	Turbomolecular pump TMU 521P, 500l/s Fore-vacuum pump (Diaphragm Vacuum Pump MV 015,15 l/min)	Compact Full Range gauge PKR251 (1000 – $5 \cdot 10^{-9}$ mbar)
TOFMS Tube ⁽²⁾ $P_{\text{TOFMS Tube}}$	$\sim 10^{-6}$ (open) $<10^{-6}$ (closed)	Turbomolecular pump TMH 261-010, 200/s Fore-vacuum pump (Diaphragm Vacuum Pump MD 4T3,3 m ³ /h)	Compact Cold Cathode gauge IKR251 (10^{-2} – $2 \cdot 10^{-9}$ mbar)

Table 12 : Inlet unit operating conditions

⁽¹⁾ Pressures are measured when the inlet unit is closed (closed) or when it is open for aerosol measurements (open). ⁽²⁾ The pressure $P_{\text{TOFMS tube}}$ is measured in each time-of-flight mass spectrometer tube (TOFMS Tube). ⁽³⁾ All the equipment was purchased by Pfeiffer Vacuum GmbH, Asstar, Germany

The pressure level reached with the current pump configuration is in agreement with the technical data provided by the inlet unit manufacturer as presented in Annex A.

The gas sampling flow rate of the inlet unit is determined by the pressure drop over the nozzle and the diameter of the nozzle orifice. As the pressure drop ratio is lower than 2 (here 0,011), the gas velocity flow through the orifice reaches the sound velocity. In this case, the flow rate is only determined by the nozzle orifice diameter, the pressure and the temperature of the gas before it enters the inlet unit. The sampling flow was measured to be 2,75 liter per minute. The calculated maximum sampling volume flow rate by Eq. 6 (from [Shapiro, 1953]) indicates a sampling flow rate of 12,2 liters per minute in case of an isentropic gas flow through the nozzle orifice. The calculated flow rate is 4,4 times higher than the measured one. The origin of this discrepancy is not determined but can probably be related to the uncertainty of the nozzle orifice size, the development of a boundary layer in the orifice that reduces the gas flow or non-isentropic flow conditions.

$$Q_v = \frac{P_{upstream} \cdot A^x}{\sqrt{T_{upstream}}} \cdot \sqrt{\frac{\gamma}{R} \cdot \left(\frac{2}{\gamma+1}\right)^{\frac{\gamma+1}{\gamma-1}}}$$

Eq. 6

4.2 Particle velocity

The inlet imparts a given velocity to the particles as they are accelerated by the sonic expansion of the carrier gas (here air) at the different nozzle and skimmer orifices. The particle velocity depends on the gas velocity and the particle size, shape and density. In particular, particles of similar shape and density can be differentiated according to their sizes what permits the determination of their diameter if they are assumed to be spherical. It is usual to consider here that the measured particle velocity corresponds to the terminal particle velocity which is reached after a long time in the same flow conditions.

The particle terminal velocity is difficult to evaluate numerically since the particle motion occurs in non-stokesian regime. Indeed in this case, the gas flow is turbulent and sonic so that the gas can not be considered as an incompressible fluid ($Re \sim 1,2 \cdot 10^4$ and $M_a \sim 1$).

A precise calculation of the velocity requires to describe precisely the gas velocity, gas pressure and the drag coefficient C_D along the particle trajectory through the nozzle and the next two skimmers. The calculation of the drag coefficient C_D in these conditions is complex even if the work of [Oskouie et al., 2002] provides mathematical relationships to evaluate it and [Dahneke et Cheng, 1979] and [Cheng et Dahneke, 1979] provide mathematical relationships for the description of the gas flow and its properties along the nozzle axis. [Tsai et al., 1998] mentioned the need of a 2D-fluid flow properties simulation after the nozzle to better characterize the particle velocity at the exit of the nozzle for particle sizes above 10 μm .

The particle velocity can however be evaluated from a semi-empirical relationship as described in Chapter 12. applied to a single supersonic nozzle without second and third skimmer. The calculated velocities for 4 particle sizes and two different densities agree within 6% with the measured data presented in this work.

This calculation is not necessary for the operation of the aerosol mass spectrometer at this stage but

can be interesting to perform to evaluate more precisely the particle Stokes Stk number for each particle after each inlet unit orifice. The Stokes number Stk represents the ability of a particle to follow the gas flow stream lines. It is defined by the ratio of a stopping distance S_d to a characteristic length L_c of the device where the particle is moving as presented in Eq. 7. The stopping distance S_d is defined as the distance necessary for a particle to completely stop. Particles tend to follow more and more the carrier gas stream lines as the Stokes number decreases.

$$Stk = \frac{S_d}{L_c}$$

Eq. 7

The calculation of the Stokes number Stk would permit a better characterization of the particle beam quality and the evaluation of the “size cut” of the nozzle, the inverted skimmer and the plane skimmer since the inlet unit can be considered in some extent as a “cascade virtual impactor”.

The measured particle velocities for PolyStyrene Latex particles (later referred as PSL particles) (Dukes Scientific, Palo Alto, CA, USA) obtained with the current inlet unit are presented in Figure. 12 and summarized in Table 13.

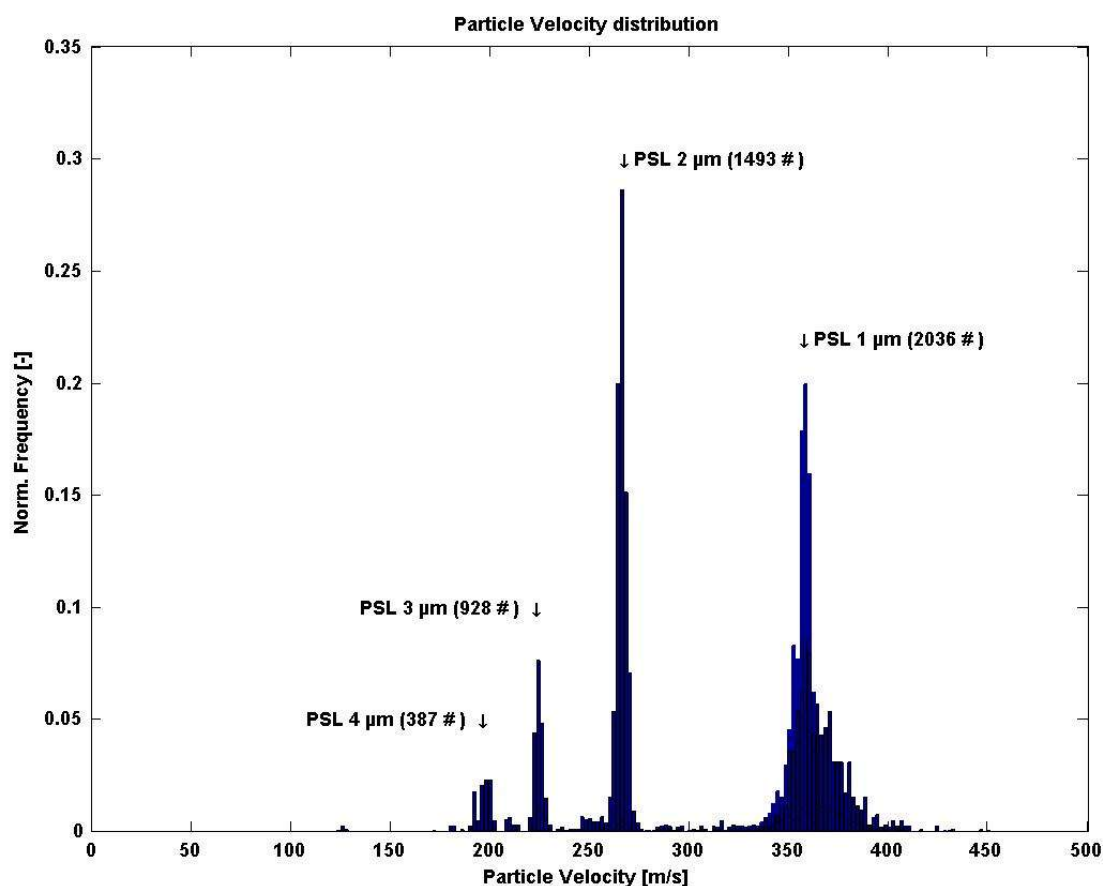


Figure. 12 : PSL particle velocity distribution obtained with the SPALMS instrument

PSL 1 μm : PSL particle of geometric diameter 1 μm , **PSL 2 μm :** PSL particle of geometric diameter 2 μm , **PSL 3 μm :** PSL particle of geometric diameter 3 μm , **PSL 4 μm :** PSL particle of geometric diameter 4 μm

<i>Particle Type ⁽¹⁾</i>	<i>Most frequent particle velocity V_p [m/s]</i>	<i>Particle velocity range ⁽²⁾ [m/s]</i>
PSL 1 μm	358	350 - 364
PSL 2 μm	266	264 - 270
PSL 3 μm	224	222 - 226
PSL 4 μm	200	192 - 202

Table 13 : PSL particle velocities in the SPALMS instrument

⁽¹⁾ PSL 1 μm : PSL particle of geometric diameter 1 μm , PSL 2 μm : PSL particle of geometric diameter 2 μm , PSL 3 μm : PSL particle of geometric diameter 3 μm , PSL 4 μm : PSL particle of geometric diameter 4 μm . ⁽²⁾ Particle velocity boundaries that contain 85% of the measured values

If the inlet unit is operated with another nozzle downstream pressure, as for example 60 mbar here, the particle velocity is different since the gas velocity at the exit of the nozzle is modified. In this case the gas velocity is reduced as presented in Table 14.

<i>Particle Diameter [μm]</i>	<i>Particle velocity [m/s] $P_1 = 12 \text{ mbar}$</i>	<i>Particle velocity [m/s] $P_1 = 60 \text{ mbar}$</i>	<i>Relative variation</i>
1 μm	360-375	310-325	-13.50%
2 μm	265	190	-28.00%
3 μm	225	160	-28.00%

Table 14 : Effect of the nozzle downstream pressure on the PSL particle velocity

By insuring that the inlet is operated in sonic flow regime i.e. at a pressure ratio P_1 / P_{atm} smaller than 0,5) and by keeping the downstream nozzle pressure constant, the sampling flow rate remains constant (here 2,75 liter per minute) and the velocity of particles of identical size, shape and density is made reproducible. In order to keep constant the gas flow rate through the nozzle, the inlet system is operated here in sonic conditions. This avoids the need of a flow controller and specific pump controllers. The measured velocities are of similar in order of magnitude with other similar inlet units of other aerosol mass spectrometry groups as presented in Figure. 13 even if their respective pressure levels in the different inlet chambers and designs are different.

The other important task of the inlet unit is to produce a low divergent particle beam. The next section presents the characteristics of the obtained particle beam with the current inlet unit.

4.3 Beam quality

As presented in Figure. 11 and observed experimentally in Figure. 14, the generated particle beam has a given divergence. The beam divergence has for effects to dilute the particles within the cross-section of the beam and to induce a significant loss over the three orifices. Table 15 presents the particle beam diameter measured at different locations in the inlet unit and the apparent particle beam divergence in the ion source.

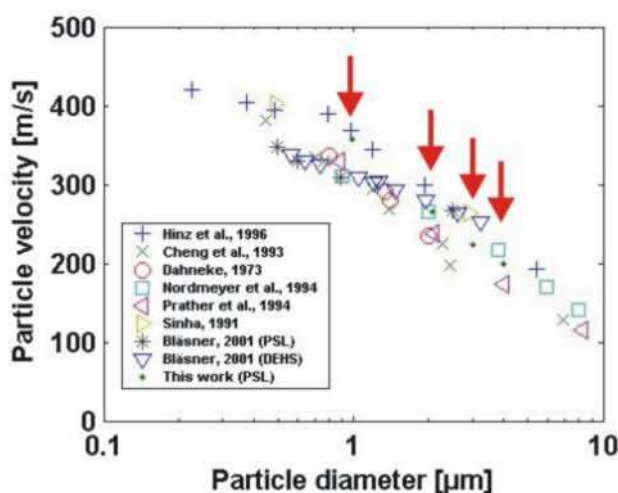


Figure. 13 : Particle velocities obtained with different aerosol mass spectrometers

(modified after [Bläsner et al., 2000]). The arrows locate the particle velocity measured in this work for four different sizes of PSL particles (1 μm , 2 μm , 3 μm , 4 μm)

Location	Particle beam diameter	Beam divergence (Half-angle)
after the nozzle on the inverted skimmer ⁽³⁾ (skimmer I)	Palas soot particles : $\text{\O} > 2 \text{ mm}$	$\sim 40^\circ$ ⁽¹⁾
after the inverted skimmer on the the plane skimmer (skimmer II)	Palas soot particles : $\text{\O} \sim 2 \text{ mm}$ PSL particles 1 μm : $\text{\O} 2 \text{ mm}$	$\sim 3,8^\circ$ ⁽²⁾
after the plane skimmer in center ion source	Palas soot particles : $\text{\O} \sim 2 \text{ mm}$	$0,9^\circ$ ⁽²⁾

Table 15 : Particle beam diameter at different locations in the inlet unit

⁽¹⁾ Calculated from the geometry of the nozzle as if particles were flying along the wall of the nozzle before passing through its orifice and after according to their initial trajectory. ⁽²⁾ Calculated from the measured size spot of the impacted particles on the different skimmers or impaction plates and the distance between the orifice exit and the impaction plate. ⁽³⁾ The calculated beam divergence after the nozzle is only a limit value for particle having a high inertia.

The most important quantity to consider from Table 15 to operate the aerosol mass spectrometer is the diameter of the particle beam in the ion source as it intercepts the desorption/ionization laser. The beam diameter is here of 2 mm which is quite important compared to the apparent size of the desorption/ionization laser of less than 1 mm what is illustrated in Figure. 14(2).

Figure. 14(1) shows the deposition of particles on the whole surface of the plane skimmer (skimmer II) where the pressure reaches ca. $5 \cdot 10^{-2}$ mbar. Particles belonging to the particle accumulation region located by the arrow (a1) in Figure. 14 can be considered to be big particles with a high inertia. Similarly particles collected in the region (b1) can be considered to be smaller than those located in (a1). The thin particle layer on the plane skimmer present far from the skimmer orifice, located by the arrow (a1)) as can be deduced from (c1) in Figure. 14 indicates that particle trajectories are still influenced by the gas expansion at the local low pressure of $5 \cdot 10^{-2}$ mbar what lets think that particles can also be further accelerated at this stage.

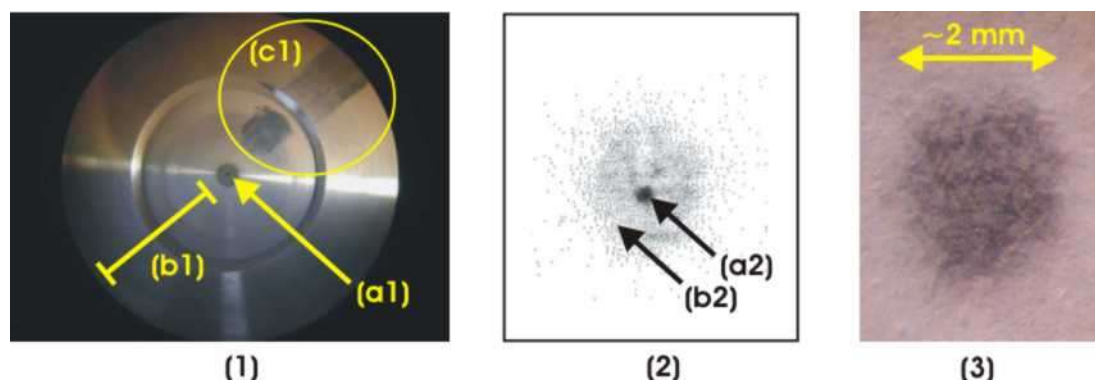


Figure. 14 : Particle beam size and particle deposition in the inlet unit

Panel (1): Accumulation of particles on the skimmer II (plane skimmer). One can clearly observe different particle accumulation patterns: High inertia particles (a1), low inertia particles (b1). The spot (c1) illustrates the particle accumulation on the skimmer II and demonstrates that the particle motion is still influenced by the gas flow at a pressure level of $5 \cdot 10^{-2}$ mbar. **Panel (2):** arrow (b2): Particle beam impactation spot in the ion source center. Arrow (a2): focus point of the desorption/ionization laser. **Panel (3):** Particle radial distribution within the particle beam in the ion source center. Particles were sampled on a piece of paper. Due to the roughness of the paper, one can not infer how particles are distributed within the beam.

In Figure. 14(2), the arrow (b2) shows the particle beam size ($\sim 1,5$ mm) and particle distribution in the beam cross-section at the center of the ion source where the particle beam intercepts the desorption/ionization laser. The arrow (a2) indicates the focus point of the desorption/ionization laser which is at least 8-10 times smaller than the particle beam. This confirms that the high particle beam divergence will dramatically limit the chemical analysis rate (CR).

Although particles seem to be distributed uniformly, it is difficult to state whether it is the case or not. Indeed the impaction plate is here a piece of paper. The examination of the particle distribution in the particle beam with a microscope for different experiments as presented in Figure. 14(3) shows that the presence of the paper fibers accumulates particles locally what masks their initial impact location. As a result, it is yet not possible to determine the most probable particle concentration profile across the particle beam cross-section. In the rest of this work, it will be considered uniform over the particle cross-section as a first approximation. The particle distribution in the particle beam is expected to depend strongly on the alignment of the nozzle and skimmer orifices and to be different after each cleaning of the inlet unit.

If the high divergence of the particle beam reduces the chemical analysis rate (CR), one can take advantage of it to sample particles by impaction on the skimmer II as long as the high divergence of the particle beam does not affect negatively the normal operation of the aerosol mass spectrometer.

4.4 Particle sampling with the inlet unit

Since all particles can not be efficiently focused in a beam by the inlet unit, the quasi-totality of the aerosol particles get impacted at different places within the inlet unit as presented in Figure. 14 and Figure. 15.

Figure. 15(a) shows the collection of liquid oil droplets from the rotary pump of the SPALMS instrument which were released in the atmosphere. These liquid and viscous particles rapidly clogged the inlet unit. This shows that they were not coming from the oil diffusion from the pumps through the pipes to the inlet unit.

Cigarette smoke components were also sampled in liquid state on the skimmer I (Figure. 15(b10) and (b11)) as well as on the skimmer II (Figure. 15(b20) and (b21)). For the case of cigarette smoke it is not clear yet if the deposited material originates from smoke particles or from the condensation of the hot gases and material of the cigarette combustion induced by the gas cooling as it expands in the inlet unit. The second explanation is the more plausible since the cigarette smoke was not diluted and sampled warm. Solid state particles such as soot or ash particles were also sampled by the SPALMS instrument and the inlet unit on both skimmers I and II as presented respectively in Figure. 15(c10), (c11) and (c20,c21).

Even if no mass spectra were obtained for the pump oil or cigarette smoke particles, the sampling of particles by impaction within the inlet unit permitted nevertheless the detection of oil as droplets and of low volatile compounds from cigarette smoke in ambient air. The sampled particles can be then analyzed by off-line conventional techniques as presented in Chapter 3. This permits therefore the detection or/and the analysis of particles that may not be detectable by the mass analysis or/and the check of the proper operation of the aerosol mass spectrometer.

It appears here that this inlet unit can also be considered as a quite special “pseudo-cascade impactor” with three stages. Table 16 summarizes the origin and the properties of the particles sampled at different locations in the inlet unit.

	<i>Pseudo impactor - Stage 1</i>	<i>Pseudo impactor - Stage 2</i>	<i>Pseudo impactor - Stage 3</i>
Location	Inner walls of nozzle before the nozzle orifice	Inverted skimmer (Skimmer I)	Plan skimmer (Skimmer II)
Particle origin	<ul style="list-style-type: none"> • Big / dense particles that can not be carried to the nozzle and that sediment in the nozzle • High inertia particles distant from the nozzle axis that impact on the nozzle walls 	<ul style="list-style-type: none"> • Particles that passed the nozzle whose radial location at the inverted skimmer is outside the inverted skimmer orifice • All fine particles that follow the carrier gas stream lines after passing the nozzle orifice 	<ul style="list-style-type: none"> • Particles that passed the inverted skimmer whose radial location at the plane skimmer is outside the plane skimmer orifice • All fine particles that follow the carrier gas stream lines after passing the inverted skimmer orifice
Practical availability for chemical off-analysis	Unpractical to collect	Unpractical to collect	Possible (once a day sampling for example) and before each cleaning
Geometric particle sampling efficiency (%) ⁽¹⁾	Not defined	99,5	93,8

Table 16 : Characteristics of the particles sampled by impaction within the inlet unit

⁽¹⁾ The geometric particle sampling efficiency is equal to the ratio of the particle beam cross-section area that is captured by the impactor plate (particle beam cross-section minus the surface area of the orifice) to the total particle beam cross-section at the impactor plate location after each nozzle/skimmer orifice.


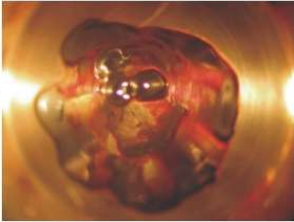
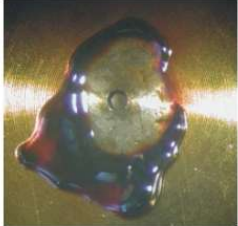
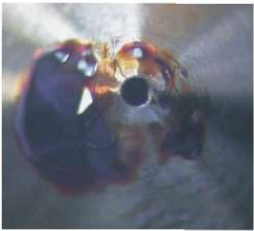
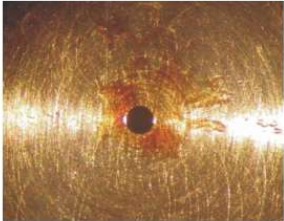


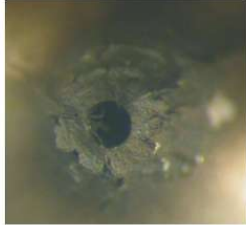

Particle impaction at the different inlet unit locations		
	Inverted skimmer (Skimmer I)	Plane skimmer (Skimmer II)
Rotary pump oil		(a) 
Cigarette smoke	(b10) 	(b20) 
	(b11) 	(b21) 
Soot/Ash particles	(c10) 	(c20) 
	(c11) 	(c21) 

Figure. 15 : Sampling of particles by impaction in the inlet unit on skimmer I and skimmer II

The calculated values of the geometric particle sampling efficiency for each impactor indicates that only a small particle fraction is transmitted from one chamber to the other. Considering this, the theoretical inlet unit transmission T can be calculated to be roughly 0.03% if the particle distribution is uniform over the particle beam cross-section. It means that roughly 0.03% of the particle transmitted by the nozzle are transmitted to the ion source. Such low transmission dramatically

limits the particle sizing rate (SR) and therefore the chemical analysis rate (CR) and the sizing and chemical analysis rate (SCR). The collected quantity of particles might be small but can potentially be used if carefully collected (washed by a solvent for example) for further off-line chemical analysis when the inlet unit is taken apart.

In this “pseudo-cascade impactor”, particles are not collected only according to their size but also according to their initial radial location before they reach the nozzle/skimmers orifice. The particle size cut of each stage of this “pseudo-cascade impactor” (nozzle, inverted skimmer and plane skimmer) has not been determined experimentally because this information is not of primary importance in the scope of this work yet and because its calculation as mentioned before is complex. Nevertheless considering the usual relationship used to calculate the particle size cut an inertial impactor as given in Eq. 8 ([Baron and Willeke, 2001]), it is possible to get some ideas of the pattern of particle size distribution of the transmitted particles.

$$d_{p,av,50} = \sqrt{\frac{18 \cdot \eta \cdot d_{nozzle}}{\rho_p \cdot C_c \cdot U_{gas}}} \cdot \sqrt{Stk_{50}}$$

Eq. 8

where $d_{p,av,50}$ is the vacuum aerodynamic diameter size cut, d_{nozzle} the diameter of the orifice diameter, ρ_p the particle bulk density, Stk_{50} the cut-off Stokes number, η the gas viscosity and C_c the Cunningham factor. From Eq. 8, each orifice has its own size cut meaning that the size distribution of the transmitted particles corresponds to the common transmitted size range for each nozzle and skimmers. Since the transmitted particles have different origins as listed in Table 16, it might also not be surprising to observe that the transmitted particle population has a three-mode size distribution. This question still remains to be answered since it was not of primary importance in this work.

5 Detection / sizing unit

Chapter 5. describes the detection/sizing unit goals, designs and characteristics. The sizing unit permits the detection, counting and sizing of the particles as they enter the aerosol mass spectrometer. The sizing unit provides also the necessary information needed to trigger the desorption/ionization laser as the particle reaches the ion source center. It consists of two laser beams that intercept the particle beam. The light scattered by the particle as it crosses the sizing laser is then processed to measure the particle velocity, therefore its size, and possibly to get additional information about its physical properties. The scattered light is collected by two photomultipliers for each sizing laser located at different angles relatively to the laser beam. Photomultipliers convert the light signal into electrical pulses that are digitized and processed off-line by a home-made program. With this setup, the real inlet unit and the particle sampling efficiency of the aerosol mass spectrometer can be evaluated.

In the following, the measurable size range is determined as well as the highest aerosol particle concentration that can be sampled without significant biases due to coincidence effects and to the data acquisition speed. Finally this chapter presents the characteristics of the sizing unit by showing that the particle sizing accuracy strongly depends on the sizing laser distance, the particle location in the sizing lasers and coincidence effects for which a treatment method is proposed.

5.1 General design

Particles are detected by the scattered light as they cross a laser beam. The scattered light by the particle is collected and conducted to a photomultiplier which detects it and converts it to an electric signal. The electric signal is then processed electronically (or numerically) to mark the time at which the particle crossed each sizing laser. The different particle detection times are then used to measure the particle velocity and further processed to trigger the desorption/ionization laser. The detection/sizing unit involves a light source (sizing laser), a detection optical line (collecting optics and photomultipliers) and a signal processing unit.

5.1.1 Light source

The light source that illuminates the particle must be powerful enough and have a wavelength that makes the scattered light by the particle be detectable. The amount of light scattered by single particles in many directions can be estimated theoretically by different light scattering models. Such modeling was considered here to be unnecessary since many groups (listed in Table 17) report experimental setups currently used in aerosol mass spectrometry that permit the detection of single particles in the range of interests for the SPALMS instrument. The choice of the laser light from a bibliographic compilation is the most pertinent since the published results take into account the quality of the optical setup, what is of the utmost importance as is illustrated in this work.

From Table 17, many laser systems are possible with different nominal powers. The nominal laser power related to the particle size range that can be detected gives a good measure of the quality of the detection/sizing unit. The work of [Gälli et al., 2001] demonstrates that it is possible to detect particles as small as 0,12 μm in optimal conditions. This clearly orients the choice of the laser to be used.

5. Detection/sizing unit

<i>Reference</i>	<i>Sizing laser characteristics</i>	<i>Mean laser power density [$\mu\text{W}/\mu\text{m}^2$]</i>	<i>Detectable particle size [μm]</i>	<i>Sizable particle size [μm]</i>
This work	Diode-laser pumped Nd:YAG, 532 nm, cw, 50 mW	0.17	0.8	0,8-4
[Gälli et al., 2001]	Diode-laser pumped Nd:YAG, 532 nm, cw, 23 mW focused to $\varnothing=490 \mu\text{m}$	0.12	0.08	0,18-2,1
[Trimborn et al., 2000]	Diode laser pumped Nd:YAVO ₄ , 532 nm, cw, 50 mW focused to $\varnothing=30 \mu\text{m}$	70.1	0.2	0,2-5,7
[Weiss et al., 1997]	He-Ne laser, 633 nm, 16 mW focused to $\varnothing=50 \mu\text{m}$ (split in two beams 42% each beams)	3.4	0.36	0,36-4
[Carson et al., 1995]	He-Cd laser, 442 nm cw, 60 mW focused to $\varnothing=300 \mu\text{m}$	0.85	0.25	>0,5
[Prather et al., 1994]	Ar ⁺ laser, 488 nm, 40 mW, focused to $\varnothing=100 \mu\text{m}$ He-Ne laser, 633 nm, 10 mW, focused to $\varnothing=100\mu\text{m}$	5,1 1,3		1-8,4 (NaCl)
[Hinz et al., 1994]	He-Ne laser, 633 nm	/	/	/

Table 17 : Sizing laser systems used in different aerosol mass spectrometers.

The power density is expressed in $\mu\text{W}/\mu\text{m}^2$ since the surface unit of μm^2 is more characteristic of the particle size (in μm range).

On the example of the ATOFMS from TSI Inc., St Paul, MN, USA and from the work of [Gälli et al., 2001], two independent sizing lasers have been chosen for the SPALMS instrument. Both lasers are Crystal Laser Nd:YAG pumped diode-laser (Model GCL-050-L, Class IIIb, Crystal Laser, Reno, Nevada, USA) that produces a laser beam with a light at $\lambda = 532 \text{ nm}$, 50 mW, continuous and vertically polarized in TEM₀₀ mode (which corresponds to a radial Gaussian distribution of the light within the laser beam). The nominal beam diameter at $1/e^2$ is given to be 0,4 mm with a half-angle divergence of 0,2 mrad. Each laser permits the illumination of the particle with a power surface density of $0,14 \mu\text{W}/\mu\text{m}^2$ without focusing elements of the laser light.

In the rest of this work, the two lasers used for the detection and the sizing of the particles will be respectively denominated Sizing laser 1 and Sizing laser 2 which are respectively the first and the second laser beam encountered by the particle on its flight.

5.1.2 Sizing laser distance

The particle velocity can be measured by measuring the time-of-flight of the particle between to distant sizing laser beams. The choice of distance between both laser beams $d_{\text{sizing lasers}}$ results from technical compromises between the particle coincidence event probability, the wished particle velocity measurement accuracy, the method used to produce two laser beams, the time response of the electronic hardwares that will process the scattered light signal produced as a particle crosses the sizing laser beam and the time delay between the electric trigger of the desorption/ionization laser and the effective light pulse. These constraints attributed to each parameter are listed in Table 18.

5. Detection/sizing unit

<i>Parameters</i>	<i>Constraints on the detection/sizing unit design</i>
Coincidence event probability	The distance between both sizing lasers $d_{\text{sizing laser}}$ should be the smallest possible
Particle velocity accuracy	The distance between both sizing lasers $d_{\text{sizing laser}}$ should be the longest possible
Production of the two laser beams	<p>If $d_{\text{sizing laser}} < 5$ mm: the laser beam can be split into two parallel displaced beams of different polarization with a birefringent crystal (calcite for example).</p> <p>If $d_{\text{sizing laser}} > 5$ mm: Two possibilities arise. Either two lasers are used or one laser can be used with an assembly of a 50% reflecting mirror to split the laser beam and a total reflection mirror. The former mirror produces the two beams by reflecting a part of the incident beam and letting the rest unchanged. The second mirror produces the second parallel beam to the first one by reflecting a second time the reflected beam on the first mirror.</p>
Signal electronic processing hardware	The distance $d_{\text{sizing laser}}$ must be long enough so that the particle time-of-flight between the detection/sizing unit and the ion source can be long compared to the laser trigger delay of the desorption/ionization laser and the reaction times of electronic devices. In practice both sizing laser beams should be spaced of at least 3 mm

Table 18 : Parameters to consider to set the distance between both sizing laser beams

Due to geometric constraints in the ion source as presented in Chapter 3., the room available between the exit of the inlet unit and the electrodes of the mass spectrometer has a length along the particle beam of 32 mm. The distance between the electrodes entrance and the center of the mass spectrometer is 18 mm. As a result, the three laser beams have to be positioned within 50 mm with the desorption/ionization laser beam (the last laser beam encountered by the particle on its flight) being located at the center of the mass spectrometer as depicted in Figure. 9.

The distance between both sizing laser beams was set to 12 mm and the distance from the second sizing laser beam to the desorption/ionization laser of 24 mm. The particle time-of-flight TOF_{sizing} between the sizing lasers lies between 20 and 120 μs while it ranges from 40 to 240 μs between the second sizing laser and the desorption/ionization laser. The particle time-of-flight between each beam is long compared to the reaction times of the photomultipliers, the signal processing electronic devices and the trigger time delay of the desorption/ionization laser. This makes therefore possible to couple electronically the sizing unit and the desorption/ionization unit.

Both laser beams are decided to be distant by 12 mm. This is achieved by using two lasers and by bringing both beams laterally displaced of 12 mm to each other by two successive reflections on 2 mirrors as presented in Figure. 16. As mentioned in Table 18, both laser beams could have been produced by splitting the initial laser beam with a 50% beam splitter. The beam splitter lets 50% of the beam energy constitutes the first laser beam whereas the reflected part is then totally reflected by a second mirror to produce the second laser beam parallel to the first one and distant from 12 mm. The first solution has been preferred because both laser beams can be adjusted independently and the high light intensity should permit the detection of smaller particles than in the case of split laser beams. However the second solution can be used in a next future for the detection/sizing unit and will give the possibility to use the second laser for the detection of incompletely volatilized particles after their desorption/ionization as presented in the work of Weiss [Weiss et al., 1997].

Each laser beam is directed to the sensing volume where the particle crosses the sizing laser beams by two mirrors (BK7, reflectivity $> 99,5\%$ at 532 nm at $AOI = 45^\circ$, Laser Star GmbH, Olching, Germany) each mounted on a 3-screws table (Linos Photonics GmbH, Göttingen, Germany) as presented in Figure. 16(a). After it adjustment, the light is then transmitted to the ion source

chamber via a window with an anti-reflection coating on both sides for $\lambda = 532 \text{ nm}$ (Laser 2000, Wessling, Germany). The anti-reflection coating is expected to block 99,9% of the reflected light at normal incidence. Once the laser beam has entered the ion source, it passes a series of diaphragms (or light baffles) that blocks the scattered light as the light meets the window surfaces (Figure. 16(b) and (c)). The laser beam passes then through a “black chamber” where it intercepts the particle beam. The laser beam reaches then an other anti-reflection window mounted with a diaphragm at the opposite side of the ion source and enters a black tube shaped as a U that acts as a light trap to stop the laser light. The presence of diaphragms on both sides of the ion source (after the entrance window and before the exit window) as depicted in Figure. 16(c) permits the parallel adjustments of both sizing laser beams and the relatively precise determination of their distance ($\pm 1 \text{ mm}$) at their intersection with the particle beam.

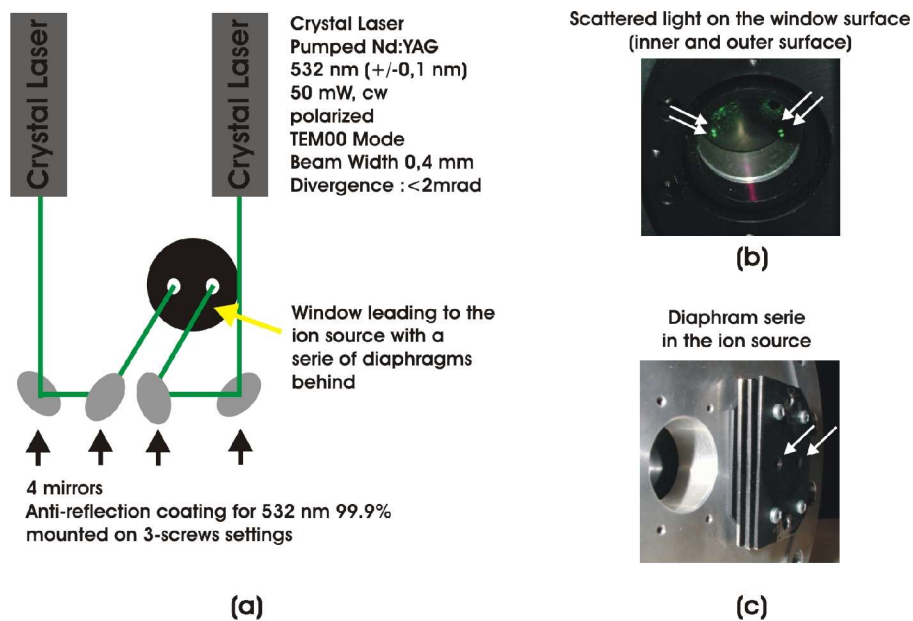


Figure. 16 : Setup of the sizing laser beams in the detection/sizing unit

(a) 3D-view illustrating the laser beam paths from the lasers to the entrance window preceding the detection/sizing unit. (b) Scattered light of the laser on both faces of the interface window (green spots on the window located by the arrows). (c) Home-made light baffle system (here denominated as diaphragm series) dedicated to capture the laser light scattered on the entrance window.

The series of diaphragms at the entrance and exit windows also permits the check of an eventual drift of the sizing laser distance. If a drift occurs, one of the sizing laser will meet the border edge of a diaphragm what is easily detected by the photomultipliers. This gives a mean to drive eventual step-motors that can be implemented to adjust automatically the mirrors.

Each sizing laser beam travels ca. 50 cm and is reflected twice between the laser exit to the sensing volume. Considering its divergence (0,2 mrad), the laser beam diameter reaches an approximative diameter of ca. 0,6 mm as it crosses the particle beam. The light intensity of both lasers was measured to be about 40 mW before they met the entrance window. Accounting for global loss of 10% for all window faces and diaphragms, the power of the sizing laser beam can reasonably be

estimated to be about 30 mW at the particle beam. The light power density on the particle beam is therefore calculated to be 10,6 W/cm² (or 0,11 mW/μm²). The calculated energy or power density is a mean which does not reflect the fact that the particle may be strongly irradiated as it crosses the center of the laser beam and much less as it crosses the border of the laser beam. The location of the particle in the laser beam is difficult to address and will be discussed in Chapter 13.

5.1.3 Optical setup for the collection of the scattered light

The particle is detected as it scatters the laser light. The light scattering occurs in all space directions whose spatial distribution depends on the light wavelength and the particle optical parameters such as its size, shape and refraction index. The main question is here to decide for the design of the scattered light collection optical setup in which direction and over which solid angle the light is to be collected. The scattering light properties of a single particle is determined by its size parameter α defined as follow in Eq. 9:

$$\alpha = \frac{\pi \cdot d_{p,g}}{\lambda}$$

Eq. 9

where $d_{p,g}$ is the particle geometric diameter and λ the light wavelength.

Three cases are to be considered depending on the value of the size parameter α . The different cases are presented in Table 19 and illustrated in Figure. 17.

α value	Appropriate theory	Comments	I_{scatt} approximation ^(*)
$\alpha \ll 1$	Raleigh theory	The particle is seen as a dielectric dipole oscillating in a uniform electric field. The light scattering pattern presents a radial symmetry if the particle is spherical.	$I_{scatt} \propto d_{p,g}^6$
$\alpha \# 1$	Lorentz-Mie theory	The electric field is not uniform over the particle. The scattered light intensity and its angular distribution depend strongly on the particle diameter and the refraction index for a spherical particle.	The ($I_{scatt}, \leftrightarrow d_{p,g}$) relationship is not monotone
$\alpha \gg 1$	Geometric theory	The law of the geometric optics can be used to evaluate the light scattering patterns. In near forward scattering region (within 20° from the light propagation axis), the scattered light is originating mainly from the light diffraction by the particle and is roughly proportional to the particle projected area and is few dependent of the shape and refraction index.	$I_{scatt} \propto d_{p,g}^2$

Table 19 : Light scattering characteristics as a function of the particle size parameter α

(*) I_{scatt} is to be considered for a given light wavelength, refractive index in a given direction over a given solid angle.

In the present case ($\lambda = 532$ nm, $d_{p,g} = 0,5$ to 4 μm), the size parameter α ranges from ~ 3 to ~ 23. The size parameter lies close to the range in which the measured amount of scattered light can not theoretically be unambiguously related to the particle diameter unless white light is used or the scattered light is collected over a very wide solid angle ([Baron and Willeke, 2001]).

Mie scattering calculations were performed by researchers developing aerosol mass spectrometers to better design their optical detection/sizing unit as presented by [Hinz et al., 1994] and illustrated in Figure. 18 below or/and to gain additional information about the particle as recently performed by [Murphy et al., 2004] and [Moffet et Prather, 2005].

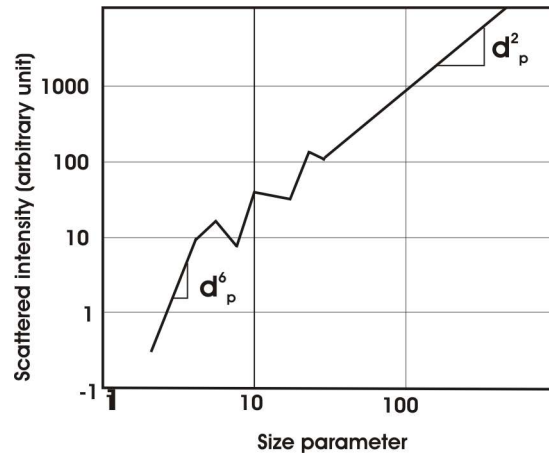


Figure. 17 : Variation of the scattered light intensity as a function of the size parameter α

This figure represents the typical dependence of the amount of scattered light by a particle as a function of the size parameter α .

Three regions can be identified: $\alpha < 7$: Raleigh theory, I_{scatt} is proportional to d_p^6 , $7 < \alpha < 70$: Lorentz-Mie theory, I_{scatt} is not monotonically dependent on d_p , $\alpha > 70$: Geometric theory, I_{scatt} is proportional to d_p^2

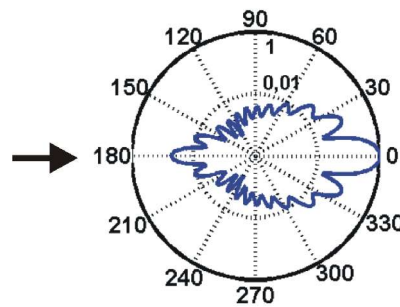


Figure. 18 : Single particle light scattering pattern

This figure presents the normalized amount of scattered light in different space directions within the scattering plane by a particle of refractive index $n = 1,55$ of geometric diameter $1 \mu m$ in polar coordinates and logarithmic scale. The incident laser light ($\lambda = 532 \text{ nm}$) is located by the arrow at the graduation 180° . The calculation were performed with the program MiePlot v3.41 [MiePlot v3.41, 2006]

5. Detection/sizing unit

The simulation presented in Figure. 18 indicates that in this light scattering regime ($\alpha = 4,9$, i.e. in the conditions that are well represented by the Mie-Lorentz theory) most of the scattered light is scattered within $\pm 68^\circ$ in the forward direction. Capturing the light within these angles should allow to easily detect particles. For practical reasons, the light is not captured in near forward direction (within $\pm 22^\circ$) due to the probable high level of parasite light near the laser beam axis and the necessity in this case to set the collection optics far away from the sizing sensing volume what is not possible for room scarcity reasons in the ion source.

In practice the scattered light is captured at $\pm 45^\circ$ across the sizing laser beam. For each laser beam, the scattered light is collected by two collimators (Soliton Laser und Meßtechnik GmbH, Gilching, Germany) respectively positioned at $\pm 45^\circ$ across each sizing laser beam. Each collimator transfers the light to an optical fiber (Soliton Laser und Meßtechnik GmbH, Gilching, Germany) which leads the light to a photomultiplier tube. The collimators have a diameter of 4 mm and are located at 5,5 mm from the sensing volume. They collect in practice the scattered light within $\pm 10^\circ$ around the collimator axis what represents a solid angle of 0,35 steradian each. For each sizing laser beam, the scattered light is collected over a total solid angle of 0,7 steradian representing 6,8% of the space directions. The optical fiber leads the light to the photocathode of a photomultiplier (Hamamatsu 931B, Side-On-Type, Hamamatsu Photonics K. K., Hamamatsu City, Japan) whose sensitive spectral band ranges from 300 to 650 nm with a maximum sensitivity at 400 nm. It permits in particular the detection of white light, the sizing laser light ($\lambda = 532$ nm) and some of the ultraviolet desorption/ionization laser light (such as nitrogen laser light, $\lambda = 337,1$ nm) or its fluorescence light as it impacts a surface. The light that exits the optical fiber illuminates at most 8,3% of the photomultiplier sensitive surface.

The particle scattered light is collected at two locations for each sensing volume for two main reasons. Firstly, one can check that a light scattering event observed by a photomultiplier corresponds to a particle by checking that the second photomultiplier also detected at the same time a light scattering event. This is particularly useful for small particles whose photomultiplier signals amplitude are close to the photomultiplier noise level. It avoids therefore false triggers due to dark spikes ([Kievit et al., 1996], [Trimbom et al., 2000]) and the noise level. Secondly, both photomultiplier signals obtained for big particles can be compared and can theoretically inform in which extent the particle shape deviates from sphericity and, in any case, confirms the observation from the other photomultiplier.

Figure. 19 illustrates the arrangement of the different components of the detection/sizing unit in the ion source. The collimators for each sizing lasers are inserted in a black chamber which positions the collimators 45° apart above and below the laser beam in the forward direction (Figure. 19(d)). It isolates each light scattering region from the other so that the scattered light from the first sizing laser is not be detected by the photomultipliers of the second sizing laser. The spatial origin of the light detected by a given photomultiplier is then unambiguous. It also isolates the collimators from parasite light from the exterior that facilitates therefore the analysis of the scattered light event.

However it appears that a fraction of the day light can still enter the black chamber and be detected by the photomultiplier as displayed in Figure. 20(a) when the desorption/ionization laser is fired. Indeed, the desorption/ionization laser light ($\lambda = 337$ nm), and maybe also the emitted fluorescence light from the surface where the light impacts, is partly reflected back into the ion source by the exit glass window and gets into the “black chamber” and proceeds to the photomultiplier. This parasite effect can be used for counting detected particles that lead to trigger the desorption/ionization laser and to determine approximatively the time origin of the ion mass spectra.

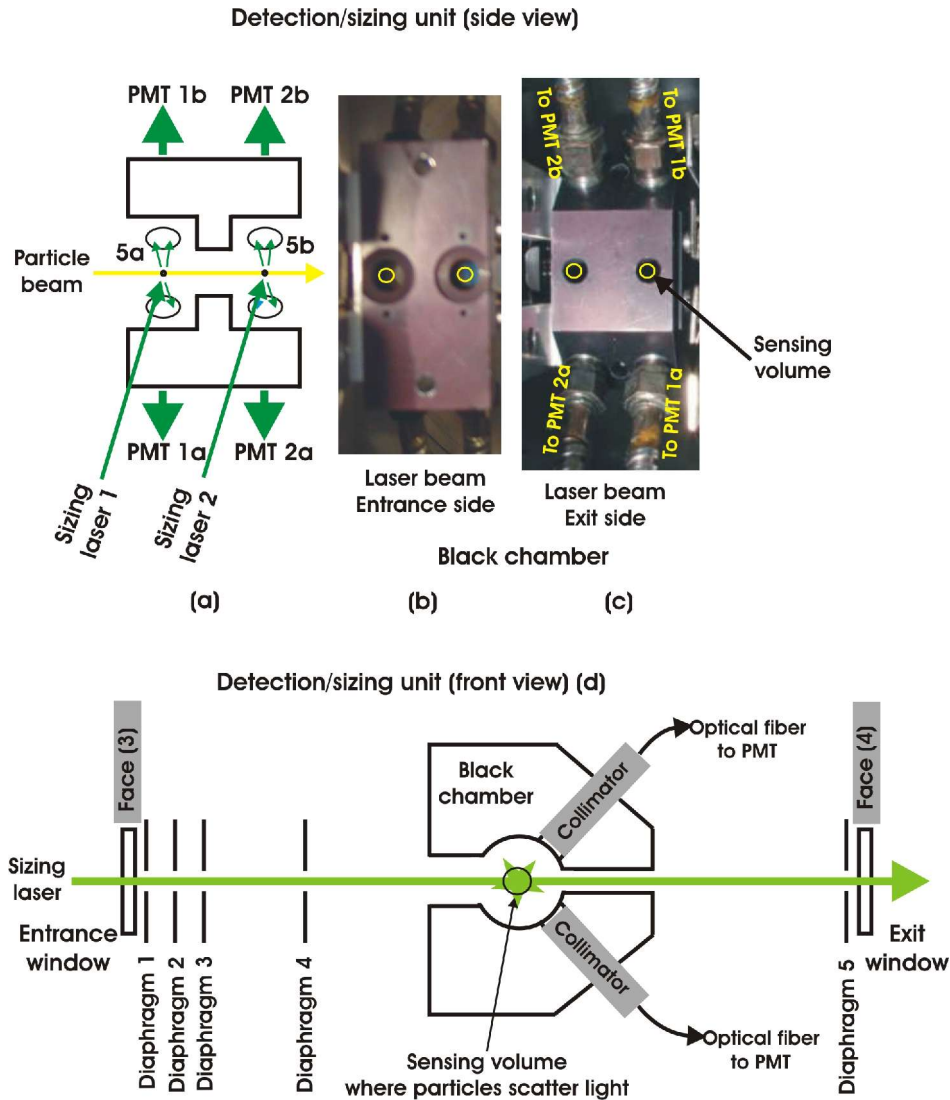


Figure. 19 : Schematic view of the detection/sizing unit located in the ion source

(a) Cross-section of the “black chamber”. (b) Photo of “black chamber” (from the entrance face of the sizing laser beams). (c) Photo of the “black chamber” (from the exit face of the sizing laser beams). (d) Arrangement of the “black chamber”, the diaphragm series (or light baffles), the light collimators and the optical fibers between the face (3) and face (4) of the ion source.

The noise level of the different photomultipliers is quantified here by the voltage signal amplitude after the photocurrent emitted by the photocathode is converted into a voltage by the current-to-voltage transformer whose settings affect the final absolute voltage amplitude. The current noise level of the photomultipliers while the sizing lasers are off reaches 10 to 20 mV with only the daylight from the outside of the instrument through the 4 open windows of diameter 25 mm that transmit the laser light in the detection/sizing unit and ion source. The noise level ranges from 50 to 200 mV when both sizing lasers are on. Fine sizing laser adjustments (which are quite time consuming) permit the reduction of the noise level down to about 50 mV by limiting the scattering of the laser light on the diaphragm edges (diaphragms 1,2,3,4 of Figure. 19(d)). The diaphragms are necessary to eliminate the scattered light (stray light) as the sizing laser beam meets the entrance

window (Figure. 19(d)). They consist of assemblies of three 1 mm thick aluminium anodized plates separated by 1 mm and 3 cm with two circular apertures of diameter of 1,5 mm distant of 12 mm that let both sizing laser beams reaching the particle beam.

5.1.4 Photomultiplier signal processing

The light transmitted to the photomultiplier is converted into a photocurrent by the photocathode and further amplified by a serie of 9 dynodes that amplify the current by a factor of 10^7 . The resulting current is then converted to a voltage that is after amplified. This is performed in our case by a DA socket assembly (Model C1556-51, Hamamatsu Photonics K. K., Hamamatsu City, Japan). The power supply of the photomultiplier and DA socket assembly were manufactured by the electronician of the GSF-Forschungszentrum with a special care to make the high-voltage supply very stable and isolated from any network perturbations.

According to the operation mode of the SPALMS instrument, the photomultiplier signal can be either electronically processed by specific electronic devices or digitized with an oscilloscope or a digitizer PCI-card. Figure. 20(a) presents the shape of typical photomultiplier signals as they are digitized with an oscilloscope (LeCroy WR6050a, LeCroy, Chestnut Ridge, New York, USA).

5.1.4.1 Photomultiplier response to a light pulse of different time lengths

The nominal fast response of the photomultiplier (within 2 ns) and the short electron transit time (22 ns) are small against the particle residence time of the particle within the sizing laser beam whose typical order of magnitude is around 1,5 μ s. Considering this, it is therefore possible to follow the time variation of the scattered light intensity as the particle crosses the sizing laser in case the light power density distribution is not uniform within the laser beam. For example if the laser has a Gaussian energy distribution, the resulting photomultiplier signal should also present a Gaussian-like shape as well.

In the present work, on the contrary to what was expected, the photomultipliers do not produce such signal patterns. To test the behavior of the photomultiplier setup, the reaction time of the detection/sizing unit was tested with an intense short light pulse of length of 8 ns (in this case the laser light pulse from the nitrogen laser, $\lambda = 337$ nm, 8ns). The photomultiplier signal needs some microseconds, from 1 to 3 microseconds, to reach its maximum before it disappears in 20 to 50 μ s. The photomultiplier signal obtained for particles who reside in the laser beam 1,5 to 3 μ s have typically a peak rising time of 1 to 3 μ s and a long tail of 20 to 30 μ s as presented in Figure. 20(b) for particle scattered light whereas the peak rising time reaches $\sim 1,6$ μ s as depicted in Figure. 20(c) for a short light pulse (8 ns).

This observation makes the interpretation of the photomultiplier signal not straightforward since one can relate neither the peak time width nor its rising time to the particle residence time τ_{particle} in the sizing laser.

The asymmetrical shape of the peak is not unusual since such a feature was also observed on a ATOFMS instrument operated at Lawrence Livermore National Laboratory (Ferge, personal communication) or on the PALMS instrument ([Cziczko, 2005]).

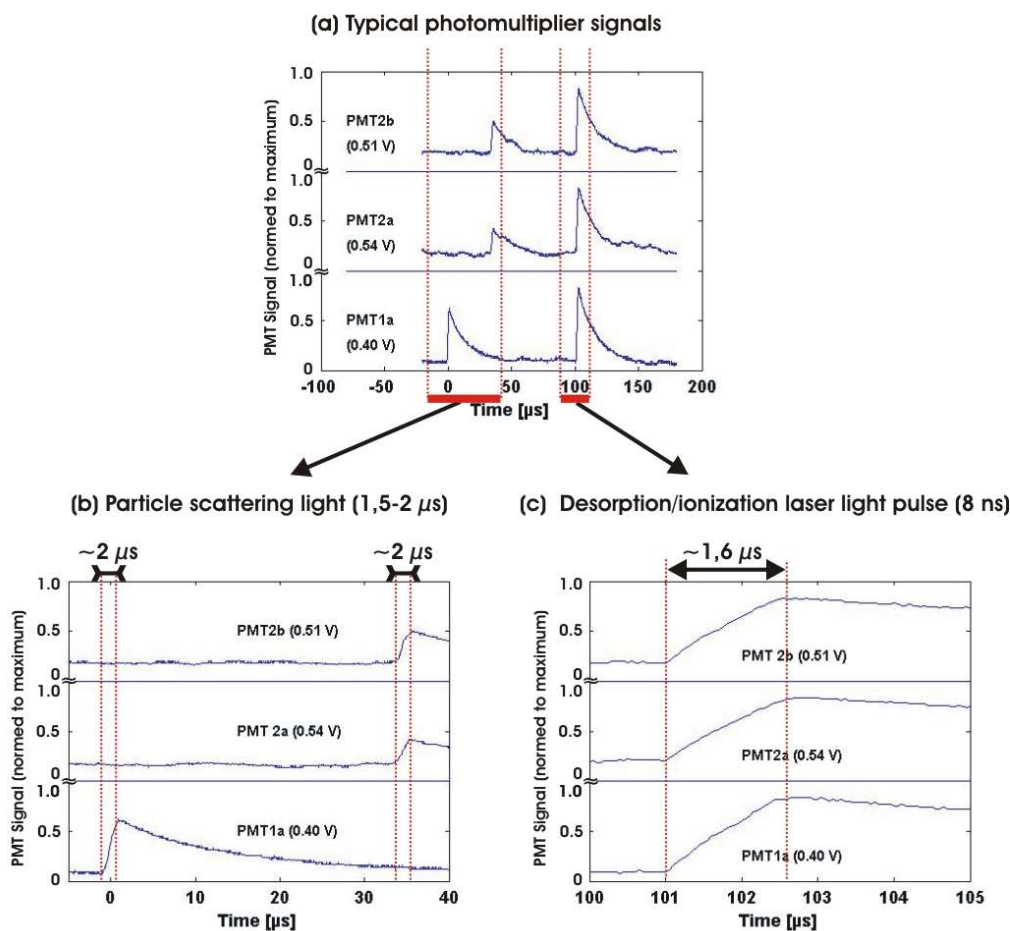


Figure. 20 : Typical time response of the photomultiplier of the detection/sizing unit

Panel (a) Typical photomultiplier signal showing the detection of a particle by both sizing lasers and of the laser light emitted by the desorption/ionization laser. **Panel (b)** Enlargement of the photomultiplier signal of the inset (a): particle detection by both laser beams. **Panel (c)** Enlargement of the photomultiplier signals of the inset(a): detection of the laser light emitted by the desorption/ionization laser. (*) The voltage indicated in parenthesis corresponds to the maximum voltage reached by the photomultiplier signal as it is digitized over the acquisition time window.

5.1.4.2 Processing of the photomultiplier signal for the particle detection and sizing

However even if the photomultiplier signal is not as optimal as it should be expected, particles can still be sized and the desorption/ionization laser can still be triggered with the current signal quality.

The photomultiplier signal from Figure. 21(a) and (b) permits the sizing of the particle since the particle time-of-flight can be easily calculated. However, only particles detected in Figure. 21(a) can potentially give mass spectra since the second observed peak for all photomultipliers at the same time corresponds to the desorption/ionization laser light that is reflected on the ion source window and reaches the photomultiplier. This illustrates the sensitivity of the photomultipliers at the wavelength $\lambda = 337$ nm. Figure. 21(c) and (d) illustrate the particle coincidence phenomena that affect both the measurement of the particle size distribution and the hit efficiency. Case (c) can not

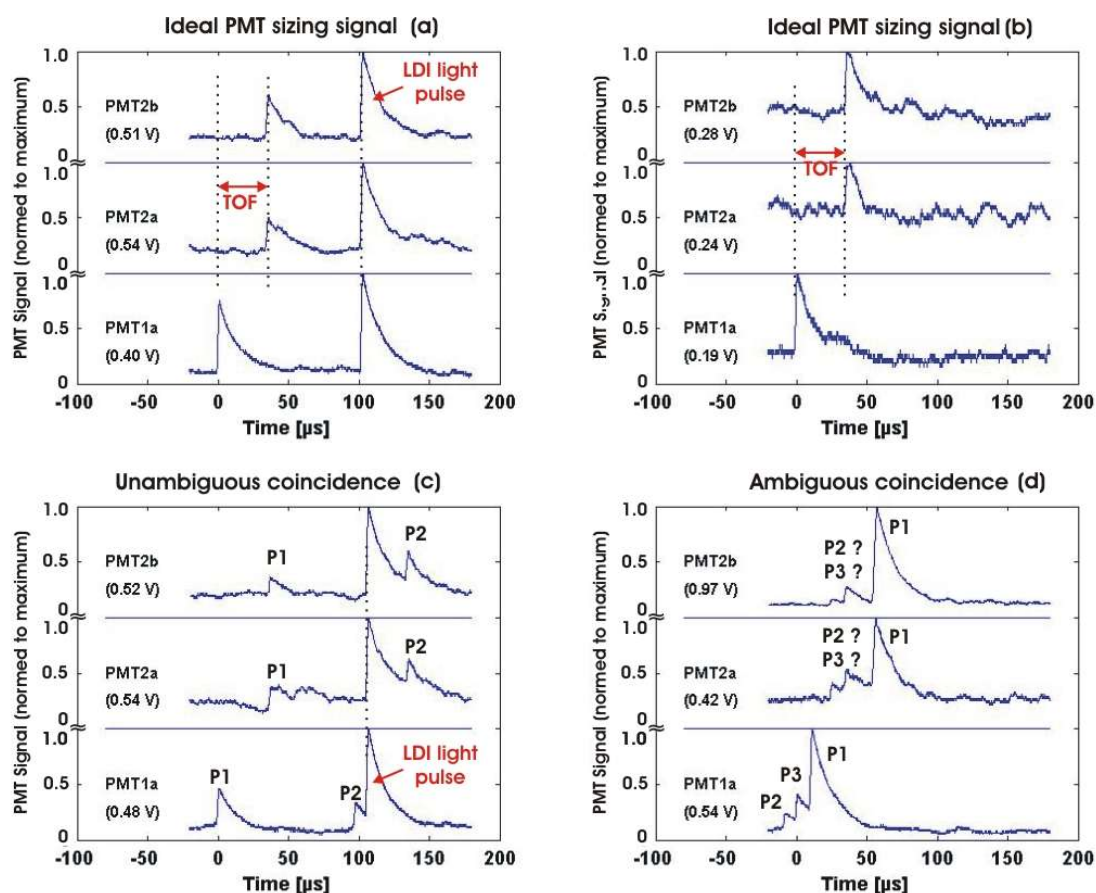


Figure. 21 : Photomultiplier signals for particle sizing

Panel (a) Particles can be sized and chemical analyzed. **Panel (b)** Particles can only be sized (the desorption/ionization laser has not been fired). **Panel (c)** Coincidence event. The first particle P1 detected can be sized and chemically analyzed whereas the second particle P2 can be sized but not chemically analyzed. **Panel (d)** Coincidence event. Either the particle P1, P2 or P3 can be chemically analyzed but it is not possible to identify which is chemically analyzed and to state if one of the particles can be sized correctly. (*) The voltage indicated in parenthesis corresponds to the maximum voltage reached by the photomultiplier signal as it is digitized over the acquisition time window.

really be considered as a “real” coincidence phenomenon since the time between two successive particles P1 and P2 is greater than the time needed for the particle to fly to the second laser.

On the opposite in the case (d) of Figure. 21, if a coincidence error is not possible for the highest peak attributed to the same particle P1, coincidence error is to be considered for the two other peaks corresponding to the particles P2 and P3.

The advantage of processing the data off-line numerically is to permit the classification and, if necessary, the elimination of the photomultiplier signals that do not correspond to detected particles as those presented in Figure. 22. Those photomultiplier signals result mainly from inappropriate experimental conditions such as the inappropriate laser adjustments (case of Figure. 22(e) and (g)), erroneous trigger due to a high noise level (case of Figure. 22(f)). The PMT1a signal in Figure. 22 (e) indicates a bad adjustment of the first sizing laser. The laser light is slightly scattered on the edge of a diaphragm and illuminates therefore the whole sensing volume. A possible explanation of the shape and the characteristics of this signal can be that the particle or group of particles scatter the light during their whole flight in the first sensing volume of “black chamber” giving rise to some

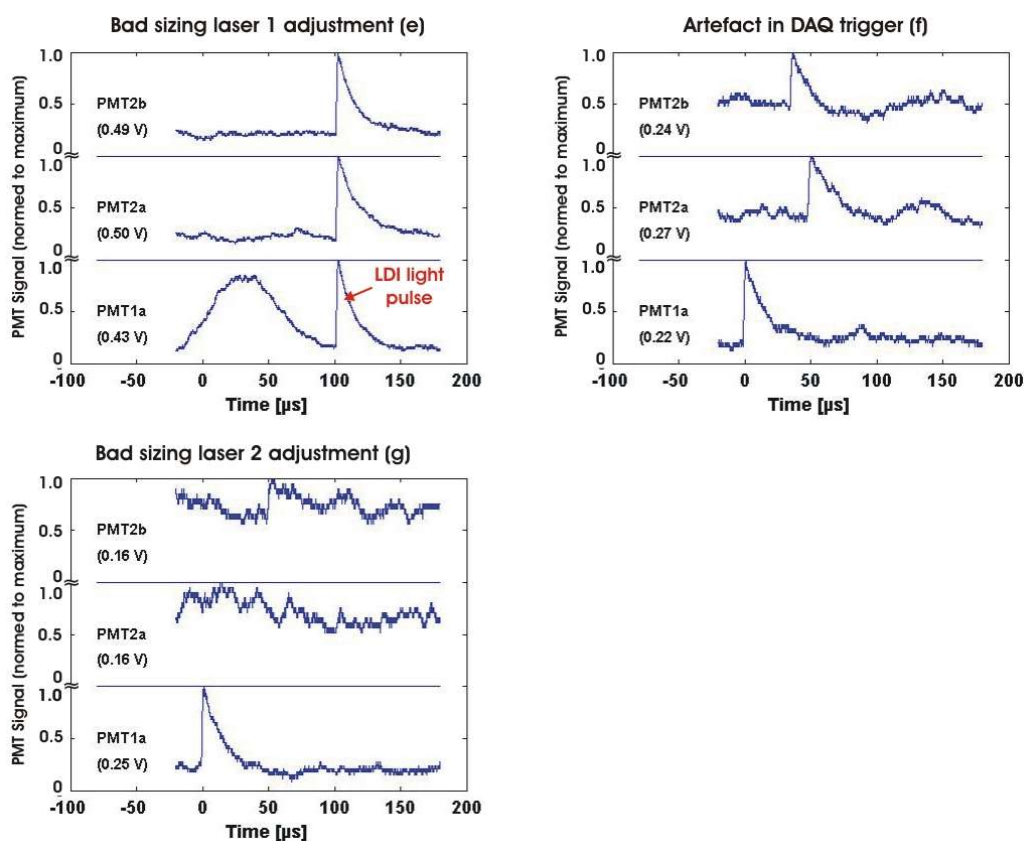


Figure. 22 : Inappropriate photomultiplier signals for particle sizing

Panel (e) Case of an inappropriate sizing laser adjustments. **Panel (f)** Case of a trigger problem specific to the simultaneous parallel use of 3 digitizers for the acquisition of the 3 photomultiplier signals. **Panel (g)** Case of an inappropriate adjustment of the second sizing laser. (*) The voltage indicated in parenthesis corresponds to the maximum voltage reached by the photomultiplier signal as it is digitized over the acquisition time window.

kind of “hill peak”. The rising time of the peak ($\sim 50 \mu\text{s}$) may be related to the travel time of the particle within the sensing volume (9 mm wide) indicating here a particle velocity of 180 m/s, i.e. the detection of the equivalent of a big particle.

The PMT2a,b signals in Figure. 22(f) and (g) have a low maximum voltage which lies between 0.16 and 0.270 V compared to clean signals that usually reach 0.43 to 0.97 V. In these cases, the photomultiplier signal acquisition is frequently triggered by the noise of the signal what explains the unexpected and chaotic signal patterns. This can also be due to the successive triggers of each digitizer that starts their acquisition at different times for the same particle due to the high frequency of the photomultiplier peak signals and to the low speed of the digitizer driving program in the current SPALMS setup. This can be the case for the signal presented in Figure. 22(g). This can be corrected by making all the digitizers ready in a shorter time, by operating the aerosol mass spectrometer with a low particle concentration and by reducing further the photomultiplier noise level that induces many false triggers in the current set-up. This shows the interest of detecting the same scattering light signal by two independent photomultipliers. Sometimes, proper particle signal can be still identified even if the photomultiplier noise signal is high as observed in Figure. 21(b).

Even if the photomultiplier signal behavior is not as ideal as expected, it permits nevertheless the detection/sizing of the particles and the trigger of the desorption/ionization laser.

5.1.4.3 Electronic processing of the photomultiplier signals

The photomultipliers that detect the particles optically are not only dedicated to their counting and sizing but also to the trigger of the desorption/ionization laser in order to obtain as many as possible mass spectra. If particles can be counted and sized by digitizing the photomultiplier signals and analyzing them by different programs, the desorption/ionization laser trigger can only be achieved with specific electronic devices which can quickly process them and send to the laser an electric trigger pulse.

Both functionalities can be included in a custom-made electronic box named Dynamic Sizing Trigger Unit (later referred as DSTU). This unit uses the particle time detection of each particle as they are detected by each sizing laser as input signal. In particular it calculates the particle time-of-flight, sends the measured time to a computer and generates a pulse electronically delayed in a certain manner so that the desorption/ionization laser can be triggered at the time when the particle will be at the center of the mass spectrometer. This approach was first introduced by [Prather et al., 1994] and is now commonly used for the analysis of particles larger than 200 nm in diameter.

To operate the DSTU, each photomultiplier signal must be first electronically processed separately. The photomultiplier signal is first lead to a constant fraction discriminator (CFA, Constant Fraction Analyzer, Model 2126 Camberra, Meriden, CT, USA) which converts the photomultiplier pulse to a square signal whose amplitude depends on the photomultiplier pulse amplitude. It has the important ability to always produce a square pulse at the same location of the photomultiplier pulse independently of its shape and amplitude.

The resulting square pulse is then sent to a coincidence analyzer (CA, Coincidence Analyzer, Model 2040, Camberra, Meriden, CT, USA) which is used here to convert the square electric pulse to a TTL pulse of a given amplitude and length. This signal is considered as the input signal for the DSTU. More important, the primary role of the coincidence analyzer is to check if two to four electric signals occur within a given time window after the first occurring photomultiplier pulse. It is in particular intended to check if a photomultiplier pulse is really corresponding to a particle and to lower the particle size detection limit by looking for simultaneous photomultiplier pulses close to the noise level that might not be related to a particle at first sight which can nevertheless be because of their simultaneous occurrence.

5.1.4.4 Data acquisition hardware of the photomultiplier signal

The time profile and amplitude of each photomultiplier signal can permit the evaluation of the residence time of the particle in the laser beam (and therefore its velocity and its size) ([Kievit et al., 1996], [Prather et al., 1994]) and bring additional information about the particle as was demonstrated by [Murphy et al., 2004] and [Moffet et Prather, 2005].

Processing the photomultiplier signals with different programs adapted to each particular case should permit a better characterization of the aerosol particle population and a better evaluation of measurement biases (such as false trigger and coincidence events).

Signals from the four photomultipliers are either digitized with a cluster of 4 digitizers Acqiris (DP210, 2Gs/s, 500Mhz, 256kPts, 8 bits, Acqiris, Geneva, Switzerland) mounted in parallel or with an oscilloscope WR6050A (Waverunner WR6050A, 5GS/s, 500MHz, 1MPts, 8 bits, LeCroy, Chestnuts Ridge, New York, USA).

Both options permit the acquisition of the four available photomultiplier signals on four different channels. The oscilloscope is very advantageous to record simultaneously data on 4 channels since

the acquisition is triggered from the signal from only one channel. The simultaneous use of four digitizers requires a complex trigger scheme since each digitizer must be individually simultaneously externally triggered to perform the data acquisition on 4 channels. The four digitizers can be all simultaneously triggered within 5 ns which corresponds to the rising time of the TTL pulse that externally triggers each of the four digitizers. The combination of the digitizers driven by a home-made Labview 6.i program permits a better management of the amount of acquired data and its adaptation to its typical time scale. Indeed one can perform data acquisition with all digitizers starting at the same time but with different sampling rate what is not possible with an oscilloscope. Moreover data can be on-line processed and/or directly stored as Labview 6.i binary files for further processing what is not possible with the oscilloscope at the present time. The data can however be quickly stored as LeCroy binary files which need to be then re-formatted into Labview 6.i binary files via their intermediate transformation into ASCII files to process them. The global data acquisition rates of both hardware options are presented in Table 20.

<i>Data acquisition device</i>	<i>LeCroy WR6050a</i>	<i>4 DP210 Acqiris digitizers⁽¹⁾</i>
Environment	PC included – Windows XP	Driven by a home-made Labview program PC – Windows 2000
Sample time	200 μ s	200 μ s
Sampling period	40 ns	50 ns
File size	4 x 6 K (LeCroy binary file)	126 K (Labview binary file)
Max. Saving Frequency	15 Hz	7 Hz
Max. Display Frequency	25 Hz	15 Hz

Table 20 : Photomultiplier signal data acquisition device characteristics

⁽¹⁾ Digitizers are triggered externally by a delay generator

From the data acquisition speed point of view, the oscilloscope is twice as fast as the combination of the 4 digitizer PCI cards. But its data, stored as small binary files, have to be reformatted in many steps to enable their processing by a home-made Labview 6.i program. Indeed any data files that are processed by the home-made Labview programs have a specific format. The data are stored in columns where each column corresponds to each acquisition channel. The first value of the data column indicates the number of acquisition points, the second precises the initial time, the third gives the sample rate and the rest corresponds to the serie of the voltage data points of the signal. This is an economic format in terms of file size. This was made possible under the assumption that the sampling period of the digitizers or the oscilloscope does not vary over the acquisition time and with the temperature. This data format is called format [nipss] (n: number of data points, i: initial time, p: sampling period and ss: signal serie as a voltage).

The data acquired either with the oscilloscope or the digitizer cluster are then formatted into a unique format. The signal from each 4 photomultipliers are formatted in the [nipss] format in 4 columns which each corresponds to a photomultiplier. The data acquisition with digitizers saves directly the photomultiplier signal in its final format whereas the data acquired with the oscilloscope have to be re-formatted first with a specific program from the oscilloscope manufacturer (ScopeExplorer 2.20, downloadable from LeCroy website <http://www.lecroy.com>) and secondly with a home-made Labview 6.i program. This conversion step is time consuming. As a result, data acquisition which requires a high acquisition rate or which is dedicated for a quick test is performed

with the oscilloscope whereas routine data acquisition is preferentially operated with the combination of 4 digitizers even if the acquisition speed is twice as slow.

Once the data are formatted in the same manner independently from their acquisition method, the photomultiplier signal have to be treated in order to extract information about the aerosol particles.

5.1.4.5 Software processing of the photomultiplier signals

Either with the oscilloscope or the digitizer cluster, the data acquisition is triggered when the photomultiplier signal that captures the scattering event of the first sizing laser exceeds a given threshold level denominated thereafter $V_{\text{sizing, trig}}$. This parameter is set according to the current noise level and determines the particle size detection limit.

The usual settings permit the data acquisition over 200 μs in order to capture any light scattering events occurring between the particle detection by the first sizing laser and the end of mass spectra acquisition for the four photomultipliers. Such acquisition is called thereafter a PMT scan. It is performed with a sampling period of 50 ns and a trigger offset of -20 μs to get an estimation of the noise level before the first photomultiplier peak occurs.

This procedure permits the detection of the particle, the measurement of its time-of-flight and the check of the occurrence of coincidence events. Further advanced data processing programs should allow to derive optical/geometric properties of the particle.

The number of PMT scans should correspond ideally to the number of particles sampled by the detection/sizing unit. Due to the high amount of data to save, a high detection and/or particle sizing rate can not be expected since it is determined by the maximum data acquisition speed, here, of 15 Hz and 7 Hz respectively of the oscilloscope and the digitizer cluster. The particle counting rate (PCR) can be made higher by using electronic hardwares to simply count and measure a particle time-of-flight. The aim of the detection/sizing unit of the SPALMS instrument is here to improve the knowledge of the single particle at the cost of the particle population. This why only a numerical data processing of the PMT scans is considered in this work.

Meanwhile data are currently saved to obtain datasets that can be later used to develop, improve and compare the different versions of home-made programs for the analysis of the PMT scans. The purpose of the home-made programs is to extract data and reformulate them so that they can be easily processed and interpreted to permit the obtention of additional information about the particle.

Once those programs will be mature enough, they will be included within the program that runs the data acquisition devices what would increase the particle counting rate, at most, double it (see Table 20) and spare the computer processor and memory place on the hard-disk.

For this purpose, all the programs were written in Labview 6.i (Austin, Texas, USA). The Labview 6.i programming environment has been chosen for compatibility reasons with other programs in the group of Prof. Zimmermann at the GSF-Forschungszentrum and because of its user friendly programming manner even if it is not the best choice for the manipulation large amount of data and for real-time applications.

Once the photomultiplier signals are stored and formated, they are first sorted as a function of the number of interpretable/identifiable peaks and then treated case by case. Two specific programs were developed to detect the peaks produced in the photomultiplier signal that can be often very noisy as particles cross the sizing laser beam.

- Peak detection method 1

Each peak of the photomultiplier signal is detected at a time named “peak detection time $t_{\text{peak detection}}$ ” as the voltage rises quickly within a short time. The digitized photomultiplier signal is subtracted from its running mean over the typical peak length (typically 25 μs). The resulting signal presents a very low noise level and reveals the peaks in the photomultiplier signal which can be related with a high probability to a particle light scattering event. The peak time detection $t_{\text{peak detection}}$ is the time when the subtracted signal level exceeds a given threshold set arbitrary which corresponds roughly to 1,5 time the maximum value of the noise level of the subtracted signal well before the first peak occurs.

- Peak detection method 2

The peak detection time $t_{\text{peak detection}}$ can also be determined by calculating for each data point the linear regression parameters of a signal portion corresponding to the typical peak rising time (typically 1 to 2 μs , here 1,5 μs). The occurrence of a peak is then detected by a sharp change, here the increase of the slope coefficient, of the line slope coefficients.

The peak detection method 1 was first developed and has been thoroughly tested. This method is therefore used for the detection of peaks in the photomultiplier signal in the rest of this work even if the peak detection method 2 gives acceptable results.

- Determination of the peak bottom time $t_{\text{peak bottom}}$ and peak top time $t_{\text{peak top}}$

Once a peak is detected, a procedure looks for the peak top after the peak detection time $t_{\text{peak detection}}$ and looks for the most probable peak bottom before the peak detection time $t_{\text{peak detection}}$ by looking respectively for the highest and lowest signal level reached after and before the peak time detection $t_{\text{peak detection}}$ within a characteristic time of the peak rising time (here 1,5 μs). The Labview program runs for any settings of the sampling time period of the digitizer as soon as it is 10 time smaller than the peak rising time.

Currently the Labview home-made programs record three different time of occurrence of a given peak. The peak detection time $t_{\text{peak detection}}$ (specific to the peak detection algorithm), the peak bottom time $t_{\text{peak bottom}}$ and peak top time $t_{\text{peak top}}$ are recorded. The two latter peak detection times can be determined only if the peak detection time is determined as previously explained. At this stage it is important to evaluate which type of peak detection time should be used for particle sizing.

The program that apply the Peak detection method 1 is tested with the photomultiplier signal of a short laser pulse from the nitrogen laser that has a pulse length of 8 ns. Such laser pulse lasts roughly 8 ns and is expected to occur within a time windows of 150 ns roughly 650 ns after the nitrogen laser is triggered. As a first test, the program should reproduces this feature. The distribution of values of the three types of peak time ($t_{\text{peak detection}}$, $t_{\text{peak top}}$ and $t_{\text{peak bottom}}$) is presented in Figure. 23 for the method 1. Figure. 23 represents the dispersion of the different peak times obtained by the program. It reproduces well the time dispersion of the laser trigger time window only if the parameter peak detection time $t_{\text{peak detection}}$ is considered. The other peak top time $t_{\text{peak top}}$ and peak bottom time $t_{\text{peak bottom}}$ present a much wider dispersion, respectively of $\sim 0,4 \mu\text{s}$ and of $\sim 0,5 \mu\text{s}$. The observation that the values are centered in Figure. 23(left panel) and Figure. 23(right panel) around 0,18 μs is due to the fact that the measured times were subtracted by the smallest measured time of the data set for graphical representation purposes.

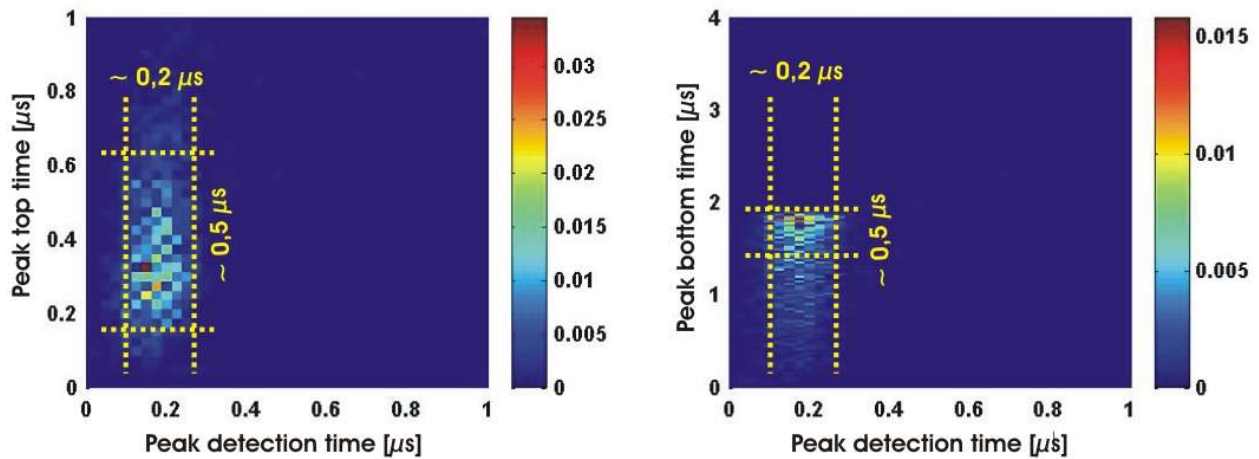


Figure. 23 : Accuracy of the different types of peak detection time.

Left panel: Normalized frequency of the peak top time $t_{\text{peak top}}$ for a given value of the peak detection time $t_{\text{peak detection}}$.
Right panel: Normalized frequency of the peak bottom time $t_{\text{peak bottom}}$ for a given value of the peak detection time $t_{\text{peak detection}}$. In both cases, the distribution of the peak detection $t_{\text{peak detection}}$ value (of $0,2 \mu\text{s}$) is much narrower than the peak top time $t_{\text{peak top}}$ value ($0,5 \mu\text{s}$) and than the peak bottom time $t_{\text{peak bottom}}$ value ($0,5 \mu\text{s}$).

On its side, Figure. 24 indicates that the program gets the peak detection time $t_{\text{peak detection}}$ with the method 1 at always the same relative peak height (between 50 and 60% of the peak height).

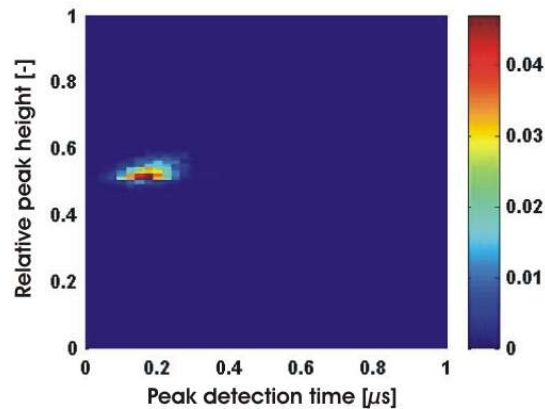


Figure. 24 : Relative peak height at the peak detection time

It represents the distribution of the relative height of the photomultiplier signal at which the peak detection time $t_{\text{peak bottom}}$ is determined as a function of the peak detection time. In most of the cases, the peak detection time occurs between 50% and 60% of the absolute peak height.

From Figure. 23 and Figure. 24, it is evident that the peak detection time $t_{\text{peak detection}}$ is the best quantity to mark the time of occurrence of a peak in the photomultiplier signal. Indeed the peak detection time $t_{\text{peak detection}}$ has the smallest dispersion and always detects a peak at half of its amplitude.

Once the peak is detected, the voltage level at the bottom, at the top and at the detection time,

respectively $V_{\text{peak bottom}}$, $V_{\text{peak top}}$, $V_{\text{peak detection}}$ are read in order to calculate the peak amplitude as follow:
 $V_{\text{peak amplitude}} = V_{\text{peak top}} - V_{\text{peak bottom}}$.

In the same manner, a peak rising time quantity is defined as the difference between the peak top time $t_{\text{peak top}}$ and peak bottom time $t_{\text{peak bottom}}$ such as $t_{\text{rising time}} = t_{\text{peak top}} - t_{\text{peak bottom}}$

It would be interesting to calculate the peak intensity (peak surface area) and to check if those values are consistent with the peak amplitude. If calculating the peak amplitude is easy, the peak integration remains tricky because of the determination of the integration limit in particular when the photomultiplier signal is very noisy.

The different peak characteristics described above can be compared in terms of peak occurrence time and amplitude for each photomultiplier and PMT scans. Considering these characteristics, all PMT scans can be classified according to different filters (i.e. sorting rules) as listed in Table 21.

<i>Filter Nr.</i>	<i>Purpose</i>	<i>Nb. Peak PMT 1a</i>	<i>Nb. Peak PMT 2a</i>	<i>Nb. Peak PMT 2b</i>
1a	Selects ideal particle sizing signal without signal from the DI laser	1	1	1
1b	Selects ideal particle sizing signal with signal from the DI laser	2	2	2
2a	Selects correct particle sizing signal without signal from the DI laser	1	1	0
2b	Selects correct particle sizing signal without signal from the DI laser	1	0	1
2c	Selects correct particle sizing signal with signal from the DI laser	2	2	1
2d	Selects correct particle sizing signal with signal from the DI laser	2	1	2
3	Selects signal attributed to noise "signal"	1	0	0
4	Coincidence signal (difficult to interpret)	>2	any	any
5	Other (due to Data acquisition failure, trigger problems)	0	any	any

Table 21 : Filter characteristics for the PMT scans

In the scope of this work, only PMT scans selected by filters Nr.1a and Nr.1b are considered. They permit the measurement of the particle time-of-flight, therefore its size, and the use of the photomultiplier signals from PMT2a and PMT2b to possibly infer optical properties of the single particles.

Filters Nr.2a, 2b, 2c, 2d permit also the sizing of the particle but the observed peaks can not be confirmed by the second parallel photomultiplier (PMT2a or PMT2b). This information can however be used for sizing purposes to a certain extent. Considering those signals increases the particle detection efficiency (PCE) and the particle sizing and analysis efficiency (SAE) but the extent in which the validity of the measured size distribution might be improved is still matter to question since the particle detection at the second laser is observed only for a sizing laser. A significant amount of scans obtained by these filters can practically be sorted by Filter Nr.1a or Filter Nr.1b by hand since peaks corresponding to particle can be clearly identified with a "human-eye" treatment whereas they can not be by the home-made program because the difference of the signal and its running mean is not big enough. Processing these PMT scans with the same program with slightly tuned parameters should permit their classification according to the Filter Nr.1a and Filter Nr.1b. It also shows that the peak detection algorithm is not pertinent enough yet.

The proportion of PMT scans from Filter Nr. 3 permits the evaluation of the quality of the whole

detection/sizing unit. It is to be used for the final adjustment of the sizing lasers. The smaller this proportion is, the better are the detection/sizing unit settings. The PMT scans from Filter Nr.4 are considered to be related to coincidence events while those from Filter Nr.5 are considered to be partly due to false triggers of the data acquisition and are not really explained.

The relative proportion of the PMT scans from Filter Nr. 2a, 2b, 2c, 2d to Filter Nr. 1a,b allows potentially the evaluation of the quality of the alignment of both sizing lasers relative to each other and to the particle beam. The more PMT scans are obtained from Filter Nr.1a,b compared to filter Nr. 2a,b,c,d the better should be the adjustments of the sizing lasers.

At this stage it is important to note that the program sorts the PMT scans according to the number of peaks in each photomultiplier signal and that it does not check the time consistency of the peak time occurrence.

Once the PMT scans are sorted in different directories according to their filter (or pattern) membership, a Labview 6.i routine specific to each case searches for the different peak times and voltage level and export them in a spread sheet data file that is ready to be processed by different specific MATLAB procedures (MATLAB 6.5.1, Natick, Massachusetts, USA) that plot the data in different manners. For example, every MATLAB home-made programs process only the particle data that meet the “time-of-flight consistency test”. Indeed it considers here only the data set whose measured particle time-of-flight lies between 20 μs and 120 μs since other values of the measured particle time-of-flight can not be related logically to a particle. These cases are simply ignored. Such feature will be in the future be included in the PMT scans Labview classification programs.

By sorting all the PMT scans according to the different filters, the inlet and the sizing unit can be characterized, the particle velocity (*in fine*, its size) and the particle size distribution, for example, can be measured.

5.2 Characteristics of the detection/sizing unit of the SPALMS instrument

The following section presents the performance of both the inlet unit and the detection/sizing unit in terms the particle counting efficiency (PCE) and rate (PCR) as well as the particle sizing efficiency (SAE) and rate (SR). The whole unit {inlet unit + detection/sizing unit} is then characterized according to the same criteria as for an usual particle sizer.

5.2.1 Particle identification from PMT scans

Before the inlet and the detection/sizing unit can be evaluated, it is necessary to evaluate in which “extent” the PMT scans and the related analysis software can identify typical photomultiplier signals from particles and how well particles can be counted and/or sized. Table 22 presents the classification score of the algorithm for ash particles. Similar scores were obtained for the other particles investigated such as PSL and soot particles.

From Table 22, it appears that the half (49,2%) of the particles are detected by all photomultipliers (Filter Nr.1a,1b) while a large fraction (34,7%) of the PMT scans recorded is difficult to interpret (Filter Nr.3,4,5). It means also that 65,3% of the PMT scans do correspond to a particle signal, which can be considered to be very acceptable considering the high noise level of 150 - 200 mV compared to the highest peak amplitude possible of 1,2 volts and the diversity of the photomultiplier signal shapes. In the cases where all PMT scans correspond in the reality to the number of detected particles, at least 65,3% can be correctly sized. According to this assumption,

the characteristics of the ensemble {inlet unit, detection/sizing unit} presented in the following sections can be scaled-up by a factor of $\sim 1,5$. However, further work is required to better understand the origin of the trigger of all unexplained PMT scans to define a better value of the scaling-up factor and more importantly, to make it get the value of 1 or 100%. Such problem is not specific to this instrument since similar remarks can be made for the APS3321 because the photomultiplier signal is processed electronically and the photomultiplier signal shape is sorted in four categories similar to those presented here (see manual of the APS3321, TSI Inc., St. Paul, MN, USA).

In the following, only PMT scans from Filter Nr.1a,b are taken into account since they offer the highest particle information potential.

<i>Filter Nr.</i>	<i>Proportion (%) of considered PMT scans</i>	<i>Number of considered PMT scans</i>
1a	36	8750
1b	13.2	3204
2a	2.5	596
2b	8.8	2139
2c	0.7	177
2d	4.1	996
3	9.5	2309
4	2.7	661
5	22.5	8644
Total	100	100 (24272)

Table 22 : Typical photomultiplier signal classification characteristics.

The half (49,2%) of the particles are detected by all photomultipliers (Filter Nr.1a,1b) while a large fraction (34,7%) of the PMT scans produced is difficult to interpret (Filter Nr.3,4,5).

5.2.2 Particle counting efficiency

To give an order of magnitude of the fraction of the aerosol particles that can be detected and sized by the detection/sizing unit, the particle counting efficiency (PCE) can be approximated geometrically by considering the intersection surface area of a cylinder (laser beam) and a disk of bigger diameter representing the aerosol beam cross-section as illustrated in Figure. 25 which also represents the geometry of the particle sensing volume in the aerosol mass spectrometer.

As mentioned above the laser has an approximative diameter at $1/e^2$ of $\sim 0,6$ mm as it crosses the particle beam. By a geometric calculation assuming that the particle beam has a diameter of roughly 300 μm at the nozzle exit and a half-divergence of $0,9^\circ$, it can be calculated that the particle beam has a diameter of about 0,74 mm and 1,1 mm when it crosses the first and second sizing laser.

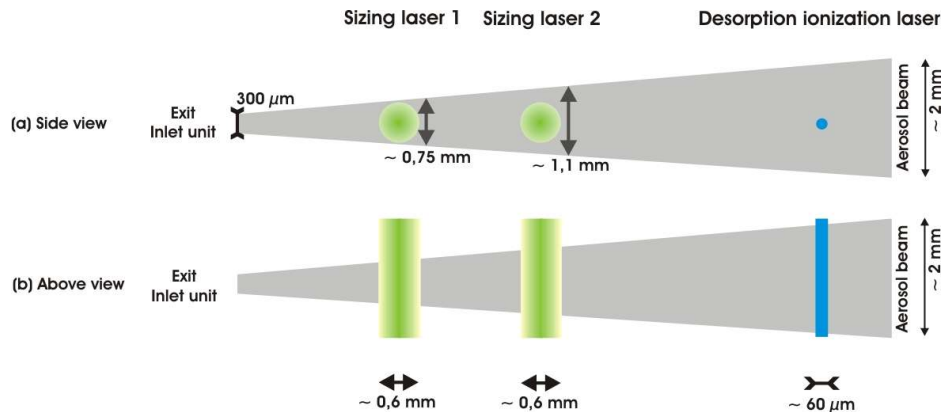


Figure. 25 : Particle sensing volumes of the different sizing laser beams.

The figure depicts the overlap of the different laser beams with the particle beam. **Panel (a):** Side view: particle beam overlap with the laser beams. **Panel (b):** Above view of the laser and particle beams overlapping.

It is clear that the sizing laser beam permits theoretically the detection of all particles. On its side, the small size of the desorption/ionization laser only allows the analysis of a small fraction of the sampled particles into the instrument.

If the particle concentration is uniform within the cross-section of the particle beam and if the symmetry axis of the laser beam and the particle beam intersect together, only 89% of the particles can be detected by the first sizing laser whereas 66% can be detected by the second one. If the particle concentration within the particle beam cross-section follows a Gaussian profile centered on the particle beam axis and the laser beam, one can expect to detect more particles.

5.2.3 Particle size detection limit

As in every particle sizing instrument, the SPALMS aerosol mass spectrometer can not detect every particle. If particle size distributions are measured, it is important to know the particle size detection limit, i.e., the diameter of the smallest and the biggest particle that can be detected. Since particles are optically detected, the size of the smallest detectable particle is strongly dependent on its optical properties, in particular its size, shape and refraction index, and on the quality of the particle detection system.

Figure. 26(a1),(b1), (c1) and (a2),(b2),(c2) show the particle velocity normalized frequency and the particle size distribution of standard PSL particles (Dukes Scientific, Palo Alto, CA, USA) with respective nominal geometric diameter of 1 μm and of 2 μm measured by the SPALMS and the APS instruments in parallel. The arrow indicates the particle velocity of the PSL 1 μm . It appears in Figure. 26(b2) that if particles smaller than 1 μm , labeled $P_{<1\mu\text{m}}$, can be well detected and sized by the APS compared to PSL 2 μm particles, the aerosol mass spectrometer detects such particles only in much smaller extent compared to the PSL 2 μm as presented in Figure. 26(a2). As a result the particle size detection limit of the SPALMS instrument is below 1 μm for PSL particles. A value of 0.8 μm can be taken as the lower detection limit. Particles smaller than 1 μm labeled $P_{<1\mu\text{m}}$ in Figure. 26 which appear frequently with PSL particles have an unclear origin.

The observed particle size distribution of the monodisperse PSL particles measured by the APS do not match the particle nominal size showing here a net underestimation (about -25%). No explanation is yet proposed for this if it is not due to a higher gas velocity in the APS nozzle nor due

to a diameter reduction from the particle aging (the PSL particles are 5 years old). It is however in the present study it is not relevant since particles were sampled simultaneously in parallel in both instruments and only comparisons studies were made.

At this stage, it is not possible to discriminate whether the particle size detection limit is due to the selectivity of the inlet unit or the sensitivity of the detection/sizing unit. Statistically, the current inlet unit (described in Chapter 4.) is expected to transmit small particles to the ion source if their initial trajectory before passing the nozzle orifice is parallel and close to the axis of the inlet unit. Considering the high noise level observed in the photomultiplier signals and the work of [Gälli et al., 2001] who reports the detection of particles as small as 120 nm with an unfocused similar sizing laser (532 nm, 23 mW), the particle size detection limit is very likely to be determined by the poor quality of the optical and signal processing part of the detection/sizing unit as clearly suggested in Table 17.

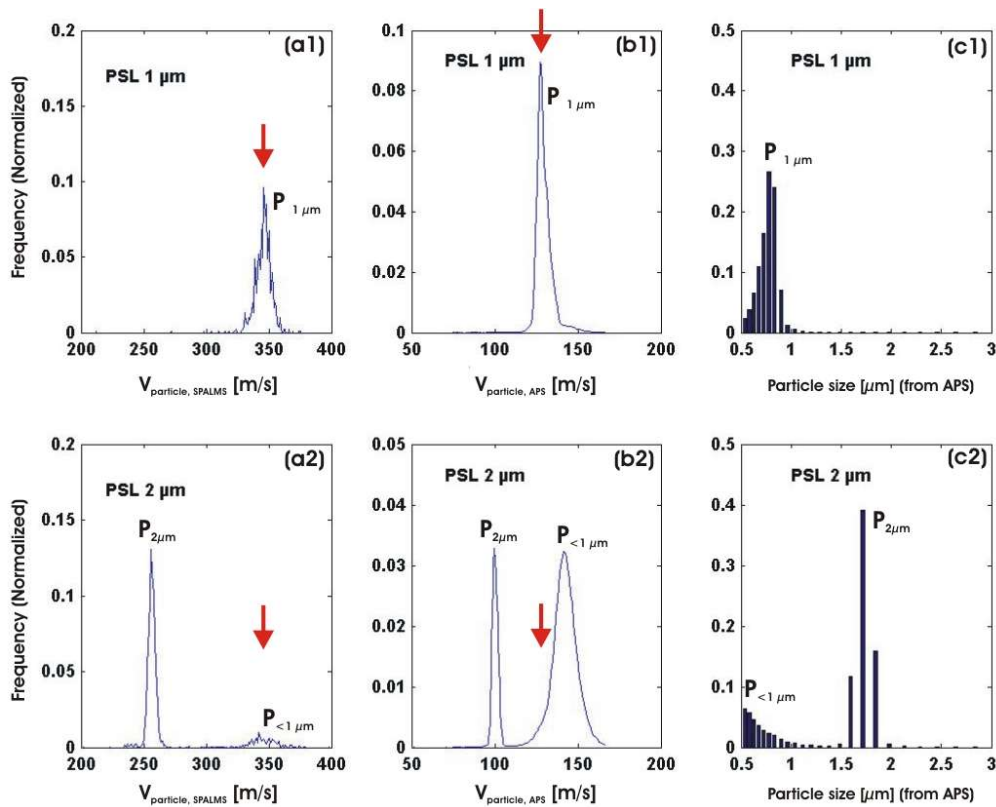


Figure. 26 : Particle size detection limit of the SPALMS instrument

(a1) Particle velocity distribution of PSL 1 μm particles measured with the SPALMS. **(b1)** Particle velocity distribution of PSL 1 μm particles measured with the APS. **(c1)** Particle size distribution of PSL 1 μm particles measured with the APS. **(a2)** Particle velocity distribution of PSL 2 μm particles measured with the SPALMS. **(b2)** Particle velocity distribution of PSL 2 μm particles measured with the APS. **(c2)** Particle size distribution of PSL 2 μm particles measured with the APS. The abbreviations $P_{1\mu\text{m}}$ refers to PSL 1 μm , $P_{2\mu\text{m}}$ refers to PSL 2 μm and $P_{<1\mu\text{m}}$ refers to unavoidable sub-micron particles, whose origin is unclear, associated with the PSL particles.

5.2.4 Counting rate

The particle counting rate (PCR) defined as dN/dt determines how fast particles can be counted. It has a direct influence on the resulting measured particle concentration and its size distribution. Indeed a low counting rate for a high particle concentration leads to an underestimation of the particle concentration. In the current setup the counting rate is determined by the particle time-of-flight between the sizing laser (from 20 to 120 μ s) and the speed of the data acquisition device (oscilloscope or digitizer) which either saves the 4 photomultiplier signals or directly interprets the particle photomultiplier signals as particle time-of-flight.

The counting rate appears to be here limited by the maximum acquisition frequency $f_{DAQ,max}$ of 7 Hz or 15 Hz according to the current acquisition device in the detection/sizing unit.

According to [Baron and Willeke, 2001], the counting rate dN/dt can be related to the sampling volume flow rate Q_v and the particle concentration c_0 by Eq. 10:

$$\frac{dN}{dt} = c_0 \cdot Q_v$$

Eq. 10

With a sampling flow of 2,75 liter per minute, the maximum apparent concentration $c_{app,max}$ that can be measured by the SPALMS is calculated by Eq. 11 to be 0,32 #/cm³.

$$c_{app,max} = \frac{dN}{dt} / Q_v = f_{DAQ,max} / Q_v$$

Eq. 11

5.2.5 Inlet efficiency

As discussed in Chapter 2., the inlet unit has a given transmission T that depends on the particle size. It is important to characterize the inlet efficiency for different particle sizes in order to relate the observed particle size distribution to the “real” particle size distribution of the aerosol.

The inlet efficiency IEF is defined here as the fraction of particles sampled by the instrument that are correctly sized. This quantity is a lumped quantity that depends on the inlet transmission T and the quality of the detection/sizing unit quantified by the particle sizing efficiency (SE). IEF is the equal to T.SE.

The inlet efficiency IEF can be approximated from geometric considerations if particles are assumed to be distributed uniformly over the whole particle beam cross-section and if the measured particle rate entering the instrument does not exceed 7 Hz. From Table 16 it can be inferred that only 0,5% of the particles reach the skimmer I and 6 % of those reach the ion source. Moreover from §5.2.2 the sizing unit can only size 66% of the particles that proceed to the detection/sizing unit. As a result, the inlet efficiency can be estimated to be equal to the product of 0,005, 0,07 and 0,66 what gives $2,3 \cdot 10^{-4}$. In other words only one particle out of 23000 can be sized.

In order to precise this order of magnitude, the inlet efficiency IEF was experimentally measured by operating the SPALMS in parallel with an APS for the particle size range of 0.5 to 4 μ m in the scope of our project.

The measured inlet efficiency (IEF) depends here on the particle sampling quality of the SPALMS and the APS instrument that serves as the reference/calibration instrument. The measured effective

inlet efficiency is presented in Table 23. In practice, the inlet efficiency IEF and inlet transmission T are often confused even if it is right when the sizing efficiency is known and equal to unity.

<i>PSL Particle diameter</i>	<i>Inlet efficiency (IEF)⁽¹⁾</i>	<i>Number of sampled particles (SPALMS / APS)</i>
0.5 µm	~ 3,5.10 ⁻⁴	219 / 3.4 10 ⁵
1 µm	~ 1,8.10 ⁻³	1974 / 604960
2 µm	~ 1,8.10 ⁻³	1213 / 363279
3 µm	~ 5.0.10 ⁻³	180 / 19538
4 µm	~ 1,5.10 ⁻²	39 / 1410

Table 23 : Inlet transmission for different PSL particle sizes

⁽¹⁾ In this case it is considered that the sizing efficiency is equal to unity so that the inlet transmission T is equivalent to the inlet efficiency IEF.

These inlet efficiencies for different PSL particles are consistent with the manufacturer technical data who reports an inlet efficiency of $>8.10^{-4}$ for 1 µm PSL particles and of $>10^{-6}$ for 0,2 µm PSL particles. This agreement was expected since the inlet unit was operated with similar pressures in each chambers (see Annex A) and the particles were detected during the manufacturer tests and in the present work at respectively 2,5 cm and 1,4 cm after the inlet exit..

The inlet efficiency values show that at most 1,5 % of the particle present in the air are sampled by the inlet unit for sizing purposes only. The observed high effective inlet efficiency for particle PSL 4 µm may be overestimated since only a small amount of PSL 4 µm was sampled by the SPALMS and the APS. The flow splitter used for this study was not adapted to isokinetic particle sampling. If it might not affect the results presented here for particles of 1 or 2 µm, the inlet efficiency might be underestimated here for 3 and 4 µm particles by a factor of 4 due to different gas flow velocities in the tubing to each instrument since the APS3321 samples 5 liter per minute whereas the SPALMS samples 2,75 liter per minute.

The measured inlet efficiency is for particles bigger than 1 µm one order of magnitude bigger than the estimated inlet efficiency based on geometry considerations. It suggests that the particle concentration is not uniform over the particle beam cross-section. The distribution can present, possibly, a bell or Gaussian shape.

Table 24 reports different inlet efficiencies for different similar nozzle-skimmers systems published in the literature.

<i>Reference</i>	<i>Inlet transmission efficiency T [-] (particle size [µm])</i>
[Van Wuijckhuijse, 2003]	0,00035 (0,7 µm) – 0,027 (1,1 µm) – 0,0075 (1,3 µm) 0,0164 (bacillus Thuringiensis 1-4 µm)
[Trimborn et al., 2000]	10 ⁻⁵ (PSL 0,2 µm) – 10 ⁻³ (PSL 0,8 µm)
[Hinz et al., 1994]	0,04 (for particle diameter 0,1-10 µm)

Table 24 : Inlet unit efficiency for different nozzle systems

The measured inlet efficiency differs from the reported inlet efficiencies in the literature for similar inlet systems in some cases up to one order of magnitude (4% compared to 0,2 % for a 1 μm particle). Compared to the other similar nozzle-skimmers units, the particle detection efficiency of the SPALMS reaches reasonable usual values.

The knowledge of the inlet efficiency permits the evaluation of the highest aerosol particle concentration that can be measured without significant coincidence biases for a given particle size.

In this regard, Eq. 11 can then be adapted by considering the inlet system efficiency E_{inlet,d_p} for a given particle diameter d_p as follow in Eq. 12:

$$\frac{dN}{dt} = c_o \cdot Q_v \cdot E_{\text{inlet},d_p}$$

Eq. 12

The maximum particle concentration $c_{\text{corr,max}}$ of a given size that the instrument can measure rigorously is then given by Eq. 13.

$$c_{\text{corr,max}} = \frac{\frac{dN}{dt}}{Q \cdot E_{\text{inlet},d_p}} = \frac{f_{DAQ,max}}{Q \cdot E_{\text{inlet},d_p}}$$

Eq. 13

For example, for PSL 1 μm , according to Eq. 13, the maximum particle concentration $c_{\text{corr,max}}$ reaches $\sim 750 \text{ \#/cm}^3$

Once the inlet efficiency IEF is known, it is then possible to operate the SPALMS instrument to obtain the particle size distribution of the aerosol as it is in the air. However its validity depends also on the particle size measurement accuracy as discussed below.

5.2.6 Accuracy of the particle velocity measurement

Particles are sized by measuring their terminal velocity after their acceleration in the inlet unit. The precision of the velocity measurement will determine the accuracy of the calibration curve which then determines the resolution and accuracy of the particle size.

It is interesting, but not mandatory if particles are to be sized only, to know where particles can be considered to have reached their terminal velocity. This is particularly important if the particle velocity is used to trigger the desorption/ionization laser. In this case, the particle velocity must be constant after its detection. According to [Hinz et al., 1996] and references therein, particles reach their terminal velocity at a certain distance after the second skimmer (here the plane skimmer). This is consistent with the observation presented in Figure. 14(1) which shows the accumulation of particles on the whole surface of the plane skimmer. It means that particles are still influenced (here deviated) by the air flow even at a pressure level as low as $5 \cdot 10^{-2}$ mbar. It is then possible to consider that particles are still accelerated at the exit of the second skimmer and possibly beyond it. Since the first sizing laser is located 14 mm after the exit of the inlet unit it is assumed at this stage that the particle has reached its terminal velocity since the gas passing through the last orifice has expanded just after. This can be checked, in a certain extent, by considering the chemical detection

time of the particle (time at which it gives a mass spectrum) as it is hit by the desorption/ionization laser and by comparing it to its detection time at the sizing laser 1 and 2. The measured times must be consistent with the relative position of the three lasers.

The velocity measurement depends not only on the accuracy of the particle time detection but also on the precise knowledge of the location where particles are detected. Indeed the particle velocity determination depends on the accuracy of the particle time-of-flight TOF_{sizing} and on its flight distance $L_{flight,sizing}$ between their detection times at both sizing lasers. Since the particle velocity is given by Eq. 14, the uncertainty of the particle velocity measurement can then be evaluated as follow by Eq. 15.

$$V_p = \frac{L_{flight,sizing}}{TOF_{sizing}}$$

Eq. 14

$$\frac{\Delta V_p}{V_p} = \frac{\Delta L_{flight,sizing}}{L_{flight,sizing}} + \frac{\Delta TOF_{sizing}}{TOF_{sizing}}$$

Eq. 15

- Measurement of the particle flight distance $L_{flight,sizing}$

The particle flight distance depends on the distance between both sizing laser beams and on the position of the particle in the laser beam as it is detected. In practice the particle location that should be considered is its position in the laser beam when the photomultiplier signal processing unit returns a time mark that indicates its detection.

Both sizing lasers are distant from each other by a nominal distance of $d_{sizing\ lasers}$ of 12 mm. The distance is constrained by the fact that both laser beams pass through a serie of diaphragm orifices that are distant from exactly 12 mm and that have each a diameter of 2 mm. Each laser beams have a nominal diameter measured at $1/e^2$ of the intensity distribution of 0,4 mm and a measured diameter that is of roughly 0,8 mm. The position of each laser beam is then known within 0,6 mm. It results that the sizing laser distance is known to be 12 mm +/-1,2 mm (i.e. within 10%).

The determination of the particle flight distance $L_{flight,sizing}$ requires also to know where the particles are detected within the laser beam, especially if the laser beam is wide (as when it is unfocused for example). For an equivalent illumination of the particle, small particles will scatter less light than bigger ones. If the light intensity distribution within the laser beam is considered to follow Gaussian distribution in a first approximation because the sizing lasers are operated in TEM_{00} mode, small particles will be detected in a smaller area than bigger particles. The detection location of particles within the sizing laser beam is therefore more accurate for small particles than for bigger ones. This is a consequence of the problem denominated “trajectory effect” by [Grehan et Gouesbet, 1986], which is illustrated in Figure. 27.

Considering a radial symmetry of the laser intensity distribution within the beam cross-section, one can consider that all particles will be detected within a half-diameter of the sizing laser beam, i.e. here within 0,4 mm. Since the particle beam has a half-angle divergence of 0.9° , the difference in the particle flight distance along the particle beam axis and its external side in the plane of both

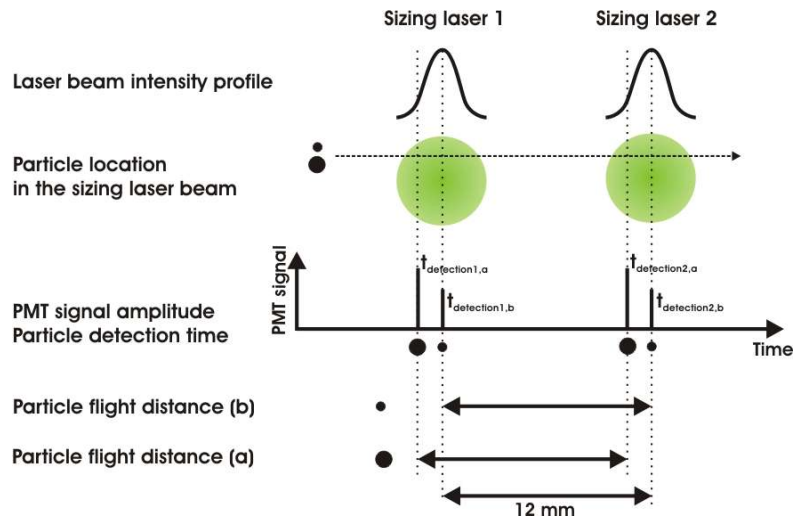


Figure. 27 : Influence of the trajectory ambiguity effects on the particle sizing

This figure shows that particles of different sizes are not necessarily detected at the same location within the laser beam. Since it occurs for both sizing lasers, it has for consequences that the measurement of the particle time-of-flight and the time of the detection of the particle at the first sizing laser are size-dependent.

sizing lasers is of $1,5 \cdot 10^{-3}$ mm which is totally negligible compared to the error induced by the “trajectory ambiguity effects” of 0,4 mm.

As a result in the absolute, the particle flight distance $L_{\text{flight sizing}}$ varies between 10,8 and 13,6 mm. The particle flight distance is known in the absolute within 2,8 mm, i.e. 23% of the nominal sizing laser distance $d_{\text{sizing laser}}$. However during the aerosol mass spectrometer operation, once both sizing lasers are ideally adjusted, the flight distance $L_{\text{flight sizing}}$ is known within 0,4 mm (a half-sizing laser beam diameter), i.e. 3% of the nominal sizing laser distance. It means that the calibration curve should be regularly checked to take into account an eventual drift of the sizing laser distance $d_{\text{sizing laser}}$ as presented in Figure. 28.

- Measurement of the particle time-of-flight $\text{TOF}_{\text{flight}}$

The accuracy of the particle time-of-flight measurement between both sizing lasers depends on the quality of the detection unit. Table 25 presents the typical measured particle time-of-flight for different PSL particles. The smallest and biggest values that contain more than 85% of the measured velocity are tabulated with their difference in parenthesis. The particle time-of-flight $\text{TOF}_{\text{sizing}}$ dispersion depends on the method used to determine the peak detection time $t_{\text{peak detection}}$. As mentioned before, the peak detection time $t_{\text{peak detection}}$ is used because of its reliability. The typical dispersion of the particle time-of-flight values is in this case of $1,5 \mu\text{s}$ and appears to be surprisingly independent of the particle size.

It is important to note that a part of the low accuracy of the $\text{TOF}_{\text{sizing}}$ measurement is here due to the trajectory ambiguity effect since there were until now no means to reduce it. Considering this, the particle velocity accuracy available with the current detection/sizing unit can be then computed. The contributions of the different parameters are presented in Table 26.

5. Detection/sizing unit

<i>PSL Particle nominal size</i>	<i>“Peak top time” method [μs]</i>	<i>“Peak detection time” method [μs]</i>	<i>“Peak bottom time” method [μs]</i>
1 μm	31,8 – 34,9 (3,1)	32,7 – 34,2 (1,5)	32,2 – 34,8 (2,6)
2 μm	43,5 – 46,5 (3)	44,2 – 45,8 (1,6)	44,2 – 46 (1,8)
3 μm	52,4 – 54,5 (2,3)	52,6 – 54,2 (1,6)	52,5 – 55 (2,5)
4 μm	60,5 – 62,2 (1,7)	60,5 - 62 (1,5)	59,6 – 62,8 (3,2)

Table 25 : Accuracy of the measured particle time-of-flight between both sizing lasers for PSL particles

The smallest and biggest particle time-of-flight values between which lay more than 85% of the measured particle velocities are tabulated with their difference in parenthesis

<i>Particle type</i>	<i>Typical TOF_{flight} [μs]</i>	<i>Contribution of the time measurement uncertainty (%)</i>	<i>Contribution of the sizing laser distance uncertainty (%)</i>	<i>Contribution of the trajectory ambiguity effect (%)</i>	<i>Relative particle velocity accuracy [%] (“absolute”)</i>	<i>Relative particle velocity accuracy [%] (“in operation”)</i>
PSL 1 μm	33	4,5	23.3	3	27.5	7.5
PSL 2 μm	45	3,3	23.3	3	26.6	6.3
PSL 3 μm	53	2,8	23.3	3	26.1	5.8
PSL 4 μm	61	2,4	23.3	3	25.7	5.4

Table 26 : Contribution of different parameters to the accuracy of the particle velocity measurement

It appears that the particle velocity measurement accuracy is mainly limited by the uncertainty of the determination of the flight distance which depends in particular on the uncertainty of the measurement of the sizing laser distance. It is interesting to note that [Weiss et al., 1997] report similar results with a different detection/sizing unit design.

The measured particle velocity is absolutely known within 28%. Once the sizing laser distance is set, the particle velocity accuracy can be estimated to be 8%. It means that particles whose velocity differs from more than 8% can be considered to be aerodynamically different. This points out the necessity of regularly checking the sizing laser distance with monodisperse particles to avoid a bias in the particle velocity measurement as presented in Figure. 28. Doing this allows the uncertainty to be kept exclusively dependent on the detection location of the particle in the laser beam and the time-of-flight measurement. It implies here that the sizing laser distance $d_{\text{sizing laser}}$, which drift with time due to vibrations in the instrument, has to be particularly reduced, if not eliminated.

Values reported in Table 26 do not report the diminution of the contribution of the trajectory ambiguity effect as the particle size decreases since it was only estimated from the half-width of the laser beam where the particle is surely detected. It is in fact difficult, if not impossible, to evaluate where the particle is detected in the laser beam since it depends on the particle optical properties (size, refraction index and shape) and on the sensitivity of the whole detection optical unit and data processing.

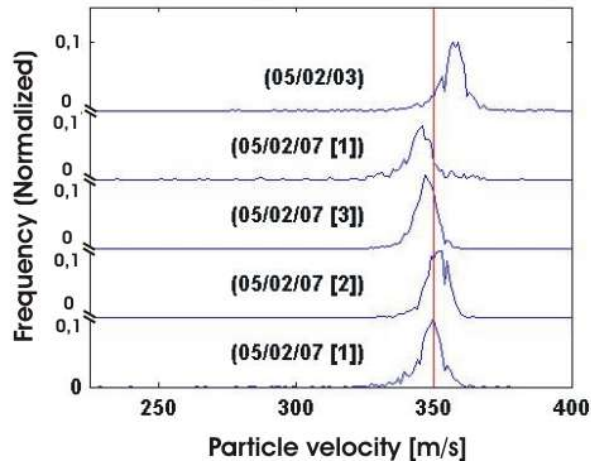


Figure. 28 : Particle velocity variations due to the drift of the sizing laser distance for PSL 1 μm particles.

The different curves correspond to different measurements performed at different times of the day 7/2/2005 and day 3/2/2005 where the distance between both sizing lasers has slightly varied.

A higher accuracy in the particle velocity measurement can be reached by first making the sizing unit more robust and isolated from vibrations, by reducing the photomultiplier noise signal, by focusing tighter the sizing lasers and by increasing the sizing laser distance $d_{\text{sizing laser}}$. Spacing the laser beams will reduce the uncertainty on the particle flight distance $L_{\text{flight, sizing}}$ and its time-of-flight $\text{TOF}_{\text{sizing}}$ measurement. Due to geometric constraints and to the large particle beam divergence, the latter solution can not be considered so that particle velocity accuracy improvements can only be achieved through the three other former propositions.

Once the particle velocity has been measured, the obtained particle velocity can be related to the particle aerodynamic diameter via a calibration curve which has to be experimentally determined.

5.2.7 Sizing unit calibration

A calibration curve for the aerosol mass spectrometer for PSL particles that relates the particle velocity to the nominal geometric particle diameter can be calculated from experimental data as presented in Table 12. The most frequent particle velocity for each particle size is used to evaluate the calibration curve. The calibration is here evaluated as a polynomial of the third degree as presented by Eq. 16 and proposed by [Gälli et al., 2001] who also weight each coefficient a_i to the number of data points and the standard deviation of the measured velocity for a given particle size.

$$d_{p,g} = \sum_{i=0}^3 a_i \cdot V_p^i$$

Eq. 16

with $d_{p,g}$ as the particle geometric diameter in [μm] and V_p as the particle velocity in [m/s]. The different a_i coefficients have the following values $a_0 = 29.9394$, $a_1 = -0.24577$, $a_2 = 7.2676 \cdot 10^{-4}$ and $a_3 =$

$7.4315 \cdot 10^{-7}$. The calibration curve is presented in Figure. 29. The curve is calculated by associating the most frequent measured particle velocity (sorted in bins of 1 m/s width) for a given particle size to its nominal geometric diameter. The confidence of the validity of the polynomial fitting coefficients has not been evaluated as [Galli et al., 2001] did. The confidence is here estimated as satisfactory by taking the most frequent measured particle time-of-flight TOF_{sizing} . Due to the drift of the sizing laser distance, the calibration has to be regularly checked with monodisperse particles (such as PSL 1 μm and PSL 2 μm). Such calibration curve after Eq. 16 is valid only for particles of similar shape and density.

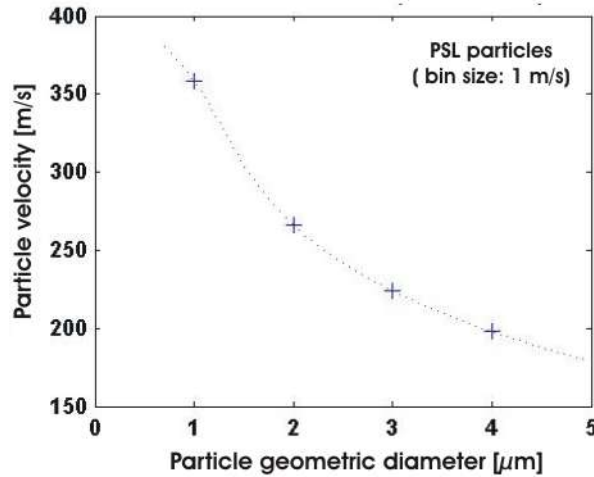


Figure. 29 : Detection/sizing unit calibration curve

$$d_p = f(V_{particle})$$

Other authors such as [Weiss et al., 1997] and [Van Wuijckhuijse, 2003] propose to include the density in the calibration curve as follow:

$$TOF_{flight} = V_p \cdot L_{flight, sizing} = b_0 \cdot \sqrt{(1 + b_1 \cdot d_{p,g} \cdot \rho_p^m)}$$

Eq. 17

with b_0 , b_1 and m as fitting parameters. Since only particles of identical density have been used for the calibration of the detection/sizing unit, the rest of this work will only consider the calibration curve computed after Eq. 16.

Once the calibration has been determined, it is possible to evaluate the particle sizing resolution of the detection/sizing unit.

Considering that particles whose velocity differs from more than 8% are different, PSL particles of diameters of 1,1 μm and 1,7 μm , 3,5 μm and 5,3 μm can be aerodynamically differentiated with a high level of confidence. The poor size resolution is due to the uncertainty in measuring the particle flight distance $L_{flight, sizing}$ and the particle time-of-flight TOF_{sizing} accurately.

The APS provides with its manufacturer calibration curve a better size resolution. Indeed, the APS

5. Detection/sizing unit

provides 8 size bins (1,037 / 1,114 / 1,197 / 1,286 / 1,382 / 1,486 / 1,596 / 1,715 in [μm]) between 1,1 and 1,7 μm and 8 size bins (3,278 / 3,523 / 3,786 / 4,068 / 4,371 / 4,698 / 5,048 / 5,425 [μm]) between 3,5 and 5,3 for PSL particles. This means that each particle size class can be clearly distinguished from each other and that the uncertainty velocity measurement is smaller for the APS than for the SPALMS instrument. Indeed 8 particles size classes are identified by the APS for only one for the aerosol mass spectrometer for the same size range. The higher accuracy of the particle velocity measurement by the APS is made necessary by the fact that particle velocities are distributed over a narrower range of values than that measured by the aerosol mass spectrometer. This is surprising since the aerosol mass spectrometer better differentiates aerodynamically particles from each other due to its higher carrier gas velocity. This particularly points out the dramatic need of reducing the uncertainty of the particle velocity measurement in order to take full advantage of the larger particle acceleration by the sonic gas flow of the SPALMS instrument that permits a better, from the instrument design, particle size resolution.

Once the SPALMS instrument has been calibrated in order to size particles, one can check the ability of the instrument to detect particle concentration changes in number or/and size distribution.

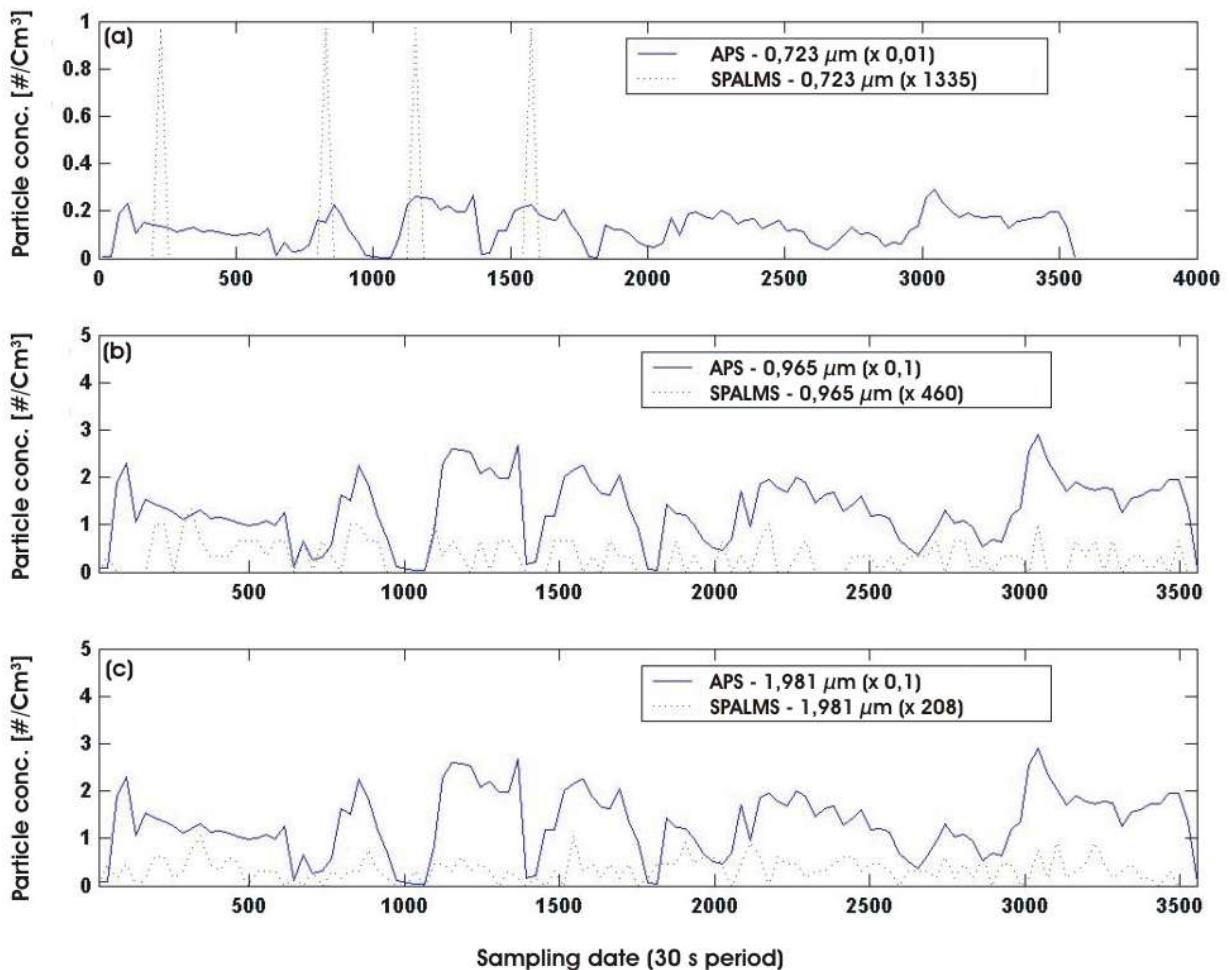


Figure. 30 : Variation of ash particle concentration in air measured with the APS and SPALMS instrument

Panel (a): Particle concentration time profile at $d_p = 0,723 \mu\text{m}$. **Panel (b):** Particle concentration time profile at $d_p = 0,965 \mu\text{m}$. **Panel (c):** Particle concentration time profile at $d_p = 0,965 \mu\text{m}$.

5.2.8 Particle concentration variation

In spite of the low inlet transmission efficiency T and the small particle detection rate, the SPALMS instrument can reproduce particle concentration time variations for a given particle diameter that is measured by the APS. This is possible only when enough particles can be detected per time unit by the aerosol mass spectrometer. Figure. 30 presents the case of a measurement of ash particles during a one hour measurement. The measured concentration by the APS lies in the range 0 to 100 #/cm³. The particle concentration variation observed by the SPALMS instrument and the APS are in agreement together in particular for big particles (here for 0,965 μm and 1,981 μm). The apparent measured concentration by the SPALMS instrument is a factor 2000 to 5000 lower for particles of diameter 0,965 μm and 1,981 μm what is consistent in order of magnitude with the inlet efficiency IEF measured with PSL particles as reported in Table 22.

For smaller particle sizes, the agreement is not obvious. The poor agreement has to be related to the low inlet efficiency and the poor particle size detection limit of the inlet/detection unit.

As a result, the SPALMS instrument can reliably detect changes in particle concentration down to 100 #/cm³ for particle sizes down to 1 μm . At high particle concentrations, coincidence phenomena and low data acquisition speed affect the measurement of the size distribution of the aerosol. Data acquisition of photomultiplier signals provides a mean to evaluate the occurrence of coincidence events whose principle is described in the next section.

5.2.9 Particle coincidence

Coincidence events result from errors in tracking particles as they are detected by both sizing lasers. Their probability increase as the particle concentration to be sampled increases and as the distance between both sizing laser beams increases. It occurs when many particles cross the first sizing laser before one of those is first detected at the second sizing laser. As an example in Figure. 31, if the particle (a) crosses the second laser after the particle (b) is detected by the first sizing laser (Case 1) or particle (b) crosses the second sizing laser before the particle (a) detected the first at the first sizing laser (Case 2), there is a “coincidence event”. Since there is no means to identify which particle (a) or (b) has crossed the first the second sizing laser, particles (a) and (b) can not be sized reliably. If one particle scatters much more light than the other, it might be possible to resolve the “coincidence event”. On the other hand, both in case 1 and 2, the particle (c) can be reliably sized since there is not coincidence.

It is normal that coincidence events occur. It is however very important to attempt to avoid them by a clever instrument design and by attempting to discriminate “normal sizing events” from “coincidence events”.

Indeed, coincidence events affect the validity of the measured particle size distribution and affect the aerosol mass spectrometer particle chemical analysis efficiency (CAE) and rate (CAR) in static and dynamic trigger mode by triggering erroneously the desorption/ionization laser. For the latter effect, coincidence has to be reduced by the design of the instrument, by making the sizing laser distance $d_{\text{sizing laser}}$ small and by operating the SPALMS instrument at low aerosol particle concentration.

The former effect can also be either treated by using three lasers and analyzing the resulting particle detection times (later referred as “three laser method”) or by smartly processing numerically the PMT scans as will be described later in Chapter 13.

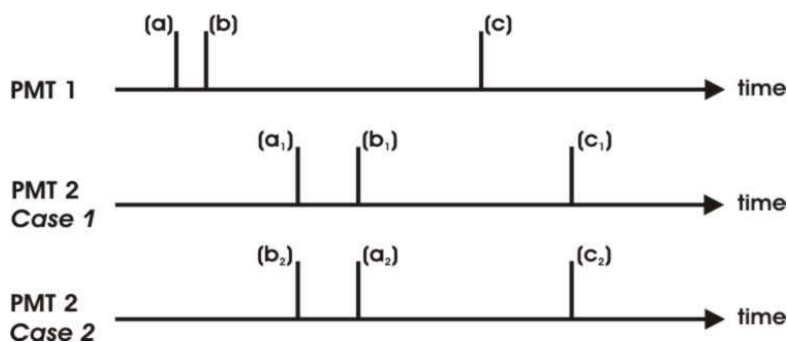


Figure. 31 : Coincidence principle

This figure represents the photomultiplier signals for the sizing laser 1 and 2, respectively noted PMT1 and PMT2 as particles are detected. In the time window, three particles (a), (b) and (c) are detected successively by the photomultiplier PMT1. The photomultiplier signal (PMT2) is difficult to interpret since two possibilities arise: in Case 1, the first particle detected (a₁) corresponds to the particle (a) detected in PMT1. This is a coincidence event since the PMT1 detects another particle (b) before. In Case 2, the first particle detected on PMT2 (b₂) corresponds to the particle (b) which arrives at the second sizing laser before the particle (a) and was detected before by the PMT1. This is also a coincidence event. On the other hand, the particle (c) does not induce any coincident event since the PMT1 does not detect any particle before the particle (c) reaches the second sizing laser after its crossed the sizing laser 1.

In this “three lasers method”, the desorption/ionization laser (that can be in principle either continuous or pulsed) is used as a third particle detection laser. The particle is detected as it produces a mass spectrum. The particle detection time at each laser are recorded and then compared together: the first particle detection time obtained for the second sizing laser and the desorption/ionization laser after a particle has been detected by the first sizing laser are considered and compared together. Since the particle velocity is constant over the distance between the first sizing laser and the desorption/ionization laser, the particle detection times must be consistent with the relative distances between each laser beam. If not, it means that the particle detected by the second sizing laser or the desorption/ionization laser is not the same as the particle detected by the first sizing laser. In this case, there is a “coincidence event”. With this method, the particle size distribution can then be corrected by eliminating the coincidence cases from the data set.

This method can be extended by implementing additional continuous sizing lasers instead of a desorption/ionization laser as undertaken by [Franck et al., 2005]. The different detection time at each sizing laser crossings are retrieved by a specific software that can state for each particle detection signal if it should be related to a coincidence event or not.

This principle is also valid for pulsed desorption/ionization laser. In this case, the frequency of coincidence events will be highly underestimated due to the fact that the desorption/ionization laser only operates at a slower rate than the particle detection rate. For example, for a nitrogen desorption/ionization laser, the particle beam is only illuminated 160 ns (there is at most 20 light pulses of 8 ns length per second) over one second one measurement, i.e. $1,6 \cdot 10^{-5}$ % of the time. As a result, one can not reasonably quantify coincidence events taking place in the detection/sizing unit. It allows at least to check that a particle that gives a mass spectrum has been sized correctly.

An other data analysis approach can be applied to quantify the coincidence events in a certain

extent. Since it requires an ideal particle photomultiplier signal, the method will be presented later in Chapter 13.

5.2.10 Particle sizing by light scattering

The particle can also be sized by considering the amount of scattered light as operated by optical particle counter instruments (OPC instruments) ([Baron and Willeke, 2001]). The detection/sizing unit of the SPALMS instrument has indeed the possibility to record a measure of the amount of the detected scattered light which should permit the measurement of the particle size as well.

Indeed Figure. 32 shows that PSL particles of 1 μm , 2 μm , 3 μm and 4 μm can be differentiated from each other with the SPALMS instrument by considering only the scattered light as can be done

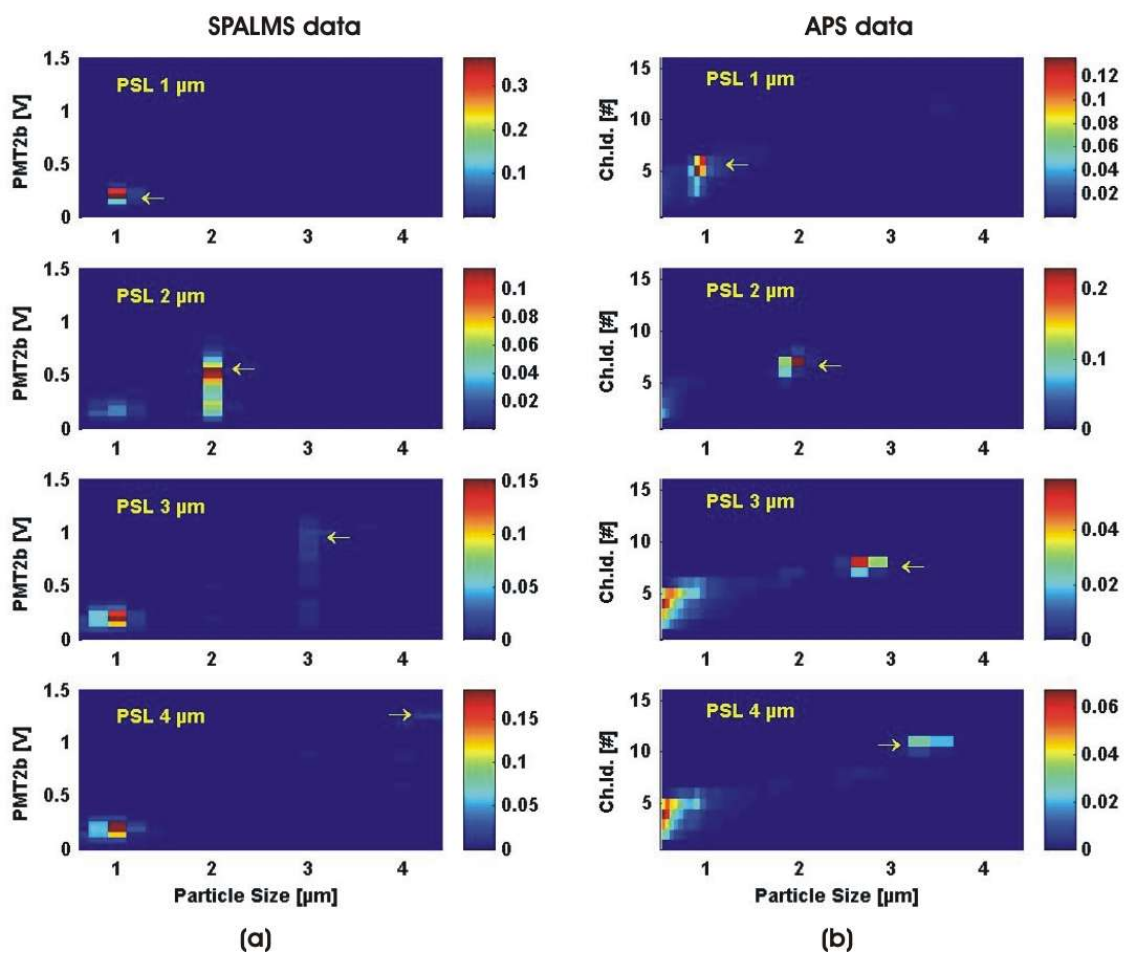


Figure. 32 : Optical particle sizing with the APS and the SPALMS instrument

Panel (a): Photomultiplier PMT2b particle signal amplitude (in V) of the SPALMS instrument for different PSL particle sizes (1 μm , 2 μm , 3 μm , 4 μm) as a function of the particle size (in μm). **Panel (b):** Particle scattered light collected by the photomultiplier of the APS expressed in Channel Id (Ch. Id. [#]) for different PSL particle sizes (1 μm , 2 μm , 3 μm , 4 μm) as a function of the particle size.

It is important to note here that the amount of scattered light is not represented in the same manner. The APS sorts the amount of scattered light in 16 bins whereas the SPALMS photomultiplier signal corresponds to the output voltage of the photomultiplier DA socket.

with an APS3221 operated in correlated mode. Scattered light measurements have a much larger dispersion than the particle velocity ones so that the particle size is less accurately measured optically than aerodynamically. The low dispersion of the scattered light values from the APS are due to the binning in 16 channels of the scattered light measured by the APS whereas it is not the case for the SPALMS instrument. In the case of the aerosol mass spectrometer measurements, this large dispersion is mainly due to the high noise level of the photomultiplier signal and due to the location where the particle crosses each sizing laser (“trajectory ambiguity effects”). The latter effect causes the particular pattern of the photomultiplier signal: the photomultiplier voltage ranges from 0V to a maximum value which is dependent on the particle size. This observation is consistent with similar measurements reported in [Moffet et Prather, 2005]. The absence of such effects for the APS instrument tends to indicate that the optical setup for the particle detection reduces efficiently the “trajectory ambiguity effect” by for example using a narrow laser beam (~ 90-100 μm). It should nevertheless be mentioned that the binning method to record the detected scattered light by the APS is not known. It is in particular not known if the “trajectory ambiguity effect” is treated.

The difficulty of precisely sizing the particle optically compared to the aerodynamic sizing is confirmed for salt particles of size of 1 μm , 2,1 μm and 3,2 μm by [Salt et al., 1996] and partly from [Kievit et al., 1996].

However, considering these uncertainties, it is satisfactory to note that the detection/sizing unit in its current state is able to reproduce the features of the APS.

5.3 Improvement possibilities

In the previous sections and chapters, it has been shown that the inlet unit and detection/sizing unit is operational and that some improvements would greatly improve the performances of the SPALMS instrument. Some improvements are proposed in the next paragraphs.

5.3.1 Current nozzle inlet unit

The inlet unit samples in the best cases less than 0,2 % of the particles of the aerosol. To reach a better representativity, the sampling efficiency (i.e. the inlet efficiency T) has to be increased.

The improvement of the current nozzle inlet unit can be achieved by first reducing the internal angle of the nozzle significantly to make the gas stream converging slowly to the nozzle orifice. This will bring slowly particles with higher inertia and those close to the nozzle walls through the nozzle orifice with a higher probability. This will also lead to a smaller particle loss due to the reduced impaction within the nozzle walls before its orifice.

Moreover the different orifices can be positioned closer together while being careful to conserve the appropriate pressure ranges in each chamber. Indeed the efficiency of the pumps to produce the vacuum in each chamber of the inlet unit decreases as the spacing distance between the nozzle and skimmers decreases. As the nozzle and skimmers orifices are close together, the aerosol beam after each orifice will be more concentrated in particles when it reach the next skimmer. The possible drawback here could be a quicker clogging of the inverted skimmer due to a higher amount of particle landing on its orifice edge.

A known alternative to nozzle inlet systems is to use aerodynamic lenses as was discussed in Chapter 2. and will be discussed in the next paragraph.

5.3.2 Aerodynamic lens

The aerodynamic lens, firstly developed by [Liu et al., 1995a] and [Liu et al., 1995b] brings a satisfactory answer to the quest of efficient inlet systems for aerosol mass spectrometers. Aerodynamic lenses consist of a series of thin distant plates mounted in serie within a housing tube. The housing tube is terminated by a nozzle which accelerates the particle. At each lens, consisting of a thin plate with an aperture, the gas flow will first converge and then expand. At each convergence/expansion, the carrier gas brings particles always closer to the aerodynamic lens axis of the lens as presented in Figure. 33.

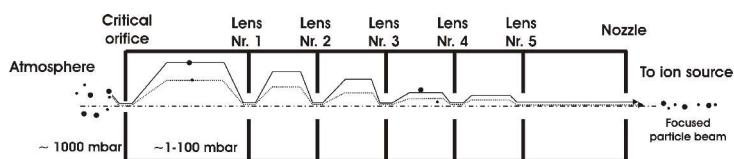


Figure. 33 : Aerodynamic lens principle

An aerodynamic lens consists of a series of apertures (denominated "lens") of decreasing diameter mounted in a housing tube. At each lens, spaced from each other by a given distance, the particle carrier gas undergoes a compression/expansion that modifies the particle trajectory. According to their inertia, particles are step by step (from left to right) brought close to the aerodynamic lens axis to form a thin particle beam.

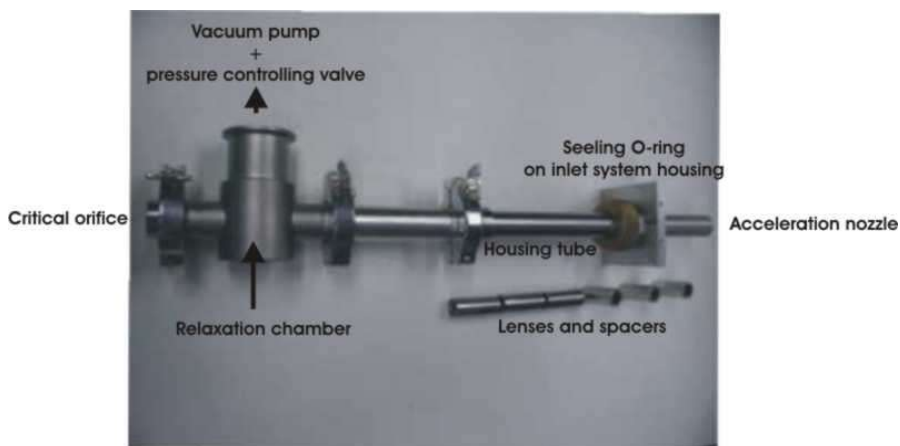


Figure. 34 : Aerodynamic lens built at GSF-Forschungszentrum

The critical orifice samples the aerosol from the atmosphere, controls the sampling flow rate and reduces the pressure to some mbars in the inlet unit. The relaxation chamber permits the expansion of the air and the particles sampled by the critical orifice to relax, i.e., slow down. The housing tube holds the different lenses which are maintained distant by the spacers. The aerosol particles flow from the relaxation chamber to the acceleration nozzle through the series of lenses which each focuses the particles into a thin beam. The acceleration nozzle permits then to impart a size-dependent velocity to the exiting particle.

An aerodynamic lens has been designed at the GSF-Forschungszentrum which still needs to be tested and implemented. Figure. 34 presents the designed aerodynamic lens. Details are presented in Annex A-3.

However, its interest is usually limited by the low desorption/ionization laser firing frequency and low data acquisition speed.

The advantages of aerodynamic lenses are of three types:

- Unity inlet transmission T over a wide range of particle sizes
- Ability to focus particles in a very thin beam down to hundreds of micrometers. This feature is very advantageous in that it will locate *de facto* particles more precisely and more reproducibly in the different laser beams. Moreover scattered light signals will then be easier to analyze since the “trajectory ambiguity effect” will be dramatically reduced.
- Ability to sample very small particles (few 10s of nanometers) efficiently. It is of particular interest for investigating soot particles from combustion processes.

5.3.3 Particle detection unit

Considering the quality of the photomultiplier signal, the electronic processing of the signal and the home-made data analysis programs, the current detection/sizing unit permits the operation of the SPALMS instrument in a routine manner to size aerodynamically the particles and fire the desorption/ionization laser in a static manner only.

As showed earlier, the transduced scattered light signal by the photomultiplier into an electric pulse does not reflect clearly the residence time of the particle in the sizing laser beams and contains a high noise level (up to 200 mV compared to less than 50 mV in the best cases) if the laser adjustments are not appropriately done. This leads to a difficult interpretation of the photomultiplier particle signal, to a bad particle size detection limit and to random unnecessary shots of the desorption/ionization laser.

It appears that an important part of the noise of the photomultiplier signal comes from the residual light which reaches the photomultipliers. It originates from the scattered light of the sizing laser beams on the diaphragm edges and on windows of the ion source. This light is to be eliminated or blocked by redesigning the sizing laser beam paths or, more globally, the way to bring the sizing laser light to the sensing volume of the detection/sizing unit.

Another problem to address is the photomultiplier response to a short light pulse that appears to be asymmetric with a sharp rise time as the particle is detected and a long tail that lasts up to 30 μs . It might be related to an unadapted frequency bandwidth of current-to-voltage transformer. Since the photomultiplier has a nominal time response of 2,2 ns with an electron transit time of 22 ns (time between the light pulse and the emission of the photocurrent) and the particle has a residence time of a few microseconds in the sizing laser beam, the photomultiplier must be able in principle to capture and reproduce the scattered light intensity variation obtained as the particle crosses each sizing laser. It appears that the current-to-voltage transducer has a bandwidth from 0 to 10kHz. It means that the transducer reproduces correctly the photomultiplier signal only if its variation occurs in a time longer than 100 μs what is 50 times longer than the particle scattering light characteristic time which corresponds typically to the particle residence time τ_{particle} in the sizing laser beam of a few μs . A solution to the problem is to replace the current current-to-voltage transducer by a current-to-voltage transducer with a more appropriate frequency bandwidth.

Another explanation of this photomultiplier signal behavior could also be a local and temporary saturation of the photocathode. In this case, the photocathode might need some time to release the sudden high quantity of emitted electrons. Indeed the collected scattered light by the collimator and the optical fiber is illuminating only 8,3% of the sensitive surface of the photomultiplier. A solution to the problem would be to make the light diffuse, either by softly polishing the exit of the optical fiber or by increasing the distance between the exit of the optical fiber and the photomultiplier sensitive surface in order to use the whole sensitive surface of the photocathode.

5.3.4 Hardware solutions for the elimination of the “trajectory ambiguity effect”

For better taking advantage of the amount of the light scattered by the particle as it crosses the sizing laser beams, the “trajectory ambiguity effect” should be reduced. A data analysis solution is presented in Chapter 13 in this work but it can also be solved by rearranging the current optical setup of the detection/sizing unit. The “trajectory ambiguity effect” is caused here by the diameter of the particle beam and/or by the large diameter of the sizing laser beam within which the energy is not uniformly distributed.

As mentioned before, “trajectory ambiguity effects” can be reduced by reducing the particle beam width so that the particles are always crossing the laser beam at the same place if their relative positions do not move. In this case, particles are always illuminated the same way. This has the advantage of not modifying the current detection/sizing unit configuration. This can be done by implementing an aerodynamic lens. On the other hand, the sizing laser beam can be further processed by focusing it tightly with a convergent lens that will make the location where the particle will be detected very accurate. The sizing laser beam can also be expanded with a cylindrical lens in the perpendicular direction of the particle beam axis and of the sizing laser beam axis so that all particles at any place in the particle beam will be irradiated approximatively similarly. In both cases, the focusing lens has to be changed. The latter solution will conserve the current particle sizing efficiency (SE) whereas the former will decrease it significantly.

6 Desorption/ionization unit

This section presents the characteristics and the experimental setup used to perform the desorption of the particle constituents and their ionization. This step has to be handled carefully since it determines the quality of the chemical analysis. Indeed, its choice orients the type of chemicals that are targeted, the type and polarity of the ions, such as fragment or molecular ions, that will be detected by the bipolar mass spectrometer. The choice of the laser systems is guided by a literature compilation on aerosol mass spectrometers that operate a one-step laser desorption/ionization. For the two-step laser desorption/ionization approach, the choice of the laser systems is further guided by usual off-line aerosol mass spectrometry ([Hauler et al., 2004], [Ferge et al., 2005]). In this case, the aerosol sample is introduced into the instrument on a plate on which the aerosol is collected whereas in the on-line approach the sample is the flying particle itself.

The aerosol mass spectrometer built in this work is dedicated to operate on a on-line basis the different desorption/ionization methods implemented in off-line aerosol mass spectrometers at the GSF-Forschungszentrum such as the desorption of the particle constituents by using a CO₂-laser followed by a soft post-ionization, ideally fragment-free, of the desorbed molecules via a REMPI process (Resonance Enhanced Multiple Photoionization) as described by [Hauler et al., 2004] or a SPI process (Single Photon Ionization) as described by [Ferge et al., 2005]. Such setup should permit in the future the detection of organic compounds such as aromatic and aliphatic compounds in aerosol single particles and to investigate further the desorption/ionization process mechanisms.

6.1 Choice of the laser based technique

The use of lasers permits the remote vaporization and ionization of the particle constituents given that the light is directed and focused to the sensing volume, i.e. the center of the extraction electrodes of the mass spectrometer. The advantage is the absence of any hardware in the close vicinity of the ion extraction electrodes of the mass spectrometer that can perturb its electric field which might affect negatively the mass spectrometer performances. This gives the possibility to add equipments for alternative, remote or not, vaporization and, more important, ionization methods under the conditions that they do not intercept the laser light. [Mühlberger et al., 2004] shows the advantages of such approach for gas analysis.

It permits also the operation of the mass spectrometer with a “standard” extraction electrode system (here, spaced plane electrodes). The ion source needs only to possess many windows for each laser beam and enough room outside to install securely the laser systems. The major concerns of the design of the SPALMS instrument is not to have room in the ion source but enough room around it in order to arrange the different laser systems and to lead easily the different laser beams to the center of the mass spectrometer, i.e., the center of the ion source.

6.2 Laser light characteristics

To perform the desorption of the particle constituents and their ionization, the laser light must supply enough energy in a given time and surface area so that the irradiated particle can produce

enough ions during its residence time in the laser beam in the middle of the ion source of the mass spectrometer otherwise the particle will not be detected. The quantity of ions produced by the ionization process (which depends on the chemical species and their respective amounts), the amount of ions captured by the mass spectrometer and the mass spectrometer sensitivity determine the ablation efficiency E_a of the SPALMS instrument. Upon the chosen desorption/ionization approach, one or two-step, different laser characteristics have to be chosen.

6.2.1 One-step desorption/ionization laser light characteristics

[Thomson et Murphy, 1993] and [Thomson et al., 1997] investigated the first for standard particle materials the suitability of different laser wavelengths for the one-step laser desorption/ionization of particles. They report that the power density of the ablation threshold has a strong dependence on the laser wavelength as well as weaker dependencies on the particle diameter, absorption coefficient and the lattice energy of the particle material. They in particular indicate that laser light at $\lambda = 193$ nm allows most compounds typically found in ambient aerosols to be detected with lower fluencies and with significantly less variation in sensitivities than at longer wavelength. In other words, the shorter the wavelength is, the more probable it is to observe particle mass spectra and the less power density is needed from the laser. They also report nevertheless the fact that pure sulfuric acid droplets are difficult to ablate and ionize what requires in this case a laser light wavelength of 157 nm. On its side, the required power density determines the laser pulse and beam characteristics (pulse energy, pulse length and beam size) to be used.

As reported in Table 27, UV lasers are the most commonly used in the field of aerosol mass spectrometry. Indeed the photon energy is high enough to photoionize chemicals for the shortest wavelengths. For wavelength smaller than ~ 300 nm, the gas phase in the ion source of the aerosol mass spectrometer can be sampled in spite of its low pressure as reported by [Prather et al., 1994], [Rodgers et al., 2004] and later in this work. [Prather et al., 1994] also reported the obtention of a particle mass spectra with a CO₂ laser (10,6 μ m) as well as [Thomson et Murphy, 1993] for very high laser power density incident on the particle.

As a result, as soon as the delivered power density at the surface of the particle is high enough, more than 0,4 W/ μ m² (in most of the cases excepted the work of [Sinha, 1984]), particle mass spectra should be obtained for most particle sizes and compositions. In this work, a nitrogen laser, a Nd:YAG laser and an excimer laser were available at GSF-Forschungszentrum so that the SPALMS was designed to operate these different lasers for different measurement purposes.

6.2.2 Two-step desorption/ionization laser light characteristics

In the case of the two-step laser desorption/ionization, two choices have to be made: the choice of the wavelength and the power density of both the desorption and ionization lasers. Table 28 summarizes some of the published different laser wavelength combinations used for the two-step desorption/ionization used in on-line single particle aerosol mass spectrometry.

The next two paragraphs precise further the characteristics of the respective laser lights with respect to the studied particles. The choice of the laser characteristics is also based on the experience in off-line two-step laser desorption/ionization mass spectrometry in Prof. Zimmermann's group at GSF-Forschungszentrum ([Hauler et al., 2004], [Ferge et al., 2005]).

6. Desorption/ionization unit

<i>Laser type</i>	<i>Reference</i>	<i>Nominal pulse characteristics</i>	<i>Mean power density (W/μm²)</i>	<i>Focused beam size in source ion</i>
Nitrogen	This work	337,1 nm, 250 μJ, 8 ns	11	Ø 60 μm
Nitrogen	[He et Murray, 1999]	337 nm, 3,5 mJ,	0.4	400 x 2000 μm
Nitrogen	[Hinz et al., 1994]	337,1 nm, 250 μJ, 3 ns,	265	Ø 20 μm
Excimer	This work	248 nm, 12 mJ, 8 ns	1.5	Ø 1000 μm
Excimer	[Rodgers et al., 2000]	248 nm, 10 ns (**)	1 (**)	
Excimer	[Carson et al., 1995]	248 nm, 5 mJ, 2,5 ns	1,3 – 31,8 (*)	Ø 200 μm
Excimer	[Murphy et Thomson, 1995]	248 nm, 4 mJ, 2,5 ns	141-282	Ø 85-120 μm
Excimer	[Reilly et al., 2000]	308 nm, 7 mJ, 20 ns	2	500 x 350 μm
Excimer	[Weiss et al., 1997]	308 nm, 5 mJ, 3 ns	5.2	400 x 800 μm
Excimer	[Reents et al., 1995]	308 nm, 130-300 mJ, 40 ns	1.35 – 3,1	800 x 3000 μm
Excimer	[Kane et Johnston, 2000]	193 nm, 7 mJ, 8 ns	7.3	Ø 390 μm
Excimer	[Murphy et al., 1998]	193 nm, 2,5 ns	4 -50 20(*)	-
Excimer	[Middlebrook et al., 1997]	248 nm, 193nm, 157 nm	-	-
Nd:YAG	[Tan et al., 2002]	266 nm, 4 mJ, 4ns	0.56	Ø 1500 μm
Nd:YAG	[Kievit et al., 1996]	266 nm, 1 mJ	300(*)	Ø 20 μm
Nd:YAG	[Prather et al., 1994]	266 nm	0,1 – 1 (*)	
Nd:YAG	[Reents et Schabel, 2001]	532 nm, 100 mJ,	40 – 2700 (*)	Ø 100 μm
Nd:YAG	[Reents et Ge, 2000]	532 nm, 1064 nm, 300 mJ,		
Nd:YAG	[Sinha, 1984]	1064 nm, 1 J, 100 μs	2.10 ⁻³	Ø 2500 μm

Table 27 : Typical characteristics of commonly used lasers in aerosol mass spectrometers.

(*) most frequently value mentioned by the author

(**) estimated from the laser fluency (W/m²) and a typical value of laser pulse length (10 ns)

<i>Group</i>	<i>Desorption laser</i>	<i>Ionization laser</i>
[Morrical et al., 1998]	10,6 μm	266 nm
[Lazar et al., 1999]	308 nm	248 nm
[Cabalo et al., 2000]	9,525 μm	193 nm
[Woods et al., 2001]	10,6 μm	118,5 nm
[Woods et al., 2002]	3,39 μm and 10,6 μm	118,5 nm
[Öktem et al., 2004]	1,064 μm	118 nm
[Nash et al., 2005]	10,6 μm	142 nm
This work	10,6 μm	248 nm

Table 28 : Laser wavelengths used in two-step desorption/ionization in aerosol mass spectrometry

6.2.2.1 Desorption laser light

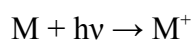
The interest of a desorption step with a laser light compared to a classical thermodesorption is its ability to vaporize quickly single particle relatively independently of the particle composition in a contact-free manner. Moreover laser desorption can be expected to be more efficient since the particle constituents are brought in the gas phase by usual vaporization and by mechanical fragmentation of the particle. Such mechanical effect occurs if the desorption energy is deposited in a sudden manner as with a short laser pulse which induces a pressure shock wave for example ([Zhigilei et Garrison, 1998]). The fragmentation of the particle helps to desorb more efficiently softly the particle constituents without fragmenting the chemical constituents if the laser wavelength is long enough and if the amount of energy deposited is not too high.

Most of the used lasers for this purpose are infrared lasers. The use of a long laser light wavelength is particularly adapted for desorbing material since the photon energy is not high enough to photoionize also the molecule. Indeed infrared electromagnetic radiation affects the relative motion of atoms within the molecules rather than the electron environment of the molecules. [Cabalo et al., 2000] and [Woods et al., 2002] take advantage of this in order to preferentially desorb certain molecules compared to others by adjusting the laser wavelength to the infrared absorption bands of molecules to be preferentially studied. The wavelength of 10,6 μm will be used in the rest of this work since it is the most used laser light for this purpose and since it is easily produced by a CO_2 -laser.

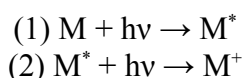
6.2.2.2 Ionization laser light

The choice of the laser wavelength for the ionization step can be made based on classical gas-phase laser mass spectrometry experiments since here the aerosol particle constituents are analyzed once they are gaseous. One can take advantage of gas phase measurement experiments or data banks to better adapt the ionization methods to the targeted chemicals.

The photoionization with lasers can occur via two pathways, SPI or REMPI, depending on the photon energy, the number of photons delivered by the laser at once and the ability of the molecule to be step-wise excited as summarized in [Boesl et al., 1994]. The ionization scheme Single Photon Ionization (SPI) is the most simple since it takes advantage of the ability of a single energetic photon to remove an electron from the molecule M as follow



The second process named REMPI (Resonance Enhanced Multiphoton Ionization) uses the ability of a photon of moderated energy compared to photons permitting Single Photon Ionization (SPI) to bring a molecule M to an excited state M^* which has a long lifetime. The excited molecule can then be further excited by another photon until the molecule gets ionized. This ionization method is more selective than SPI and is well suited for the ionization of polyaromatic compounds (PAHs) whose aromatic cycles stabilize their excited state. The ionization takes place as follow:



Both ionization methods produce essentially cations and are considered to be “soft ionization” methods, which produce mainly molecular ions. Both methods are illustrated in Figure. 35.

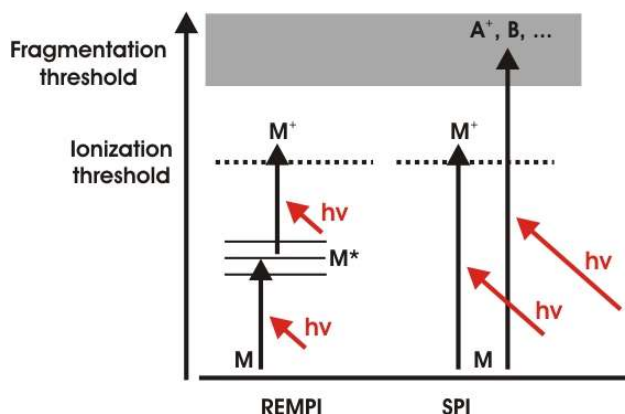


Figure. 35 : REMPI and SPI ionization process principle

Left: REMPI ionization. A photon of energy $h\nu$ brings a molecule M to an excited state M^* that has a long life time. During its life, the excited molecule M^* can receive a second photon of energy $h\nu$ that permits the removal of an electron what therefore ionizes the molecule M . **Right: SPI ionization.** The incident photon of energy $h\nu$ on the molecule M has enough energy to remove the electron for the molecule M which is therefore ionized. If the photon energy exceeds a fragmentation threshold for the molecule M , it leads to the fragmentation of the molecule.

It is usual for SPI ionization methods to use of the ionization energy IE to determine roughly the required laser wavelength to ionize given chemicals. This is justified since photoionization was thoroughly used to measure the ionization energy of many compounds ([NIST, Weekbook]). The energy brought by a photon of a given wavelength can be calculated by Eq. 18

$$E_{\text{photon}} = h \cdot \nu = h \cdot \frac{c}{\lambda}$$

Eq. 18

with E_{photon} the photon energy in [J], ν the light frequency in [Hz], h the Planck constant ($h = 6,626 \cdot 10^{-34}$ J.s), c the light velocity (~ 300000 m/s) and λ the light wavelength in [m].

Figure. 36 shows the number of species for a given laser wavelength that can be ionized via a SPI process (Single Photon Ionization). All the compounds whose ionization potential IP (rigorously ionization energy IE) are lower than the corresponding energy brought by a photon of a given wavelength can be ionized. Moreover a greater probability of fragmentation can be expected as the difference between the molecule ionization potential and the incident photon energy increases. The reported laser wavelengths in Figure. 36 are the laser wavelengths that can be operated in Prof. Zimmerman's group at GSF-Forschungszentrum at the exception of the laser light ($\lambda = 142$ nm).

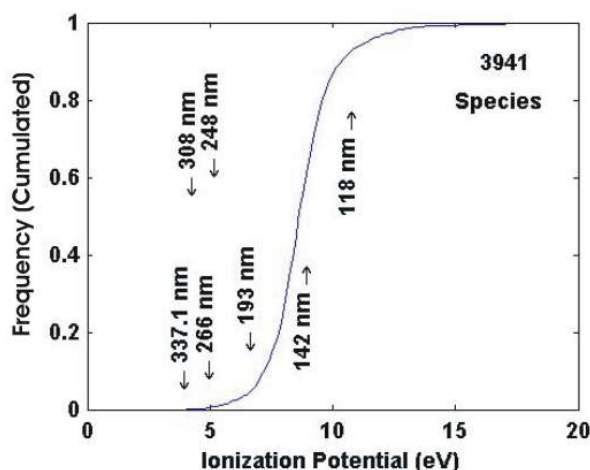


Figure. 36 : Number of ionizable chemical species for a given photon energy ([NIST, Weekbook])

Ionization potentials of 3941 species compiled in [NIST, Weekbook] are sorted in bins of 0,02 eV and plotted as a cumulative histogram. It represents the number of molecules that can be theoretically ionized via a SPI ionization process only for different laser wavelengths.

Figure. 36 shows the advantage to operate the ionization with a light of wavelength $\lambda = 118$ nm to confer to the aerosol mass spectrometer an “universal” detection ability. It shows also that such photoionization can not be considered to be selective as the laser wavelength decreases. One can nevertheless conclude that SPI ionization is selective for the species that can not be ionized for a given wavelength.

As a result the choice of the laser ionization method (SPI versus REMPI) will orient the category of chemicals than can be detected by the SPALMS instrument. In this work, polyaromatic compounds (PAHs) are the targeted compounds. To produce molecular ion of these compounds via a REMPI ionization process, laser systems of wavelength of 266 nm or 248 nm are good candidates.

For other compounds, the photoionization at a wavelength of 118 nm is ideally interesting but its interest seems limited for practical reasons. The low photon density in laser pulses producing 118 nm light would only ionize few chemicals via a SPI process. On the other hand at a wavelength of $\lambda = 193$ nm, the probability of photo-ionizing molecules via a REMPI process increases as the photon density in the laser light increases. Due to the high photon density in excimer laser light at $\lambda = 193$ nm, a high amount of energy can be transferred to the molecules and lead to the molecule fragmentation. Indeed for example, 2 photons at $\lambda = 193$ nm represent a total energy of 12,86 eV what is well beyond the ionization energy of the most molecules, typically ranging from 7 to 9 eV. For this reason it is preferred, for such high photon density, to use laser light whose photons are not too energetic and which permit REMPI ionization processes. Laser wavelengths of $\lambda = 266$ nm or $\lambda = 248$ are therefore preferred.

6.3 Laser operation characteristics

If the light wavelength and energy delivered by the laser pulse are of importance for the particle analysis, the trigger characteristics of the laser are also important. Indeed, in contrary to the gas

phase, an aerosol is not a homogeneous medium. Particles come practically randomly in the ion source where they must be volatilized and ionized. This implies that the desorption/ionization laser has to be fired at the time a particle is present at the center of the extraction zone of the mass spectrometer.

The desorption/ionization laser can be either fired periodically (free-running mode) as performed for fine particles but this approach lead to a low hit efficiency HE and therefore hit rate HR. To increase the chance of the laser light to hit a particle, the laser light must be emitted at the time the particle will be in the ion source. In all laser systems, the laser light is always emitted with a given time delay (laser trigger time delay $t_{\text{trig,delay,laser}}$) after an electric trigger informed the laser to fire. This laser trigger time delay depends on the laser type. For example, gas lasers react much quicker than Nd:YAG lasers. Indeed the trigger time delay depends on the rapidity of the laser medium to build up the population inversion of excited atoms that will produce the laser light. Nd:YAG lasers have a solid state medium that requires more time than the gas laser. This explains why Nd:YAG lasers have a long time delay between the trigger and the light pulse and why they are more adapted to be triggered internally and periodically.

The value of laser trigger time delay $t_{\text{trig,delay,laser}}$ is not problematic in aerosol mass spectrometry as long as it is stable enough from shot-to-shot and is small enough compared to the trigger system time scale $t_{\text{trig,system}}$. It means here that the laser trigger system should take in consideration this delay to calculate the time of the trigger pulse that will let the laser fires at the right time. In the present case, the trigger time scale $t_{\text{trig,system}}$ of the trigger system is of the order of magnitude of 20 μs . This means that the trigger time delay $t_{\text{trig,delay,laser}}$ of the laser system should not exceed the trigger time scale $t_{\text{trig,system}}$ here of 20 μs

If such long trigger time delay can be accepted for the one-step laser desorption/ionization approach, it can not be accepted for the ionization laser in the two-step laser scheme. Indeed, the ionization laser must be fired shortly after the desorption laser in order to keep the distance between the desorption laser beam and ionization laser beam close enough to insure that enough molecules can be ionized and detected by the mass spectrometer after their desorption. Indeed the desorption process creates from the particle constituents a cloud of molecules that quickly expand (typically at a velocity of 200-500 m/s). The short distance between the desorption and ionization laser beams determines therefore the maximum trigger time delay acceptable for the ionization laser. Considering the case of a laser beam distance of ~ 1 mm with a particle velocity of 350 m/s, it requires a laser trigger time delay equal or shorter than 2,8 μs . Table 29 presents the different trigger time delay $t_{\text{trig,delay,laser}}$ of the used laser systems in this work.

6.4 Optics arrangement

Since the desorption/ionization step in aerosol mass spectrometry has to be handled with great care and a high degree of modularity, the optical setup that leads the laser lights for the desorption and the ionization process into the ion source has been designed such that either one- or two-step desorption/ionization can be operated by the SPALMS instrument and such that it has not to be re-designed for each laser system.

6. Desorption/ionization unit

<i>Laser system</i>	<i>Trigger time delay</i>
Nitrogen laser	660 μs +/- 15 ns
Excimer	< 1 μs
Nd:YAG laser (*)	~ 185 μs (depends on the energy to be delivered) The light is delivered by the Q-switch within 70 +/-2ns (at 50 mJ, at 1064 nm)
CO ₂ -laser	~ 1-2 μs

Table 29 : Laser trigger time delays for selected laser systems

(*) In the case of the Nd:YAG laser, the laser light is let out by the action of a Q-switch whose principle is as follow: the laser light is reflected back and forth between two mirrors located at both sides of the laser resonator to produce the inversion population of the excited atoms. The position change of one of the mirror $M_{Q\text{-switch}}$ to a specific orientation let the light out of the resonator. The Q-switch corresponds to the motion of this mirror $M_{Q\text{-switch}}$. The Q-switch is activated in the present Nd:YAG laser only ~ 185 μs after the electric pulse that triggered the laser. This corresponds to the time needed to induce the inversion population of the excited atoms. Once the Q-switch activated, the laser light is only emitted after 70 +/-2 ns. As a result, the trigger time delay of the Nd:YAG laser is measured to be 185 μs + 70 ns, i.e., ~ 185 μs .

Indeed the designed optical system permits the introduction of the laser light from any used laser systems from the left side of the instrument into the ion source. It just requires the new positionment of only one mirror (called later interface mirror $M_{\text{interface}}$) within the rack I in addition to the positionment of a mirror close to the exit of the beam of the laser system. This mirror brings the laser light to the rack I and to the interface mirror $M_{\text{interface}}$ if the laser system is not mounted within the rack I as it is the case for the excimer laser. From there, the optical setup is set and contains the devices that permit the direction (via mirrors), the attenuation (via diaphragms, neutral glasses and beam splitters) and the focusing (via lenses) of the laser light into the ion source. It also permits the monitoring of the laser pulse energy (laser pulse sensors, Dual Laser Star, Ophir, Jerusalem, Israel) before the light enters the ion source. Only optics may have to be adapted for the different used laser light wavelengths if necessary. The optical set-up includes two laser lines as presented in Figure. 37 below.

Both laser lines are designed in the same way. Each laser beam is directed by a series of 4 mirrors that lead the light to the center of the extraction electrodes of the mass spectrometer. For the first test of the instrument, the mirror $M_{3,\text{ionization}}$ was the interface mirror for the ionization laser line. The interface mirror $M_{\text{interface}}$ for the desorption line is showed in $M_{1,\text{desorption}}$ since the desorption laser is located at at higher level depicted in Figure. 37. In the final state of the instrument, the mirrors $M_{1,\text{ionization}}$ and $M_{2,\text{ionization}}$ of the ionization laser line will be used to lead the ionization laser light to the instrument on the leftest side of the optical set-up (see the dashed line in Figure. 37, left panel). This will let room to install the nitrogen-laser and to allow a rapid exchange of the laser light by simply moving the mirror $M_{1,\text{ionization}}$ (the interface mirror) to the nitrogen-laser beam output. The mirror $M_{4,\text{ionization}}$ and $M_{4,\text{desorption}}$ direct both laser lights to the center of the extraction electrodes of the mass spectrometer. Figure. 38 and Figure. 39 depict the desorption and ionization laser beams arrangement in the ion source. Both laser beam waists are separated by a distance of $d_{\text{desorpt,ion}} \sim 1$ mm as they cross the particle beam. The value of ~ 1 mm was set for preliminary tests after the value reported by [Cabalo et al., 2000]. Indeed, the distance $d_{\text{desorpt,ion}}$ has to take into account the velocity of the particle and the mean velocity of the desorbed constituents.

6. Desorption/ionization unit

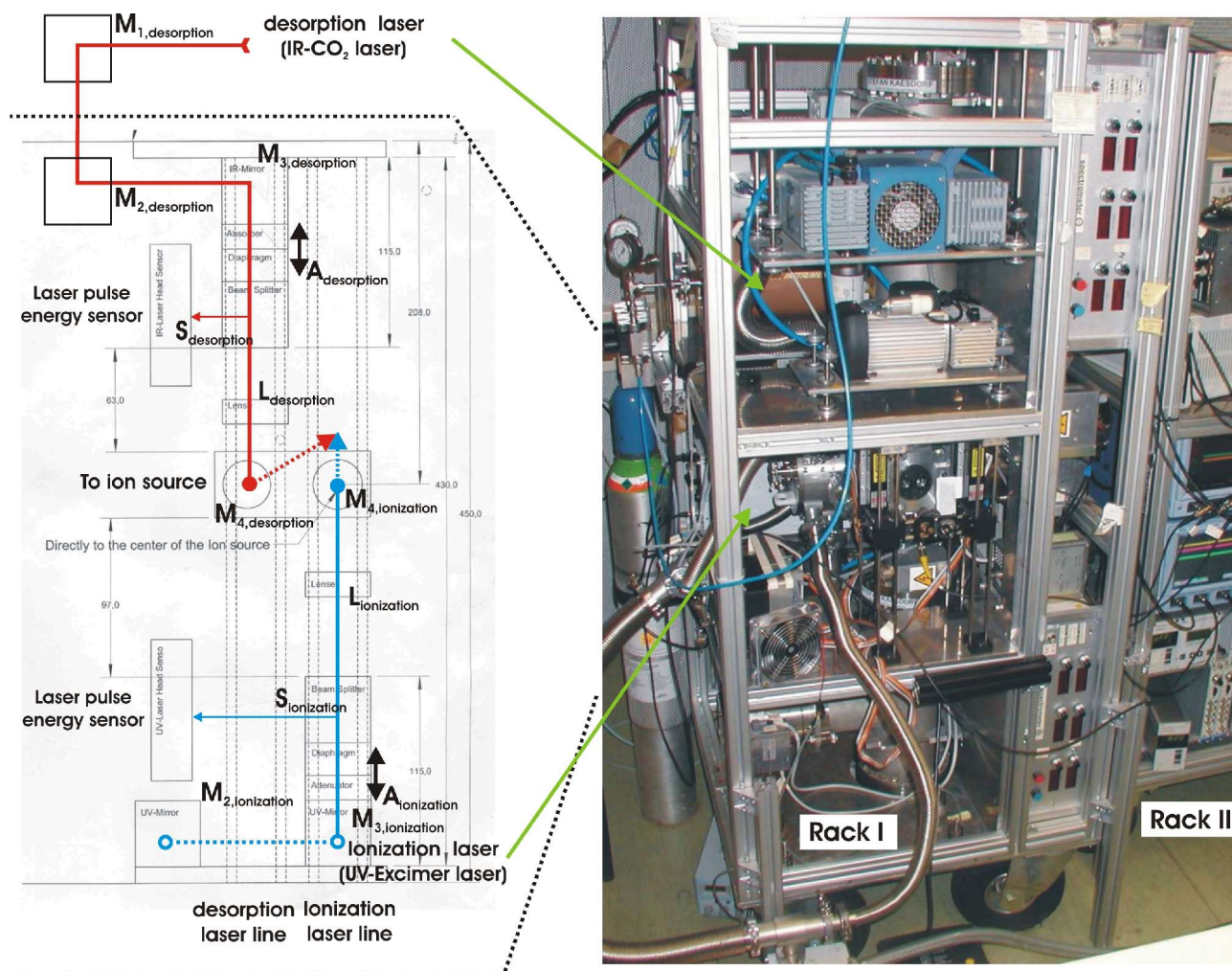


Figure. 37 : Laser desorption/ionization optical setup of the SPALMS instrument

<i>List and location the optical elements</i>	<i>Desorption line</i>	<i>Ionization line</i>
First directional mirror (interface mirror in final state)	M _{1,desorption}	M _{1,ionization} ^(*)
Second directional mirror (interface mirror in final state)	M _{2,desorption}	M _{2,ionization} ^(*)
Third directional mirror	M _{3,desorption}	M _{3,ionization}
Energy beam attenuation devices (beam splitter, diaphragm)	A _{desorption}	A _{ionization}
Beam splitter that reflects ~ 10% of the laser light onto the laser energy sensor. The rest goes to the ion source.	S _{desorption}	S _{ionization}
Focusing lens	F _{desorption}	F _{ionization}
Last directional mirror before the ion source	M _{4,desorption}	M _{4,ionization}

(*) only positioned in Figure. 37(left panel) and not in Figure. 37(right panel)

Each laser line is designed similarly. Each laser line leads the light from the laser to the center of the extraction electrodes of the mass spectrometer by successive reflections on 4 mirrors M₁, M₂, M₃, M₄. A beam splitter S, an assembly of intensity filter and a diaphragm A are mounted between the mirrors M₃ and M₄. The beam splitter leads a fraction of the laser light to a laser sensor that measures its pulse power whereas the assembly A reduces the laser pulse power if necessary. Before the light is reflected by the mirror M₄, the light is focused by a lens that adapts the power surface density incident on the particle to a given level.

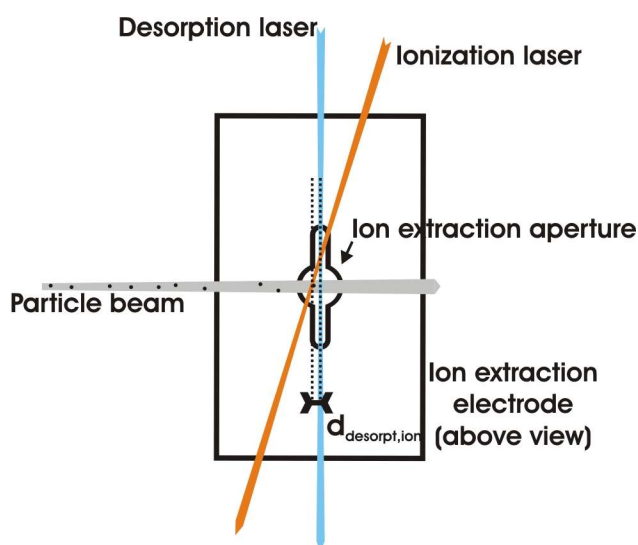


Figure. 38 : Relative positions of the desorption and ionization laser beams (view from above)

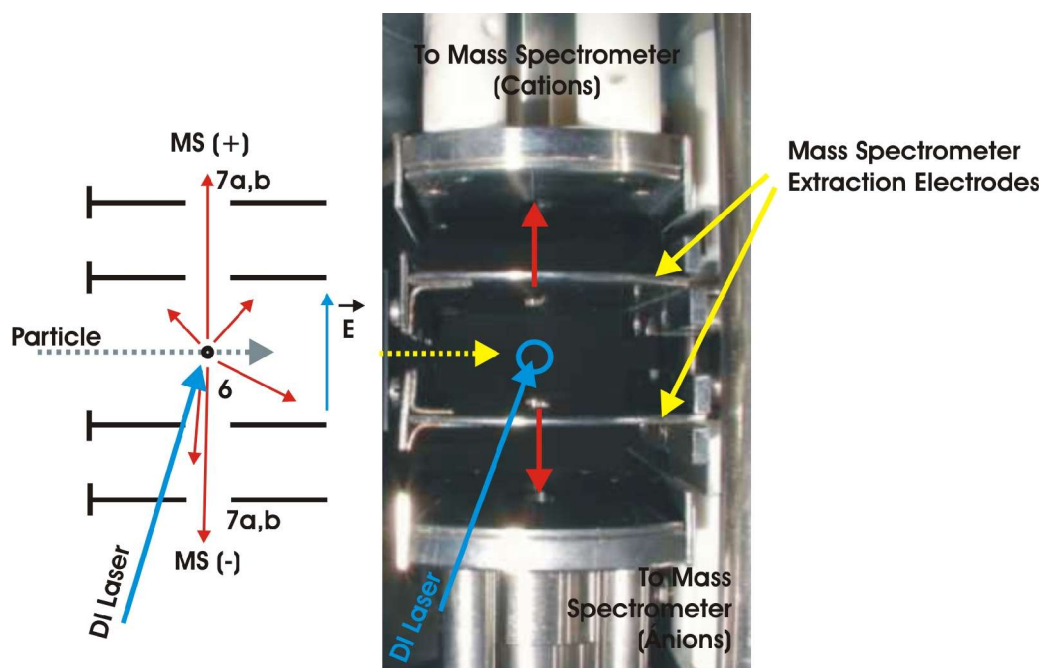


Figure. 39 : Desorption/ionization unit (side view)

The desorption/ionization laser beam (labeled here DI laser) is directed to the center of the extraction electrodes of the mass spectrometer (located by the open circle in the photo and by the number 6 in the drawing on the left). The extraction electrodes consist of two parallel plates across which a voltage is applied. Each plate has an aperture through which ions can be transmitted to both mass spectrometers. The electrostatic field between the extraction electrodes accelerates the cations and the anions in opposite directions to both mass spectrometer tubes (in the present illustration, the cations are accelerated upwards whereas anions are accelerated downwards). Particles are admitted in the ion source from the left side of the extraction electrodes in this picture (dashed arrow).

With this setup, the SPALMS instrument can operate either the one-step or two-step laser desorption/ionization with different laser systems which are presented in the next section. Indeed one-step desorption/ionization can be operated by firing only the ionization laser with a higher power than in the case of a two-step desorption/ionization mode.

6.4.1 Laser systems for one-step desorption/ionization

The task of the one-step desorption/ionization laser is to supply in one time enough energy to desorb and produce ions from the particle that can be detected by the mass spectrometer. The laser systems used in this mode are described below.

- Nitrogen laser

For the test of the different equipments of the SPALMS instrument and the validation of the aerosol mass spectrometer technical choices, a nitrogen laser (337,1 nm, VSL-337ND-S, C-763, Class IIIb, LSI Inc., Newton, MA, USA) has been used for the one-step laser desorption/ionization. The advantages of the nitrogen are its compactness (for a mobile instrument), its short and stable trigger time delay (660 ns +/- 15 ns), its sealed gas cartridge and its long wavelength that does not permit the ionization of gas phase components.

The laser light is directed to the sensing volume by a series of 4 high mirrors (high reflection grade $R > 99\%$ at $\text{AOI} = 45^\circ$, UV-fused silica, Laser Star GmbH, Olching, Germany and Topag Lasertechnik GmbH, Darmstadt, Germany) with a high reflecting coating for the light at $\lambda = 337.1$ nm) and is focused by a UV-lens (Laser Star GmbH, Olching, Germany) with a focal distance of 250 mm which produces a laser beam with a diameter of $\sim 60 \mu\text{m}$ when it meets the particle beam. The light is transmitted into the ion source through a UVFS window with an anti-reflection coating on both sides at $\lambda = 337,1$ nm (Laser2000 GmbH, Wessling, Germany). Such setup provides a power density of up to $10,6 \text{ W}/\mu\text{m}^2$ on the particle. The power density of the laser experienced by the particle can be reduced either by moving the focusing lens or by simply introducing a series of glass plates before the light enters the ion source. This is a easy mean to moderate the laser energy since each glass plate attenuates by $\sim 10\%$ the laser power. Both methods can lead to displace significantly the beam waist of the laser which might then not any more match the center of the particle beam. It is then preferable to move the focusing lens to increase the laser beam size what, if the power density remains sufficient, has a positive effect of the chemical analysis efficiency CAE since a broader part of the aerosol beam is irradiated. The laser light is stopped by impaction on a piece of paper that fluoresces as the UV-light impacts. In addition, a photodiode is placed behind the piece of paper to detect the light pulse and to produce an electric pulse that is displayed on an oscilloscope. The photodiode signal is used to give the time origin for the mass spectra. For safety reasons, the nitrogen laser was replaced by a similar more recent one that can return a TTL pulse (from the OptoSync connector) as the light pulse is emitted from the laser. In this laser, the embedded photodiode returns a TTL signal that indicates the light emission within 50 ± 1 ns after the light pulse. The laser can be fired periodically internally triggered up to 20 Hz or externally triggered at a rate of up to 30 Hz in burst mode.

- Nd:YAG laser

The Nd:YAG laser (266 nm, UltraCFR, Class 4, BigSky Laser Technologies, Inc., Bozeman, MT, USA) provides in particular a laser light pulse at $\lambda = 266$ nm (by frequency tripling of the ground laser light at 1064 nm) of 4 mJ per pulse of 6 ns length at up to 20 Hz. The laser pulse energy can be varied from the laser control panel. Due to its unpractical external trigger properties, the Nd:YAG laser was always used in internal trigger mode in which the laser is fired at a given frequency that can be set on the control panel from 0 to 20 Hz. The light is transmitted into the ion source via a classical UVFS window without any specific coating (Laser Star GmbH, Olching, Germany).

The principal use of this laser was to check the good operation of the bipolar mass spectrometer by sampling polyaromatic compounds in gas phase such as benzene, toluene and naphthalene for example. Casually, a Nd:YAG laser was installed in addition to the nitrogen laser (see Chapter 14.). In the latter configuration, the Nd:YAG laser was mounted on the SPALMS instrument so that it points the laser beam directly into the ion source. Both laser beams were adjusted almost in parallel and were propagating in toward each others. Such configuration permits the simultaneous analysis of the particles and the gas phase of an aerosol.

- Excimer laser

Currently, an Excimer laser ($\lambda = 248$ nm, KrF, Optex, Class 4, LamdaPhysik, Göttingen, Germany) is used alternatively for one-step and two-step laser desorption/ionization. In spite of its large size which makes the SPALMS instrument unsuitable for field measurements, it permits the ionization of the gas phase molecules either from the gas carrier gas or from the particle after its desorption by a CO₂-laser. It permits in addition a higher particle hit rate in free-running mode due to its higher firing frequency (200 Hz) and its higher output energy that allows its laser light to be less focused compared to the nitrogen laser. It produces a laser light with a power density for unfocused light of $9,8 \cdot 10^6$ W/cm² (22 mJ per pulse, 8 ns pulse length with a rectangular beam shape of size 7 mm x 4mm). The other advantageous feature of this laser is its “easy” change of the laser light wavelength by changing the gas-mixture that is used to produce the laser light. Indeed, wavelengths such as 193 nm, 248 nm, 308 nm and 351 nm can be respectively operated with different gas mixtures (respectively ArF, KrF, XeCl and XeF). The change of the light wavelength may require to adapt the optics used for transmission grade reasons. The advantage of this laser is that it makes possible to perform experiments over a wide range of laser wavelengths on the example of the PALMS instrument described by [Thomson et al., 1997] and [Middlebrook et al., 1997].

The laser light is conducted from the laser to the ion source in the same manner as with the nitrogen laser. The light is re-directed 4 times on high reflection grade mirrors at 45° AOI suited for the wavelength 248 nm (Topag Lasertechnik GmbH, Darmstadt, Germany) before being focused with a UVFS lens of focal distance $f = 250$ mm (Topag Lasertechnik GmbH, Darmstadt, Germany) and transmitted to the ion source by a UVFS window (Laser Star GmbH, Olching, Germany).

6.4.2 Laser systems for two-step desorption/ionization

For the two-step laser desorption/ionization, the desorption is here performed with an infrared laser ($\lambda = 10.6$ μ m, 100 mJ/pulse, 50 ns, 20Hz, Model MTL-3 Mini TEA CO₂ Laser, Class 4, from Edimburgh Instrument Ltd., Edimburgh, England). The infrared light is conducted and focused into the ion source by 4 gold coated mirrors, a focusing lens (ZnSe) of focal distance $f = 150$ mm and a ZnSe window before it reaches light trap with a funnel shape.

The ionization of the chemicals resulting from the particle desorption is then performed by an excimer laser ($\lambda = 248$ nm, 22 mJ/pulse, 8 ns pulse length, gas mixture KrF, Class IV, Model Optex from LambdaPhysik. Göttingen, Germany) presented before.

7 Coupling of the detection/sizing unit with the desorption/ionization unit

As presented before, the SPALMS instrument has a detection/sizing unit and a desorption/ionization unit that respectively permit the determination of the particle size and the preparation of the aerosol particle for the mass analysis of its constituents. Both units can in practice be operated independently. Operating that way would limit the potential of the SPALMS instrument since they are not coupled. In order to obtain size information and chemical composition of the same particle, both units have to be coupled together. This coupling makes possible, and this is its main purpose, a high sizing and chemical analysis efficiency (SCAE) and rate (SCR) by insuring a high hit efficiency (HE) and hit rate (HR). Such high efficiency is wished in order to obtain a statistical data set to describe correctly the aerosol.

The different coupling modes, free-running mode, static mode and dynamic mode, are presented below with their respective principles, technical characteristics and operating conditions. The free running mode fires the desorption/ionization laser without coupling its trigger with the detection/sizing unit. This mode is the only mode that can be operated with optically undetectable particles such as fine particles (smaller than 500 nm in the present case). On the opposite, the static trigger and dynamic modes link the trigger of desorption/ionization laser to the optical detection and sizing of a particle. The static mode has to be operated for a given particle size whereas the dynamic mode is independent of the particle size.

7.1 Free-running mode

In free-running mode, the desorption/ionization laser is simply triggered periodically (either internally or externally) at its usual maximum frequency in order to have the more chances possible to hit particles. Mass spectra are obtained when a particle is by chance in the desorption/ionization laser beam at this time. As an example, in the case of the nitrogen laser, the ion source of the center of the mass spectrometer is illuminated only 160 ns per second. At the maximum particle detection rate 7 Hz (i.e., for an aerosol load of $\sim 760 \text{ \#/cm}^3$) of the detection/sizing unit, particles are present in the middle of the extraction electrodes of the mass spectrometer and can be illuminated by the desorption/ionization laser beam only during 1,25 μs . The probability per second that a particle is desorbed and ionized is therefore very low.

This mode is operated mostly when particles can not be detected (here optically) by the detection/sizing unit (typically particles smaller than 0,5 μm here) or when the concentration of particles in the aerosol is high enough ($> 2000 \text{ \#/cm}^3$). This mode is independent of the particle size and can give the size information, with a specific data processing routine, of the particles for which mass spectra were acquired.

In our case, particle mass spectra were obtained in this mode for aerosols of high particles concentration but the analysis lasted only a few minutes since the inlet unit got quickly clogged due to the accumulation of particles at one of the inlet unit orifices. This mode is however not recommended due to its very low hit efficiency (HE) and rate (HR).

7. Coupling of the detection/sizing unit with the desorption/ionization unit

As a result specific trigger schemes are required to increase the probability to hit particles. The first improvement is the firing of the laser with a given delay after a particle has been detected.

7.2 Static Mode

In static mode, the desorption/ionization laser is triggered after a given time following the detection of the particle by the first or the second sizing laser as presented in Figure. 40. In this case, only particles of a given velocity, and therefore size, are met by the desorption/ionization laser light. This approach was firstly operated by many groups [Weiss et al., 1997], [Hinz et al., 1994], [Trimborn et al., 2000],[Murphy et Thomson, 1995] because of its simplicity and its robustness before an active trigger scheme was developed. As in the case of free-running mode, one has to wait for a particle with the given velocity (corresponding to the set trigger time delay) to arrive in the desorption/ionization laser beam path.

The advantage of this mode is that all uncertainties due to the different time delays of all electronic devices that are necessary to trigger the desorption/ionization laser as well as those due to the particle detection time (consequence of the “trajectory ambiguity” and particle optical properties) are made irrelevant by setting a given fixed time delay and by analyzing polydisperse aerosol particles. In those conditions, particles of nearly the targeted size can be hit by the desorption/ionization laser light. The size range that can be analyzed can be widened if the desorption/ionization laser has enough power to have a larger beam size as it intercepts the particle beam.

The static trigger mode is a very easy and efficient method to use to focus on particles of given sizes but also to check and calibrate the proper operation of the SPALMS instrument. By comparing the particle time-of-flight between both sizing lasers and the time when a mass spectrum occurs, one can evaluate the delay due to the trigger electronic chain. Unfortunately due to the insufficient current accuracy of the particle detection time, this method could not be successful. On the other hand, the selected particle size is determined by the fixed trigger time delay dt of the desorption/ionization laser and checked afterward off-line by analyzing numerically the photomultiplier signals recorded by the detection/sizing unit. Considering this, the optimal conditions can be set for a future analysis of monodisperse particles.

As first step in the development of the SPALMS instrument, the static trigger mode was used to fire the desorption/ionization laser and to get the order of magnitude of the total time delay generated by the different electronic devices in the laser trigger chain.

The trigger scheme is presented in Figure. 40 and the resulting time delays are listed in Table 30. In practice, the photomultiplier signals are monitored with an oscilloscope. The used oscilloscope (WR6050a, LeCroy, Chestnuts Ridge, New York, USA) has a specific feature that can produce a square shape electric pulse as the oscilloscope is triggered to capture/display a signal/waveform on its screen. The trigger signal, when a particle is detected by the photomultiplier PMT1a, from the oscilloscope is first sent to a first delay generator DG535 (DG1) that lets the input pulse out with a minimum period of 50 ms. It acts as a frequency filter to avoid the desorption/ionization nitrogen laser firing above its maximum firing rate of 20 Hz. The signal from the first delay generator is then sent to a second delay generator DG535 (DG2) which delays the input pulse by the wished time delay of dt (here 90 to 120 μ s starting after the signal from the PMT1a). This pulse triggers then the desorption/ionization laser. In the trigger chain, the initial photomultiplier signal used to trigger the

7. Coupling of the detection/sizing unit with the desorption/ionization unit

laser is successively processed by 4 devices that each add some time delays. These delays have to be evaluated and eventually compensated by adjusting manually the time delay dt of the delay generator DG2 in order to focus the analysis on a given particle size.

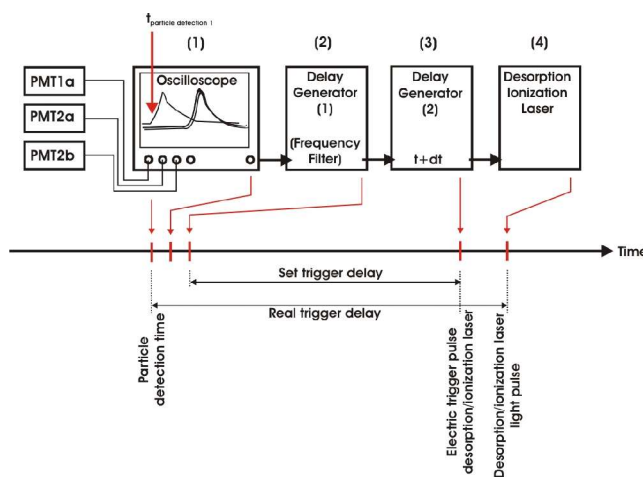


Figure. 40 : Desorption/ionization laser static trigger mode flow chart

The particle detection signal from the photomultiplier PMT1a is processed by the oscilloscope (1) that triggers a serie of delay generators ((2) and (3)), that respectively removes high frequency trigger events (2) and adds a time delay (3) to the particle detection signal from the oscilloscope (1). The resulting delayed signal is then used to trigger the desorption/ionization laser (4).

Step	Time delay origin	Functions / Comments	Time delay
1	Oscilloscope WR6050a (Aux. Trig. Output)	Displays and stores the photomultiplier signals Generates a trigger pulse as the PMT1a detects a particle	~ 40 ns
2	Delay Generator DG535(1)	Acts as a frequency filter to avoid the desorption/ionization laser firing above its maximum firing frequency	~ 80 ns
3	Delay Generator DG535(2)	Adds a given delay to the trigger pulse from the oscilloscope to fire the laser at the wished time	~ 80 ns
4	Nitrogen Laser	Volatilizes and ionizes the aerosol particle constituents	660 ns +/- 15 ns
	TTL peak rising time	2 x 5 ns	~ 10 ns
	Total delay time		~ 795 ns

Table 30 : Typical time delays encountered in the desorption/ionization laser static trigger mode scheme

The time delay of the whole desorption/ionization laser trigger chain reaches ~ 795 ns what is small compared to the characteristic trigger time scale $t_{\text{trig, scale}}$, here of 20 μs . The electronic chain has therefore enough time to react and to make the nitrogen ready to fire. It is only the case for the nitrogen laser and for the excimer laser, whose trigger time delays are shorter than 1 μs .

7. Coupling of the detection/sizing unit with the desorption/ionization unit

All of the measurements of this work were performed using this trigger scheme. The efficiency of the static trigger mode $E_{\text{stat, trig, mode}}$ is presented here as the ratio of the number of trigger events that lead to a mass spectrum to the number of produced trigger signals for the targeted particle size. This efficiency depends on the particle beam divergence since the particle beam size is ~ 10 times bigger than the desorption/ionization laser if the nitrogen laser is used for the desorption/ionization step. Based on the typical total number of detected particles (typically ~ 20000) and obtained mass spectra (~ 100) over a one-hour measurement for a particle concentration of $\sim 200 \text{ \#/cm}^3$, the static trigger mode efficiency $E_{\text{stat, trig, mode}}$ is practically smaller than 0,05%. Since it considers all particle sizes, a size correction is needed. Another approximation based on geometric consideration gives a maximal static trigger mode efficiency $E_{\text{stat trig mode}}$ for the present SPALMS setup of 10% as depicted in Figure. 11. Further data treatment, corrected from the particle size influence, should be performed to evaluate more precisely the static trigger mode efficiency $E_{\text{stat, trig, mode}}$ which is expected not to exceed 10%.

A drawback of this scheme is that it triggers the laser each time a particle is detected independently of its time-of-flight between both sizing lasers (and therefore of its size). To overcome this problem, i.e. to be more selective with regards to the particle size, a more complex trigger scheme was used in order to check if the particle time detection of the particle $t_{\text{particle detection2}}$ at the second sizing laser is consistent with the set trigger time delay of the delay generator. In these conditions, the laser is fired only if the probability to hit a particle is high. The laser can therefore be spared.

This requires the use of an additional third delay generator (DG3), of a coincidence analyzer unit (CA Model 2040, Camberra Industries, Meriden, Connecticut (CT), USA) and of a second oscilloscope (LT374, LeCroy, Chestnut Ridge, New York, USA) with a trigger feature (Auxiliary Trigger Output connection) as presented in Figure. 41.

This new desorption/ionization laser trigger scheme consists of two parallel lines. Each line waits for the particle detection time $t_{\text{particle detection1}}$ and $t_{\text{particle detection2}}$ of the particles as they cross the first and second sizing laser by detecting the PMT1a and PMT2a signals on two oscilloscopes (WR6050a and LT374). Each scope produces a trigger pulse (at the Auxiliary Trigger Output connector on the rear panel) that is respectively delayed by dt_1 and dt_2 by two delay generators DG1 and DG2 so that the resulting delayed output pulses can practically fire the desorption/ionization laser at the same time for the same particle. The values of dt_1 and dt_2 reflect the instrument geometry and the particle velocity. The coincidence of these pulses is then checked by a coincidence analyzer. If both input pulses are time-coincident, i.e., occurring within a defined time window of 500 ns (6.2 times the type particle residence time in the ionization laser beam), an output pulse is generated that is then frequency filtered. The resulting output pulse from the last delay generator DG3 triggers then the laser. The trigger sequence is presented in Figure. 41 while the different resulting trigger time delays are listed in Table 31.

Since this scheme is more complex because more devices are used, the value of dt_1 and dt_2 have to be carefully tuned and since it did not brought significant improvements compared to the previously described static desorption/ionization laser trigger mode scheme, this trigger scheme was not frequently used. In addition, this trigger scheme is not very good for the laser since by waiting for the proper particle to come, it makes the laser wait and lead to a lower power of the next laser pulse.

This improved trigger scheme still focuses on a given particle size that keeps the particle hit efficiency low. The trigger scheme presented in the next section, referred as dynamic trigger mode, should bring a more satisfactory answer than both trigger schemes previously described.

7. Coupling of the detection/sizing unit with the desorption/ionization unit

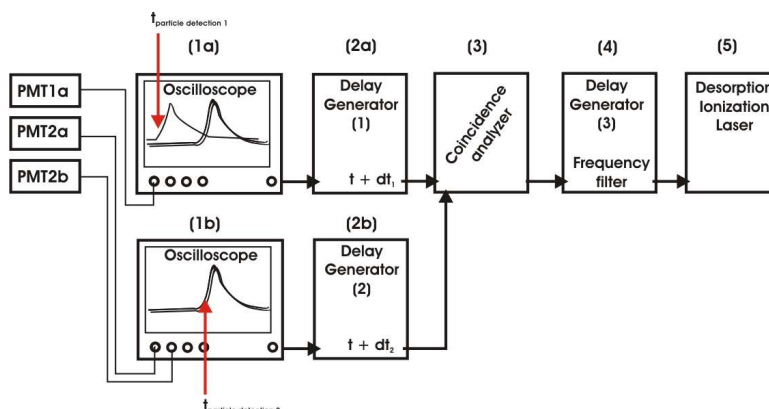


Figure. 41 : Desorption/ionization laser static trigger mode with coincidence test flow chart.

The photomultiplier signals of the detected particle by the PMT1a and the PMT2a are displayed by the oscilloscopes (1a) and (1b) that respectively sends a trigger signal to two delay generators (2a) and (2b). Each delay generator adds a time delay, respectively dt_1 and dt_2 , such that both generated trigger pulses occur at the same time and are tested by the coincidence analyzer (3). If the emitted trigger signals by the delay generators (2a) and (2b) are simultaneous, the coincidence analyzer (3) sends a trigger pulse which is first frequency filtered by a third delay generator (4) and which then triggers the desorption/ionization laser (5).

Step	Time delay origin	Functions / Comments	Time delay
1a	Oscilloscope WR6050a (Aux. Trig. Output)	Displays and stores the photomultiplier signals Generates a trigger signal as the PMT1a detects a particle	~ 40 ns
1b	Oscilloscope LT374 (Aux. Trig. Output)	Displays and stores the photomultiplier signals Generates a trigger signal as the PMT2a detects a particle	~ 40 ns
2a	Delay Generator DG535(1)	Adds a given delay dt_1 to the trigger pulse from the oscilloscope WR6050 to fire the laser at the wished time	~ 80 ns
2b	Delay Generator DG535(2)	Adds a given delay dt_2 to the trigger pulse from the oscilloscope LT374 to fire the laser at the wished time	~ 80 ns
3	Coincidence analyzer	Checks if the desorption/ionization laser trigger pulses from both delay generators occur within a given time window after the first pulse (here within 500 ns)	~ 800 ns
4	Delay Generator DG535(3)	Acts as a frequency filter to avoid the desorption/ionization laser firing above its maximum firing frequency Triggers the desorption/ionization laser	~ 80 ns
5	Nitrogen Laser	Volatilizes and ionizes the aerosol particle constituents	660 ns +/- 15 ns
	TTL peak rising time	4 x 5 ns	~ 20 ns
	Global time delay		~ 1680 ns

Table 31 : Typical time delays encountered in the desorption/ionization laser static trigger mode (coincidence test)

7. Coupling of the detection/sizing unit with the desorption/ionization unit

7.3 Dynamic mode

The static trigger mode is suited for the study of only one particle size range determined by its time-of-flight between the sizing lasers. Only a particle fraction can then be analyzed what reduces then the number of particles analyzed. To analyze more particles, one should analyze them as they come independently of their size. The appropriate trigger mode for this purpose is referred here as dynamic mode. Its principle was first introduced by [Prather et al., 1994] and is used by many groups now such as by [Reilly et al., 2000], [Van Wuijckhuijse, 2003] or [Hinz et al., 2005].

In this case, the particle detection time at the first and at the second sizing laser, $t_{\text{particle detection1}}$ and $t_{\text{particle detection2}}$, are recorded. These two time marks are then processed by an electronic device named DSTU (Dynamic Sizing Trigger Unit) that generates a trigger pulse that triggers the desorption/ionization laser at the time when the particle reaches the desorption/ionization laser beam in the center of the bipolar mass spectrometer. This requires to calculate accurately this time. The time accuracy requirements for such an unit are defined by the residence time of the particle in the desorption/ionization laser and by the accuracy of the particle time detection as it crosses both sizing lasers. A time precision of half of the particle residence time in the desorption/ionization laser beam should be sufficient. Its value depends on the desorption/ionization beam width in the ion source and on the particle velocity.

The DSTU unit simply multiplies the particle time-of-flight of the particle TOF_{sizing} between the two sizing lasers by a factor f_{DSTU} which is specific of the instrument geometry (i.e. the relative distance between the sizing lasers, 12 mm, and the desorption/ionization laser, 24/36 mm). It adds this calculated time to the particle detection time at the second sizing laser $t_{\text{particle detection2}}$ and subtracts any generated time delay $t_{\text{delay electronic}}$ in the photomultiplier signal processing chain. The relationship which permits the calculation of the desorption/ionization trigger time $t_{\text{trig,DI laser}}$ is given in Eq. 19.

$$t_{\text{trig,DI laser}} = f_{\text{DSTU}} \cdot TOF_{\text{sizing}} + t_{\text{particle detection2}} - t_{\text{delay electronic}}$$

Eq. 19

Since such an electronic device is not commercially available, a custom-made device, named DSTU (Dynamic Sizing Trigger Unit), was purchased whose practical principle is as follow and depicted in Figure. 42. Two versions of DSTU were purchased by two manufacturers (Jungbauer, Munich, Germany and University of Augsburg, Augsburg, Germany). Both DSTU devices work after the same principle and are driven by a computer via a serial port RS-232.

The operation of the Dynamic Sizing Trigger Unit (DSTU) requires TTL pulses as input signals. The TTL pulses are produced by processing the photomultiplier signal from PMT1a and PMT2a respectively by two delay generators DG535, respectively DG1 and DG2. The TTL pulse is generated ~ 80 ns after the photomultiplier signal has exceeded a given threshold with a positive slope (Leading Edge method). The Leading Edge method used to return a time mark as a peak is detected was chosen because of the apparent slow response of the photomultiplier to the scattered light. Indeed the peak top of the photomultiplier signal appears not to be the more reliable characteristic of the photomultiplier signal to use as a time mark for the particle detection for this purpose. The detection threshold for the peak detection is adapted for each photomultiplier signal according to their respective noise level. Once converted into TTL pulses, the photomultiplier signals are sent to the DSTU.

7. Coupling of the detection/sizing unit with the desorption/ionization unit

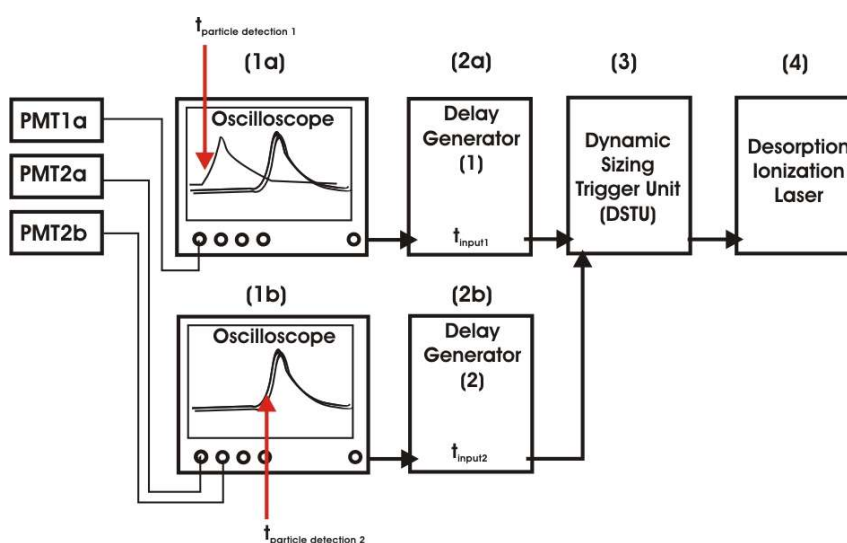


Figure. 42 : Desorption/ionization laser dynamic trigger mode flow chart

The photomultiplier signals that detect the particle at the PMT1a and the PMT2a are displayed by the oscilloscopes (1a) and (1b) that respectively send a trigger signal to two delay generators (2a) and (2b). Both generated TTL pulses from both delay generators (2a) and (2b) respectively at t_{input1} and t_{input2} are processed by the Dynamic Sizing Trigger Unit (DSTU) (3) which triggers the desorption/ionization laser (4).

The operation principle of the Dynamic Sizing Trigger Unit (DSTU) is depicted in Figure. 43. The DSTU waits for a TTL pulse that indicates the detection of a particle by the first sizing laser on a input 1 (BNC connector). The DSTU waits for a second TTL pulse on a second input 2 (BNC connector) that indicates the detection of a particle by the second sizing laser. All incoming TTL pulses from the delay generator DG1 (from the PMT1a) on the DSTU input 1 before the occurrence of a TTL pulse at the DSTU input 2 are ignored. The measured time (which corresponds to the particle time-of-flight, TOF_{sizing}) between the TTL pulses from the input 1 and 2 is multiplied by the geometric factor f_{DSTU} . This calculated time is then added to the time at which the TTL pulse has arrived on the DSTU input 2 and is then subtracted from a given time $t_{delay\ electronic}$ corresponding to the electronic processing time and the laser trigger time delay. At this calculated time, a TTL pulse, which must be compatible with the external trigger specifications of different laser systems, is generated and sent to the laser system that produces, with a given time delay inherent to the laser system, the wished laser light pulse. The laser light pulse occurs then at the time when the particle is in the center of the mass spectrometer where the particle can be volatilized and ionized.

Moreover the DSTU has additional features to filter the incoming pulse signals at each DSTU inputs to select the signals due to particles, to limit the desorption/ionization firing rate and to take into account the electronic time delays. Indeed all measured time-of-flight smaller than $20\ \mu s$ or greater than $120\ \mu s$ are rejected since such values of the particle time-of-flight TOF_{sizing} are not physically possible in the present setup. In these cases, the DSTU is reinitialized and waits for the next input signals.

7. Coupling of the detection/sizing unit with the desorption/ionization unit

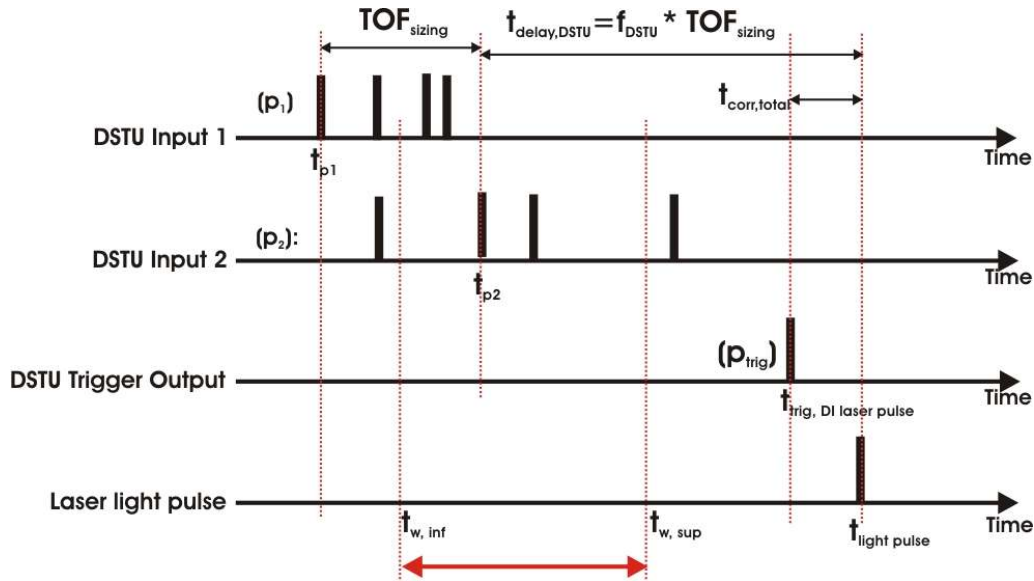


Figure. 43 : Dynamic Sizing Trigger Unit (DSTU) time diagram

This figure presents the time diagram of the DSTU operation. The time occurrence of the pulse (p_1), t_{p1} and (p_2), t_{p2} sent respectively to the DSTU Input 1 and DSTU Input 2 are compared by the DSTU. The time between (p_1) and (p_2), TOF_{sizing} , is measured and case-checked. If TOF_{sizing} lies in the interval $t_{w,inf}$ ($20 \mu s$) and $t_{w,sup}$ ($120 \mu s$) which corresponds to the only physically possible particle TOF_{sizing} values, the DSTU multiplies this time TOF_{sizing} by the factor f_{DSTU} , adds it to the time t_{p2} at which the pulse (p_2) occurred and subtracts from it the total electronic time delay $t_{corr,total}$ so that the generated the laser trigger pulse (p_{trig}) fires the laser at $t_{light pulse}$ when the particle reaches the center of the mass spectrometer. In cases where TOF_{sizing} is smaller than $t_{w,inf}$ exceeds $t_{w,sup}$, the DSTU is reinitialized and waits for the next pulses (p_1) and (p_2).

The DSTU acts also as a filter frequency by limiting the frequency of the desorption/ionization trigger pulse at the maximum rate of the laser. Simultaneously the DSTU measures all the correct particle sizing events, i.e. for the expected value of TOF_{sizing} , and sends the data to a computer via a serial port RS-232. Values of TOF_{sizing} are sent with a label that mentions if the sizing event has been followed or not by a desorption/ionization laser trigger pulse. In this manner it is possible to obtain the particle size distribution of the aerosol. Since the particle counting rate (PCR) of the DSTU is expected to be higher than the photomultiplier processing method described earlier in Chapter 5. because all signals are electronically processed, the measured particle size distribution should be more representative of the aerosol.

The DSTU is driven by a home-made Labview program that starts, stops, transmits the measured values of TOF_{sizing} and sets the different operating parameters such as the f_{DSTU} factor, a correction time for the input 1 $t_{corr,start}$, a correction time for the input 2 $t_{corr,stop}$, a correction time for the electronic timedelay $t_{delay electronic}$, the maximum possible time between both input 1 and input 2 pulses $t_{dead,cycle}$ and the minimum time period between two consecutive trigger pulses $t_{min,period}$). The relationships between some of the previously listed parameters are given by Eq. 20 and Eq. 21.

$$t_{trig, DI laser} = f_{DSTU} \cdot ((t_{particle detection 2} - t_{corr, stop}) - (t_{particle detection 1} - t_{corr, start})) + t_{corr, total} \quad \text{with}$$

Eq. 20

7. Coupling of the detection/sizing unit with the desorption/ionization unit

$$t_{corr, total} = t_{particle\ detection} - t_{corr, stop} - t_{delay\ electronic}$$

Eq. 21

The most important parameters to adjust to obtain the maximum chemical analysis efficiency (CAE) are the DSTU factor f_{DSTU} and the total correction time $t_{corr, total}$ which are discussed below.

- Choice of the DSTU factor f_{DSTU}

The factor f_{DSTU} permits the operation of the DSTU to any relative position of the sizing lasers and the desorption/ionization laser. The fine tuning of the factor f_{DSTU} permits ideally the determination of the best settings to maximize the hit efficiency (HE) of the SPALMS instrument. For practical and technical reasons, the value of the factor f_{DSTU} can only be discrete and ranges from 1 to 50. Indeed the more precision the factor f_{DSTU} has to have, the more complex is the electronic board design. On the other hand, the more precise is this factor, the easier is the fine tuning of the DSTU. Both constraints determine the precision of the factor f_{DSTU} .

As an example, in the case of a PSL 1 μm particle with a velocity of 358 m/s, the measured time-of-flight TOF_{sizing} is of 33,5 μs . Due to geometric considerations, the f_{DSTU} value is theoretically 2. A precision of 0,1 of the factor f_{DSTU} leads to a calculated laser trigger time of $67 + t_{particle\ detection}$ μs for $f_{DSTU} = 2$, $70,35 + t_{particle\ detection}$ μs for $f_{DSTU} = 2,1$ and $73,7 + t_{particle\ detection}$ μs for $f_{DSTU} = 2,2$.

According to the different values of the factor f_{DSTU} , the particle position offset is of 1,2 mm and decreases for particle with smaller velocity. It means that if the value of f_{DSTU} is changed, the position of the desorption/ionization laser beam has to be changed as well of 1,2 mm to insure that the laser light pulse hits the particle. The maximum offset range of the DSTU factor f_{DSTU} is determined by the extraction electrode design of the mass spectrometer. In the present setup, the extraction electrode can allow the ion source location, here the intersection point of the desorption/ionization laser beam and the particle beam, to move of +/- 2 mm around the geometric center of the ion source of the mass spectrometer. As a result, a precision of the factor f_{DSTU} of 0,1 can be accepted. The choice of the f_{DSTU} value is not influenced by the particle velocity (i.e. particle time-of-flight) as demonstrated in Figure. 44(a).

- Accuracy of the correction time $t_{corr\ total} = t_{detection} - t_{delay\ electronic} - t_{corr, stop}$

If the value of f_{DSTU} is set independently of the particle velocity, the total correction time $t_{corr\ total}$ can not. Figure. 44(b) shows a simulation that illustrates this effect. Figure. 44(b) presents the distance (labeled as "Particle rel. Position" in Figure. 44(b)) of the particle from the desorption/ionization beam waist ideal position when the laser is fired. If this distance is greater than the desorption/ionization laser beam diameter at the center of the mass spectrometer, the particle will not be hit. Negative values means that the particle is located between the desorption/ionization laser and the last sizing laser whereas positive ones mean that the particle is beyond. It shows in particular that the position where the particle should be to be irradiated by the desorption/ionization laser varies significantly with the particle time-of-flight (i.e., velocity) for a given time correction $t_{corr\ total}$.

7. Coupling of the detection/sizing unit with the desorption/ionization unit

Depending on the width of the desorption/ionization beam only particles with a given $\text{TOF}_{\text{sizing}}$ will be hit for a given time correction $t_{\text{corr, total}}$.

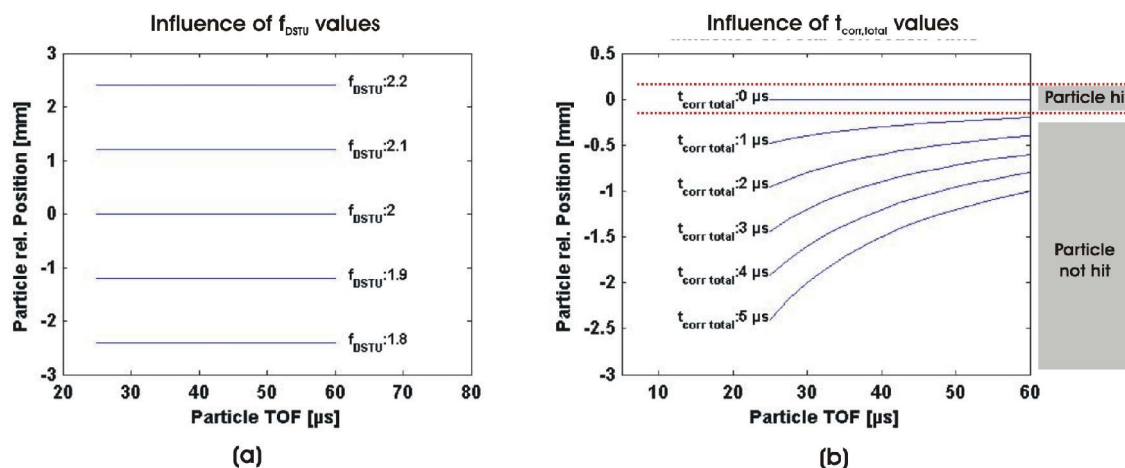


Figure. 44 : Influence of 2 parameters of the Dynamic Sizing Trigger Unit

Both graphs report the position of a particle at the desorption/ionization laser trigger time from the center of the mass spectrometer as a function of the particle time-of-flight measured by the detection/sizing unit for different values of the DSTU factor f_{DSTU} and the total correction time $t_{\text{corr, total}}$. The desorption/ionization laser focus point is located at the position "Particle rel. Position" = 0. **Left panel (a):** Each value of f_{DSTU} requires a specific adjustment of the desorption/ionization laser position which is independent of the particle time-of-flight (i.e. of the velocity). **Right panel (b):** The particle size range of the particle that can be hit by the desorption/ionization laser depends strongly on the value of the total correction time $t_{\text{corr, total}}$.

As a result it is important to evaluate precisely the value of $t_{\text{corr, total}}$ or to position the desorption/ionization laser beam so that the particles of interests will have the more chances to be hit. Table 32 presents the time delay that have to be accounted for for the different dynamic trigger setups.

Step	Origin of the time delay	Function(s) / Comments	Time delay
1a	Delay generator (1)	Generates a TTL pulse as a particle is detected by the PMT1a	~ 80 ns
1b	Delay generator (2)	Generates a TTL pulse as a particle is detected by the PMT2a	~ 80 ns
2	DSTU Box (Jungbauer)	Accuracy of the trigger time calculation varies with measured $\text{TOF}_{\text{sizing}}$	10,6 μs (systematic offset of 1,6 μs)
	DSTU Box (Augsburg)	(at most 15% of the particles can be hit)	~ 100 ns and ~ 1,6 ns
3	Nitrogen Laser	Measured in December 2004	660 ns +/- 15 ns

Table 32 : Time delays to be accounted for the desorption/ionization laser trigger with the DSTU unit

According to the devices chosen for the dynamic trigger mode, the DSTU must includes a time correction $t_{\text{corr, total}}$ whose value varies over 0,5 to 12 microseconds. It is not critical if this time delay is less accurate than +/- 100ns since it corresponds to the half of the residence time of the particle in

7. Coupling of the detection/sizing unit with the desorption/ionization unit

the desorption/ionization laser in the case of the nitrogen laser whose beam width in the ion source is $\sim \varnothing 60 \mu\text{m}$. The time precision required will be less if the laser beam is wider. In this case, the requirements for the DSTU can be less constraining.

Up to now, both DSTUs are available but some problems still need to be fixed as summarized in Table 33. They are implemented yet in the SPALMS instrument.

<i>DSTU 1</i> (Jungbauer, Munich, Germany)	<i>DSTU 2</i> (Electronic Workshop, University of Augsburg, Augsburg, Germany)
<ul style="list-style-type: none"> • Systematic overestimation of the particle time-of-flight $\text{TOF}_{\text{sizing}}$ of $1.6 \mu\text{s}$ • Time accuracy of the desorption/ionization laser trigger pulse deviates from its theoretical value as a function of $\text{TOF}_{\text{sizing}}$ as an U-shape curve 	<ul style="list-style-type: none"> • The time of the desorption/ionization laser trigger pulse has two discrete values instead of one separated by $\sim 1,6 \mu\text{s}$ • Only 15% of the photomultiplier trigger signals are followed by the right desorption/ionization laser trigger pulse.

Table 33 : Current technical problems of the Dynamic Sizing Trigger Units (DSTU)

<i>Item</i>	<i>Free running</i>	<i>Static trigger</i>	<i>Dynamic trigger</i>
Principle	The laser is fired periodically in this work 20 Hz.	The desorption/ionization laser is trigger after a given time after the detection of the particle by the first sizing laser. It can also be trigger after the second sizing laser.	The desorption/ionization laser is triggered as a function of the measured particle time-of-flight in the detection/sizing unit.
Laser trigger time scheme	No dependency between the particle detection time and desorption/ionization trigger time $t_{\text{LDI, trig}} = 1/f_{\text{LDI, periodic}}$	$t_{\text{LDI, trig}} = t_{\text{particle detection1}} + t_{\text{delay}}$	$t_{\text{LDI, trig}} = f_{\text{DSTU}} \cdot \text{TOF}_{\text{sizing}} + t_{\text{corr, total}}$
Hit particle probability (relative to each other)	Low	Middle	High
Comments	Hits randomly particle of any size Not influenced by the particle size detection limit	Hits predominantly particle with a specific aerodynamic size	Hits particle of any size
Size specificity	No	Yes	No
Required hardware	None	Oscilloscope with trigger Output Delay generator	Specific Electronic Unit
Operation facility	Easy	Easy to operate and rather easy to calibrate	Difficult to calibrate

Table 34 : Overview of the characteristics of the different desorption/ionization laser trigger modes of the SPALMS

7. Coupling of the detection/sizing unit with the desorption/ionization unit

7.4 Summary

As a result, the SPALMS instrument will be operated with the dynamic trigger mode for the particle size range that can be optically detected (currently 0,8 - 4 μm) once the DSTU and the detection/sizing unit will be corrected from their current imperfections. What concerns smaller particles, the option will be to operate an aerodynamic lens in free-running mode. The low hit efficiency HE of the free-running mode will be in some extent compensated by the high transmission efficiency T of the aerodynamic lens. In this study, measurements have been operated with the static trigger mode. The differences between each trigger mode are summarized in Table 34.

8 Mass spectrometer unit

Once the aerosol particle has been detected, sized, volatilized and a part of its chemical constituents ionized, the ions can be mass analyzed. The mass analysis of the ions permits the identification of the chemicals present initially in the particle. Since the particle should be considered as a mixture of many constituents, it is important to obtain at this level the maximum of information by designing carefully the extraction zone, characterizing the ion detector behavior and by operating specific mass calibration procedures. The design and the technical characteristics of the mass spectrometer used in this study will be first presented here. The geometry of the extraction zone, “the entrance gate of the ions into the mass spectrometer”, will then be shortly discussed in the perspective of the physics of the desorption event. Finally the principle and behavior of the microchannel plates, “the ion detectors”, and the calibration procedures of the mass spectrometer proposed for this study will be presented.

8.1 General principle

The major interest of time-of-flight mass spectrometers is its ability to analyze at once different ions of different mass-to-charge ratio (later referred as m/z) for one single ionization event at a high rate with a high transmission. The high rate corresponds to the ability to perform the mass analysis at a high frequency typically up to at least 10^4 Hz. The high transmission concerns the ability of the mass spectrometer to sample and lead to the detectors the majority of the ions created by the ionization event. Such ion analyzers are therefore particularly suited for mixture of chemicals which needs to be analyzed at high frequency..

Time-of-flight mass spectrometers (later referred as TOFMS) measure the ratio mass-to-charge m/z of ions by measuring their time-of-flight between their source and the detector which detects them. The typical geometry of a time-of-flight mass spectrometer is depicted in Figure. 45(a). Ions are first extracted and accelerated by an electric field in the extraction zone of the mass spectrometer before the ions enter an electric field-free region (called drift zone) where the ions fly at a constant velocity since they do not experience any further acceleration. The velocity reached by the ions as they enter the electric field-free region depends on their ratio m/z , on the extraction and acceleration voltages and on the acceleration distance relative to their initial position and velocity. Due to their inertia, small ions are much more accelerated than bigger ions are. As a result, ions with small m/z reach the detector before ions with bigger ratio m/z so that ions of different ratio m/z are separated according to the arrival time on the ion detector. The separation power, usually denominated mass resolution, quantifies the ability of the mass spectrometer to differentiate ions with close m/z ratios for a given ion mass m and is expressed as a ratio $m/\Delta m$, where Δm stands for the smallest mass difference that can be detected by the mass spectrometer for a given ion mass m . In time-of-flight mass spectrometry, the mass resolution increases with the length of the drift zone. The most simple setup is a tube as illustrated in Figure. 45(a). One end holds the ion extraction electrodes and the other end holds the detector. This configuration is called linear TOFMS. The theoretical ion time-of-flight in such setup can be calculated as follow.

Figure. 45(b) presents in details the principles and the typical design of the extraction electrodes

whose aim is to extract and accelerate the ions. For simplification reasons, the acceleration stage is not considered in the calculation here but the mathematical treatment is similar. One will only consider here the ion acceleration by the extraction electrodes.

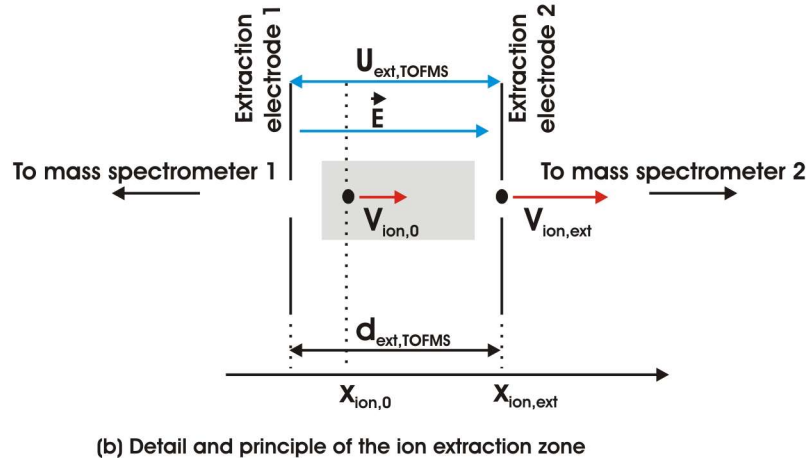
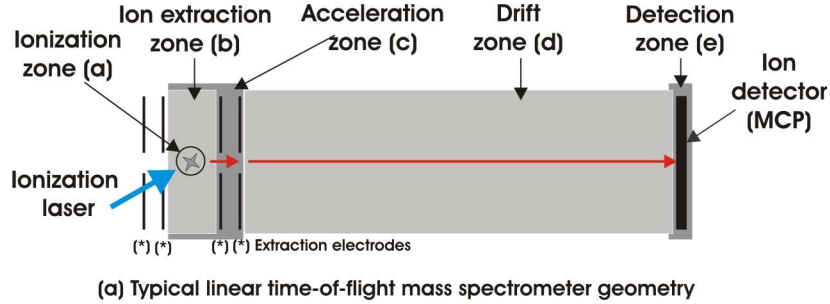


Figure. 45 : Typical geometric design of the time-of-flight mass spectrometer

Top panel (a): Typical geometric design of a monopolar linear time-of-flight mass spectrometer. Ions are created in the ionization zone (a). From there, ions are first extracted (b), accelerated (b), (c) and directed to the drift zone (d) where the ions travel at the velocity they reached at the exit of the extraction zone (b),(c). Ions are finally detected in the detection zone (e). Ions are moderately separated according to their m/z ratio in the acceleration zone (b), (c) and mainly in the drift zone (d). **Bottom panel (b):** Typical extraction zone geometry and voltage arrangement.

The velocity of the ion $V_{ion,ext}$ at the exit of the extraction electrostatic field (at $x_{ion,ext}$) depends on the initial position $x_{ion,0}$ and velocity $V_{ion,0}$ of the ion as given by Eq. 22:

$$V_{ion,ext} = \sqrt{\frac{2 \cdot e \cdot z}{m_{ion}} \cdot \frac{U_{ext,TOFMS} \cdot (x_{ion,ext} - x_{ion,0})}{d_{ext,TOFMS}} + V_{ion,0}^2}$$

Eq. 22

The time required by the ion to quit the extraction zone $t_{ion,acc}$ can be calculated from Eq. 23:

$$t_{ion,acc} = (x_{ion,ext} - x_{ion,0}) \cdot \int_{x_{ion,0}}^{x_{ion,ext}} \frac{dV_{ion}}{V_{ion}}$$

Eq. 23

The time-of-flight of the ion $t_{ion,drift}$ in the drift zone can be calculated by Eq. 24 as follow:

$$t_{ion,drift} = \frac{L_{drift\ zone}}{V_{ion,ext}}$$

Eq. 24

The total time-of-flight TOF_{ion} of the ion in the mass spectrometer is then given by Eq. 25.

$$TOF_{ion} = t_{ion,acc} + t_{ion,drift}$$

Eq. 25

If the initial ion velocity $V_{ion,0}$ is negligible against the ion velocity at the exit the extraction region $V_{ion,ext}$ and if the ion acceleration time $t_{ion,acc}$ is small compared to the ion time-of-flight in the drift region (as is usually the case since the ion path in the extraction zone is small compared to the drift zone), the ion time-of-flight TOF_{ion} can be expressed by Eq. 26 as follow:

$$TOF_{ion} \approx L_{ion,drift} \cdot \sqrt{\frac{d_{ext,TOFMS}}{2 \cdot e \cdot U_{ext,TOFMS} \cdot (x_{ion,ext} - x_{ion,0})}} \cdot \sqrt{\frac{m_{ion}}{z}}$$

Eq. 26

Eq. 26 usually leads to calibrate of the mass spectrometer with a two-parameters linear equation presented in Eq. 27.

$$TOF_{ion} \approx A + B \cdot \sqrt{\frac{m_{ion}}{z}}$$

Eq. 27

where A is a constant that represents the effects of the data acquisition (the determination of the time origin of the mass spectrum for example) and B is a parameter that reflects the geometry and the operation parameters of the mass spectrometer ([Guilhaus, 1995], [Vera et al., 1996]).

[Vera et al., 1996] propose in the case of matrix-assisted laser desorption/ionization (MALDI) to express the ion time-of-flight TOF_{ion} by a linear polynomial of the quantity m_{ion}/z at the power $p = 0, 1/2, 3/2$ as illustrated in Eq. 28 in order to take into account the specificities of multiple charged ions and ions with long time-of-flight TOF_{ion} that have high masses or whose motion is affected by ion/neutral clouds produced by the desorption/ionization process. Indeed, ions created from the desorption/ionization of the particle can experience different accelerations due their collisions within the desorption/ionization plume constituents and due to shielding effects of the extraction voltages by the outermost species of the ion/neutral cloud.

$$TOF_{ion} \approx A + B \cdot \left(\frac{m_{ion}}{z}\right)^{\frac{1}{2}} + C \cdot \left(\frac{m_{ion}}{z}\right)^{\frac{3}{2}}$$

Eq. 28

It is important to note here that the ion time-of-flight in the mass spectrometer depends not only of the mass spectrometer characteristics but also on the initial position and velocity of the ion as demonstrated in Eq. 26. A group of ions of identical m/z of different initial positions and velocities will not have the same time-of-flight TOF_{ion} up to the detector. This will result in an error in the measurement of the m/z ratio of the ion. However, it does exist along the ion trajectories a focal point F_1 where all ions of the same m/z reach the same position at the same time. Beyond this point, the ion positions will differ again. The position of the focal point F_1 is usually too close to the extraction zone so that ions of different m/z can not be separated efficiently what leads to a low mass resolution.

To diminish the effect of the initial position and initial velocity, the ion analysis can be performed with a reflectron time-of-flight mass spectrometer (usually denominated ReTOFMS). Instead of a linear instrument as previously presented, the ions are produced and accelerated as in a linear TOFMS but at the end of the drift zone, they are reflected by an electrostatic field backward so that ions of the same m/z will focus again at another focal point F_2 where the ion detector is placed. The ion reflector reflects the ions according to their velocity as they arrive at the ion reflector. Indeed ions with high velocity penetrate further in the ion reflector due to their higher inertia than ions with smaller velocities and will be therefore more delayed. This way ions of identical m/z arrive at the same time on the detector independently of their initially velocities and positions. The use of reflectron permits also the improvement of the mass spectrometer resolution by doubling the drift zone length.

The effect of the different initial velocities can also be reduced in some extent by operating the mass spectrometer in delayed extraction (DE). In this case, the ions are extracted and accelerated by the TOFMS with a given delay after the ion production. Indeed in normal conditions, all emitted ions are accelerated as they are produced what accentuate the spread of the ion velocities at the extraction electrodes. On the opposite, if the electrostatic field is applied with a given delay, the ion whose position is close to the exit of the extraction zone will not be as accelerated as the slower and remoter ions will be. Delayed extraction therefore homogenizes the velocity of ions of same m/z ratio as they leave the extraction zone what contributes to a better mass resolution for a given ion mass-to-charge ratio m/z . For further details about time-of-flight mass spectrometry, the reader is reported to [Guilhaus, 1995].

Usually time-of-flight mass spectrometer can only analyze one ion polarity at once. Time-of-flight mass spectrometers that permit the simultaneously analysis of both ions polarities at a time were also developed and operated first by [Hinz et al., 1996]. It simply consists of a second tube mounted on the opposite side of an existing monopolar time-of-flight mass spectrometer.

8.2 Technical details of the bipolar mass spectrometer

The aim of the aerosol mass spectrometer developed at the GSF-Forschungszentrum is to obtain the most comprehensive possible, both qualitatively and quantitatively, information about the single particles of an aerosol. The features of the mass spectrometer to be implemented are determined by the necessity of limiting the influence of the initial position and velocity of the created ions by the desorption/ionization process on the mass analysis accuracy and resolution, by the need to capture as much as possible ions to obtain a representative description of the single particle composition and by the need to perform a quick extraction of the ions in order to limit the development of secondary

reactions in the desorption/ionization plume that will affect the interpretation of the mass spectra.

Indeed the one-step laser desorption/ionization of the particle creates from the particle a cloud of ions and neutrals with a large range of velocities but whose initial positions are close together and located within the laser beam diameter at its beginning. In two-step desorption/ionization, a given time delay occurs between the desorption and the ionization process. During this time, the cloud of neutral species spread radially and the molecules are ionized over the whole ionization laser beam volume. If the time delay between the desorption and the ionization is large, a large distribution of ion initial position and of the initial velocities will have to be accounted for. Furthermore the choice of ion polarity to be investigated by the mass spectrometer is guided by the particularity of the one-step desorption/ionization process that produces simultaneously cations and anions.

Considering these elements, a custom-made bipolar time-of-flight mass spectrometer was purchased (Stefan Kaesdorf, Geräte für Forschung und Industrie, München). The mass spectrometer geometric design is presented in Figure. 46 and its characteristic dimensions are listed in Table 35.

<i>Characteristics</i>	<i>Values</i>
Extraction plates distance	14 mm
Length 2 nd Acceleration stage	11,5 mm
Drift zone	801 mm
Aperture extraction plate	4 mm
Aperture entrance plate liner	6 mm
Angle between incident and leaving ion beam in reflector	6.1°
Distance entrance-middle electrode reflector (stage 1)	22,5 mm
Distance middle-end electrode reflector (stage 2)	94,5 mm

Table 35 : Bipolar time-of-flight mass spectrometer geometrical dimensions

The operating conditions of the mass spectrometer are presented below. The values presented in Table 36 correspond to the preliminary voltage settings that give proper mass spectrometric signals even if it might still need to be optimized.

<i>Stage</i>	<i>Voltage</i>
Extraction plate cation	1 kV
Extraction plate anion	1 kV
Liner ^{(1),(2)}	3 kV
Lens ^{(1),(2)}	5,2 kV
Middle reflector grid ^{(1),(2)}	1,1 kV
End reflector grid ^{(1),(2)}	1,1 kV
MCP ^{(1),(2)}	1,6 kV

Table 36 : Bipolar time-of-flight mass spectrometer voltage settings used in this work

The voltages listed here were used for the measurements of this study. The same voltages are applied for both the cation ⁽¹⁾ and anion ⁽²⁾ mass spectrometer tube electrodes.

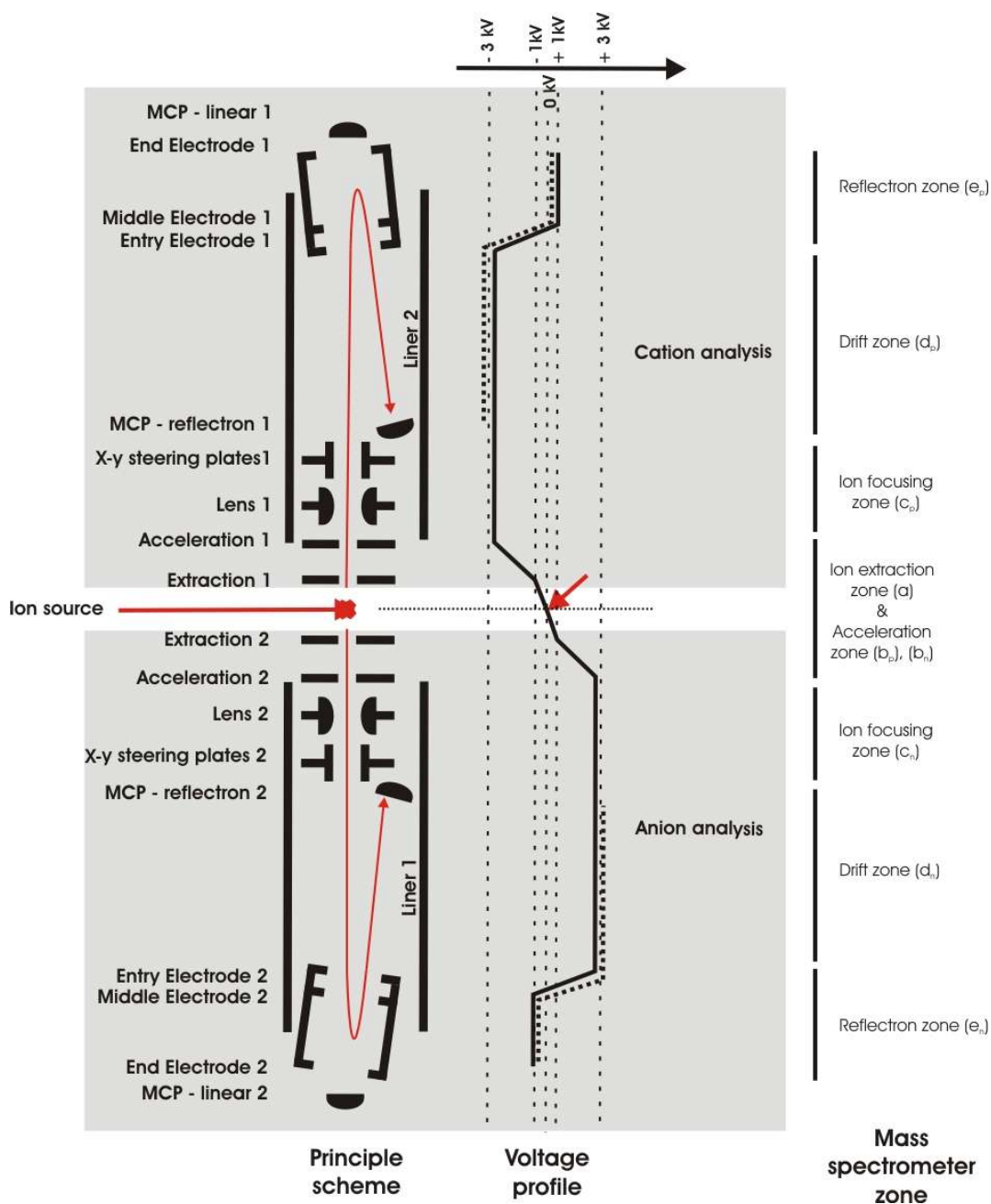


Figure. 46 : Details of the bipolar time-of-flight mass spectrometer of the SPALMS instrument

Ions created by the desorption/ionization process in zone (a) are extracted in opposite directions according to their positive and negative polarity later respectively accelerated in zone (b_p), (b_n). Ions are first focused in zone (c_p), (c_n) before they drift in zone (d_p), (d_n) to the reflectron zones (e_p), (e_n) where they are reflected to the detectors (MCP – reflectron 1 and 2) through the drift zone (d_p), (d_n). The middle panel (labeled “Voltage profile”) illustrates the voltage levels at the different locations of the mass spectrometer that permits the bipolar ion mass analysis.

The mass spectrometer can be operated in two different modes in linear mode or in reflectron mode. It is also equipped with a two-stage acceleration and a second order ion reflector for each ion polarity. These equipment features permit a reduction (if needed) of the effect of the initial position and velocity of the ions on the mass resolution.

The mass spectrometer has also specific features that permit the control of the mass spectrometer electrode voltages and the ion detector voltages to address the problematic of the “quasi” simultaneous chemical analysis of the particle surface and particle core and to permit the operation of a combined ionization of the single particle constituents as proposed in Chapter 2. Indeed the extraction electrode voltages can be applied in the mass spectrometer in a constant or pulsed manner and can be switched over to the other polarity as will be described below.

Ions can be extracted for their mass analysis by a constant electric field or a pulsed electrostatic field which can be triggered with an external usual delay generator. With constant extraction voltages, given a ion time analysis $t_{\text{ms,analysis}}$ of 100 μs , the ion mass analysis can be performed at a rate up to $1/t_{\text{ms,analysis}}$ of 10kHz. The mass spectrometer can also be operated in pulse mode up to 1 kHz which still let 1000 μs to perform the mass analysis. In this case, the voltage on the extraction electrodes can be applied within ~ 10 ns. This delay time needs to be considered in the laser trigger scheme in order to synchronize the laser light pulse with the ion extraction. In both cases, the mass analysis rate of the mass spectrometer is limited by the maximum firing frequency of the laser of at most 200 Hz (in the case of the excimer laser) and by the maximum data acquisition rate.

In addition to this, the anion mass spectrometer can be converted to a cation mass analyzer that can perform the analysis of positive ions a short time after a first cation analysis. In this case the voltages of the mass spectrometer are switch over to the other polarity so that the anion mass spectrometer can analyze positive ions. This feature only exists for the anion mass spectrometer which means that only cations can be analyzed twice for the same ionization event. In such mode the mean time between two cation analyses should be at least ~ 5 μs in order to set the new voltages values in the mass spectrometer. Such operating mode will impose very specific and controlled trigger schemes of the mass spectrometer and of the data acquisition unit. This feature is of great interest to investigate on a on-line single particle basis the homogeneity of single particles.

Both mass spectrometers include an electrostatic lens and two steering plates that can focus the ion beam more tightly to correct the angular deviation of the ion trajectory away from the mass spectrometer axis if necessary. This reduces the effect of the ion velocity component from the initial particle (along the particle beam axis) or from the created ions by making to them coming onto the MCP detectors. An alternative of the steering plates would be the implementation of a guiding wire set at a given potential in the drift zone that centers the ion flying away for the mass spectrometer flight tube axis as performed by [Franck et al., 2005].

Ions are detected by microchannel plate detectors (MCP, Burle Chevron Typ S3040-10-D, Part-Nr. 1332-4004, pore size 10 μm , thickness sensitive surface 0,5 μm , diameter 40 mm). One MCP is mounted for each operation mode (linear and reflectron mode) for each mass spectrometer tube. The MCP signals are recorded either on a oscilloscope or digitizers that samples the voltage signal in 8 bits. In the case of digitizers, two digitizers can be used in parallel for the same MCP in order to record the MCP signal over a wide dynamic range (one digitizer with a large dynamic range 0-5 V) and to conserve a good voltage resolution for weak MCP signals (a second digitizer with a narrow voltage range 0-1V or less). Such procedure is also be possible with a 4 channels oscilloscope. By sampling a MCP signal on two channels, one should be careful to avoid eventual artefact signals and loss of signal due to the splitting of the MCP signal.

The different extraction, liner, reflector stage 1, reflector 2, ion lens, x-and y-steering plates and the MCP voltages can be set either manually, as during this work, or via a computer.

8.3 Geometry of the extraction zone

The extraction zone permits the sampling of the created ions by the mass spectrometer. Its design is very important to capture as many as possible ions so that a representative composition of the single particle can be inferred. The knowledge of the typical pattern of material ejection from the particle during the desorption event should help to design the extraction electrode of the mass spectrometer.

According to the work of [Zhigilei et al., 2003] and presented in Figure. 47, the particle constituents are mostly emitted along laser beam axis backwards to the laser light in case the surface material is absorbing the laser light more efficiently than its core. In the case the core of the particle absorbs better the laser light than its overlaying material, the ejected material are distributed uniformly in any space direction.

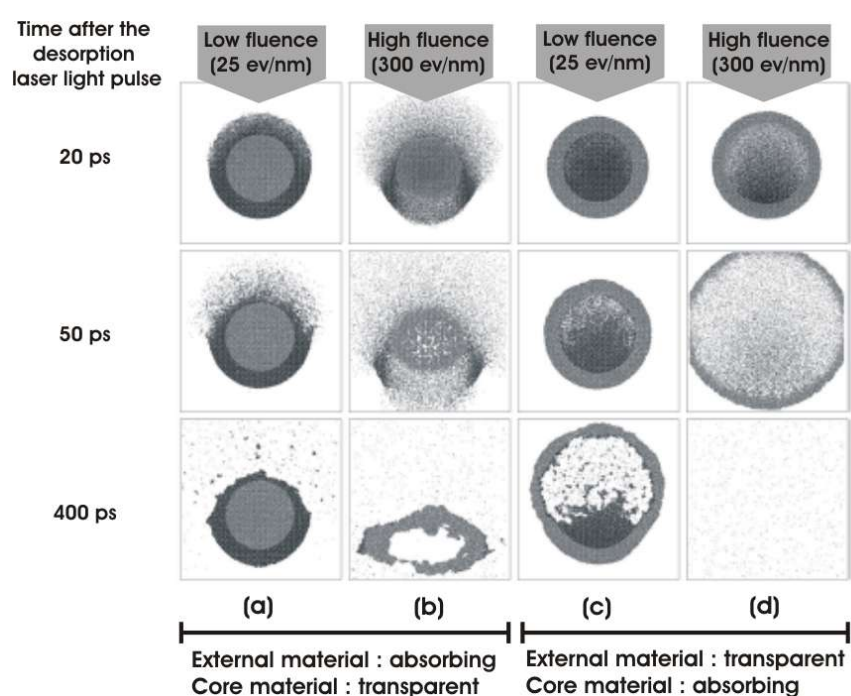


Figure. 47 : Desorption plume in the Matrix-Assisted Laser Desorption process

This figure is modified after [Zhigilei et al., 2003]. It presents different material ejection patterns during the particle desorption according to different repartition of an absorbing and a non-absorbing material in the particle obtained from a 2D-numerical simulation. The desorption is more complete in the case of an absorbing material located in the core of the particle. In this case the ejected materials are emitted uniformly in all space directions.

It is then important to capture the ions around the particle position in any direction in particular along the laser beam axis to catch as much as possible the emitted ion in the one-step laser desorption/ionization. It is even more necessary when the laser desorption/ionization is operated in two-steps since the desorbed neutrals from particle have more time to expand compared to one-step laser desorption/ionization and since the ions are created along the whole ionization laser light beam.

An inappropriate design of the extraction electrodes can be corrected by the use of a high extraction voltage that samples the ions emitted in any direction into the mass spectrometer. To be on the safe side, the extraction electrode sampling aperture has been specifically designed. The extraction electrodes have been designed so that their apertures are parallel to the ionization laser beam direction and contain a bigger aperture at its center. As a result, the extraction electrode aperture has a diameter of 4 mm and a slit centered on the aperture center of ~ 15 mm length and ~ 1 mm width (i.e. projected surface area of ~ 62 mm²) as depicted in Figure. 48. The narrow slit is not expected to modify significantly the electric field between the extraction electrodes.

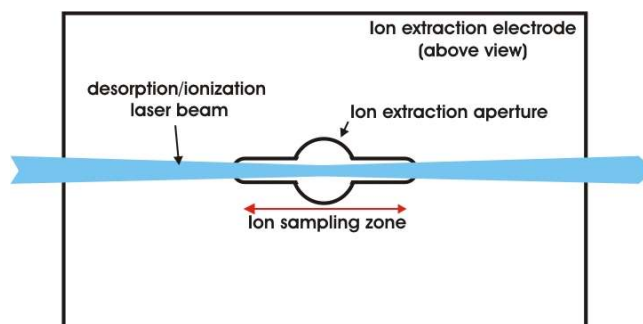


Figure. 48 : Extraction electrode design

The extraction electrodes are distant of 14 mm from each other (see Figure. 39) what allows the sampling of the ions into the mass spectrometer over a solid angle of 0.26 steradian from the center of the ion source: the ions contained within a cone of aperture angle of 32° are sampled. If anions and cations are emitted uniformly as presented for the desorption process in Figure. 47(c) and Figure. 47(d) in any direction, at most 2% of the ions can be detected which corresponds to a minimum ion sampling efficiency by the extraction electrodes. The ion extraction efficiency rises as the extraction voltage is applied on the extraction electrodes. In addition, the size of the extraction electrodes permits the interception of the ions over a solid angle of 7,5 radians i.e. $\sim 60\%$ of the space directions.

It is usual for such mass spectrometer type to have an extraction electrode as a grid and not as a plate with an aperture. The choice of a perforated plate for the extraction electrode is justified by the high ion transmission within the extraction plate orifice of diameter 4 mm and the by low degree of deviation of the ions as they pass through the extraction electrode. Indeed the electrostatic field is little distorted since the curvature radius of the edge of the aperture is made big by using a ~ 1 mm thick electrode. On the opposite of the extraction electrodes designed in the form of metal plates, extraction electrodes consisting of a grid/mesh can catch up to $\sim 10\%$ of the emitted ions before they enter the mass spectrometer tube. In addition, the wires of small diameter of which the grid consists of induce a strong electric field gradient in the immediate vicinity of the thin wires that deviates significantly the ions and affects negatively the mass spectrum quality ([Guilhaus, 1995]).

8.4 Microchannel plates (MCP) behavior

The microchannel plates MCP detect the ions or neutrals as they arrive onto the detector. The detector is made up out of a stack of plate of semiconductor with a high surface density of microchannels that are not perpendicularly oriented relative to the plate surface. On each plate the

microchannel tubes are slightly angled. A second plate is mounted below with an opposite inclination so that ions and neutrals meet the walls of the microchannels with a high probability and then emit electrons which are then multiplied by their successive impacts within the microchannels. The resulting current is then amplified and converted into a voltage.

Ions or/and neutrals are detected when they impact the microchannels with enough kinetic energy (i.e. a high enough velocity). The impact triggers the emission of electrons from the microchannels which is measured as a current. The resulting current measured as a function of time provides the mass spectrum of the detected ions. It has for consequences that the detector response for ions of different m/z is different. This also implies that only ions with the same ratio m/z are detected in the same manner. One can therefore compare together only ions with the same m/z from mass spectra to mass spectra

If too much ions impact at the same time the detector, the detector can saturate at the point it can mask the mass spectrum signal corresponding to the next incoming ions of greater m/z ratio and/or it can modify the detector response. It might then badly affect the detection of high m/z ratio ions (arriving later on the detector) and unable the comparison of mass spectra. This illustrates the interest of inserting a mass filter within the mass spectrometer to avoid a high quantity of given ions reaching the detector. This way one can focus on the analysis of high m/z ratio ions. The mass filter simply deviates the ions from their trajectory so that they do not reach the MCP detector. This is of particular interest for the analysis of ambient aerosols with a high content of sodium and potassium which can mask the other m/z positively charged ions such as magnesium or calcium.

8.5 Calibration procedure

The mass calibration of the mass spectrometer is of crucial importance since it conditions the validity of the results. Due to the uncontrolled desorption/ionization processes that produce ions with different initial positions and energies, the stability of the mass calibration of the mass spectrometer from particle to particle is to be evaluated. If the usual calibration procedure using two different ions of different m/z representative of the mass range to analyze is valid, the comparison of the arrival time of carbon clusters C_n ($n=1, \dots$) of different masses (of different n) for carbonaceous particles for different laser pulse power densities gives a measure of the calibration stability for different values of m/z simultaneously. It gives also a measure of the confidence that should be attributed for the measured m/z at different m/z values. Figure. 49 shows that the ion time-of-flight TOF_{ion} for different m/z varies from particle to particle in particular from negatively charged carbon clusters bigger than C_5 . It also shows in particular that for small m/z (typically $m/z \sim 50$) the mass calibration is satisfactory and that its quality decreases dramatically for higher ion masses.

It particularly points out that mass spectra should be calibrated individually in particular if ions of high masses are studied. The calibration must be performed for both polarities of the mass spectrometer since both calibration parameters are susceptible to be affected in different manners from particle to particle.

Figure. 49 highlights the interest of carbon cluster ions as a mass spectrometer calibration standard. Indeed carbon clusters can be easily produced from any carbon containing particle such as organics or soot particles. They present a carbon cluster pattern in both mass spectra polarities ([Silva et Prather, 2000]) which can be of different intensities according to the quantity of carbon in the particle and to the laser energy used for the desorption/ionization. In spite of the variable intensity

of the mass spectrum signal for such cluster ions, the periodicity of their m/z ratio ($m/z = 12 \times n$ with $n = 1, 2, 3, 4, \dots$) makes their assignment to carbon clusters C_n easy and valuable to use for calibration purposes in this study.

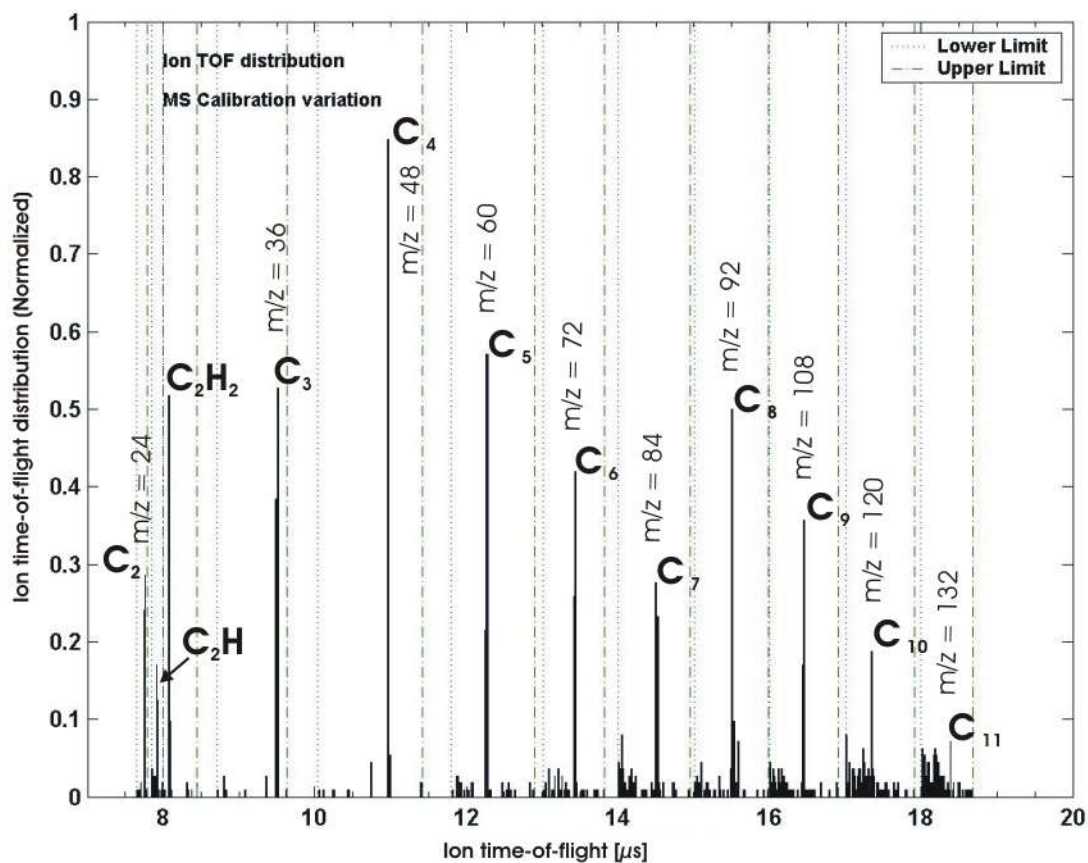


Figure. 49 : Variability of the ion time-of-flight for given m/z value from particle to particle

This graph presents the ion time-of-flight TOF_{ion} distribution (ion time-of-flight) of different negative carbon cluster ions C_n ($n=2,3,4,\dots$). As the m/z of the ion increases, the stability of the mass calibration of the mass spectrometer decreases. This variability can be related to the desorption/ionization and ion extraction processes. The mass calibration of high ion masses requires therefore a spectrum to spectrum specific calibration.

9 Data acquisition unit

The analysis of particles by aerosol mass spectrometry involves different physical and chemical processes. Each of these processes is to be considered as a potential novel/additional source of information. To exploit and check these advantages, many data acquisition devices have been implemented in the SPALMS instrument to record these information which can be then off-line analyzed by different home-made programs or theoretical tools. This chapter first lists the different sources of information. It first presents the data acquisition setup used in this work and illustrates its modularity. Finally the processing method of the data will be shortly addressed.

9.1 Inventory of the available information from the SPALMS instrument

In the rest of this work, the concept of primary and secondary information will be used to qualify the type of data according to their origin and how they were obtained. Primary information refer to directly measurable parameters, such as particle velocity, that describes the particle/aerosol while the secondary information are physical/chemical properties deduced from the primary information via a transfer function F . As an example, the vacuum aerodynamic diameter is a secondary information obtained from the particle velocity (a primary information) via a calibration curve (the transfer function F). The secondary information are here the classical parameters needed/used by aerosol scientists.

Table 37 lists the different measurement steps with their related data acquisition setups and the corresponding measured aerosol properties as primary information.

The primary information can be processed either alone or together using either calibration methods or theoretical models. This permits the improvement of the confidence of the analysis of the single particle (Improvement Type 4), the obtention of additional information about the aerosol population (Improvement 1) and about the physical particle properties (Improvement Type 3). Improvements of type 2 are more achievable by hardware solutions rather than with a complex data analysis scheme.

The quality of the function transfer T is of primary importance for the trueness and accuracy of the secondary information deduced from the primary information. The development of these transfer functions F is a major concern of aerosol mass spectrometrists in particular for the interpretation of the mass spectra to infer from them the particle composition of the particle, useful data for aerosol scientists.

9.2 Standard data acquisition scheme (DAQ Scheme Nr.1)

The data acquisition unit consists here of two independent parts: a high rate data acquisition unit (“high-rate DAQ”) and a low rate data acquisition unit (“low-rate DAQ”) as performed by the ATOFMS TSI Inc., St. Paul, MN, USA and [Noble et Prather, 1996] for example). It is intended to capture all measurement events as they come. Its experimental setup is presented in Figure. 51.

9. Data acquisition unit

<i>Measurement step</i>	<i>Hardware</i>	<i>Primary information</i>
Parallel aerosol sampling with the APS	APS3321	Particle concentration in air Particle velocity distribution in subsonic flow regime Correlation particle diameter – light scattering levels
Aerosol sampling with the SPALMS inlet unit (2)*, (3)*, (4)*	Current inlet unit → <i>Impactor like</i>	Collection of not transmitted particles Content of particles of a given size range (middle inertia)
Particle detection and sizing (5a)*, (5b)*	Oscilloscopes Digitizers	Particle velocity distribution in supersonic flow Particle light scattering level distribution Correlation particle velocity – light scattering levels Apparent particle concentration in air
Particle desorption (6a)*	Laser energy sensor Laser characteristics	Desorption energy level Desorption laser wavelength
Particle ionization (6b)*	Laser energy sensor Laser characteristics	Ionization energy level Ionization laser wavelength
Ion mass analysis (7a)*, (7b)*	Oscilloscopes Digitizers	Mass-to-charge ratio m/z of ions Apparent relative abundance of anions and cations in the particle
Particle collection by impaction (8)*	Impactor plate	Collection of transmitted but not hit particles

Table 37 : Measurement steps and their related accessible information

* The number in parenthesis refers to the measurement steps as depicted in Figure. 5, Figure. 7 and Figure. 10.

The high-rate data acquisition unit plays the role of an advanced particle counter and particle sizer. It captures and stores the photomultiplier signals in order to count particles, to determine their velocity and to infer their amount of scattered light. As exposed before, the maximum counting rate operated here is 7 Hz and was performed by digitizing each photomultiplier signals with a digitizer each (Acqiris DP210, PCI-Card, Geneva, Switzerland).

The low rate data acquisition unit (“low-rate DAQ”) records all the particle information when a mass spectrum is produced. All photomultiplier signals as well as the signals from both mass spectrometers and the laser light pulse trigger are digitized. It is to be noted that the data acquisition system is dependent on the trigger mode of the desorption/ionization laser, here, the static trigger mode. Indeed the trigger configuration used here is adapted to permit the data acquisition since the trigger configuration has not only to trigger the desorption/ionization laser but also the data acquisition unit what makes the trigger hardware setup complex.

The “modular/composite” data acquisition unit offers 12 digitizer channels to record the signal from different sensors whose respective attributions are presented in Table 38. The data acquisition unit is shown in Figure. 50.

The simultaneous operation of all digitizer channels is presented as a flow chart in Figure. 51 and

Low rate DAQ
 - All PMTs signal
 - DI laser Trig. Pulse
 - MS signal (MSP & MSN)
 - Photodiode signal

High rate DAQ
 - All PMTs signal



Figure. 50 : Setup of the SPALMS data acquisition unit (scheme Nr.1)

<i>Acquisition device</i>	<i>Channel Id.</i>	<i>Signal source</i>	<i>Accessible primary information</i>
Acqiris digitizers driven by a home-made Labview 6.i program (“High rate DAQ”)	DP210 Nr.0	PMT1a	Particle TOF _{sizing} Scattering light signal intensity Number of laser desorption / ionization trigger event
	DP210 Nr.1	PMT2a	
	DP210 Nr.2	PMT2b	
	DP210 Nr.3	Desorption/ionization laser trigger pulse from DG535(1)	
Oscilloscope LT374 (“Low Rate DAQ”)	Channel 1	PMT1a	Particle TOF _{sizing} , related to particles giving mass spectra Scattering light signal intensity related to particles giving mass spectra Statistics on the laser trigger delay
	Channel 2	PMT2a	
	Channel 3	PMT2b	
	Channel 4	Desorption/ionization laser trigger pulse from DG535(1)	
Oscilloscope WR6050A (“Low Rate DAQ”)	Channel 1	Desorption/ionization laser trigger pulse from DG535(1)	Time origin of the mass spectra Anion mass spectrum Cation mass spectrum
	Channel 2	Photodiode	
	Channel 3	Anion TOFMS MCP	
	Channel 4	Cation TOFMS MCP	

Table 38 : List of primary information accessible with the different digitizer channels

performed as follow. In this scheme, the data acquisition is adapted to the static trigger mode. The photomultiplier signals are digitized as they occur by the Acqiris PCI-digitizers. The digitizers DP210 are individually triggered externally by a delay generator DG1 which processes the PMT1a signal. It sends then a trigger signal to the other digitizers DP210 when the PMT1a signal exceeds a given threshold of typically 80 mV or 150 mV according to the noise level with a positive slope. This trigger signal does occur within ~ 5 ns and ~ 80 ns after the input trigger of the DG1 from the PMT1a. Considering the selected sampling period of the digitizers (50 ns), the acquisition is considered to be simultaneous for all digitizers. This delay generator DG1 sends also a trigger signal to the second delay generator DG2 that only lets out trigger pulses whose period is longer than the minimum firing period of the desorption/ionization laser. The resulting trigger pulse from the delay generator DG2 is then sent to a third delay generator DG3 that delays the trigger pulse according to the particle size to be investigated and fires the desorption/ionization laser.

The low-rate data acquisition unit consists of two oscilloscopes coupled together. The data acquisition is triggered by the oscilloscope WR6050a as a particle mass spectrum occurs. It saves both MCP signals, the electric and light pulse electric signal of the desorption/ionization laser with a high digitizing rate (down to 200 ps if necessary) and triggers externally the data acquisition with the oscilloscope LT374. This oscilloscope saves all the photomultiplier signals corresponding to the particle that produced a mass spectrum as well as the electric trigger pulse of the desorption/ionization laser in order to have the same time reference for both oscilloscope signals. The data from the digitizers DP210 are stored directly on a computer whereas data from oscilloscopes are first stored within the oscilloscope and then transferred via an USB-stick or network connection to a host-computer.

The current use of such different data acquisition devices is not optimal in term of acquisition speed due to the long sampling period and to the short sampling rate for both the digitizers (200 μ s, 50ns) and the oscilloscopes (200 μ s, 50 ns and 50 μ s, 200ps respectively for the oscilloscope WR6050a and LT374 where the first mentioned value corresponds to the sampling period while the second to the digitizing period). It is intended to have a high enough time resolution to develop and validate the data analysis program and further optimize the SPALMS instrument. Once in routine and the analysis program is mature enough, the sampling rates and sampling periods will be optimized. However, its still represents a giant amount of data (typically 1 Gb per hour) to be stored on-line and later on processed.

The data acquisition scheme is complex and tricky to operate. Indeed each trigger level of each device has to be individually set and the time delays generated by the different devices have to be carefully evaluated. Moreover the interconnections between all the sensors, data acquisition devices and delay generators have to carefully respect the load impedances of each device otherwise false trigger effects and/or absence of trigger signals might occur.

A major drawback of this data acquisition unit is the need to merge off-line the data from both oscilloscopes since one triggers the other. If the data acquisition by the oscilloscope WR6050a is not followed at the same time by the data acquisition by the oscilloscope LT374, both data sets will not contain the same number of particle data and therefore one can not any more have a complete data set containing the size and mass spectra information for a given particle. Such events occur frequently when the trigger rate from the oscilloscope WR6050a is high because both oscilloscopes do not have the same data acquisition features. It occurred for example many times as the oscilloscope WR6050A received a high frequency signal on its trigger channel what triggered a chaotic high rate data acquisition.

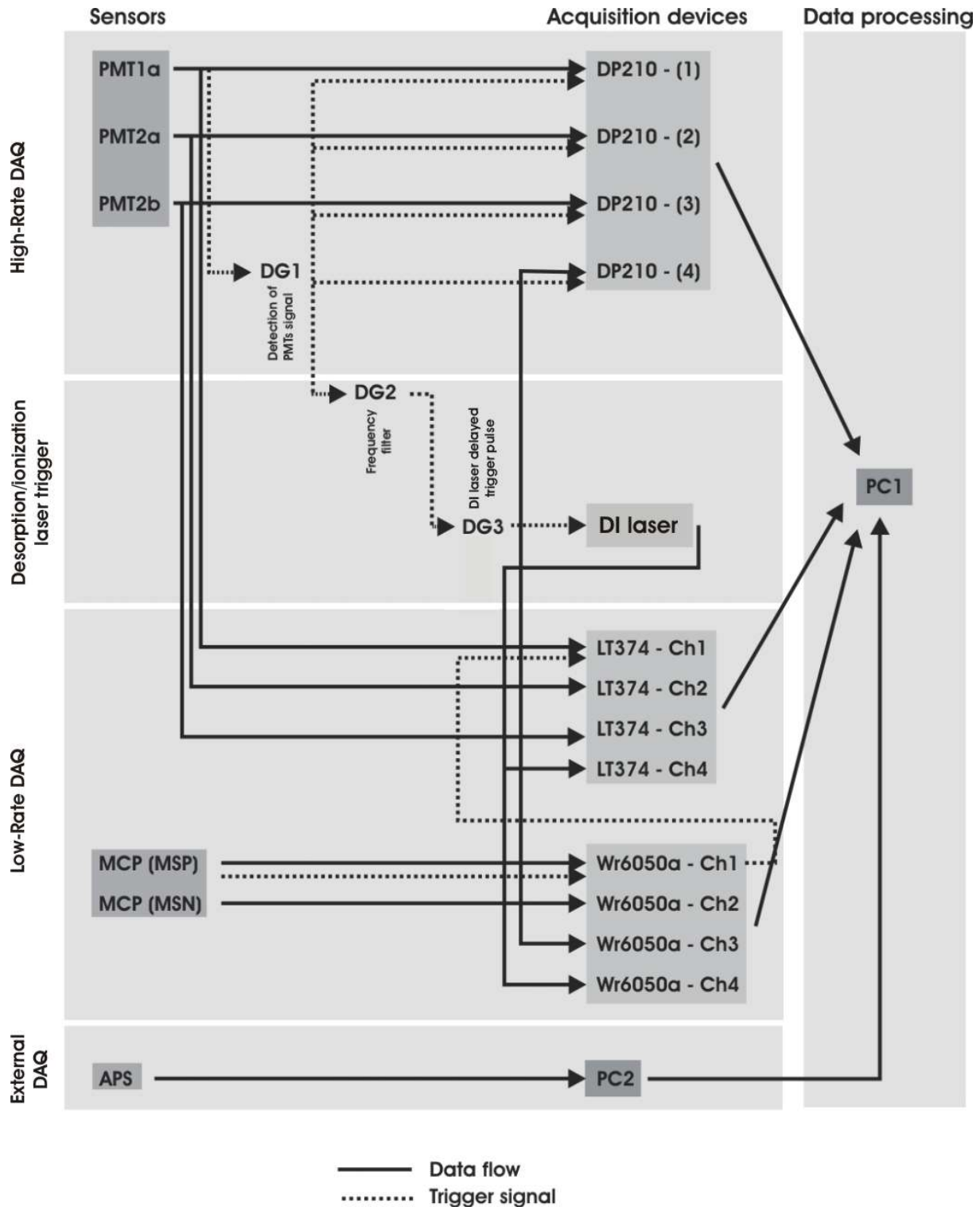


Figure. 51 : Chart flow of the data acquisition scheme Nr.1

PMT1a,2a,2b: Photomultiplier 1a,2a,2b. **MCP (MSP,MSN):** MicroChannel Plates (respectively of the positive and negative ion mode mass spectrometer). **APS:** Aerodynamic Particle Sizer. **DP210 -(1),(2),(3),(4):** Acqiris digitizer DP210, respectively Nr.1,2,3,4 **DG1,2,3:** Delay generator respectively Nr.1,2,3. **LT374:** LeCroy Oscilloscope LT374, **Wr6050a:** LeCroy Oscilloscope Wr6050a, **Ch.1,2,3,4:** Channel Nr. Of the oscilloscope. **PC1, PC2:** Personal Computer 1 and 2 for the data acquisition and storage

The data acquisition can be completed by recording with the mass spectra (on Channel 1 of the oscilloscope WR6050A for example) the laser pulse energy time profile as the light is emitted by connecting a laser sensor to the oscilloscope via a specific interface. Due to scarcity of time, this was not undertaken but it remains possible with the current data acquisition unit described here and the available laser sensor Dual Laser Star (Ophir, Jerusalem, Israel).

The signal of the Channel 2 from the oscilloscope WR6050a permits the recording of the time origin for the mass spectra. This signal depends on the desorption/ionization laser used. In the case of the nitrogen laser, this signal is produced by the photodiode included in the laser: a square pulse is returned when the light is emitted. In the case of the other lasers, this signal corresponds to the output of an external photodiode placed behind the desorption/ionization laser beam stop (a piece of paper) that fluoresces as the light meets the paper. The emitted light is then captured by the photodiode which generates an electric pulse that returns the time origin of the mass spectra.

Once the data are saved and merged, data have to be processed and to be converted to secondary information representative of the aerosol particles that are practical to handle and interpret.

9.3 Data processing program for the DAQ Scheme Nr.1

The data are first gathered on the same computer PC1 whereas the data issued from the cluster of 4 digitizers DP210 and the oscilloscopes are formatted in Labview 6.i files where each channel signal is stored in the format [nipss]. The formatted data consist of 3 files of 4 columns which represent each one of the 12 acquisition channels. One file corresponds to the “high-rate DAQ” that contain the photomultiplier signal acquired with digitizers DP210. The two other files correspond to the “low-rate DAQ” acquired data by both oscilloscopes.

- High-rate DAQ

Data from High-rate DAQ are processed in the same manner as the photomultiplier signals are processed as presented in Chapter 5. This data set provides information about the aerosol particle size distribution and about the aerodynamic and optical properties of the particle as will be described in Chapter. 13.

- Low-Rate DAQ

Data from the oscilloscope LT374 are treated identically as the data set acquired in High-rate DAQ since it corresponds to the same quantities, i.e. the aerodynamic and optical properties of the particle. The data set from the oscilloscope WR6050a is processed to extract the mass spectra for both ion polarities. Indeed, one of the channel records the signal from the desorption/ionization laser light pulse. This signal is processed to get the time mark that returns the time origin of the mass spectra for a given particle. Once the time mark has been found, the mass spectra can be extracted and stored in a file.

The obtained mass spectra are later further processed and plotted using different home-made MATLAB programs (MATLAB 6.5.1, Mathworks, Natick, Massachusetts, USA). In particular, mass spectra are mass calibrated either using a two-coefficients equation (Eq. 27) or a three-coefficients equation (Eq. 28) for each polarity. Due to the current limited hit efficiency of the SPALMS instrument and to the limited number of obtained mass spectra as presented in the next section, no thorough work has been carried out yet to process the mass spectra data.

10 Standard aerosol particle mass spectrometric analysis

This chapter presents the chemical analysis of different types of particles with the SPALMS instrument under standard operating conditions where only the particle size and the bipolar mass spectra of the particle are acquired.

It presents first test mass spectra of the mass spectrometer with a mixture of gas phase aromatic compounds before it presents typical mass spectra patterns of soot particles from Palas GmbH (Karlsruhe, Germany), soot particles from the combustion of wood in a small scale incinerator, PAHs rich soot particles (Sample #10) and ash particles from the incineration of construction wood material from a private fire place. The mass spectrometric analysis of other investigated particles such as PSLs or containing silica, sodium chloride, magnesium chloride or manganese chloride are discussed. The particle analyses were formed at two different laser wavelengths ($\lambda = 337.1$ nm and $\lambda = 248$ nm) and power level in order to test the wavelength dependency of the obtained mass spectra.

From this section it is demonstrated that the different soot particles of different origins can be differentiated since they all present a typical mass spectrum pattern. Palas soot particle mass spectra only contain pure carbon clusters whereas the typical signature of soot from wood combustion in mass spectra indicates the presence hydrogenated carbon clusters and shows the presence of sodium and potassium. The analysis of the ash particles illustrates on its side the interest of the single particle analysis by showing that the particle composition is particle-to-particle dependent. It also illustrates the ability of the aerosol mass spectrometer to detect heavy metals, such lead, and to provide some information about the element speciation. Finally, first results of 2-step laser desorption/ionization will be presented.

10.1 Gas phase analysis

The SPALMS instrument was first tested with the home-made nozzle inlet unit whose initial purpose was to check the correct operation of the mass spectrometer, to set its parameters to obtained mass spectra and to perform a first mass calibration. It also demonstrated the possible use of aerosol the mass spectrometer to operate gas-phase analysis with an aerosol inlet unit that does lead the gas phase to analyze to the center of the mass spectrometer where the ionization laser is fired.

In this experiment, a liquid mixture of toluene, toluene and naphthalene was sampled by the inlet unit. The depression created over the liquid sample connected to inlet unit made the liquid volatilized and filled up the whole aerosol mass spectrometer. The aromatic compounds atmosphere produced in the mass spectrometer reached a pressure of $\sim 5 \cdot 10^{-6}$ mbar in the ion source. The gas mixture was ionized with a Nd:YAG laser at 266 nm with a power density of $0,2 \text{ W}/\mu\text{m}^2$ (3 mJ/pulse , 8 ns , beam diameter, $\sim 1,5 \text{ mm}$) via a REMPI process which leads to the formation of cations as presented in Figure. 52. No negative mass spectra were obtained what is normal since the REMPI ionization process does exclusively produce cations.

At this pressure the quantity of material potentially able to be ionized and captured by the mass spectrometer can be estimated using the perfect gas law to be $2 \cdot 10^{-4} \text{ mol}/\text{m}^3$ what corresponds to $3 \cdot 10^{12}$ molecules in an ionization volume $V_{\text{ionization}}$ of $\sim 25 \text{ mm}^3$ ($\sim 2,5 \cdot 10^{-8} \text{ m}^3$) calculated after

10. Standard aerosol particle mass spectrometric analysis

Figure. 48. Considering the ionization/absorption cross-sections of the diverse chemicals and the mixture proportion of the three different chemicals, one may calibrate roughly the ion detector (MCP) at three different masses for the current mass spectrometer settings, here for the molecular ions (benzene at $m/z = 78$, toluene at $m/z = 91/92$ and naphthalene at $m/z = 128$) in the absence of fragmentations. The calibration can also be performed with a pure chemical.

Such detector calibration procedure can be used to evaluate further the quantitativity of the aerosol particle analysis in particular in two-step desorption ionization.

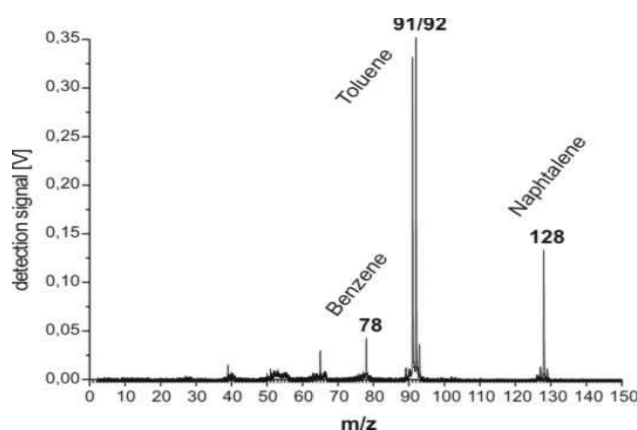


Figure. 52 : Gas-phase mass spectrum of aromatic compounds (Nd:YAG laser, $\lambda = 266$ nm)

The SPALMS instrument can sample gas phase compounds with its aerosol inlet unit. This figure presents the analysis of a mixture of benzene (78), toluene (91/92) and naphthalene (128) ionized via a REMPI process.

10.2 One-step laser desorption/ionization particle analysis

This section presents the analysis operated with a one-step desorption/ionization approach for different soot, ash and mineral particle samples with two different laser systems (with laser light wavelengths $\lambda = 337.1$ nm and $\lambda = 248$ nm).

10.2.1 Palas GmbH soot particles

The Palas soot particle sample was obtained from the company Palas GmbH (Karlsruhe, Germany) which is produced by collecting soot particles from the incomplete combustion of an alkane gas. Due to their synthesis method, soot particles are expected to contain only elemental carbon. Palas soot particles were extensively used in the present study to optimize the working conditions of the SPALMS instrument. Indeed even if the particle size distribution of the Palas soot is not appropriate for the inlet unit and the detection/sizing unit, the particle fraction in the range of $\sim 0,8$ to $3 \mu\text{m}$ in

10. Standard aerosol particle mass spectrometric analysis

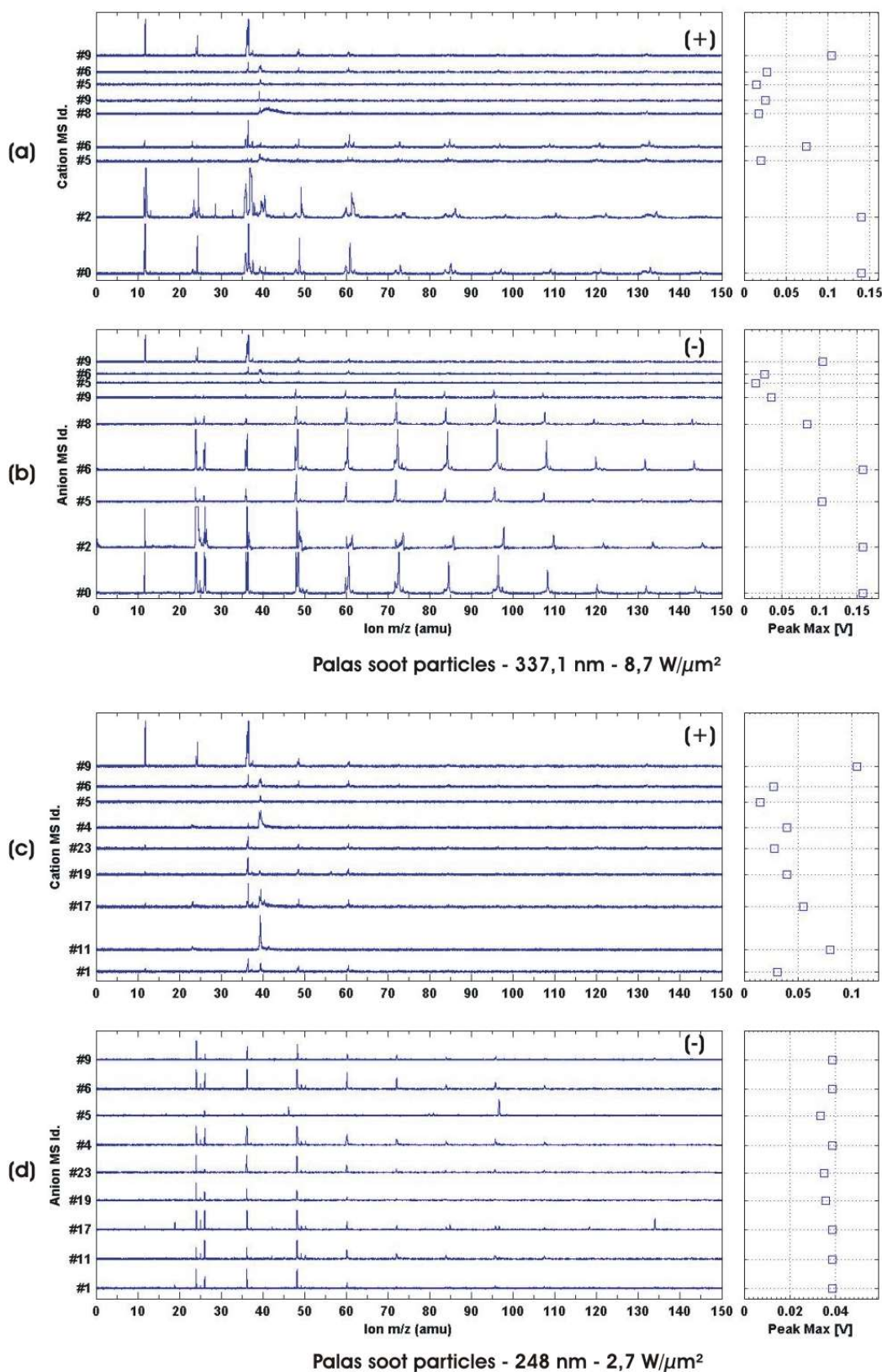


Figure. 53 : Positive and negative mass spectra of Palas soot single particles (at $\lambda = 337,1$ nm and at $\lambda = 248$ nm)

10. Standard aerosol particle mass spectrometric analysis

diameter is low but high enough to conduct experiments with the aerosol mass spectrometer in its current state. The advantage of soot particles for this study is their ability to easily produce mass spectra upon one-step laser desorption/ionization with the nitrogen laser ($\lambda = 337,1$ nm) or the excimer laser ($\lambda = 248$ nm) which can be easily calibrated.

Typical examples of Palas soot particle mass spectra are presented in Figure. 53. Figure. 53(a) and Figure. 53(b) present respectively particle cation and anion mass spectra obtained with the nitrogen laser ($\lambda = 337.1$ nm, $8,7$ W/ μm^2) whereas those of Figure. 53(c) and Figure. 53(d) were acquired with the excimer laser ($\lambda = 248$ nm, $2,7$ W/ μm^2). The common feature of each positive and negative mass spectrum is the occurrence of carbon cluster series $\text{C}_n^{+/-}$ with n varying from 1 to 11. The m/z scale presented here goes up to 150 since beyond this mass no peaks are to be differentiated from the noise level of the detector. In some cases, apparently hydrogenated carbon clusters are observed such as C, CH, CH₂ as well as, casually, carbon clusters with the generic formula $\text{C}_{n=5-7}\text{H}_{m=1-4}$ as showed in Figure. 53(a) and Figure. 53(b) sample #2. In Figure. 53(a) and (c), carbon clusters for the positive mass spectra are mainly observed with the casual apparition of peaks at $m/z = 39$ (#0, #2, #9, #5, #6 at $\lambda = 337.1$ nm and #1, #11, #17, #4, #5, #5 at $\lambda = 248$ nm) and sometime $m/z = 23$ (#0, #2, #5, #6, #8, #9 at $\lambda = 337.1$ nm and #11, #17, #4 at $\lambda = 248$ nm) indicating respectively the detection of potassium (K, 39) and sodium (Na, 23). In most cases, carbon clusters appear to be much more frequent in the negative than positive mass spectra.

It is surprising to observe mainly negative carbon clusters compared to positive carbon clusters. A default setting of the positive time-of-flight mass spectrometer and its detector can be ruled out since sodium and potassium can be detected easily detected. Such an observation is perplexing since one would have expected a clear signal for positive carbon clusters. This can be explained by the fact that potassium and sodium have a low ionization potential (respectively 4,34 eV and 5,14 eV) compared to the positive carbon clusters (respectively higher than 6 eV for C_n , with $n=1$ to 10, [Van Orden et Saykally, 1998]). This observation can also be explained by the work of [Shibagaki et al., 2000] which reports the common consensus that small carbon clusters are produced by the ionization of neutral cluster within the ablation plume after the laser ablation of a graphite surface. The conjunction of both phenomena give therefore a fairly plausible explanation of the observed low amount of positive carbon cluster ions detected by the mass spectrometer.

It is also interesting to note the higher proportion of C^+ produced compared to C^- and a tendency of producing negative carbon clusters with a higher mass than positive ones. Moreover for negative mass spectra, the relative occurrence of carbon clusters with an even or odd carbon atom number shows a particular pattern which is discussed below.

In the negative mass spectra of soot particles, carbon clusters containing an even-number of carbon atoms are proportionally more frequent than cluster ions containing an odd-number as illustrated Figure. 54(a) and (b). The error bars represent the range over which spans the peak intensity for a given peak corresponding to a given carbon cluster while the line which joins every error bars marks the corresponding mean of the peak intensity.

The observed tendency appears to be independent of the used laser wavelength and the power density incident on the particle as presented in Figure. 55. The peak intensity of each carbon cluster is in mean higher when the desorption/ionization of the particle is operated at $\lambda = 337,1$ nm due probably to the higher power density used at this wavelength.

Such behavior is consistent with the observation of particles containing organics/soots by different groups operating aerosol mass spectrometers on ambient particles at different wavelengths such as 193 nm [Lee et al., 2002] or 266 nm [Silva et Prather, 2000].

10. Standard aerosol particle mass spectrometric analysis

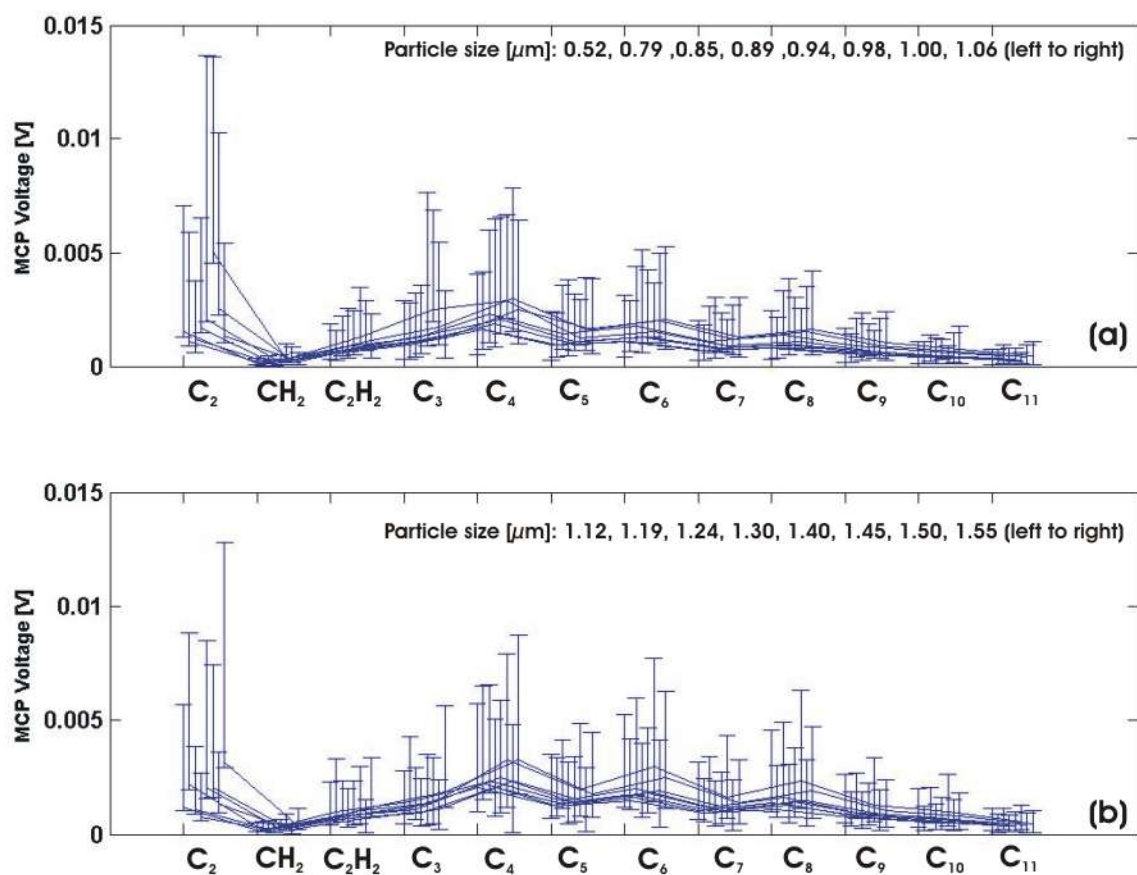


Figure. 54 : Carbon cluster anions C_n peak intensity

The error bars represent the range over which spans the peak intensity for a given peak corresponding to a given carbon cluster while the line which joins every error bars marks the corresponding mean of the peak intensity.

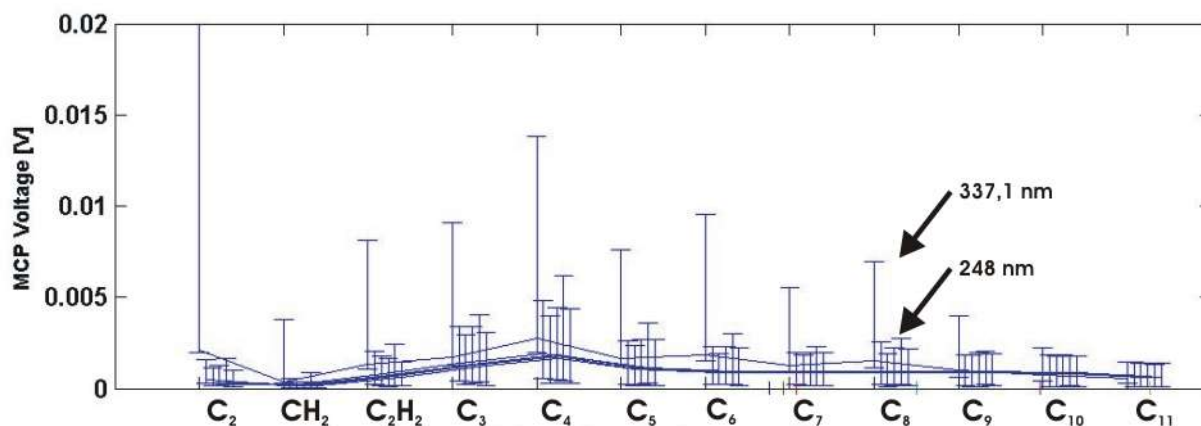


Figure. 55 : Carbon cluster anions C_n peak intensity at $\lambda = 337,1 \text{ nm}$ and $\lambda = 248 \text{ nm}$

10. Standard aerosol particle mass spectrometric analysis

It is also consistent with the mass spectra from the work of [Shibagaki et al., 2000] who reports for the ablation of a graphite target at a wavelength of 1,06 nm ($0,5 \text{ W}/\mu\text{m}^2$) in a LMMS experiment a similar behavior of the predominance of the even-number of carbon cluster anions over the odd-number carbon clusters.

Interestingly, [Shibagaki et al., 2000] reports the opposite behavior for positively charged odd-number carbon clusters which are preferentially present in the positive mass spectra compared to even-number carbon clusters. Unfortunately not enough positive carbon clusters have been observed yet to confirm the work of [Shibagaki et al., 2000]. Further work is needed to investigate the origin of the default of positive signal for the carbon clusters for soot particles.

In this direction, the review of [Van Orden et Saykally, 1998] proposes some lights on the previous observations. As illustrated in Figure. 56, odd-number carbon clusters are generally more stable than even-number carbon clusters what explains the results of [Shibagaki et al., 2000]. The difficulty of observing positive carbon clusters might be linked with their respective very high ionization potential which lies globally above 8 eV for the cluster size range investigated here combined with the possible charge transfer effects with low ionization metals such as sodium and potassium. On its side, the preferential occurrence of the negative even-number carbon clusters should be linked to the balance between the better odd-number carbon clusters stability and the high electron affinity of even-number carbon clusters unless the presence of an additional electron has a stabilizing effect on the carbon cluster what needs to be verified.

In order to gain more insights into the carbon cluster ion formation processes, this experiment should be performed again with sodium- and potassium-free soot or graphite particles to eliminate the probable effect of charge transfer from the carbon clusters to the metal ions (here Na, K) which attenuates signal of the positive carbon clusters. In this regard, the SPALMS instrument is a good instrument to deepen the work of [Shibagaki et al., 2000] since it can perform the simultaneous analysis of small carbon cluster cations and anions with possibly the investigation of the ablation plume aging by delay extraction. One might also be able to evaluate the role of the ions of both polarities in the carbon cluster ions growth.

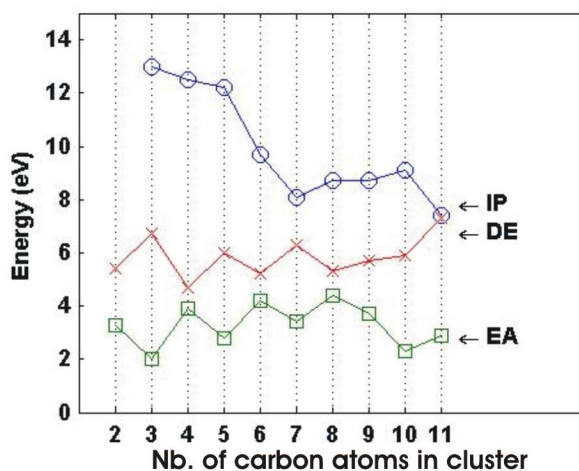


Figure. 56 : Thermochemical data of carbon clusters

EA: Electron Affinity (eV), **DE:** Dissociation energy (eV), **IP:** Ionization potential (eV) (data from [Van Orden et Saykally, 1998])

10.2.2 Observation of PAHs in combustion soot particles from incineration plant

Figure. 57 presents positive mass spectra obtained in free-running mode with a Nd:YAG laser ($\lambda = 266$ nm) (Figure. 57(a) and (b)) and a nitrogen laser ($\lambda = 337,1$ nm) (Figure. 57(c)) of soot particles from the combustion of wood. In spite of the high degree of fragmentation observed at low masses, one still does observe a small amount of compounds with high masses (Figure. 57(b)). Some of these peaks correspond to molecular ions ($m/z = 276$ and 300) which can be attributed to polyaromatic compounds (PAHs) of formulas $C_{21}H_{12}$ and $C_{24}H_{12}$ such as for example anthanthrene and coronene, respectively.

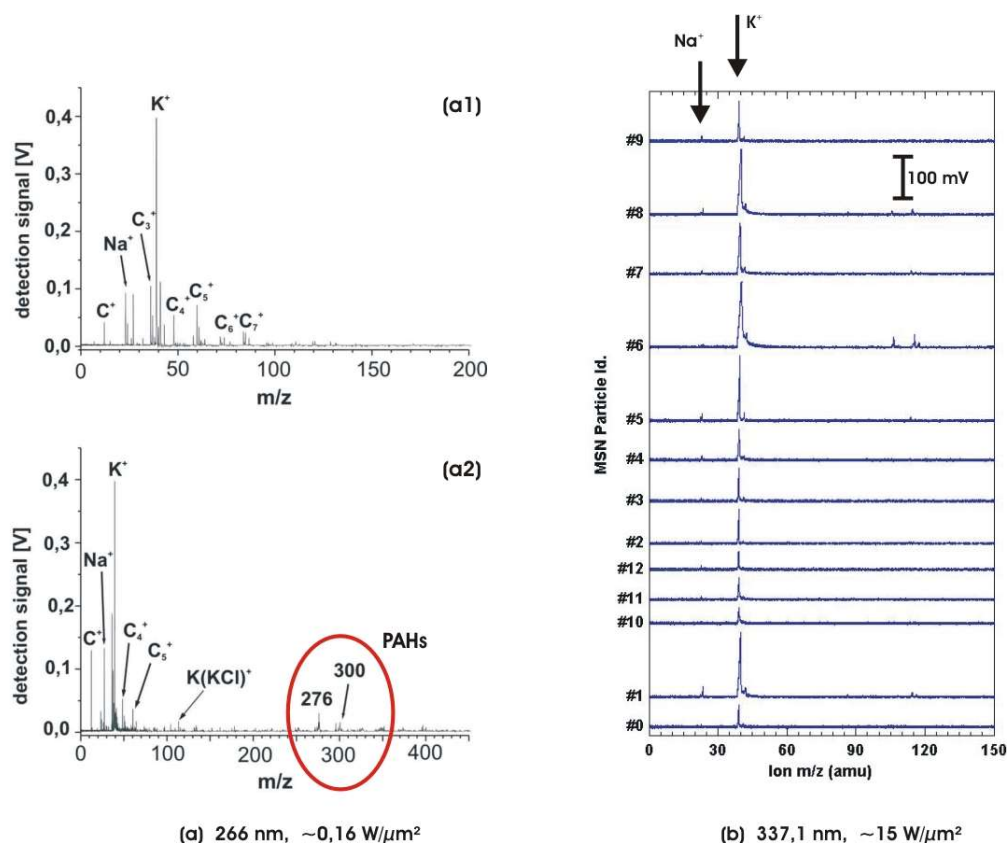


Figure. 57 : Biomass soot single particle positive mass spectra at $\lambda = 266$ nm and $\lambda = 337,1$ nm

The observation of such compounds can be expected considering the ionization process at $\lambda = 266$ nm. Indeed, these compounds can be detected here due their photoionization via a REMPI process once the molecules are brought into a gas phase. On the other hand, mass spectra of the same sample investigated with the nitrogen laser wavelength $\lambda = 337,1$ nm presented in Figure. 57(c) only demonstrates the presence of sodium and potassium which is consistent with their observation with the Nd:YAG laser at $\lambda = 266$ nm. However, the low amount of particles observed in both conditions can not exclude that polyaromatic compounds (PAHs) can not be detected by using a nitrogen laser at 337,1 nm for their ionization. Indeed even if PAHs can not be photoionized at 337,1 nm, [Hinz et al., 2005] report nevertheless the observation of compounds considered to be PAHs using a nitrogen laser for the desorption/ionization of the particle constituents, what suggests that the PAHs were chemically ionized in that case. Thus the analysis of particles with different laser lights leads to the observation of given types of chemicals and to a better understanding of the

10. Standard aerosol particle mass spectrometric analysis

ionization processes occurring during the laser desorption/ionization.

10.2.3 Wood combustion soot particles

Figure. 58 presents positive and negative mass spectra of wood combustion soot single particles obtained with a one-step desorption/ionization with a nitrogen laser at $\lambda = 337,1$ nm. The biogenic origin of these soot particles is suggested by the high amount of potassium (K, 39) which always saturates the detector as well as by the apparent lower amount of sodium (Na, 23).

This sample is significantly different from the Palas soot particles even if from the powder visual aspect they seem identical. The negative mass spectra permit the detection of the presence of organic compound containing hydrogen atoms as suggested by the series of carbon clusters of formula $C_nH_{m=1-4}$ for $n = 2$ to 7 and less clearly up to $n = 10$ where the fragments C_nH_3 or C_nH_4 tend to be more frequent at high masses (starting from $n = 8$, i.e. from $m/z = 84$).

It is interesting to note that peak aggregates C_nH_{1-4} corresponding to even-number of carbon atoms are always more intense than peak aggregates C_nH_{1-4} with n an odd-number as was observed for pure carbon clusters. This might suggest that the hydrogen content of the hydrogenated carbon clusters does not modify dramatically the intrinsic properties of the pure carbon clusters.

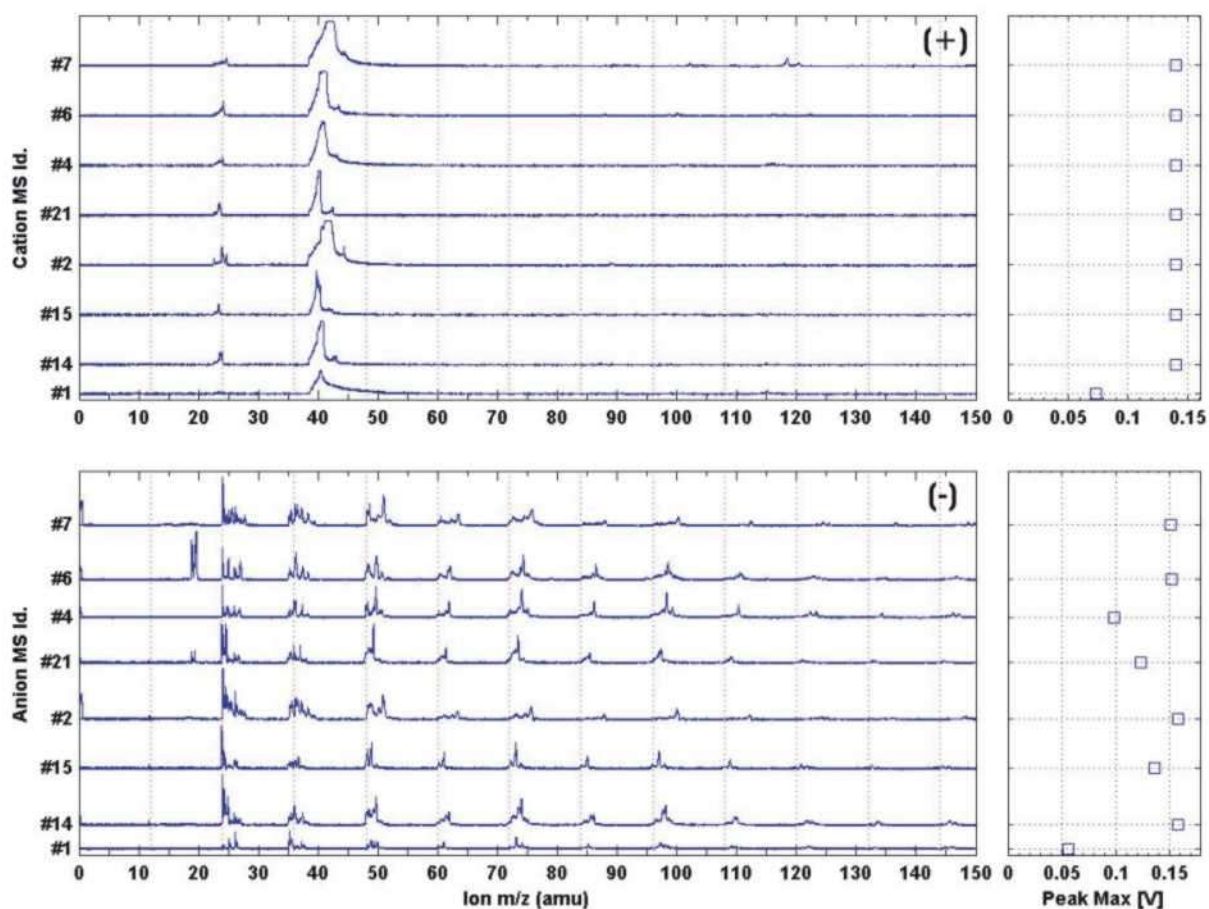


Figure. 58 : Positive and negative mass spectra of soot single particles from wood combustion at $\lambda = 337,1$ nm

10. Standard aerosol particle mass spectrometric analysis

For high masses starting at $m/z \sim 84$, the calibration of the mass spectrometer does not assign the ion clusters to the classical carbon clusters C_n from mass spectra to mass spectra. According to the observation presented in Chapter 8, this can be linked to an inappropriate mass calibration or/and to the higher occurrence of carbon clusters with a high content of hydrogen than pure carbon clusters. In the former case, the deviation from the mass calibration reflects here most probably the probable total ablation of the particle and the high power density delivered by the laser on the surface of the particle. In the later case, the higher peak of each peak aggregate seems to have the following composition C_nH_2 , C_nH_3 or C_nH_4 since each peak aggregate seems to start at a mass corresponding to the hydrogen-free corresponding carbon cluster C_n . This points out the need of (i) more control on the desorption/ionization event and (ii) to adapt the calibration curve to each particle.

This series of mass spectra illustrates the possibility of differentiating the organic- from elemental carbon-containing particles by detecting the hydrogenated carbon clusters in the mass spectra of the particles. Maybe classes of organics detected in the mass spectra as hydrogenated carbon clusters of general formulas C_nH_m can be differentiated from each other on the basis of specific value associations of n and m which are specific of the laser desorption/ionization process. It should be noted here that the usual fragmentation rules of organics used in mass spectrometry (by electron impaction for example) to identify molecules (as for example, fragment of $m/z = 14$ for $-CH_2-$ that indicates an aliphatic carbon chain) can not be applied here because the laser desorption/ionization process induces most of the time the fragmentation of the molecules and their possible rearrangement in the desorption plume. From the aerosol mass spectrometry literature, it appears that all organics appear as carbon clusters with variable content of hydrogen. The presence of C_nH_m peaks indicates here the presence of organic carbon in the particle rather than elemental carbon that may also be present. This suggests that the proportion of peaks in mass spectra due to C_nH_m and to C_n carbon clusters can be used as a mean to measure the OC/EC ratio (organic carbon/elemental carbon) of single particles as reported in [Ferge et al., 2005a].

For this reason, it is important to investigate further the formation of carbon clusters for diverse carbon source materials in order to know if the observed carbon cluster patterns in negative and, if any, positive mass spectra can be related to the initial form/speciation of the carbon atoms in the particle.

It is also interesting to note the particular shape of some of the mass spectra observed for C_2 , C_2H and C_2H_2 . For these clusters, the corresponding peaks appear to be divided into two peaks corresponding to the same m/z . This feature will be later discussed, as a mean to characterize the desorption/ionization conditions.

10.2.4 Particle mass spectra from rich PAHs particles (Sample #10)

Sample #10 was obtained during a measurement campaign on a middle scale incineration plant in Clausthal, Germany (see [Zimmermann et al., 2000] for further details). This sample has been thoroughly analyzed by different laser microprobe mass spectrometers and also by the ATOFMS instrument of TSI, Inc. According to [Zimmermann, 2005], polyaromatic compounds (PAHs) were detected in similar samples by an aerosol mass spectrometer operating a nitrogen laser ($\lambda = 337,1$ nm) as a desorption/ionization laser. For this reason, it was interesting to further test the SPALMS instrument with this sample with the nitrogen laser ($\lambda = 337,1$ nm).

Due to the low hit-rate of the SPALMS instrument (operated here in static trigger mode and a nozzle), only very few particles were hit. Globally, this sample can not be differentiated from the soot from wood combustion presented before (Figure. 58). Since no significant signal was observed

10. Standard aerosol particle mass spectrometric analysis

beyond the mass $m/z = 150$, no PAHs were detected. This was expected since the particles containing PAHs are in low amount ($\sim 7\%$), the number of particles hit is not significant (less than 20) and the quantity of Sample #10 was insufficient for obtaining enough mass spectra. Furthermore, the wavelength of $\lambda = 337,1$ nm (nitrogen) is not the most appropriated for the detection of PAHs.

10.2.5 Particle mass spectra of Ash particles from a private fireplace

The SPALMS instrument was also tested with an ash sample from a private fireplace where construction wood wastes were burned. The wood wastes contained a lot of iron nails which were mainly rusted and a lot of rests of paintings originating from the years 60's where color pigments often contain heavy metals such as lead. Furthermore these wood wastes were stored in dusty place so that the ash is also expected to contain some soil materials. The ash sample was first filtered and sieved to keep only the fraction of particles smaller than $160 \mu\text{m}$ (the lowest available size of the sieve). The resulting powder was then sampled into the SPALMS instrument with a small scale powder disperser (SSPD, TSI Inc., St Paul, MN, USA) which only re-disperses in air particles from the powder sample whose diameter is smaller than $5 \mu\text{m}$. Figure. 59(a),(c) presents the summed mass spectra (respectively of 80 mass spectra for $\lambda = 337,1$ nm and 77 for $\lambda = 248$ nm) of the ash particles. The sum of the mass spectra illustrate the diversity of the chemical species detected by the SPALMS instrument. It is worth to note the great similarity of the particle mass spectra for both polarities for both laser wavelengths and different laser powers. The peak assignment of the mass spectra with species is here tentative.

All positive particle mass spectra are similar and illustrate the presence of sodium (Na, 23), potassium (K, 39), iron (Fe, 56) and possibly magnesium (Mg, 24) and calcium (Ca, 40) in the ash particles considering its origin. In some cases, lead (Pb, 208) is detected as illustrated in Figure. 59 (c). The large peak width of the summed mass spectra is attributed first to the high amount of sodium, potassium, iron and possibly magnesium and calcium and secondly to the summing process of all mass spectra whose calibration differ slightly from particle to particle as illustrated in Chapter 8. The examination of the single positive mass spectra confirms that the width of the peak for sodium, potassium and iron is due to their high amount in the particle. The peak width due to the isotope distribution of an element can also be the cause of the peak width. It is the case of, due to the expected low amount in each particle, lead (Pb, 208) since its isotopes are of similar natural abundance. This is further accentuated by the loss of mass resolution at high masses. This is however not justified for sodium, potassium or iron as suggested by the natural occurrence of different elements listed in Table 39.

The sum of the positive mass spectra also shows the presence of soot particles only in the summed mass spectra at $\lambda = 248$ nm. Such observation is consistent with the results obtained for the other soot particles investigated in this study. The reasons of absence of carbon cluster in the positive sum mass spectra at $\lambda = 337,1$ nm are not clear. A first possible explanation could be the summing effect of the mass spectra.

10. Standard aerosol particle mass spectrometric analysis

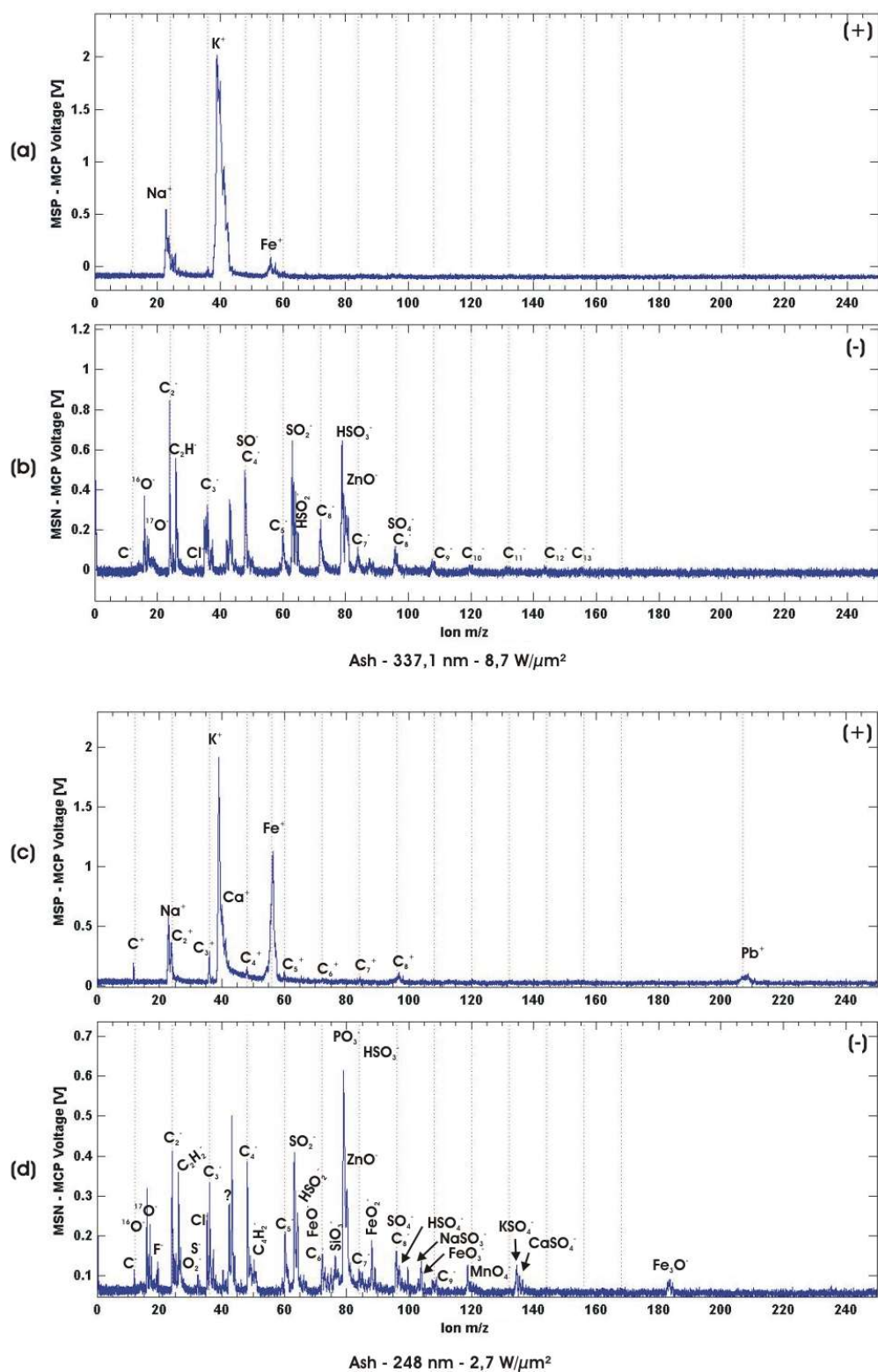


Figure. 59 : Summed mass spectra of ash single particles at $\lambda = 337\text{nm}$ and $\lambda = 248\text{ nm}$
 (a),(b) Sum of 80 mass spectra for $\lambda = 337.1\text{ nm}$. (c),(d) Sum of 77 mass spectra for $\lambda = 248\text{ nm}$

10. Standard aerosol particle mass spectrometric analysis

<i>Element</i>	<i>Most abundant isotopes</i>	<i>Nominal mass</i>	<i>Natural abundance (%)</i>
O	¹⁶ O	16	99.76
Na	²³ Na	23	100
Mg	²⁴ Mg	24	78.99
	²⁵ Mg	25	10
	²⁶ Mg	26	11.01
Al	²⁷ Al	27	100
Si	²⁸ Si	28	92.21
	²⁹ Si	29	4.67
	³⁰ Si	30	3.1
P	³¹ P	31	100
	³² P	32	95.03
	³⁴ P	34	4.22
Cl	³⁵ Cl	35	75.77
K	³⁹ K	39	93.25
	⁴¹ K	41	6.73
Ca	⁴⁰ Ca	40	96.94
	⁴⁴ Ca	44	2.09
Fe	⁵⁴ Fe	54	5.9
	⁵⁶ Fe	56	91.72
	⁵⁷ Fe	57	2.1
Pb	²⁰⁴ Pb	204	1.4
	²⁰⁶ Pb	206	24.1
	²⁰⁷ Pb	207	22.1
	²⁰⁸ Pb	208	52.4

Table 39 : Natural abundance (>1%) of some usual isotopes

Figure. 60 presents the different typical negative mass spectra of ash single particle obtained at $\lambda = 248$ nm. The nature of the ions represented in each mass spectrum class is listed in Table 40.

Negative mass spectra show a much more complex composition so that the peak assignment in Figure. 60 is very tentative. The negative mass spectra can be better interpreted by sorting the mass spectra into different classes based on their similarity. Since only 80 and 77 mass spectra were obtained for ash particles due to the current low hit efficiency of the SPALMS instrument, the obtained mass spectra were therefore sorted manually. A significant fraction of the obtained single particle mass spectra, 29% for $\lambda = 337,1$ nm and 48% for $\lambda = 248$ nm, can be attributed to be “pure soot particles” since their typical negative mass spectra are very similar to that obtained for the Palas soot particles. This suggests a contamination of the sampling line during previous measurements of soot particles.

10. Standard aerosol particle mass spectrometric analysis

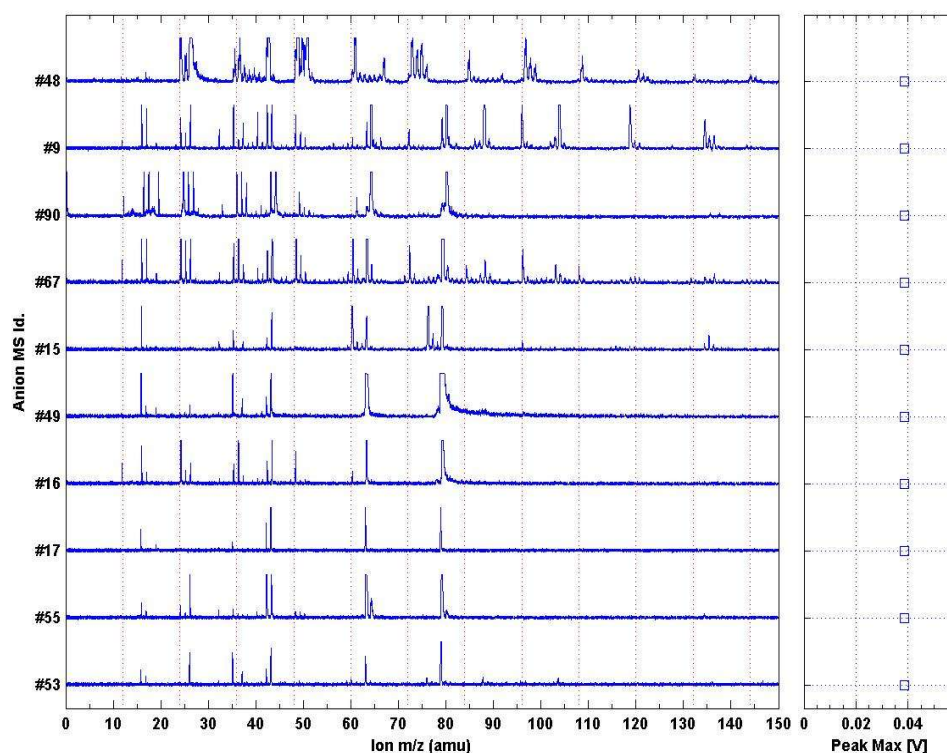


Figure. 60 : Typical classes of negative mass spectra of ash single particles at $\lambda = 248$ nm.
The tentative peak identification is presented in Table 40 for each typical mass spectrum

The analysis of the negative mass spectra of the ash single particles obtained with the nitrogen laser at $\lambda = 337,1$ nm results in a smaller number of classes. The characteristics of the sorted classes are presented in the following Table 41

Mass spectra obtained at $\lambda = 248$ nm appear to be more rich in variety and number of ions than at $\lambda = 337,1$ nm. This might be related to a higher fragmentation efficiency of the ions of low mass at $\lambda = 337,1$ nm compared to $\lambda = 248$ nm since the power density incident on the particle is higher for the former. It is however difficult to judge this hypothesis since the voltage acquisition range of the mass spectra was 0,04 V for $\lambda = 248$ nm as opposed to 0,15 for $\lambda = 337,1$ nm due probably to a bad acquisition device setting.

A low voltage acquisition range permits a better detection of weak signals. As a result, measurements with the nitrogen laser with the same data acquisition device settings might show similar mass spectra as those obtained at $\lambda = 248$ nm. Due to the limited set of mass spectra and the experimental conditions to still tune, one can not assess precisely the influence of the wavelength and the power density on the obtained mass spectra.

From the negative mass spectra at $\lambda = 248$ nm, it can be concluded that ash particles contain sulfates, iron and silicon species with certitude. Indeed these species appear with redundancy within the mass spectra. Indeed sulfates appear with S^- (32), SO^- (48), HSO^- (49), SO_2^- (64), SO_3^- (80), SO_4^- (96), $NaSO_3^-$ (103), KSO_4^- (135), $CaSO_4^-$ (136). Iron species are detected via the ions FeO^- (72), FeO_2^- (88), FeO_3^- (104) and with Fe^+ in positive mass spectrum whereas silicon species are with SiO^- (44), SiO_2^- (60), $HSiO_2^-$ (61), SiO_3^- (76). Aluminium and chlorine seem to be present since some peaks suggest them even if only one peak indicates their presence (AlO^- (43), Cl^- (35) and ClO^- (51).

10. Standard aerosol particle mass spectrometric analysis

<i>MS</i>	<i>Occurrence(%)</i>	<i>List of species</i>
#53	3.9	O ⁻ (16), Cl ⁻ (35), ³⁷ Cl ⁻ (37), SO ₂ ⁻ (64), SO ₃ ⁻ (80), FeO ₂ ⁻ (88), FeO ₃ ⁻ (104)
#55	2.6	O ⁻ (16), C ₂ ⁻ (24), C ₂ H ₂ ⁻ (26), AlO ⁻ (43), SiO ⁻ (44), SO ₂ ⁻ (64), HSO ₂ ⁻ (65), SO ₃ ⁻ (80)
#17	22.1	O ⁻ (16), AlO ⁻ (43), SiO ⁻ (44), SO ₂ ⁻ (64), SO ₃ ⁻ (80)
#16	1.3	C ⁻ (12), O ⁻ (16), OH ⁻ (17), C ₂ ⁻ (24), C ₂ H ⁻ (25), C ₂ H ₂ ⁻ (26), S ⁻ (32), Cl ⁻ (35), C ₃ ⁻ (36), C ₃ H ⁻ (37), AlO ⁻ (43), SiO ⁻ (44), C ₄ ⁻ (48), SO ⁻ (48), C ₅ ⁻ (60), SiO ₂ ⁻ (60), SO ₂ ⁻ (64), SO ₃ ⁻ (80)
#49	1.3	O ⁻ (16), OH ⁻ (17), C ₂ H ₂ ⁻ (26), S ⁻ (32), Cl ⁻ (35), C ₃ ⁻ (36), ³⁷ Cl ⁻ (37), AlO ⁻ (43), SiO ⁻ (44), SO ₂ ⁻ (64), SO ₃ ⁻ (80)
#15	2.6	O ⁻ (16), OH ⁻ (17), C ₂ ⁻ (24), C ₂ H ₁ ⁻ (25), C ₂ H ₂ ⁻ (26), S ⁻ (32), Cl ⁻ (35), C ₃ ⁻ (36), ?(37), AlO ⁻ (43), SiO ⁻ (44), SiO ₂ ⁻ (60), HSiO ₂ ⁻ (60), SO ₂ ⁻ (64), SiO ₃ ⁻ (76), SO ₃ ⁻ (80), SO ₄ ⁻ (96)
#67	1.3	C ⁻ (12), O ⁻ (16), OH ⁻ (17), C ₂ H ₂ ⁻ (26), S ⁻ (32), Cl ⁻ (35), C ₃ ⁻ (36), C ₃ H ⁻ (37), ?(41), ?(42), AlO ⁻ (43), SiO ⁻ (44), C ₄ ⁻ (48), SO ⁻ (48), C ₄ H ⁻ (49), HSO ⁻ (49), C ₄ H ₂ ⁻ (50), C ₅ ⁻ (60), SiO ₂ ⁻ (60), C ₃ H ⁻ (61), HSiO ₂ ⁻ (61), SO ₂ ⁻ (64), HSO ₂ ⁻ (65), C ₆ ⁻ (72), FeO ⁻ (72), C ₆ H ⁻ (73), SiO ₃ ⁻ (76), SO ₃ ⁻ (80), C ₇ ⁻ (84), FeO ₂ ⁻ (88), C ₈ ⁻ (96), SO ₄ ⁻ (96), NaSO ₃ ⁻ (103), FeO ₃ ⁻ (104), C ₉ ⁻ (108), C ₁₀ ⁻ (120)
#90	1.3	C ⁻ (12), O ⁻ (16), OH ⁻ (17), F ⁻ (19), C ₂ ⁻ (24), C ₂ H ₁ ⁻ (25), C ₂ H ₂ ⁻ (26), S ⁻ (32), Cl ⁻ (35), C ₃ ⁻ (36), C ₃ H ⁻ (37), ?(41), ?(42), AlO ⁻ (43), SiO ⁻ (44), C ₄ ⁻ (48), SO ⁻ (48), C ₄ H ⁻ (49), HSO ⁻ (49), C ₄ H ₂ ⁻ (50), SiO ₂ ⁻ (60), SO ₂ ⁻ (64), SO ₃ ⁻ (80)
#9	5.2	C ⁻ (12), O ⁻ (16), OH ⁻ (17), C ₂ H ₂ ⁻ (26), S ⁻ (32), Cl ⁻ (35), C ₃ ⁻ (36), ³⁷ Cl ⁻ (37), C ₃ H ⁻ (37), ?(41), ?(42), AlO ⁻ (43), SiO ⁻ (44), C ₄ ⁻ (48), SO ⁻ (48), C ₄ H ⁻ (49), HSO ⁻ (49), C ₄ H ₂ ⁻ (50), SiO ₂ ⁻ (60), SO ₂ ⁻ (64), HSO ₂ ⁻ (65), FeO ⁻ (72), C ₆ H ⁻ (73), SiO ₃ ⁻ (76), SO ₃ ⁻ (80), ⁵⁴ FeO ₂ ⁻ (86), ?(87), FeO ₂ ⁻ (88), SO ₄ ⁻ (96), NaSO ₃ ⁻ (103), FeO ₃ ⁻ (104), NaSO ₄ ⁻ (119), ?(120), ?(134), KSO ₄ ⁻ (135), CaSO ₄ ⁻ (136), ?(137)
#48	1.3	C _{n=1-11} H _{m=0-4} , AlO ⁻ (43) or SiO ⁻ (44), ?(67)
Soot	48	C _{n=1-11} H _{m=0-4} ,
Rest	9.1	Only one peak at different m/z

Table 40 : Tentative ion identification of the negative mass spectra peaks of ash single particles at $\lambda = 248$ nm

<i>Proportion (%)</i>	<i>Typical pattern</i>
15,0	like mass spectrum #17 at $\lambda = 248$ nm
27,5	like mass spectrum #16 at $\lambda = 248$ nm
28,7	Soot like mass spectra
Rest	Mass spectra with weak signal with one or two peaks

Table 41 : Main characteristics of the negative mass spectra of ash single particles at $\lambda = 337,1$ nm

One should note that the mass spectra #16, #67, #90, #9 indicate an internal mixture of carbon (most probably soot), sulfate, silicon oxides, iron oxides, aluminium oxides and chlorine whereas mass spectra #49, #15, #17 show mineral only containing particles with sulfates, aluminium oxides and silicon oxides. The occurrence of aluminium oxides as well as silicon oxides indicate the presence of aluminosilicates compounds which clearly originate from soil material. The mass spectrum #48 precises the occurrence of organic material remaining in the ash due to its C_{n=1-10}H_{m=1-4} peaks pattern.

As a conclusion, the mass spectrometric analysis is consistent with the origin of the particle sample. It is to note that no nitrates were detected as NO₂⁻(46) or NO₃⁻(62) as well as some phosphates as PO₂⁻(63) or PO₃⁻(79).

10.2.6 Other investigated particles

Other particles were used to test further the performances of the SPALMS instrument. The studied particles were chemically pure and some of them present a monodisperse size distribution. Their analyses are presented here since these particles were optically detected but did not give mass spectra.

- Monodisperse particles

For this study, the SPALMS instrument was operated in static trigger mode. This makes the obtention of particle mass spectra for monodisperse particles very difficult, sample consuming and/or time consuming since the appropriate time delay is to be found. It is needed in this case to test the trigger time delay by steps of ~ 80 ns (for a PSL $1 \mu\text{m}$ particle, particle velocity ~ 350 m/s) over ~ 65 discrete values to scan the different possibilities to make sure that particles can be hit by the laser light of the desorption/ionization laser.

PSL particles are commonly used as standard particles to test aerosol analyzers such as APS, SMPS or aerosol mass spectrometers. If the detection/sizing unit can be well characterized with PSL particles, no particle mass spectra were obtained for PSL particles. PSL particles can nevertheless be observed with a nitrogen laser at power density of $265 \text{ W}/\mu\text{m}^2$ as reported many times in the work of [Hinz et al., 1994] or [Vera et al., 2005].

Since the SPALMS instrument is operated in static trigger mode, the reason can be that the desorption/ionization laser was never fired at the right time but always too early or too late. Another reason can also be that the laser power density operated here, $11 \text{ W}/\mu\text{m}^2$, was too low to produce a mass spectrum compared to the work of [Hinz et al., 1994].

On the other hand, the extent in which the PSL particle dryness in the aerosol generator affects the mass spectra obtention is yet not known and might be of importance as presented in [Neubauer et al., 1998] where the effects of particle humidity on mass spectra are discussed. Indeed the presence of a water layer at the surface of the PSL particle might shield the particle against the laser light. On the other hand, the vaporized water molecules in the desorption plume might have a quenching effect that reduces the ionization probability of the molecules.

Similarly no mass spectra were obtained for monodisperse spherical silica particles (geometric diameter $1,25 \mu\text{m}$, later referred as SiO_2 particles) even if they were aerosolized in a dry manner by a small scale particle disperser (SSPD3433, TSI Inc., St Paul, MN, USA). [Reents et al., 1995] reports the obtention of mass spectra of SiO_2 particles at $\lambda = 308 \text{ nm}$ for a power density of $200 \text{ W}/\mu\text{m}^2$ by detecting Si^+ (28) and SiO_2^+ (60). In this case, the low laser power of the desorption/ionization laser of the SPALMS instrument might be the most fundamental and most probable, explanation for the difficulty of obtaining mass spectra of silica particles even if the reasons invoked for PSL are also valid here.

- Polydisperse particles

Mineral particles of sodium chloride (NaCl), magnesium chloride (MgCl_2) and manganese chloride (MnCl_2) were also tested and produced by grinding their dry salts in a ball grinding mill. The resulting particle size distribution of each particle type measured with an APS showed that the resulting powder contains enough particles of aerodynamic diameter between $0,7 \mu\text{m}$ and $2 \mu\text{m}$ permitting its sampling and analysis by the SPALMS instrument. No mass spectra were obtained for each sample. It is not clear yet whether the non-obtention of mass spectra was due to a problem

10. Standard aerosol particle mass spectrometric analysis

in the aerosol transmission through the nozzle and the desorption/ionization zone or due to unappropriated laser desorption/ionization conditions. Considering the nature of the powder, a default of the particle transmission would appear the most probable since NaCl particles can be readily observed in aerosol mass spectrometry. It is not known yet in which extent particles obtained by grinding from their pure dry salt can be readily analyzed by aerosol mass spectrometry since such particles are usually produced by dissolving the corresponding salt in water and drying the wet particle to its dry state.

10.3 Two-step laser desorption/ionization particle analysis

By separating the desorption from the ionization process, one can conserve some information about the structure of the molecules contained in the aerosol particle and better investigate a mixture of chemicals as illustrated in Figure. 61 for particles from an incomplete wood combustion. Indeed, molecules are usually fragmented during the one-step desorption/ionization process (Figure. 61(a)).

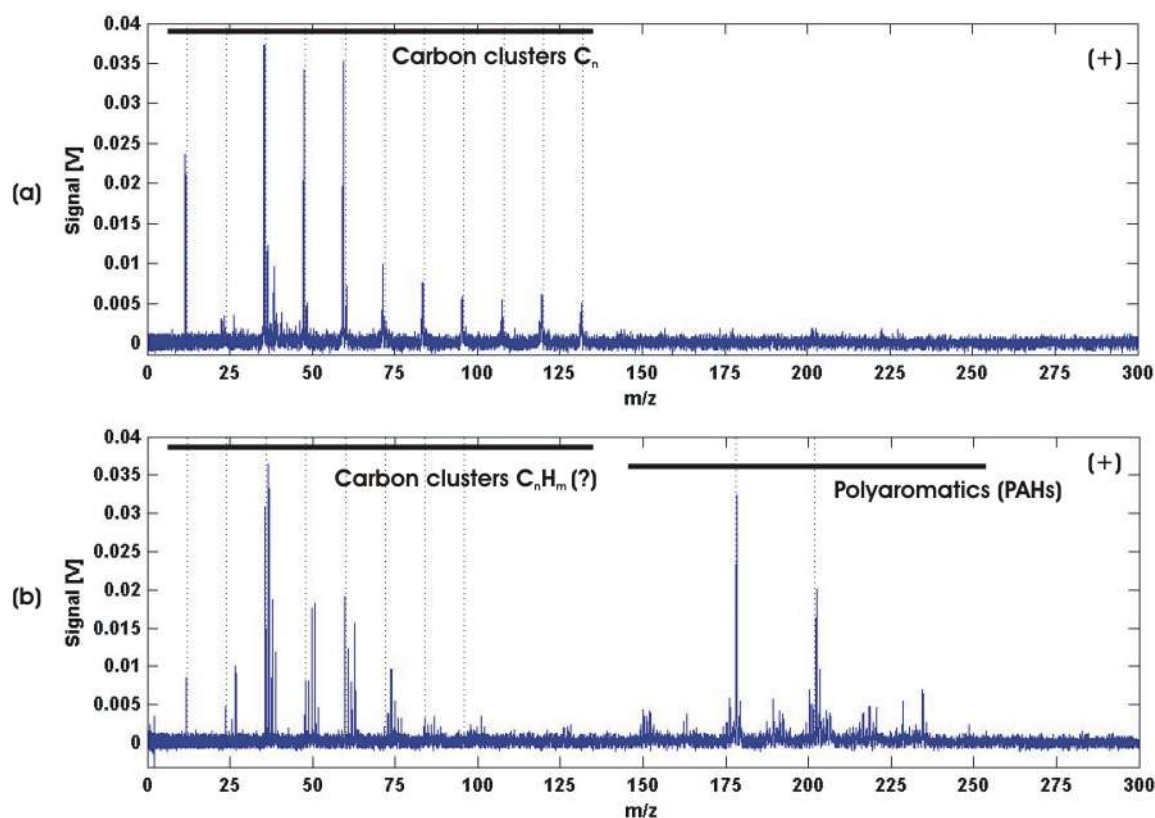


Figure. 61 : Wood soot particles processed with a one- and two-step laser desorption/ionization

This figure presents the positive mass spectra of wood soot particles analyzed according to two laser desorption/ionization approaches. The vertical dotted lines before $m/z = 150$ correspond to each carbon cluster C_n mass such that $m/z = 12.n$. **Panel (a)**: One-step desorption/ionization, $\lambda = 248$ nm, 5.4 W/ μm^2 , $\varnothing_{\text{beam}} = 1$ mm. **Panel (b)**: Two-step desorption/ionization (desorption laser: $\lambda = 10,6$ μm , 2.0 W/ μm^2 , $\varnothing_{\text{beam}} = 1$ mm, ionization laser: $\lambda = 248$ nm, 5.4 W/ μm^2 , $\varnothing_{\text{beam}} = 1$ mm, time delay between both laser pulse: 1 μs).

10. Standard aerosol particle mass spectrometric analysis

In the positive mass spectra obtained with the two-step laser desorption/ionization (Figure. 61(b)), one can observe in particular many compounds with high masses such as $m/z = 150, 178, 192, 202, 206, 220, 234, 248$ which can be attributed to polyaromatic compounds PAHs. This suggests that the particles have been produced in incomplete burning conditions. This later conclusion can not be inferred when the analysis is performed with a one-step desorption/ionization.

In Figure. 61(b) one can also observe the occurrence of small carbon containing molecules similar to the carbon clusters C_nH_m observed before in one-step desorption/ionization. It is interesting to note from Figure. 62(a) and Figure. 62(b) that these clusters are richer in hydrogen when they are produced from a two-step laser desorption/ionization. The origin of these ions in positive mass spectrum is surprising since, from Figure. 56, carbon clusters have a high ionization potential that is above 8 eV so that their photoionization with the excimer laser at $\lambda = 248$ nm (5.0 eV) is unlikely and since no chemical ionization processes are expected in a two-step approach. It would suggest either that the ionization laser power is too high so that vaporized molecules are fragmented and cations are produced during the fragmentation or that it performed, unexpectedly, a one-step desorption/ionization of the eventual rest of the particle.

If the corresponding negative mass spectra report the presence of some negatively charged carbon cluster ions, it would suggest that a one-step laser desorption/ionization of the particle rest occurred. The negative mass spectra (not presented here) however do not indicate any produced ions. At this stage of the work, it is difficult to propose a reliable explanation since only few particles, which have a complex composition, were investigated under limited experimental conditions. To better understand this observation, the particle has to be better tracked, the ionization laser power density incident on the particle better controlled and the relative position of both lasers should be varied. Indeed the spatial-offset of the ionization laser beam off the particle beam should answer the question reliably.

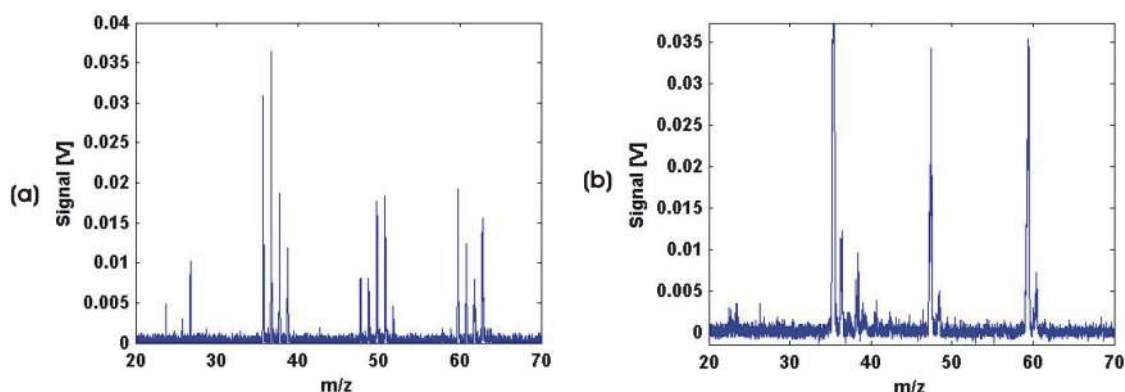


Figure. 62 : Low mass carbon ions detected with a two-step and one-step laser desorption/ionization

The low mass carbon clusters observed with two-step laser desorption/ionization are richer in hydrogen than in the one-step approach. It is also interesting to note the better mass resolution obtained with a two-step laser desorption/ionization compared to the one-step approach. **Panel (a):** Two-step desorption/ionization (desorption laser: $\lambda = 10,6 \mu\text{m}$, $2,0 \text{ W}/\mu\text{m}^2$, $\Phi_{\text{beam}} = 1 \text{ mm}$, ionization laser: $\lambda = 248 \text{ nm}$, $5,4 \text{ W}/\mu\text{m}^2$, $\Phi_{\text{beam}} = 1 \text{ mm}$, time delay between both laser pulse: $1 \mu\text{s}$). **Panel (b):** One-step desorption/ionization, $\lambda = 248 \text{ nm}$, $5,4 \text{ W}/\mu\text{m}^2$, $\Phi_{\text{beam}} = 1 \text{ mm}$.

11 Particle measurement steps integration

This chapter is an introduction for the next three chapters that describe different analytical approaches that can be followed to improve the knowledge of the aerosol characteristics based on the current aerosol mass spectrometer setup at the GSF-Forschungszentrum.

As presented many times in this work, a special care has been given to implement devices dedicated to collect all available information possible and retrieve them so that each information type can be cross-checked. An overview of the relationships between the different information sources is presented in Figure. 63 where PE1, PE2, PE3 and PE4 respectively stand for Particle Ensemble Nr.1, 2, 3 and 4 which each concerns less and less particles but not always the same. This reflects the parallel use of the Aerodynamic Particle Sizer (APS) and SPALMS mass spectrometer even if both instruments could have been operated in series or tandem. The setup of the APS and SPALMS instrument in tandem would have been complex, induced probably a high loss of particles between the exit of the APS and the inlet unit of the aerosol mass spectrometer. Furthermore the tracking of the single particle between both instruments would have not been possible.

The ensemble PE1 concerns the group of particles analyzed by the APS which permits the measurement of the size distribution, of the aerodynamic and optical properties of the aerosol single particles. The ensemble PE2 concerns all particles collected in the aerosol mass spectrometer which are not transmitted to the sizing unit nor to the chemical analysis unit (here the desorption/ionization unit and mass spectrometer unit). The information from PE2 should be considered as particle bulk information especially for further off-chemical analysis. The ensemble PE3 provides a similar data set as obtained by the APS but concerns a much smaller number of particles. Finally the PE4 ensemble corresponds to the group of single particles that are sized and chemically analyzed by the SPALMS instrument.

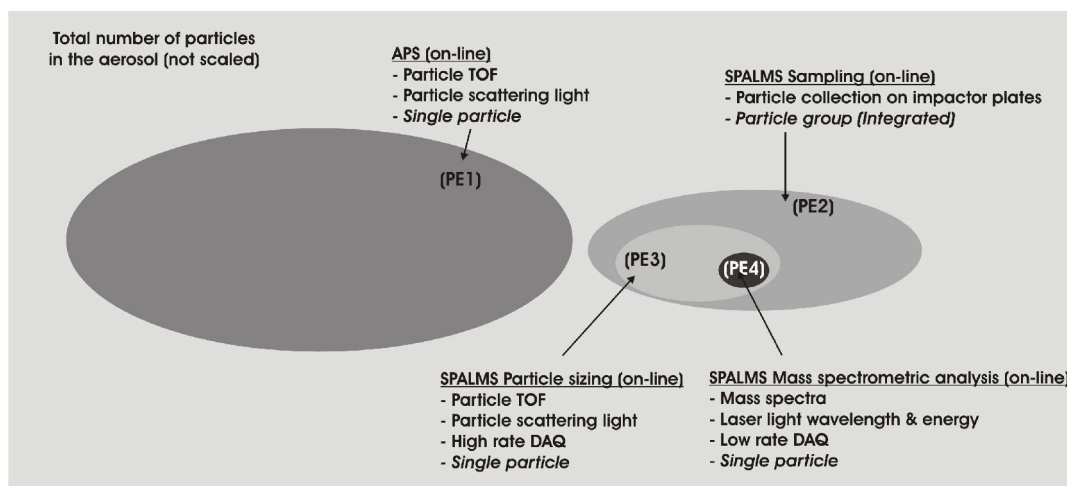


Figure. 63 : SPALMS - APS information balance (weight and relationships)

The size of the ensembles is not scaled to the relative amount of the available data presented in Table 42

11. Particle measurement steps integration

The confidence to accord to each information source is to be considered in terms of number of particles that were sampled and in terms of reproducibility of the quantity being measured. This needs to evaluate the amount of particles analyzed compared to the number of particle sampled for each ensemble. For this purpose, a particle balance of the experimental setup is evaluated and presented in Table 42. This gives an idea of the confidence attributed to each information for a given measurement step.

<i>External sampling system</i>	<i>Internal sampling/sensing system</i>	<i>Estimation of the particle proportion analyzed at each {SPALMS+APS} measurement step location (%)</i>
APS	Nozzle	100 ⁽¹⁾
	Sizing laser	100 ⁽¹⁾
SPALMS	Nozzle	100 ⁽¹⁾
	Skimmer I + pump system 1	99,5 ⁽²⁾
	Skimmer II + pump system 2	0,47 ⁽²⁾
	Sizing laser 1	0,2 ⁽²⁾
	Sizing laser 2	0,1 ⁽²⁾
	Desorption/ionization laser	0.1 ⁴⁽³⁾
	Impactor behind the Desorption/ionization laser	0,1 ⁽²⁾

Table 42 : Particle number balance for the {SPALMS+APS} measurement setup

⁽¹⁾ estimated to be unity for the particle size range considered (0,7 μm to 3 μm), ⁽²⁾ estimated from geometric considerations after Chapter 5., ⁽³⁾ estimated after Chapter 7.

From Chapter 5 and from Table 42, if the particle size distribution determined by the aerosol mass spectrometer can be considered rather true, it can not be the case for the chemical analysis. In the following chapters, its will be presented how the correlation of information from each measurement unit, corresponding to the four particle ensembles identified in the Figure. 63, can be complementary or cross-check each others.

From (PE1) and (PE3), the particle size distribution can be inferred in a reliable way for the particle size range from 0,8 to 3 μm . If the aerosol mass spectrometer limits the size range, it provides with the data of (PE3) a better particle aerodynamic size resolution than the APS. By binning the aerosol mass spectrometer sizing data appropriately, the APS size distribution can be deduced.

Both (PE1) and (PE3) permit the optical differentiation of particles having the same aerodynamic diameter what principally leads to their density for a given refractive index and shape. By constraining two of the three parameters between particle size, refractive index or shape, the value of the third one may be deduced. In this logic, since the optical setups for the particle detection for the APS and the SPALMS instrument are similar, information from (PE1) and (PE3) are not equivalent but complementary and confirm each others.

The data set (PE4) gives the chemical signature of the particle and permits the characterization of its mixing state. Due to the low proportion of chemically analyzed particles (0,01%) and the imperfect chemical analysis of the particle, the data set (PE4) can not be used to infer a chemical bulk composition of the aerosol.

11. Particle measurement steps integration

By combining the data from (PE2) and (PE4), one can obtain with a high confidence the aerosol bulk composition for the non-volatile chemical constituents fraction for targeted chemical species. In this regard, the contribution of the data set (PE4) should be considered, due to the low amount of particle chemically analyzed, of low confidence and as minor if not negligible .

To attempt to evaluate how representative is the aerosol chemical composition inferred from the data set (PE4), the observed aerodynamic-optical properties of the single particles can be compared to the aerodynamic-optical properties obtained from the data set (PE3). Indeed since the refractive index and the density depend on the chemical composition, their respective values should be reflected in the observed chemical composition of the single particle from the data set (PE4). This might not work since the variability of the refractive index and density are much less diverse as the chemical composition is. This method can nevertheless be useful to state if particles of given properties are more preferentially chemical analyzed than other what biases the inferred chemical bulk composition from the data set (PE4). Indeed the laser ablation efficiency depends on the size and the chemical composition of the particle.

As described previously it is evident that the SPALMS instrument in its current state, as operated up to now by most of the aerosol mass spectrometry groups using laser based instruments, involves many physical principles that are not fully exploited yet. The merge and the confrontation of all data set from PE1, PE2, PE3 and PE4 ensembles should fully exploit this potential. This is why the instrument presented in this work has been designed with an exhaustive data acquisition facilities. This approach should lead to provide reliable and practical to use particle information to aerosol scientists.

However, as mentioned before, the current basic characteristics of the SPALMS instrument, a high transmission T and hit efficiency HE , are poor compared to other aerosol mass spectrometers. It is therefore very important to improve T and HE such that the ensembles PE3 and PE4 are the main particle source information instead of PE2. Furthermore PE3 and PE4 should concern the same particles. Indeed the vocation of an aerosol mass spectrometer is to characterize aerosols relying only on PE3 and PE4.

The next chapter presents the principles and results of the benefits of the additional sampling units to the usual aerosol mass spectrometer setup whereas the two following ones present and propose principles, results or bibliographic feasibility studies of hardware improvements, data analysis or analytical procedures to gain more information about the particle/aerosol and more confidence in each measurement event.

12 Benefits of additional particle sampling devices

This chapter illustrates the benefits of adding particle sampling devices to the aerosol mass spectrometer. Indeed, as previously mentioned, particles can be sampling by impaction at different locations within the inlet unit. This permits later an off-line further chemical analysis of the collected aerosol with more accurate or/and adapted technique for specific non-volatile compounds such as mineral chemicals. For this type of chemicals, a co-located impactor could be considered to be superfluous. Even though such an approach seems to be contradictory with the primary motivation of an aerosol mass spectrometer, it does nevertheless convert the inlet unit imperfections and the low chemical analysis rate (CAR) into additional instrument capabilities to get further information about the aerosol without affecting the operation of the instrument. Indeed, in Chapter 2 it was indicated that analyzing particles at 20 Hz for an aerosol containing 250 particles per cm³ permits only the analysis of 2,4% of the particles contained in one liter in 5 minutes. The cascade impactor behavior of the aerosol mass spectrometer inlet unit permits in particular the characterization of a larger significant fraction of the other particles. For similar reasons, the addition of a parallel on-line instrument permits the sampling of a high amount of particle to, first, confirm the measurement of the aerosol mass spectrometer for the same quantity and also, by comparison, to infer additional information.

This chapter illustrates the benefits of the impactor capabilities of the SPALMS instrument for the analysis of the ash sample presented in Chapter 10 where a PIXE analysis (Proton-Induce X-ray Emission), which gives its elemental analysis and helps the interpretation of the mass spectra, is completed by the mass spectrometric analysis which provides some insights about the element speciation. This association concerns the improvement of the experimental setup of Type 1 and 4 as defined in Chapter 2. Later, the comparison of the particle velocity in the APS and the SPALMS instrument is discussed to investigate its interest for the determination of the particle density and shape. This later approach addresses the improvement of type 2 of the aerosol mass spectrometer.

12.1 Impactor sampling (Improvement type 4 and 1)

This section investigates the benefits from the comparison between the single particle mass spectrometric analysis and the PIXE analysis for the aerosol collected within the inlet unit.

12.1.1 Impactor capabilities of the inlet unit

It was shown before that the current setup of the SPALMS instrument permits the chemical analysis of at most only 0.2 % of the particle sampled by the inlet unit. In these conditions the observed chemical composition from the mass spectra can not be extrapolated to the entire particle population. A solution to address the problem is simply to compare the single particle observed composition with the bulk chemical composition of the aerosol sampled by impaction within the SPALMS instrument itself.

Indeed particles can easily be sampled and collected by impaction at two locations that do not affect in practice the operation of the SPALMS instrument as an on-line analyzer. Particles can be

12. Benefits of additional particle sampling devices

sampled on the skimmer II later referred as “Impactor A” and on the impaction plate located on the protecting grid of the ion source turbomolecular pump (later referred as “Impactor B”) after particles passed the desorption/ionization laser(s).

Figure. 64 illustrates that, at both indicated locations, particles can be efficiently sampled by impaction.

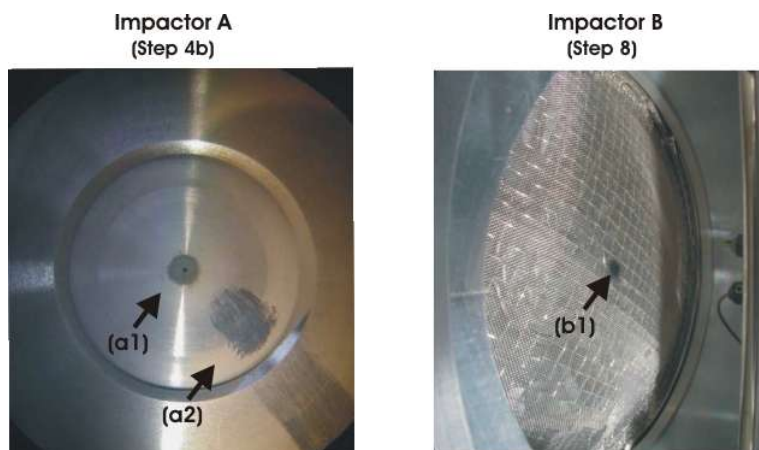


Figure. 64 : Particle sampling by impaction in the inlet unit

(a1): Particles sampled on the plane skimmer (skimmer II). These particles have a large size since they belong to the particle beam. **(a2):** Particles sampled on the plane skimmer (skimmer II). These particles correspond to the fraction of particles of small size. **(b1):** Particles sampled on the ion source turbomolecular pump grid after the desorption/ionization laser. These particles correspond to transmitted particles to the ion source which are not hit nor partially hit by the desorption/ionization laser.

The impactor A has a high sampling rate since it collects all the particles that are not transmitted in the ion source. It can represent $\sim 0,5\%$ of the sampled particle at the inlet unit entrance (from geometrically estimated inlet efficiency after Chapter 4.). Each time the inlet unit is cleaned, particles on the plane skimmer can be collected and analyzed. The observed bulk composition is then to be related to any particles sampled since the last inlet unit cleaning.

The impactor B samples particles slower than the impactor A since it only captures particles that are transmitted to the ion source chamber, are not or not completely hit by the desorption/ionization laser and do not bounce off out of the impactor plate B. It samples practically $0,03\%$ of the particles transmitted in the ion source (from geometrically estimated inlet efficiency after Chapter 4.). This impactor plate can easily be mounted on an arm that holds it in the particle trajectory. With a system of double valves, one can replace the impactor plate during the SPALMS operation from the side of the instrument. Such an impactor plate could be the same as those used for the LMMS instrument of the group ([Hauler et al., 2004], [Ferge et al., 2005]) so that off-line two-step laser desorption ionization analysis of the particles can be quickly performed after sampling.

The analysis of the particle can be performed by any usual off-line technique that targets different chemicals. This will lead to a better characterization of the particle chemical composition of non-volatile compounds that can be found in the atmosphere, such as high mass PAHs, polymers ([Kalberer et al., 2004]), mineral dusts or substances of biological origin ([Matthias-Maser et

Jaenicke, 1995]) for example.

For the same sample, both bulk analysis and single particle analysis are then available so that the mixing state of the aerosol can be elucidated. The bulk analysis and the single particle mass analysis can be advantageously processed after the methodology developed by [Ferguson et al., 2001] and more recently by [Zhao et al., 2005].

The critical step in this approach is nevertheless the transfer of the particles collected in the inlet unit into the sample inlet system for the off-line analysis instrument. Indeed some contaminations and loss of samples can easily occur, in particular for the aerosol collected on the Impactor A, if it must be removed and re-deposited on another other surface. For such an impactor, particles can be brought into a liquid solution that can be analyzed by different chromatographic techniques such as ion chromatography for example. On the other hand, the Impactor B can be designed and adapted for a given off-line analyzer such as a LMMS instruments.

12.1.2 Ash particle composition inferred from the SPALMS and PIXE analysis

The example of the ash sample described previously illustrates the interest of performing an off-line analysis of the aerosol along with a single particle mass spectrometric analysis. The ash sample analyzed in this study has not been sampled in the inlet unit on the impactor A or B as described in the previous section but could have been since the quantity of ash particles sampled after 12 hours operation is sufficient for a PIXE (Proton-Induced X-ray Emission) analysis in this study.

The motivation of this analysis is to check if most of the constitutive elements of the detected species by the SPALMS instrument are indeed detected by the PIXE analysis and vice versa. This also permits in a first extent the confirmation of the analysis by aerosol mass spectrometry and also the obtention of more information about the elemental speciation.

Table 43 lists the relative proportion of the elements in the ash particles measured by the PIXE analysis compared with their occurrence in the obtained single particle mass spectra at $\lambda = 337,1$ nm and $\lambda = 248$ nm. The PIXE analysis was performed by Dr. Wenzel and Mr. Reznikov at the PIXE installation at GSF-Forschungszentrum. The analysis corresponds to the analysis of $\sim 1\mu\text{g}$ of ash particles spread on an acetate filter and gives a measure of the relative abundance of the different elements.

The comparison of the chemical composition obtained from the SPALMS and PIXE analyses is rich in information. Under the assumption that the relative intensity of each element can be used as a measure of the relative elemental composition in the PIXE analysis, the detection and proportion of the different elements help to better interpret the mass spectra.

Indeed when elements have a close mass-to-charge ratio and are present in high quantity, the resulting detection peak in the mass spectrum is wide so that it can overlap other peaks of greater, and maybe smaller, mass-to-charge ratio. The peak assignment, even with an appropriate mass calibration, is therefore uncertain and tricky. In the analysis of the ash sample, the peak at m/z around 23 can be sodium (23) and/or magnesium (24) for positive summed and for single particle mass spectra. The PIXE analysis gives here a globally higher abundance of sodium (Na, 23) than magnesium (Mg, 24) in the particle bulk sample which suggests that the peak at $m/z = 23$ has to be mainly attributed to sodium and secondary to magnesium in the positive mass spectrum.

12. Benefits of additional particle sampling devices

<i>Element data</i>		<i>PIXE analysis ⁽¹⁾</i>		<i>SPALMS analysis ⁽²⁾</i>		
<i>Atomic Number</i>	<i>Element</i>	<i>Energy (keV)</i>	<i>Relative Intensity (a.u.)</i>	<i>m/z</i>	<i>Presence in MS at 337nm</i>	<i>Presence in MS at 248 nm</i>
11	Na	1.041	1000	23	Present in MS(+) as Na ⁺	Present in MS(+) as Na ⁺ Maybe present in MS(-) as NaSO ₃ ⁻
12	Mg	1.254	395.6	24	Maybe present and masked in MS(+) by Na ⁺	Maybe present and masked in MS(+) by Na ⁺
13	Al	1.487	193.7	27	Present as AlO ⁻ in MS(-)	Present as AlO ⁻ in MS(-)
14	Si	1.740	474.1	28	Present in MS(-) as SiO ⁻ (44), SiO ₂ ⁻ (60), HSiO ₂ ⁻ (61), SiO ₃ ⁻ (76)	Present in MS(-) as SiO ⁻ (44), SiO ₂ ⁻ (60), HSiO ₂ ⁻ (61), SiO ₃ ⁻ (76)
15	P	2.015	309.3	31	Maybe calibration problem because of species PO ₂ ⁻ (63), PO ₃ ⁻ (79)	Maybe calibration problem because of species PO ₂ ⁻ (63), PO ₃ ⁻ (79)
16	S	2.307	393.8	32	Present in MS(-) as S ⁻ (32), SO ⁻ (48), HSO ⁻ (49), SO ₂ ⁻ (64), SO ₃ ⁻ (80), SO ₄ ⁻ (96), NaSO ₃ ⁻ (103)	Present in MS(-) as S ⁻ (32), SO ⁻ (48), HSO ⁻ (49), SO ₂ ⁻ (64), SO ₃ ⁻ (80), SO ₄ ⁻ (96), NaSO ₃ ⁻ (103)
17	Cl	2.622	769.3	35	Supposed presence in MS(-) with species Cl ⁻ (35), ³⁷ Cl ⁻ (37), ClO ⁻ (51)	Supposed presence in MS(-) with species Cl ⁻ (35), ³⁷ Cl ⁻ (37), ClO ⁻ (51)
19	K	3.312	1378	39	Present in MS(+) due to a strong signal around m/z 39/40	Present in MS(+) due to a strong signal around m/z=39/40 Maybe present in MS(-) as KSO ₄ due to a signal around m/z =135
20	Ca	3.690	4190.0	40	Present in MS(+) due to a strong signal around m/z=39/40	Present in MS(+) due to a strong signal around m/z=39/40 Maybe present in MS(-) as CaSO ₄ due to a signal around m/z =136
21	Sc	4.088	187.6	45	No clear evidence	No clear evidence
22	Ti	4.508	30.2	48	No clear evidence	No clear evidence
23	V	4.949	28.5	51	No clear evidence	No clear evidence
24	Cr	5.411	12.5	52	No clear evidence	No clear evidence
25	Mn	5.895	47.5	55	No clear evidence	Maybe present in MS(-) as MnO ₄ ⁻ (119)
26	Fe	6.400	804.6	56	Present in MS(+) as Fe (56)	Present in MS(+) as Fe (56) Present in MS(-) as FeO (72), FeO ₂ (88), FeO ₃ (104), maybe as Fe ₃ O (184)
27	Co	6.925	0	59	No clear evidence	No clear evidence
28	Ni	7.472	1	57	No clear evidence	No clear evidence

12. Benefits of additional particle sampling devices

Element data		PIXE analysis ⁽¹⁾		SPALMS analysis ⁽²⁾		
29	Cu	8.041	3.3	63	No clear evidence	No clear evidence
30	Zn	8.631	270.6	64	No clear evidence	No clear evidence
33	As	10.530	9.7	75	No clear evidence	No clear evidence
35	Br	11.910	1.6	79	No clear evidence	No clear evidence
	Pb				No clear evidence	Present in MS(+) due to a signal at m/z = 206, 207, 208
82		10.552	483.1	207		206Pb, 207Pb, 208Pb

Table 43 : Ash sample analysis by PIXE and SPALMS

⁽¹⁾ the relative intensity emitted is assumed to be representative of the proportion of the corresponding element in the sample. ⁽²⁾ The mass spectrometric analysis relies on the summed spectra presented in Figure. 61, Figure. 60 and in Table 40.

The relative amount of sodium relative to magnesium can not be evaluated on a particle-to-particle basis since the signal intensity is still very high for single particle mass spectra even though the relative sensitivity factors (RSF), as defined by [Gross et al., 2000], for sodium (Na) and magnesium (Mg) are known. Negative mass spectra show no intense signals that permit a good peak mass resolution and that can be related to specific tracers of sodium and magnesium. In negative mass spectra, sodium or magnesium anions are not observed so that some of their corresponding oxides, NaO and MgO for example, are considered as their respective tracers. No observations in Figure. 60 and Figure. 61 show the presence of these oxides. Their absence can be either due to their low amount or absence in the particle or to the fact that they are not or can not be detected. From the negative mass spectra, it is also not possible to evaluate the relative content of sodium and magnesium in single particles.

Furthermore, a similar discussion can be initiated for potassium (K, 39) and calcium (Ca, 40) where clearly Ca dominates in the ash sample according to the PIXE analysis. Moreover in Figure. 60 and Figure. 61, no strong signal is observed on the negative mass spectra at m/z = 55 (KO) nor m/z = 56 (CaO). However, peaks do occur at m/z = 135 (KSO₄⁻), 136(CaSO₄⁻) what suggests the presence of K and Ca in the particle. The attribution of the mass-to-charge ratio m/z = 135 and 136 to KSO₄ and CaSO₄ is supported by the fact that it can not be AlO₂.SiO₂O and (SiO₂)₂O. Such ions usually appear when ions such as AlO₂, SiO₂, AlO₂.SiO₂ and (SiO₂)₂ are also present in the negative mass spectrum. Finally the occurrence of ion of m/z = 64, 80, 96 support further the presence of sulfates in the particle.

The peak at m/z = 135 appears to be stronger both in Figure. 60(#9) and in Figure. 61(d) than that of m/z = 136 suggesting here a higher amount of K in the single particle #9 of Figure. 60 and in the whole aerosol as suggested by Figure. 61(d) if KSO₄⁻ and CaSO₄⁻ are identically easily formed, detected and if their natural occurrence at the respective mass m/z = 135 and m/z = 136 are similar. The observation of the negative mass spectra suggests that potassium and calcium are significantly present in the ash sample as sulfates. The apparent higher abundance of potassium sulfate KSO₄ compared to calcium sulfate CaSO₄ suggests that the latter is less ionizable/detectable than the former one and/or that calcium is also present in an other form in the particle. This points out the necessity to better understand the origin of the observed sulfate ions and their negative ionization mechanism.

If such species can be detected, one must be then certain of their origin if one wish to infer the speciation of the element in the particle sample. Indeed it is not known whether such oxides can be

12. Benefits of additional particle sampling devices

originally present in the ash, what would be expected since the ash is coming from a combustion in air or from soil constituents, or can be formed during the laser desorption/ionization process, what would be here unlikely since the oxygen pressure in the desorption/ionization unit is extremely low.

Independently of the information from positive mass spectra, the comparable amount of aluminium (Al, 27), silicium (Si, 28), phosphorus (P, 31) and sulfur (S, 32) in the particles from the PIXE analysis raises the question of the right attribution of the mass spectrum peaks of sulfates. Indeed all their oxides or sulfate combinations appear to be similar by a mass unit what can lead to a probable miscalibration of the mass spectra of a mass unit. This suggests not to use in the present analysis any of such oxides or sulfates as means to calibrate the mass spectra. The interpretation of the negative mass spectra for these compounds is tricky and requires to better know the relative abundances of these different oxides and sulfates in the environment and their fate during the desorption/ionization process. The calibration quality of mass spectra presented in Figure. 60 is also negatively affected by the limited voltage range of the acquisition device which truncates a large number of peaks.

On the opposite side, the iron oxides and carbon clusters are of great importance here to tune appropriately the mass calibration since their mass can be efficiently discriminated from the other peaks. The relative amplitude of the peaks can unfortunately not help here since the voltage range is limited to a low level for the mass spectra obtained at $\lambda = 248$ nm. Furthermore the presence of a series of different iron oxides such as FeO (72), FeO₂ (88) and FeO₃ (104) suggests the presence of iron in the ash sample as oxides what is plausible since a lot of rusted iron parts were present with the burned wood. At this stage, it is not possible to determine what is the precise iron speciation in the sample. This clearly requires further studies to state how elements and their oxides are affected during the laser desorption ionization under similar conditions.

In addition of this the PIXE analysis permitted, in the present case, the detection of trace elements such as titan Ti, vanadium V, chromium Cr, manganese Mn, nickel Ni, copper Cu, arsenic As and bromine Br. The SPLAMS instrument did not detected these elements for various reasons as diverse as: (i) limited number of particles processed, (ii) matrix effects, (iii) detection efficiency of each specie and (iv) low amount of these elements. In order to evaluate whether the difficulty of detection of these elements is due to the laser desorption/ionization process, more particles should be investigated with the SPALMS instrument and also with LMMS (Laser Microprobe Mass Spectrometry).

As a whole, the PIXE analysis leads to an easier interpretation of the particle mass spectra. Indeed it can orient the attribution of a peak having a large width to a probable mass. Furthermore, the mass spectrometric analysis give the possibility to give hints about the element speciation and information related to single particles. On the other side, PIXE analyses can reveal the presence of specific element undetected by the SPALMS instrument either because the sampled aerosol was not representative enough, because they are in small amount in the particle or because they can not be detected with the current operation conditions.

12.2 Parallel operation of the APS and the SPALMS instrument (Improvement of type 2)

As mentioned above in Chapter 11, an APS instrument (APS3321, TSI., Inc, St. Paul, MN, USA) can be operated in parallel with the SPALMS instrument. The primary purposes are (i) to obtain a more representative particle size distribution and (ii) to control the state of the inlet unit and the detection/sizing unit of the aerosol mass spectrometer. It checks if the inlet got clogged or if the sizing lasers deviated away from the particle beam. The parallel operation of an APS also offers a

12. Benefits of additional particle sampling devices

mean (i) to confirm the measurement of the SPALMS instrument and (ii) to attempt to provide additional information about the particles.

Indeed, the inlet unit and the detection/sizing unit of both instruments are different. By combining measurements from both methods to a monodisperse aerosol, it might possible the gain additional information about the particles.

12.2.1 APS principle

The principle of the Aerodynamic Particle Sizer, APS, (APS 3321, TSI Inc., St Paul, MN, USA) is very close to the sizing principle of the SPALMS instrument since it measures the particle size by measuring its terminal velocity in a given gas flow. It is achieved by measuring the particle time-of-flight between two laser beams that permit the detection of the particle by light scattering.

In practice, the particle is brought into the sensing volume by focusing it aerodynamically by a sheath air flow. The particle is then accelerated through a nozzle to its terminal velocity by the carrier gas, here air, having a velocity of ~ 150 m/s. The terminal velocity of the particle depends on its size, shape and density. Both laser beams originate from a unique laser whose beam is split by a birefringent calcite crystal into an ordinary beam that continue in the same direction of the incident beam which is horizontally polarized and into an extraordinary beam which is laterally displaced by 90-100 μm and vertically polarized. The scattered light is collected by an elliptical mirror which leads the collected light to a photomultiplier which converts the light signal into a voltage. The signal is then processed electronically to calculate the particle size distribution for a particle size range of 0,5 μm to 20 μm . The conversion of the particle velocity distribution is performed according to a given calibration curve which depends on the particle type to be measured.

The APS3321 can be operated in summed mode or correlated mode. The summed mode simply measures the particle time-of-flight that is then converted to a particle size. On the opposite side, the correlated mode associates to each analyzed particle its size (0,5 μm to 20 μm) and a scattering light level, quantified as a bin number. Indeed the light signal is binned into 16 bins identified by a number (1 to 16).

The APS3321 can be controlled via a serial port interface RS-232 by a PC-computer via the TSI software or a home-made Labview driver. The measurements can be saved in the computer and processed as wished since both processed data and raw data can be exported as a text file. The APS raw data consist, depending on the export options of the TSI software, of the particle size distribution binned into 50 bins, the particle time-of-flight distribution binned into 1024 bins of 4 ns width each, the particle light scattering level distribution expressed in bins and the particle number distribution as a function of the particle diameter and the light scattering channel identification number. It offers also the possibility to observe the raw photomultiplier signal after its amplification via a BNC connector (labeled "Pulse Out") and an oscilloscope. One can then develop a home-made Labview program to analyze the photomultiplier signal shape to gain additional information about the particle.

12.2.2 Comparison of the detection/sizing units of the APS and SPALMS

The APS and the SPLAMS offer different operating conditions for the particle focusing, acceleration and detection/sizing unit which are synthesized in Table 44

If operating conditions can be seen as similar for the optical detection unit, they are not for the

12. Benefits of additional particle sampling devices

aerosol sampling and its flow regime. This particularity can be used to try to further differentiate particles by using their different aerodynamic behavior in the different gas flow regimes.

	<i>APS3321 (TSI, Inc)</i>	<i>SPALMS</i>
Gas flow regime	Subsonic regime ($M_a \sim 0.5$) non-Stokesian regime	Supersonic regime ($M_a > 1$) non-Stokesian regime
Gas velocity	~ 150 m/s	> 365 m/s
Particle incident laser light properties	680 nm, cw, 30 mW, polarized	532 nm, cw, 50 mW, polarized
Mean incident laser light fluency	$0,9 \mu\text{W}/\mu\text{m}^2$ ⁽¹⁾	Max. $0,1 \mu\text{W}/\mu\text{m}^2$
Light scattering capture angle	$+55^\circ$ to -55° ⁽²⁾	45° ($\pm 10^\circ$)
Solid angle scattering light capture	2,43 steradian (19,4%) ⁽²⁾	0,82 steradian (6,8%)

Table 44 : Operating conditions of the sizing unit of the APS and SPALMS instrument

⁽¹⁾ estimated (if laser beam size of $\varnothing 20 \mu\text{m}$), ⁽²⁾ rough estimation from APS3321 manual

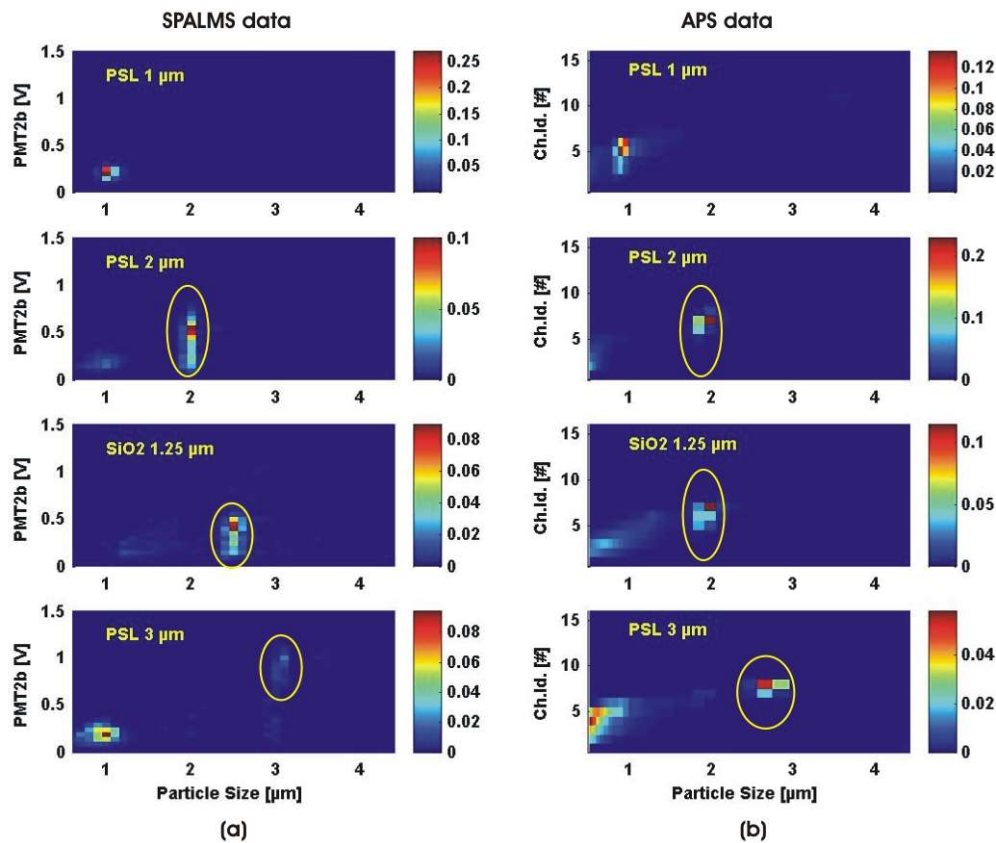


Figure. 65 : Light scattering signals of the SPALMS and APS for PSL and SiO₂ particles

This graph presents the proportion of particles that have a given diameter and a given amount of scattered light. The particle observed with a diameter smaller than $1 \mu\text{m}$ are impurities or fragments of the PSL particles which are not considered in this study. **Panel (a):** Data obtained with the detection/sizing unit of the SPLAMS instrument. The amount of light scattered by the particle is measured by the photomultiplier PMT2b signal amplitude in [V]. **Panel (b):** Data obtained for the APS. The scattered light amount is returned in bin Id.

12.2.3 Comparison of the particle sizing data from APS and SPALMS

Figure. 65 presents the particle scattering light level versus particle diameter for the sizing of different particles by both instruments. The case of the PSL 2 μm and SiO₂ 1.25 μm particles (monodisperse silica particles of geometric diameter of 1,25 μm) is interesting since they can not be significantly differentiated by the APS either in particle diameter nor in terms of scattered light. The scattered light level is binned in bins Nr. 6 and 7 and the particle size is given to be 1,9-2 μm . The SPALMS however does indicate a clear difference both in terms of amount of scattered light, respectively 0.5-0.6 V and 0.4-0.5 V for PSL 2 μm and SiO₂ 1.25 μm for the most frequent measured values, and in terms of particle size, respectively 2 μm and 2,5 μm for PSL 2 μm and SiO₂ 1.25 μm .

The scattered light intensity information obtained from the APS can not differentiate both particle types whose light amount levels belong to Channel 6-7. It is first due to the binning of the scattered light measured levels in close bins. It masks in particular the scattering light level difference if they are similar but significantly distinct as it should be expected considering the difference observed with the SPALMS sizing unit. A similar comment can be proposed for the measured particle diameter which is represented for the APS data in the Figure. 65(b) with the particle diameter binning method from TSI.

If the scattering light level may differentiate the PSL 2 μm particles from SiO₂ 1.25 μm particles, their measured particle velocity in the APS however can not as shown in Figure. 65(b). Indeed to eliminate the merging effects of the binning operation, the particle velocity in the APS for the same particles are presented in Figure. 66(b) which shows that the PSL 2 μm and the SiO₂ particle cannot practically be differentiated by the APS.

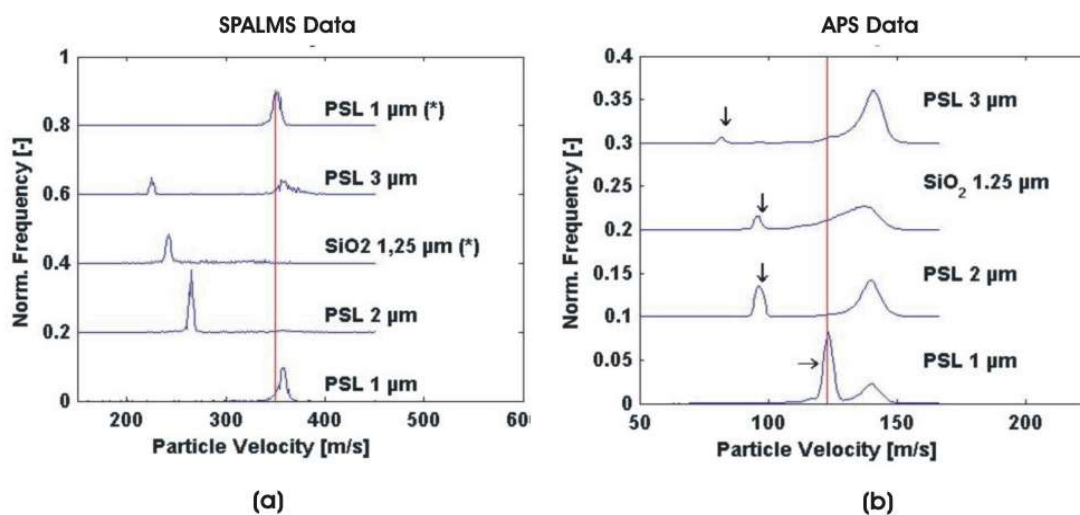


Figure. 66 : Particle velocity distribution measured for PSL and SiO₂ particles by the SPALMS and the APS

Panel (a): Particle velocity measured with the detection/sizing unit of the SPALMS. **Panel (b):** Particle velocity measured with the detection/sizing unit of the APS. (*) The PSL 1 μm and SiO₂ 1,25 μm particles were analyzed a different day as for the other particles. Particles whose velocity is above 130 m/s in the APS measurements (panel (b)) correspond to aerodynamic contamination or PSL fragment particles which are not considered in this study. This figure illustrates the aerodynamic differentiation of the PSL 2 μm and SiO₂ 1,25 μm particles with the SPALMS at the opposite of the APS.

12. Benefits of additional particle sampling devices

The particle differentiation by the SPLAMS is not surprising since the gas velocity is much higher. In these conditions, the drag force experienced by the particle is greater so that the effects of the particle size, density and shape are therefore greater for the SPLAMS than for the APS. This leads to a better particle aerodynamic differentiation as illustrated by the example of the PSL 2 μm and SiO₂ 1,25 μm particles in Figure. 66(a).

A similar approach to remove the binning effects of the APS for the scattered light level would be interesting to perform. It is possible but it requires to acquire the PMT signal of the APS and to process it with a home-made program. Even if it was done for ambient air particles, this has not been done for PSL 2 μm particle and SiO₂ 1,25 μm particles due to scarcity of time and limited interests at the time the measurement were done. However such work should increase the measurement potential of the APS instrument.

12.2.4 Particle velocity in APS and SPALMS instrument

In the previous paragraph, one can see that the SiO₂ 1,25 μm particles can be both optically and aerodynamically differentiated from the PSL 2 μm particles by using the SPALMS instead of the APS instrument. The problem of both instruments is that the calibration curve is only valid for particles of the same shape and density if the size information only is required for each instrument. This appears to be a limitation of both techniques. The comparison of the particle velocity in both instruments could be interesting and increase the potential of the SPALMS if the particle size and density can be unambiguously differentiated for spherical particles.

For this purpose, one takes advantage of the different particle acceleration conditions in both instruments. Indeed the particle acceleration conditions in the SPALMS are assumed to be very similar to those encountered in the Aerosizer instrument (API, Amherst, MA, USA) since particles are accelerated by a sonic nozzle which differ from the APS where the carrier gas reaches a velocity of ~ 150 m/s. Surprisingly no publications were reported that clearly compare the particle velocity in the APS and the Aerosizer as a function of their size and density.

To evaluate the success of the method, it is interesting to compute the relationship between the particle velocity in the SPALMS and the APS as a function of the particle size and the density. This will lead to evaluate if both the particle size and density can be obtained directly and unambiguously from simultaneous measurements with both instruments in the case of monodisperse spherical particles.

The particle velocity in the APS can be computed from the study of [Tsai et al., 2004] whereas it is calculated after the work of [Cheng et al., 1993] for the SPALMS instrument considering that the later instrument behaves like an Aerosizer as it accelerates the aerosol particles. The calculated velocities for both instruments are summarized in Table 45 and presented in Figure. 67.

The relationships given by [Tsai et al., 2004] for the APS are expected to reproduce within 6% the particle velocity of different particle types for the APS 3300 (earlier version of APS3321). It is assumed here to be valid for the APS3321 since the measurement principle and conditions are the considered to be similar. In addition, the relationship from [Cheng et al., 1993] for the SPALMS is semi-empirical and is found to be valid for particles with density smaller than 10 g/cm^3 (10000 kg/m^3).

Table 45 indicates that the computed particle velocities are well predicted by both models (within 5% except for PSL 3 μm and PSL 4 μm for the APS where the deviation is smaller than 15%). It can be considered to be acceptable considering all approximations made by both models.

12. Benefits of additional particle sampling devices

<i>Particle Type</i>	<i>SPALMS (measured)</i>	<i>SPALMS (simulated)</i>	<i>Deviation (%)</i>	<i>APS (measured)</i>	<i>APS (simulated)</i>	<i>Deviation (%)</i>
PSL 1 μm	357	349	2,2	120	125	-4,2
PSL 2 μm	265	253	4,5	94	97	-3,2
PSL 3 μm	223	211	5,4	80	73	8,8
PSL 4 μm	199	193	3,0	72	63	12,5
SiO ₂ 1,25 μm	242	243	-0,4	96	93	3,1

Table 45 : Computed and measured particle velocities with the APS and SPALMS instrument

As both models are validated within 10% in our study, one can plot the particle velocity in the APS and in the SPALMS as a function of its size and its density. The particles are considered to be here spherical. The curves are presented in Figure. 67.

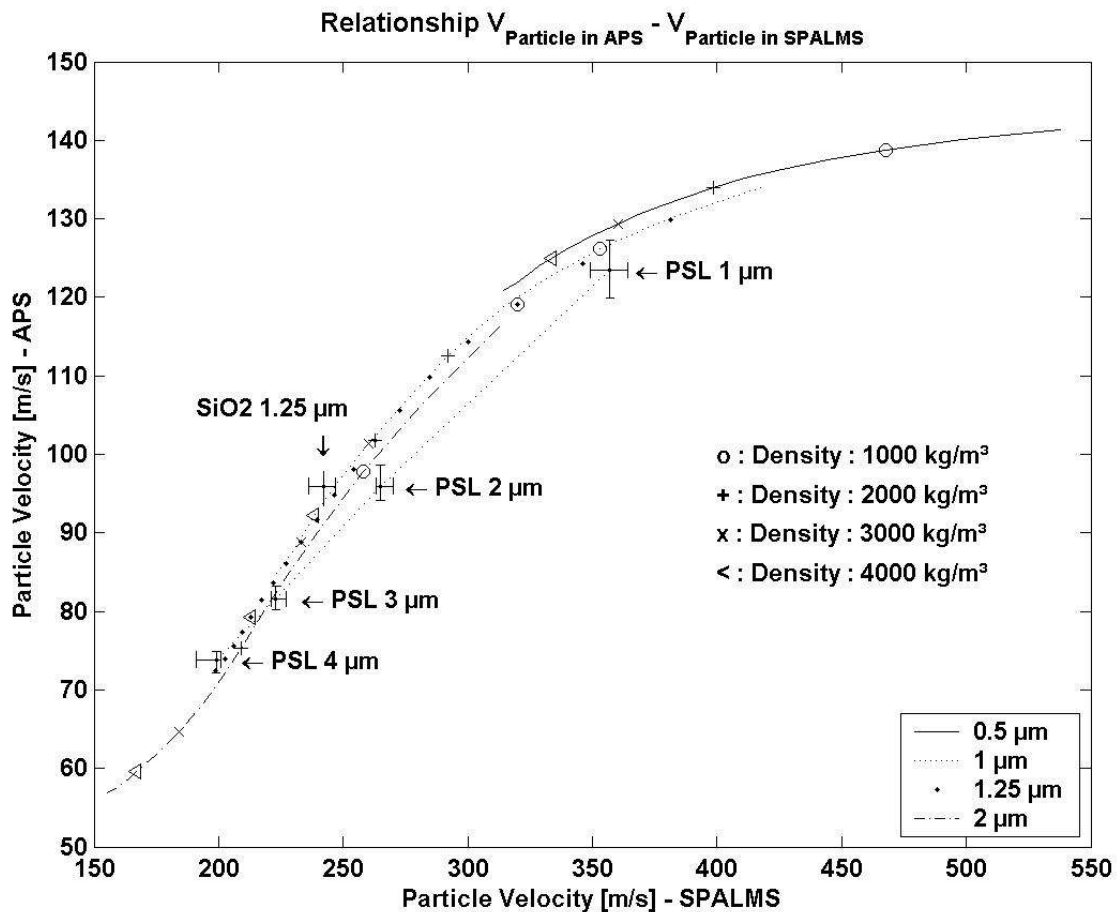


Figure. 67 : Computed and measured particle velocity for the APS and the SPALMS instruments

The computed curves are not expected to give an exact value for prevision purposes since many variables describing the gas flow and the particle behavior are approximated. Its goal is to state whether the measurement of the variables ($V_{\text{particle,AMS}}$ and $V_{\text{particle,APS}}$) permits the knowledge of both the size and the particle density from simple particle velocity measurements.

12. Benefits of additional particle sampling devices

It seems to exist a trend that for a given particle velocity in the SPALMS, the particle velocity in the APS decreases as the size increases and the particle density decreases. For a given particle velocity in the APS, the particle velocity in the SPALMS decreases as the size decreases and the particle density increases what is explicitly illustrated by the comparison of the PSL 2 μm and SiO₂ particles.

To confirm these tendencies in a more convincing way, more experiments with different monodisperse particles of different sizes and densities are needed. Moreover the uncertainty of the models used to calculate the particle velocity in the APS and the SPALMS needs to be better evaluated.

However, this method, in case it can be successful, is currently not convenient with the SPALMS due to the necessity of very accurate particle velocity measurements. Besides this methodology has only interests if monodisperse particles are sampled in parallel by both instruments. Polydisperse particles could be analyzed if one has a mean to make sure that the same particles (in terms of size, density, shape, chemical composition) were analyzed by both instruments. It raises the questions whether particles can be tagged in any manner, for example, optically as presented in the next section.

13 To a better characterization of the particle physical properties

This chapter discusses methodologies that can be used to further interpret the data obtained by the detection/sizing unit in order to better describe the physical properties of the single particles of the aerosol. As mentioned many times, the aerodynamic and optical properties of the particle are linked to its size, density and shape and also depends on its refractive index for the latter.

Since the detection/sizing unit is rich in information, the interpretation of the aerodynamic and optical measurements should reduce the uncertainty of the measured physical parameters. Both measurement types can be used in two manners. The first manner consists to infer directly the particle density, for example, from the measured apparent aerodynamic and optical diameters under specific approximations. The second manner is to use one measurement type, aerodynamic size, as a mean to better characterize the observation conditions of the second measurement type, optical size.

If the first approach is essentially addressed by [Murphy et al., 2004] and [Moffet et Prather, 2005] in particular, the second will be presented here. It permits in particular the determination of the location where particles are irradiated by the sizing laser light in similar manner such that particles within the same aerosol sample can be optically compared in terms of size or non-sphericity. This approach permits also the development of innovative methods to treat the particle coincidence in the detection/sizing unit which is described at the end of this chapter. Furthermore this section will illustrate how the combination of the aerodynamic and optical single particle properties can lead to evaluate how representative of the aerosol is the single particle chemical analysis.

13.1 Introduction based on the APS optical system

As mentioned many times, the light scattering signal from the detection/sizing unit of the SPALMS can not be properly analyzed due to the high noise level of the signal and the strange observed photomultiplier signal pattern, a sharp leading edge with a long tail. As a result, the proposed methodology is presented using the particle scattering light signal measured by the optical system of the APS3321 since its photomultiplier particle signals are Gaussian like, symmetrical and represent more precisely the radially symmetric variation of the intensity of the light within the laser beam than the SPALMS current detection/sizing unit does.

A typical sizing photomultiplier signal of the APS is presented in Figure. 68 and has been recorded for ambient air particles (with a size mode at $\sim 0,7 \mu\text{m}$) by recording it from the rear panel BNC connector “Pulsed Out” of the APS with an oscilloscope.

Many particle signals were recorded and processed with different home-made Labview 6i programs that first only select “clean signal” and lead to the particle size measurement. The typical pattern of such signal is presented in Figure. 69. The selected signals are processed so that for each signal, the particle $\text{TOF}_{\text{particle}}$ (time between each pulse top), the peak heights, the peak width at a given threshold slightly above the noise level, the peak surface and the peak surface under a fitted Gaussian curve are calculated.

Thanks to the photomultiplier peak symmetry, its peak width can be well defined at a given threshold and can be attempted to be related to the particle $\text{TOF}_{\text{sizing}}$ between both laser beams.

13. To a better characterization of the particle physical properties

Figure. 69 shows a linear relationship between the particle TOF_{sizing} and the peak width. In these conditions, the peak width is related to the particle transit time in the laser beam. The white lines are presented shifted upward for presentation purposes to show the linear dependency between between both quantities.

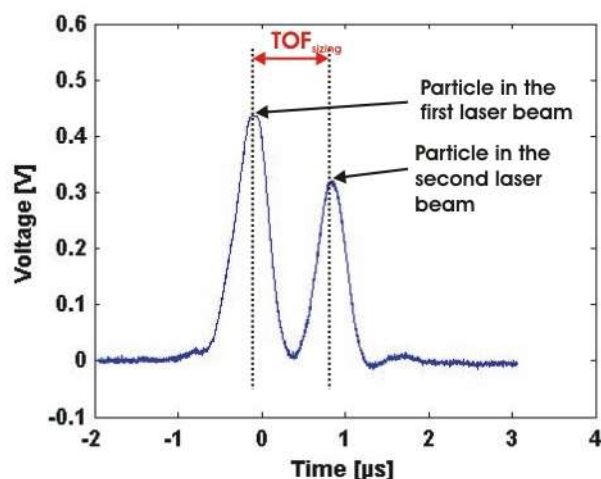


Figure. 68 : Photomultiplier signal pattern of the APS3321

This graph presents the shape of the photomultiplier signal of the APS that permits the sizing of a particle. Each peak corresponds to the particle detection at each sizing laser beam. The time between each peak TOF_{sizing} gives a measure of the particle diameter.

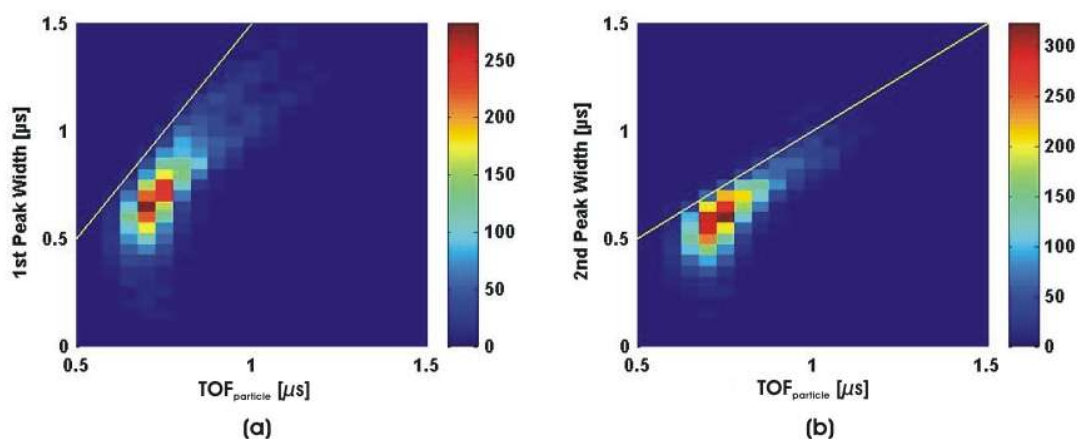


Figure. 69 : Particle time-of-flight and photomultiplier peak width equivalence for the APS

Panel (a): Number of particles with a given TOF_{sizing} and a given Peak time width (here labeled 1st Peak width) of the photomultiplier signal as the particle crosses the first sizing laser beam of the APS. **Panel (b):** Number of particles with a given TOF_{sizing} and a given Peak time width (here 2nd Peak width) of the photomultiplier signal as the particle crosses the second sizing laser beam of the APS. It shows clearly that most values of TOF_{sizing} and the peak width are closely linked and follow a linear relationship. The white line above the data points is drawn only to illustrate the linear dependency of both quantities. The presented data correspond to polydisperse ambient air particles.

13. To a better characterization of the particle physical properties

The line parameters, the slope and 0-intercept, for each case (a) and (b) are different and the causes of these differences are not known yet but would essentially be attributed, among other, to the choices of the threshold levels taken to calculate the peak width, to the size of the crossed laser beams and/or the different beam intensities of both lasers. To find the origin of this discrepancy, the method should be tested over a wider range of particle sizes and with much better known particles such as PSL particles what has not been done yet due to scarcity of time. However, it demonstrates that the peak width can be used to evaluate the particle velocity as was already mentioned by [Hinz et al., 1994] and [Kievit et al., 1996] for the detection/sizing unit of aerosol mass spectrometers but never for APS instruments.

In these conditions by evaluating roughly a nominal laser beam size, one has two ways of measuring the particle velocity. This has two important applications which are described in the following sections: (i) the reduction of the measurement biases due to the “trajectory ambiguity effects” and (ii) a new additional method to evaluate the coincidence phenomena that biases the particle size distribution measurements.

13.2 Reduction of the impact of the “trajectory ambiguity effects”

[Kievit et al., 1996] and [Salt et al., 1996] precise that the inaccuracy of the sizing of particles with the measurement of the scattered light is due to the ignorance of the particle shape, its refractive index, the non-monotone relationship {particle scattered light – particle size} when the parameter size is around unity and the intensity ambiguity problem (in other terms, “trajectory ambiguity problem ([Prather et al., 1994],[Baron and Willeke, 2001])). The trajectory ambiguity problem can nevertheless be partly solved if the particle velocity is known and its residence time in the laser beam can be approximated. Moreover the laser intensity spatial distribution within the beam must stay constant over time and present a certain symmetry in the plane of the laser beam perpendicular to the particle beam.

Indeed the knowledge of the particle velocity and the length of the photomultiplier peak signal as the particle crosses the sizing laser permits the relative location of the particle in the laser beam and therefore the evaluation the exposition conditions of the particle (length and intensity) to the laser light.

To differentiate optically particles, the photomultiplier signal must be compared for particles which are irradiated by the same amount of light and during the same time. Figure. 70 presents the consequences of the trajectory ambiguity effect.

For particles of the same size, the amount of scattered light, their detection duration and their measured residence time within the laser beam will depend on their location within the laser beam as it is the case for the big particles (a1), (a2) and (b1), (b2) for smaller particles depicted in Figure. 70. From an other point of view, particles of different sizes can have the same residence time and a similar or different amount of scattered light at different locations within the laser beam as it is the case for particles (b1) and (a2) in Figure. 70. The raw obtained information from the particle is in reality a quantity than merges the particle location in the laser and the optical particle properties. To deconvolute these parameters, specific observation conditions have to be met whose choices are presented as follow.

13. To a better characterization of the particle physical properties

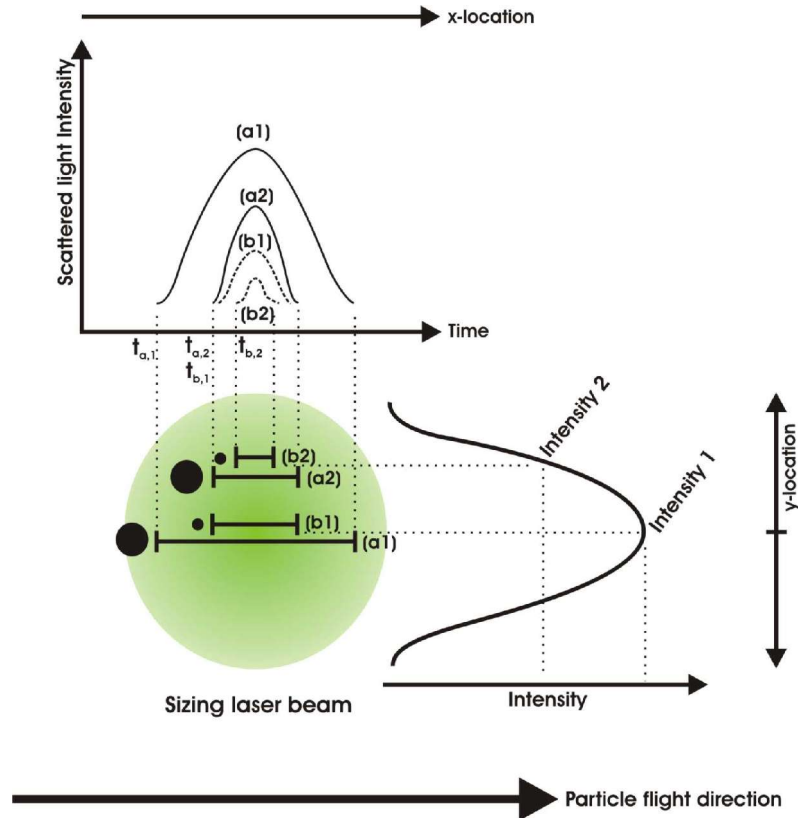


Figure. 70 : Characteristics of the “trajectory ambiguity effect”

In this figure, the laser beam intensity profile is assumed to have a radial Gaussian energy distribution. Particles of identical size scatter different amount of light according to their different location in the laser beam. Similarly, big and small particles can scatter the same amount of light and/or during the same time if they cross the laser beam at different locations. In this case, big particles met the edges of the laser beam while small particles met exclusively the center.

If the particle velocity is known, an arbitrary residence time of the particle within the laser beam $\tau_{\text{arbitrary}}$ can be defined by dividing a characteristic laser beam diameter by the particle velocity measured by its time-of-flight $\text{TOF}_{\text{particle}}$ between both sizing laser beams. By dividing the measured particle residence time in the laser beam τ_{particle} estimated here by the measured photomultiplier peak width at a given voltage level of the detection/sizing unit by the particle arbitrary residence time $\tau_{\text{arbitrary}}$, one obtains a relative particle residence time τ_{relative} (Eq. 29).

$$\tau_{\text{relative}} = \frac{\tau_{\text{particle}}}{\tau_{\text{arbitrary}}}$$

Eq. 29

This approach contains the hypothesis that the amount of scattered light by the particle increases and decreases slower than the photomultiplier reaction time as the particle enters and exits the laser beam. The validity of this hypothesis depends on the radial intensity profile of the laser beam, the particle velocity and the reaction time of the photomultiplier.

13. To a better characterization of the particle physical properties

If the photomultiplier peak is not symmetric as it is for the SPALMS, one can consider instead the peak rising time of the signal. Considering the peak rising time as such is not very rigorous since it does not physically represent the particle residence time, or more precisely, the particle detection time duration in the laser beam. As the particle exits it, the photomultiplier signal needs some time to reach its initial state. For this reason, the PMT peak rising time only can be used as an approximation of the particle residence time in the sizing laser.

Figure. 71 represents the photomultiplier peak rising time for different particle types of different sizes and shows that the peak rising time in the case of the SPALMS can be considered as a measure of the particle transit time in the sizing laser beams. Indeed the peak rising time increases with the particle size.

Figure. 72 presents the relative particle residence time distribution measured for the PMT2a and PMT2b photomultiplier signals for different particles. It shows that the relative particle residence time τ_{relative} appears to be independent of the particle velocity and particle type. The diagonal lines in Figure. 71 and Figure. 72 indicate the line $y = x$, meaning the equality of the values of the PMT2a and PMT2b photomultiplier signals measured quantities.

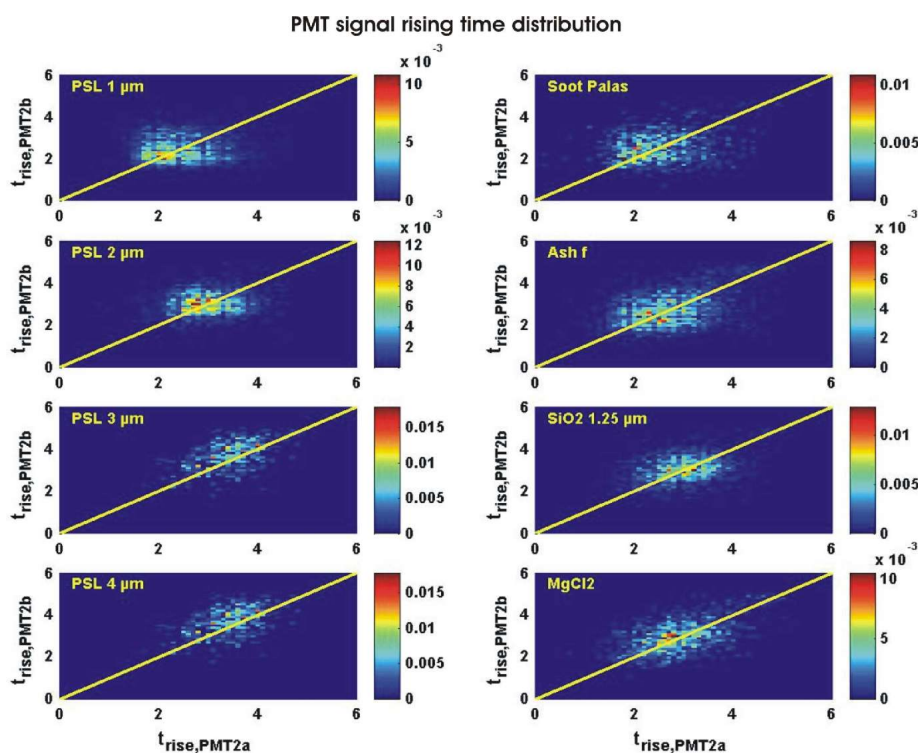


Figure. 71 : Photomultiplier peak rising time distribution for PMT2a and PMT2b for different particle types

This figure shows the proportion of particles of with a given peak rising time measured from the PMT2a and from the PMT2b signal, $\tau_{\text{rise,PMT2a}}$ and $\tau_{\text{rise,PMT2b}}$. The white line represents the line $\tau_{\text{rise,PMT2a}} = \tau_{\text{rise,PMT2b}}$ and illustrates that both photomultipliers react to the scattered light in the same manner. Indeed the values of $\tau_{\text{rise,PMT2a}}$ and $\tau_{\text{rise,PMT2b}}$ are all centered around values of $\tau_{\text{rise,PMT2a}} = \tau_{\text{rise,PMT2b}} = \tau_{\text{rise}}$ with $\tau_{\text{rise}} = 2.1 \mu\text{s}$, $2.8 \mu\text{s}$, $3.6 \mu\text{s}$, $3.6 \mu\text{s}$, $2.2 \mu\text{s}$, $2.4 \mu\text{s}$, $3 \mu\text{s}$ and $2.7 \mu\text{s}$ respectively for PSL $1 \mu\text{m}$, PSL $2 \mu\text{m}$, PSL $3 \mu\text{m}$, PSL $3 \mu\text{m}$, Soot Palas, Ash f, SiO₂ $1.25 \mu\text{m}$ and MgCl₂ particles.

13. To a better characterization of the particle physical properties

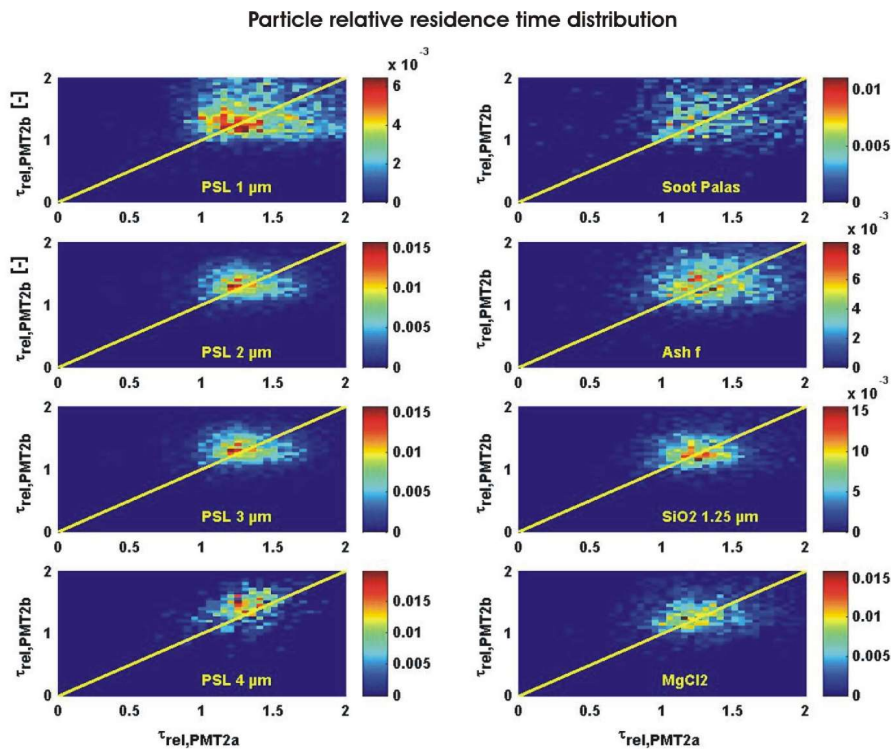


Figure. 72 : Particle relative residence time distribution for different particle types

This figure shows the proportion of particles of a given relative residence time $\tau_{rel,PMT2a}$ and $\tau_{rel,PMT2b}$ respectively evaluated from the PMT2a and PMT2b signals. The white line represents the line $t_{rise,PMT2b} = t_{rise,PMT2a}$ and illustrates that both photomultipliers react to the scattered light in the same manner. It is important to note that all values of $\tau_{rel,PMT2a}$ and $\tau_{rel,PMT2b}$ for the different particle types investigated in this study are centered around 1,25

From Figure. 71 it appears that each photomultiplier signals give different particle residence time (i.e. peak rising time) for the same particle type and therefore a different relative particle residence time as in Figure. 72. This should be attributed to the high noise level that makes the photomultiplier peak difficult to recognize and their rising time and amplitude to be measured accurately. The difference in the peak rising time obtained from the photomultiplier PMT2a and PMT2b tend to decrease as the particle size increases. This is expected since the signal can be better differentiated from the noise level.

However all values of the relative particle residence time become invariant and are centered around 1,25. It means that even if the photomultiplier signals are not optimal, the measured peak rising time is nevertheless unambiguously related to the particle residence time in the sizing laser beam. From this observation in this particular case, the photomultiplier peak rising time is considered to be a valid approximation of the particle residence time in the sizing laser.

The distribution of the relative particle residence time is surprisingly distributed between 1 and 1,5 around a median value of 1,25. At first sight it means that the sizing laser axis is vertically displaced relatively to the particle beam axis and that only a limited fraction of the particle flight along the whole sizing laser beam diameter. If both the laser beam axis and the particle beam axis intersect ideally (case of Figure. 73(b)), the highest relative residence time value will be the most frequent. The other values will then be smaller and less frequent as presented in Figure. 73(left panel).

13. To a better characterization of the particle physical properties

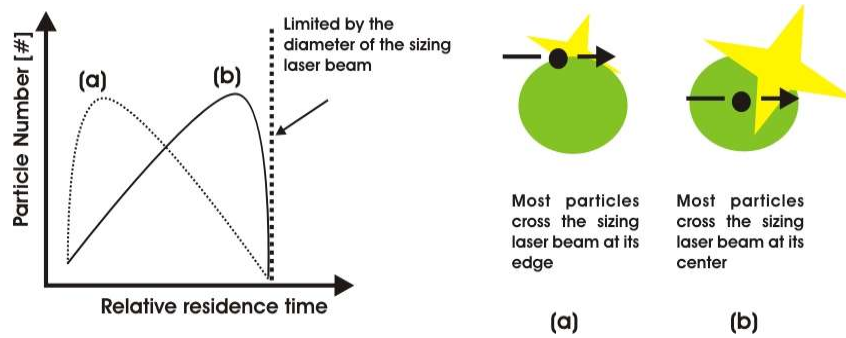


Figure. 73 . Particle distribution of given relative residence time

The distribution of the relative residence time can permit theoretically the evaluation of the relative position of the particle beam within the sizing laser beam.

Unfortunately the bad quality of the photomultiplier signals and the poor agreement between both PMT2a and PMT2b signals do not permit a reliable conclusion about the relative position of the laser and particle beams.

As a result, with the assumption of a cylindric shape of the sizing laser beam, what is an acceptable hypothesis since both sizing lasers are operated in TEM₀₀ mode, the relative particle residence permits the location in a relative manner of the particle within the laser beam. At this point, particles of similar relative particle residence time can be considered to be irradiated in the same manner.

Particles with the same velocity and the same relative particle residence time are then considered to be irradiated during the same time and at the same “place” in the laser beam, i.e. in the same manner. Particles can therefore be, in principle, better optically differentiated.

13.3 Particle optical properties

In order to characterize optically the particle, one can examine the peak amplitude and the ratio of the peak amplitude to the peak rising time for a given particle velocity and given relative particle residence time. The eventual observed differences would suggest that either or all together the geometric diameter, the refractive index or the shape are different. Figure. 74 presents qualitatively how the photomultiplier voltage, which is a measure of the amount of scattered light, varies when a particle physical property varies.

The amount of scattered light for a given refractive and given shape increases globally as the particle diameter increases. This is the case for particles with a given aerodynamic diameter and decreasing density. This increase is not monotone when the parameter size α has a value around 1 as illustrated in Chapter 5. Similarly for a given particle size and shape, the scattered light amount increases as the refractive index increases.

Considering this, the ability of the detection/sizing unit of the SPALMS to differentiate optically particles can be tested as presented below.

13. To a better characterization of the particle physical properties

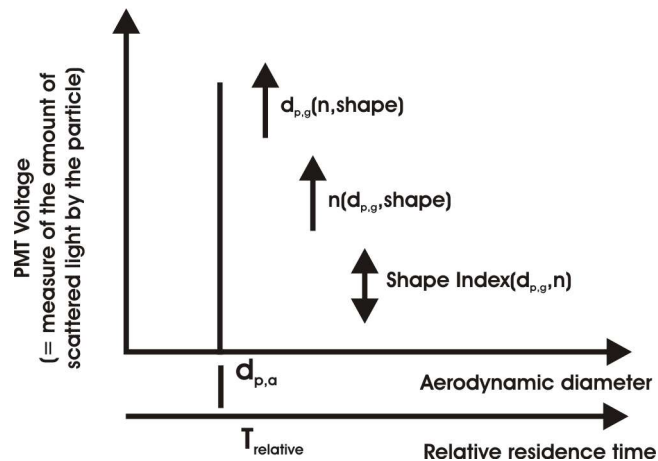


Figure. 74 : Optical particle properties behavior for a given particle velocity and relative residence time

The photomultiplier voltage signal amplitude represents in this study a measure of the amount of scattered light by the particle. This figure illustrates that under similar light irradiation conditions defined by a similar aerodynamic diameter $d_{p,a}$ and a similar relative residence time in the sizing laser beam, the photomultiplier voltage increases as the particle geometric diameter $d_{p,g}$ increases (equivalent to a given aerodynamic diameter with a decreasing density) or/and as the refractive index n increases. The effect of the shape on the photomultiplier voltage is undefined since a shape index as first to be defined for given shapes.

- Differentiation of particles having a similar aerodynamic behavior

The same data analysis is performed to compare the PSL 1 μm , soot and ash particles with here the same velocity range. The photomultiplier peak amplitude distribution is presented in Figure. 75 for a particle velocity ranging from 350 to 365 m/s and a relative residence time of 1,2-1,3. The value range was set to consider enough particles to consider a statistical significant data set.

Unfortunately, all the different particle types can be not differentiated in a reliable way. At this stage, PSL 1 μm , soot and ash particles can not be differentiated as it would be expected at least for PSL 1 μm and soot particles. The detection level of the photomultiplier was set to 150 mV in this case what is very close to noise level of the photomultiplier voltage. The measurement of the peak amplitude corresponding to the photomultiplier particle signal is there strongly affected by the close proximity of the noise level. Tests with bigger particles should be performed to better state the interest of this method.

- Differentiation of particles having similar aerodynamic behavior and identical shape

Figure. 76 presents the comparison of PSL 2 μm and SiO₂ 1.25 μm particles, in spite of their different but close velocities (242 m/s for SiO₂ 1,25 μm and 265 m/s for PSL 2 μm). Both particle types are of spherical shape. Any difference in the photomultiplier signal are therefore to be related to the particle size and the refractive index. This can principally lead to differentiate qualitatively particles according to their different density if their respective refractive index are similar.

13. To a better characterization of the particle physical properties

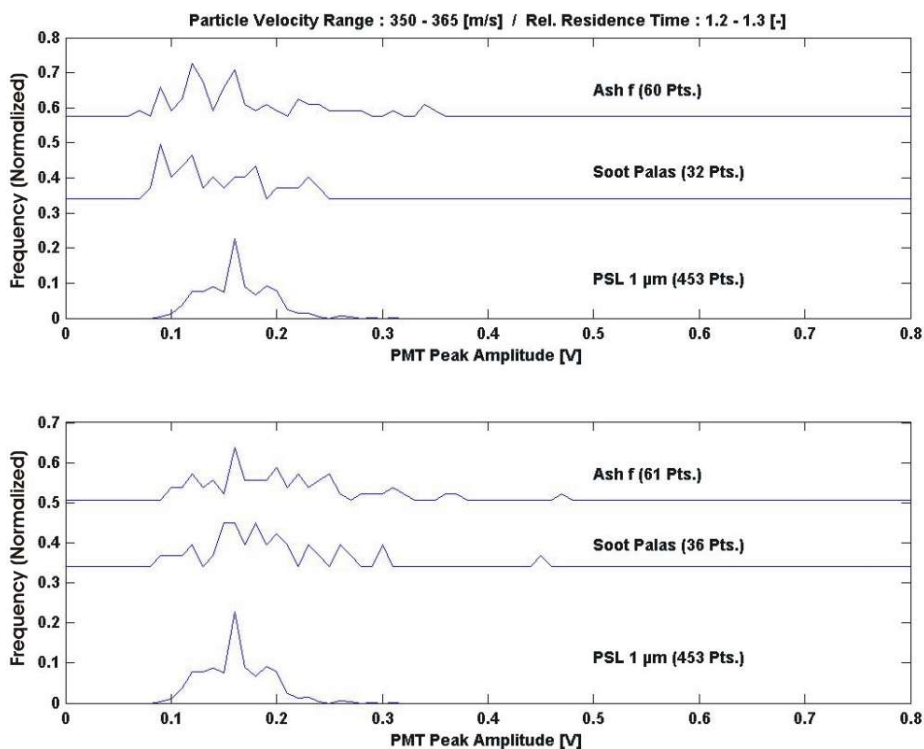


Figure. 75 : PMT2a signal amplitude for particles with similar velocity and relative residence time (1)

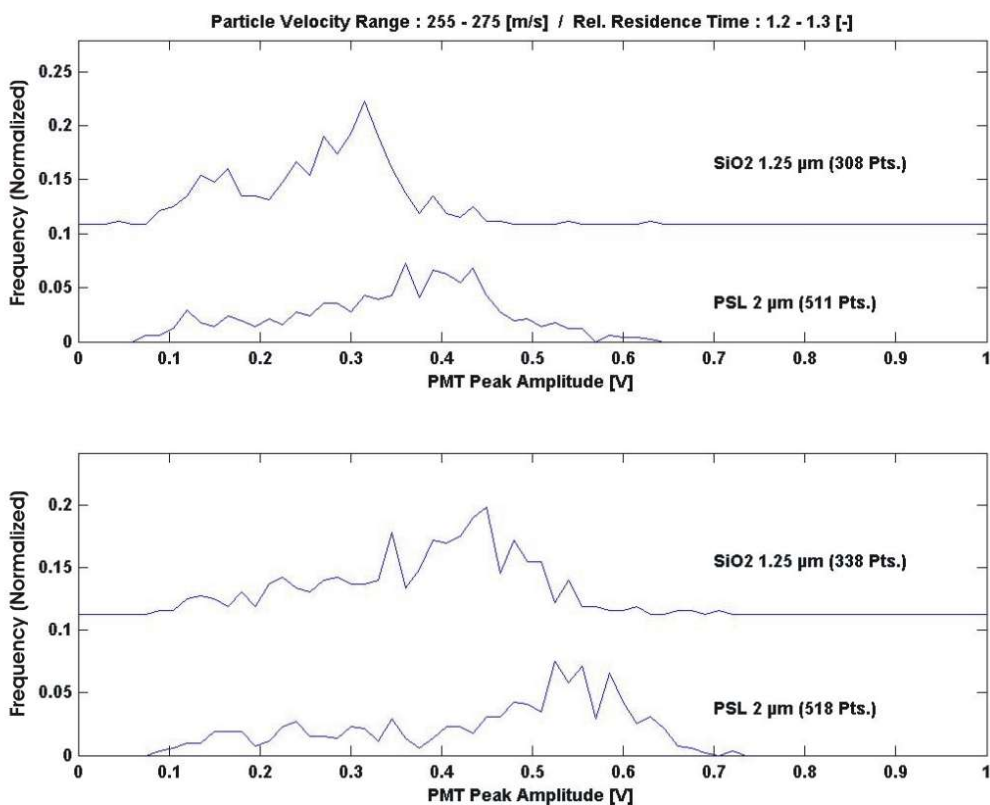


Figure. 76 : PMT2a signal amplitude for particles with similar velocity and relative residence time (2)

13. To a better characterization of the particle physical properties

The photomultiplier peak amplitude for PSL 2 μm particles is stronger than for SiO₂ 1.25 μm particles. Both particles can be here reliably differentiated. However as presented in Chapter 5., the comparison of the particle time-of-flight and the photomultiplier signals without a complex treatment already permitted their reliable differentiation. Fortunately the correction of the data by the methodology presented here confirms the results from the “raw data” presented in Chapter 5. Particles can be here, as predicted, reliably optically differentiated. The large range of measured amplitude of the photomultiplier signal can be attributed to errors in the peak amplitude measurement due to the high noise level of the photomultiplier signal.

A remarkable shift of the photomultiplier peak amplitude between PMT2a and PMT2b is observed. This shift is due to apparently different settings of the photomultipliers, probably the voltage across the dynodes series that amplifies the photocurrent or a light transmission loss in the optical line since it occurs for all particle types.

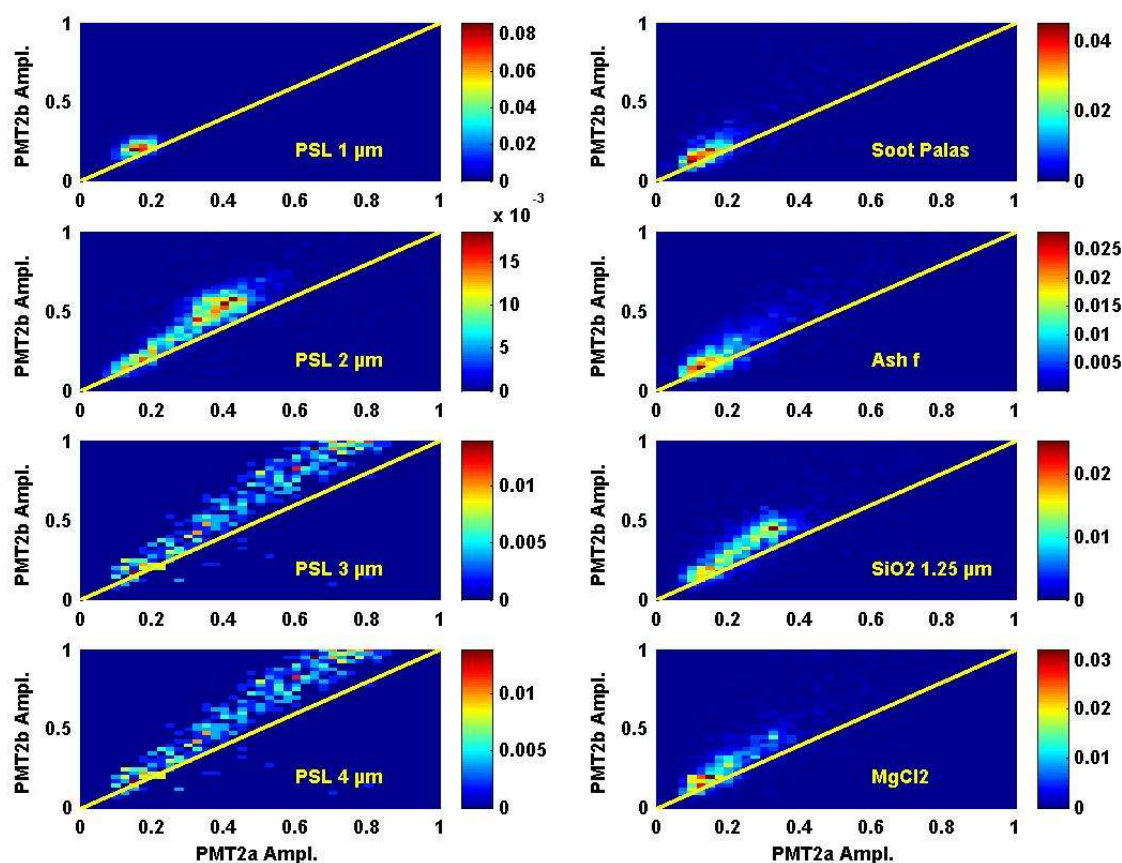


Figure. 77 : Photomultiplier peak amplitude correlation between PMT2a and PMT2b

This figure shows the proportion of particles of a given photomultiplier signal amplitude from PMT2a (denoted here PMT2a Ampl.) and from PMT2b (denoted here PMT2b Ampl.). The white line represents the line PMT2a Amplitude = PMT2b Amplitude and illustrates that both scattered light collection optics and detectors do not react to the scattered light in the same manner. The higher signal amplitude observed for PMT2b compared to PMT2a for all particles indicates an experimental bias due to the collection optics and/or photomultiplier settings. This figure also illustrates that the comparison of both photomultiplier signals PMT2a and PMT2b can not inform, in these conditions, about the particle shape or its deviation from sphericity.

13. To a better characterization of the particle physical properties

- Evaluation of the particle symmetry

An advantage of this instrument is the capture of the particle scattered light at two locations across the sizing laser beam axis. The comparison of the photomultiplier signals at each location might inform about the particle the sphericity. Figure. 77 shows the comparison of the photomultiplier signal amplitude distribution of the PMT2a and PMT2b signals.

In all cases, the distribution range of the photomultiplier peak amplitude can not be differentiated from PMT2a and PMT2b. A wider photomultiplier peak amplitude distribution is expected for the soot and ash particles compared to PSL 1 μm particles since their shape are expected to be more irregular than PSL 1 μm . Such a behavior is not observed here. In the current state of the detection/sizing unit of the SPALMS, particle sphericity can not be accessed.

If the low quality of the photomultiplier signals can not permit the obtention of additional information about the particle, it can nevertheless be used to treat the coincidence events and to evaluate the representativity of the particle chemical analysis of the SPALMS instrument.

13.4 Coincidence events evaluation

As mentioned in Chapter 5. coincidence events affects negatively the measurement of the particle size distribution. If a very narrow particle beam, down to a diameter of 100s of μm , can be produced as with an aerodynamic lens, a second method can be tried to evaluate the coincidence occurrence. This method uses the property that the particle velocity can be determined either by using the particle time-of-flight $\text{TOF}_{\text{sizing}}$ between the two laser beams or by measuring their transit time through each beam.

The need of a narrow particle beam compared to the sizing laser beam is necessary to insure that the particle irradiation conditions are the same for each particle in order to reduce the “trajectory ambiguity effects”. In this case, each particle crosses the sizing laser beam anytime at the same location. Giving this, the measured time can quasi exclusively be related to the particle velocity and size once the distance between both sizing lasers is known as well as their respective beam diameters.

In these conditions, the signal from each of the 4 photomultipliers are digitized during the time needed by the particle to fly from the first sizing laser to the desorption/ionization laser beam. For the SPALMS instrument, a typical time period of 200 μs is sampled with a sampling rate of 50 ns. The peak width of each peak from each photomultiplier signal is calculated as well as all combinations of particle time-of-flight $\text{TOF}_{\text{sizing}}$ between peaks from the PMT1a signal and PMT2a and PMT2b signals. If more than one peak is detected by the PMT1a before the first peak is detected either or by both PMT2a and PMT2b, there is a risk of coincidence event. This event is then counted as a potential coincidence event. These signals are then further processed as follow.

The particle velocity is calculated in two manners and then compared together. The particle velocity Type 1, $V_{p,1}$, is calculated from the particle time-of-flight between both sizing lasers. The particle time-of-flight $\text{TOF}_{\text{sizing}}$ that is here considered is the time between the first peak detected by the photomultiplier PMT1a and the first peak detected by the PMT2a and/or PMT2b. The particle velocity Type 2, $V_{p,2}$, is then calculated from the particle residence time in the sizing laser beam using a nominal or measured sizing laser beam diameter and the photomultiplier peak width (expressed in time).

This gives 3 values of the particle velocity: one particle velocity Type 1, $V_{p,1}$ and two values of the particle velocity Type 2, $V_{p,2}$. If the three calculated particle velocities are of similar order of

13. To a better characterization of the particle physical properties

magnitude then likely no coincidence events occurred. If the calculated particle velocities differ from each other then coincidence has very probably happened. Figure. 78 sums up the coincidence and non-coincidence situations, respectively (case(a)) and (case(b)). Table 47 summarizes the conditions of the different values of the particle velocity Type 1 and Type 2 for the coincidence and non-coincidence events.

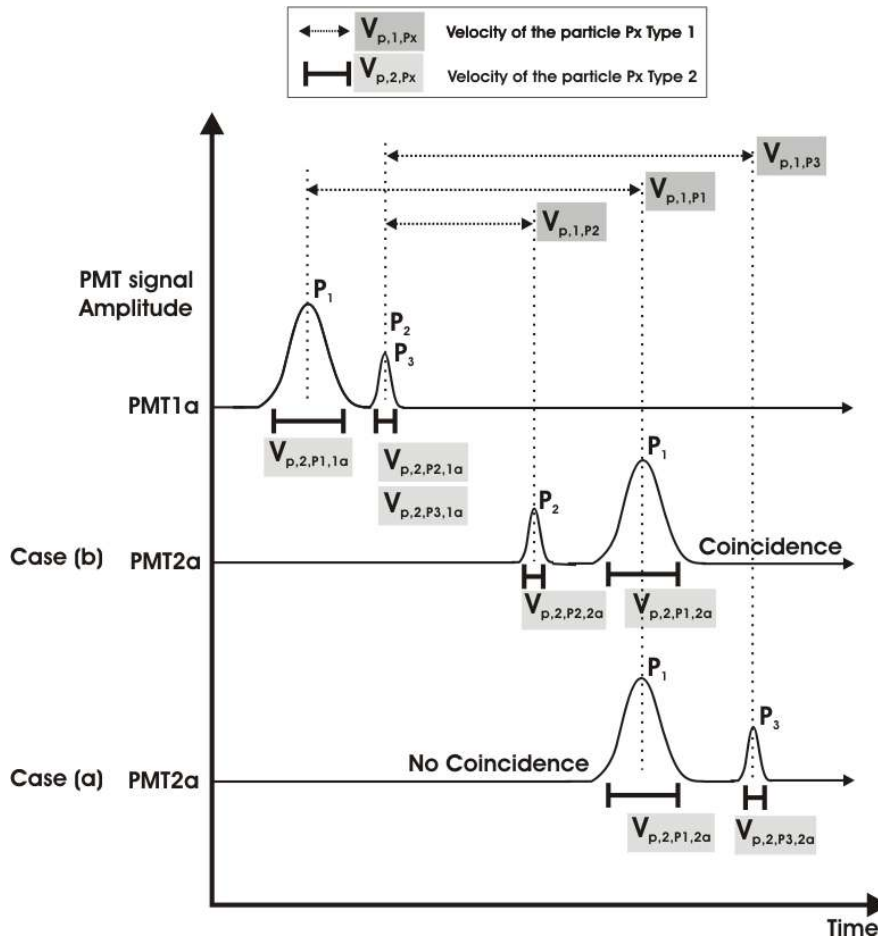


Figure. 78 : Treatment of the coincidence using particle velocity (type 1 & 2).

The velocity of the particle is calculated in two manners. The particle velocity Type 1 $V_{p,1,P}$ is calculated from two photomultiplier signals. The second particle velocity type 2 $V_{p,2,P}$ is evaluated from the peak width from each photomultiplier signal. The comparison of the values of each calculated particle velocities deduced from the different photomultiplier signals leads to evaluate the probability of coincidence events. Their relationships are presented in the next table. Note: The drawing does not respect the scale of the quantities described.

Coincidence state	Conditions
Case (a) : No Coincidence	<ul style="list-style-type: none"> $V_{p,2,P1,1a} = V_{p,1,P1}$, $V_{p,2,P1,2a} = V_{p,1,P1}$, $V_{p,2,P1,1a} = V_{p,2,P1,2a}$ $V_{p,2,P3,1a} = V_{p,1,P3}$, $V_{p,2,P3,2a} = V_{p,1,P3}$, $V_{p,2,P3,1a} = V_{p,2,P3,2a}$
Case (b) : Coincidence	Other combinations than those listed for case(b)

13. To a better characterization of the particle physical properties

By calculating the particle velocities Type 1, $V_{p,1}$ and Type 2, $V_{p,2}$, for all photomultiplier peak combinations, one can attribute in principle the different peak to their particle, quantify the coincidence events and correct accordingly the measured particle size distribution.

The efficiency of the method is strongly dependent on the quality of the photomultiplier signals, the repartition of the intensity within the sizing laser beams, the stability of the relative position of the narrow particle beam through the sizing laser beams and the precision of the flight distance of the particle between its detection times. In the present setup, it can only theoretically quantify the coincidence events for acquired photomultiplier signals at a maximum counting rate up to 7 Hz. It is currently few but it checks the coincidence events for more particles than with the three lasers method described before.

However, the calculation of the particle velocity is tricky because of the measurement of the time and because of the uncertainty on the flown distance $L_{\text{flight,detection}}$ by the particle between both sizing lasers as well as within each sizing laser beams. This makes the value of the calculated particle velocities of Type 1 $V_{p,1}$ and Type 2 $V_{p,2}$ much too uncertain. Such uncertainty makes therefore the use of this method to evaluate the importance of the coincidence events on the particle size distribution not reliable.

13.5 Analysis representativity inferred from the aerodynamic-optical particle properties

As seen before in Chapter 12, it is potentially possible to differentiate particle optically when these particles have an identical aerodynamic diameter by considering the data couple {aerodynamic diameter – scattering light intensity}. One can refine the differentiation by considering in addition the particle residence time in the laser beam. The differentiation occurs due to a difference in either density, refractive index or shape. The access to these properties can lead to confirm or infirm the observed particle composition inferred from the mass spectra as did [Murphy et al., 2004] or as proposed here to evaluate in which extent the observed particle chemical composition can be representative of the of the aerosol.

For this purpose an experiment was conducted with the SPALMS during which a special care was given to reduce the photomultiplier noise level by careful adjustments of the sizing lasers and the precise positioning of the light diaphragms. In these settings, a low noise level was reached down to 40 to 50 mV compared to the usual level of 150 to 200 mV. PSL particles with sizes ranging from 1 μm , 2 μm and 3 μm as well as Palas Soot particles were investigated. As expected, Figure. 79 shows that PSL particles and Palas soot particles can be differentiated when the photomultiplier signal has a low noise level. The dotted horizontal line precises that the photomultiplier signal acquisition device has not correctly been set and recorded voltages above 0,3V as 0,3 V so that the photomultiplier signal for PSL 3 μm particles is always distorted since it lies above 0,3 V. Nevertheless, as observed with a worse photomultiplier noise level, the scattered light level increases as the particle size increases.

The fact that PSL particles and Palas soot particles can be differentiated here leads to conclude that the data pair {particle time-of-flight $\text{TOF}_{\text{sizing}}$ or aerodynamic diameter - particle scattered light} can help to evaluate the representativity of the single particle chemical analysis.

Indeed with the used desorption/ionization laser trigger mode, the static trigger mode, one can only hit Palas soot particles which are polydisperse whereas PSL particles due to their monodisperse character can not be hit since the trigger delay is not appropriated. In the case a mixture of both particles types is investigated, one would only observe Palas soot particles with typical mass spectra as presented in Figure. 53 whereas no PSL particle mass spectra would be observed. In case PSL

13. To a better characterization of the particle physical properties

mass spectra would be obtained, there are different enough from those of Palas soot so that both particle types can be clearly differentiated. Indeed examples of mass spectra of PSL particles are presented in [Vera et al., 2005] and show a clear C_nH_m cluster pattern with $m = 1$ to 4 for any values of n as opposed to soot particles.

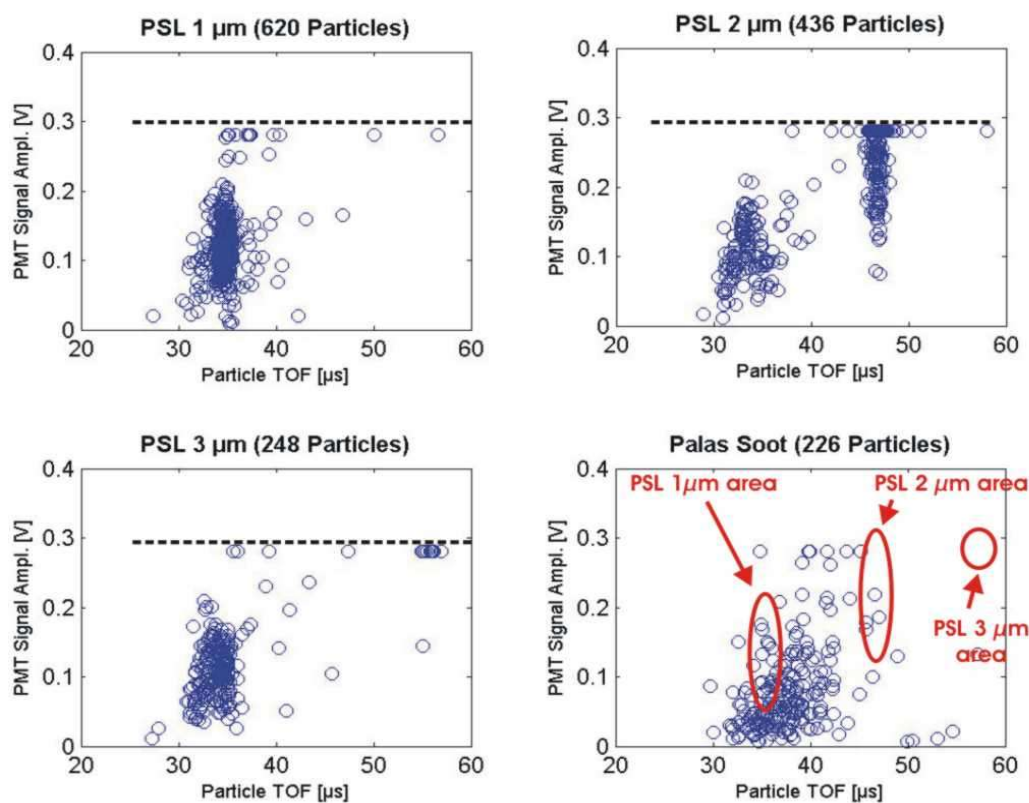


Figure. 79 : Particle scattered light versus particle time-of-flight at low photomultiplier noise level

The dotted line marks the upper range voltage of the data acquisition devices. It truncates/distorts the signal at 0,3 V what does not permit the observation of many PSL 3 μm particles. It is here to observe that PSL and soot particles can be clearly differentiated based on the particle time-of-flight TOF and the photomultiplier signal whose noise level is low.

In the case a mixture of soot and PSL particles in the aerosol would have been analyzed, it would have been easy to conclude from the mass spectra analysis only that the mixture would only contain soot particles while it is not the case. As a result, the chemical composition representativity of the aerosol inferred from the single particle mass spectra should be interpreted in the light of the aerodynamic-optical properties of all the detected single particles. Indeed one has to check that the scattered light and time-of-flight of particles giving a mass spectra are consistent with the rest of the aerosol.

13.6 Modification of the particle light scattering collection optics

The reformulation of the particle light scattering collection optics can increase in different manners the potential of the SPALMS. The light can be collected over a wider solid angle and at different positions and directed to a CCD camera or an array of photomultipliers. It can also be adapted to

13. To a better characterization of the particle physical properties

measure the scattered light intensity in its different polarization states. Both solutions should permit the obtention of additional information about the particle shape.

- Location and capture solid angle of the scattered light collection optics

For a sizing laser, one collimator should be positioned in near forward scattering region to lower the particle size detection limit since most of the scattered is located in the forward scattering zone (up to 20° for example) (see Figure. 18) and to have access to a light signal almost independent of the particle optical properties for big particles if the size parameter α of the particle is greater than unity. [Baron and Willeke, 2001].

In addition, the scattered light collecting optics can be installed asymmetrically relative to the sizing laser beam to take advantage of different incident angles of the laser light relative to the detector. Indeed [Kievit et al., 1996] operated an aerosol mass spectrometer whose scattered light collection optics capture the scattered light at 45° and 90° from the detection laser in the scattering plane. They took advantage of different amount of light scattered in both directions in order to estimate the particle size from the ratio of the photomultiplier signal areas whose standard deviation is much smaller than that of the absolute signal area (respectively 17% vs. 50% of the mean value) what reduces the impact of the trajectory ambiguity effects. Even if its comparison to the Mie theory prediction can not permit the precise determination of the particle size because the size relationship to the amount of scattered light is not monotone, the measured ratio increases as the particle diameter increases what give a size information.

This approach is interesting because (i) no correction of trajectory ambiguity effects has to be accounted for and (ii) it gives access to the geometric particle diameter $d_{p,g}$ allowing then the particle density by combination with the aerodynamic diameter $d_{p,a}$ to be inferred.

[Baron and Willeke, 2001] mentions an easy way to bypass the non monotonic function dependency of the scattered light intensity to the geometric particle diameter by using white light or increasing the solid angle over which the scattered light is captured.

In addition, the review of [Jones, 1999] about the use of light scattering to analyze single particles indicates many optical setups that could be easily implemented in the SPALMS instrument. In particular, the particle light collection with an elliptical mirror whose light is focused on a CCD camera seems interesting. Indeed by recording the scattered light pattern that can be specific of a particle shape, particles can be differentiated according to their shape.

- Light polarization

The SPALMS sizing lasers are vertically polarized (polarizing ratio 100:1) as well as are both laser beams of the APS in the detection chamber what gives the opportunity to take advantage of it. The purpose of this approach is to measure the depolarization ratio which quantifies the relative amount of light scattered respectively in the parallel and perpendicular polarization plane after the incident polarized light is scattered by the particle. The depolarization of the light can be rich in information. On one hand, the depolarization leads to shape information since spherical particles do not depolarizes light as do irregular shaped particles ([Hinds, 1999]). In addition, the measure of the depolarization ratio can also bring some chemical information as presented by [Card et Jones, 1995] who demonstrated the possibility of evaluating the carbon content in coal single particles of diameter ranging from ~ 2-3 μm up to 100 μm .

14 To a better chemical characterization of the aerosol gas and particle phases

This chapter presents the different combinations of laser systems used with the bipolar mass spectrometer operated by the SPALMS instrument with a specific trigger scheme to improve the knowledge of the chemical composition of the aerosol. The content of this chapter concerns mainly possibilities and proofed methods from the SPALMS development time and reported from the literature that require further experimental work to be validated. This chapter is aimed at better orienting the further development of the SPALMS instrument.

The chapter first presents how the SPALMS instrument can be used to analyze alternatively the gas and the particulate phase of the aerosol by firing two lasers whose characteristics better capture the features of each aerosol phase. Later on a discussion is presented on how to better characterize the desorption/ionization conditions and to evaluate the amount of ionization light incident on the particle. This knowledge is important in order to compare the particle mass spectra together and to evaluate if the surface or the whole particle is indeed analyzed. In this direction, the smart analysis of the mass spectra can inform about the quantitativity of the particle ablation by the laser as do the preferential directions in space of the ejected material from the particle during the desorption process.

Finally different laser systems and mass spectrometer trigger schemes are presented that have the potential to provide more information about the particle composition by operating the desorption/ionization in different manners to ionize the chemicals. Finally it will be discussed the interest of using high resolution mass spectrometers for a better identification of ions resulting from the soft laser desorption/ionization of the particle constituents by taking advantage of the mass deficiency parameter.

14.1 Simultaneous particle and gas-phase analysis

Many authors report the measurement of the aerosol gas phase within the mass spectrometer ([Prather et al., 1994], [Cabalo et al., 2000]) which is often considered as an artefact source or sometimes wished for their analysis purposes as performed by [Rodgers et al., 2004] by deliberately firing the laser so that it misses the particles. Sometimes, it is needed to consider the gas phase measurement as a blank measure to correct the obtained mass spectra of the particle from the biases due to the gas phase. Such biases are to be expected as the ionization laser wavelength decreases, typically starting from 266 nm.

This indicates that in spite of the low pressure of the gas in the ion source (some 10^{-6} mbar), there is enough material that can produce mass spectra as observed, for example, with the SPALMS instrument. Figure. 52 presents a mass spectrum from benzene, toluene and naphthalene at a pressure of $\sim 10^{-6}$ mbar obtained by photoionization with a Nd:YAG laser periodically triggered at 20 Hz at the wavelength of $\lambda = 266$ nm for PAHs.

Since the nozzle unit of the SPALMS instrument permits the analysis of the gas phase, it can be used to investigate both the gas phase and the particle of the aerosol at the same time. This is of particular interests for the study of combustion processes or the formation of aerosols at high temperatures. In order to attribute without any ambiguity the mass spectra to the analysis of either

14. To a better chemical characterization of the aerosol gas and particle phases

the gas phase or the particulate phase and to keep a simple laser trigger scheme, either one or two lasers can be used.

In the case of one laser, the laser is simply operated in free running mode. The mass spectra are attributed to either the gas phase or the particulate phase by the off-line processing of the photomultiplier and mass spectra signals which are acquired over the whole duration, typically 0,5 ms, of the particle analysis. Indeed all mass spectra occurring within a given time after the detection of the particle by the sizing unit can be attributed to the particle phase whereas other mass spectra are attributed to either the gas phase or particles that can not be detected by the sizing unit, i.e. fine particles. However as presented before, the free running mode usually gives a low hit efficiency.

One has then interests to operate the SPALMS instrument in static or dynamic trigger mode but in this case with a combination of two lasers. One laser is dedicated to the particulate phase, here the nitrogen laser, whereas the other is dedicated to the gas phase, here the Nd:YAG laser. This combination is presented in Figure. 80. The use of the nitrogen laser insures that the obtained mass spectra are related to the particle phase since its photon energy is not high enough to ionize gas phase compounds while the Nd:YAG laser can do it for specific gaseous compounds such as PAHs for example. The nitrogen laser can be easily triggered as particles come randomly and the Nd:YAG laser is periodically trigger allowing therefore the gas phase analysis.

If one wish a more exhaustive gas phase composition with the analysis of aliphatics compounds and other air constituents for example, the Nd:YAG laser ($\lambda = 266$ nm) can be replaced by a more energetic laser with a more energetic light such as VUV light (vacuum ultra violet light) for example at $\lambda = 193$ or 118 nm.

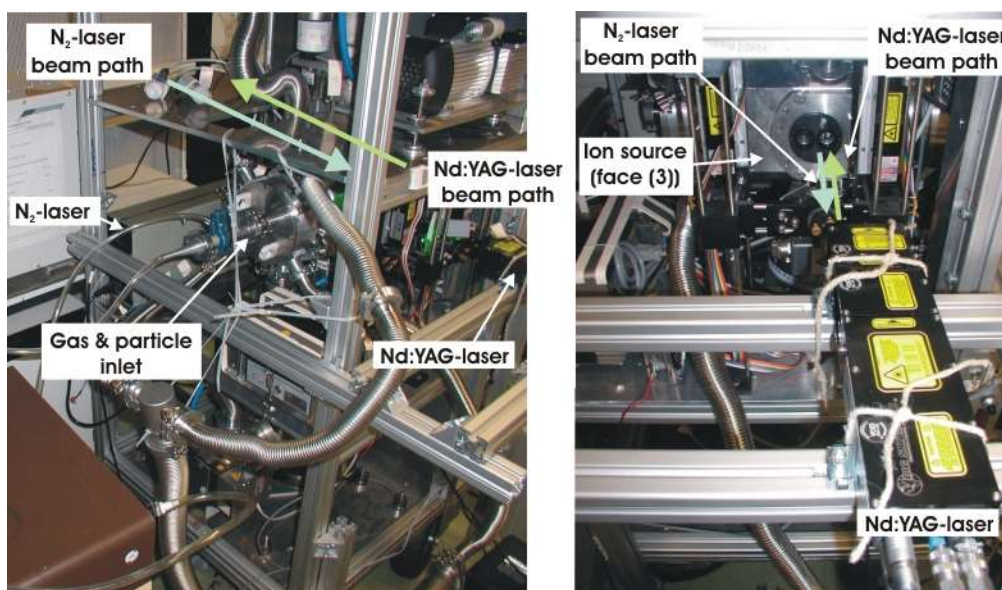


Figure. 80 : Simultaneous gas & particle analysis SPALMS setup

The nitrogen laser and the Nd:YAG laser are fired in parallel in opposite directions. The nitrogen laser permits the analysis of particles whereas the Nd:YAG laser ionizes specific gaseous compounds of the gas phase such as PAHs.

At this stage, the problem is to handle the data from the mass spectrometer properly and to attribute them to the right laser, *in fine*, to the aerosol phase that is analyzed, i.e., the gas or the particle

14. To a better chemical characterization of the aerosol gas and particle phases

phase. For this both mass spectra are acquired on the same oscilloscope on two channels Ch.1 and Ch.2 while the two other channels Ch.3 and Ch.4 are respectively recording the trigger pulse from the desorption/ionization laser for the particle phase and the ionization laser for the gas phase. The data acquisition is triggered as a mass spectrum is obtained. The occurrence of a trigger pulse on one of the channels, Ch.3 or Ch. 4, indicates which laser was triggered and, as a result, which aerosol phase was analyzed. The mass spectra attribution can be performed off-line by a home-made program that checks on which oscilloscope channel the laser trigger pulse occurred. Figure. 81 presents in more details the trigger scheme. A second oscilloscope is to be used to record the photomultiplier signals as presented in Chapter 9. which is synchronized with the first oscilloscope (similarly to the scheme presented in Figure. 51). This checks that the mass spectra recorded for a particle has a high probability of originating from a big particle. Indeed the sizing lasers must detect the particle in a given time window before the mass spectra occurs as presented in Chapter 7.

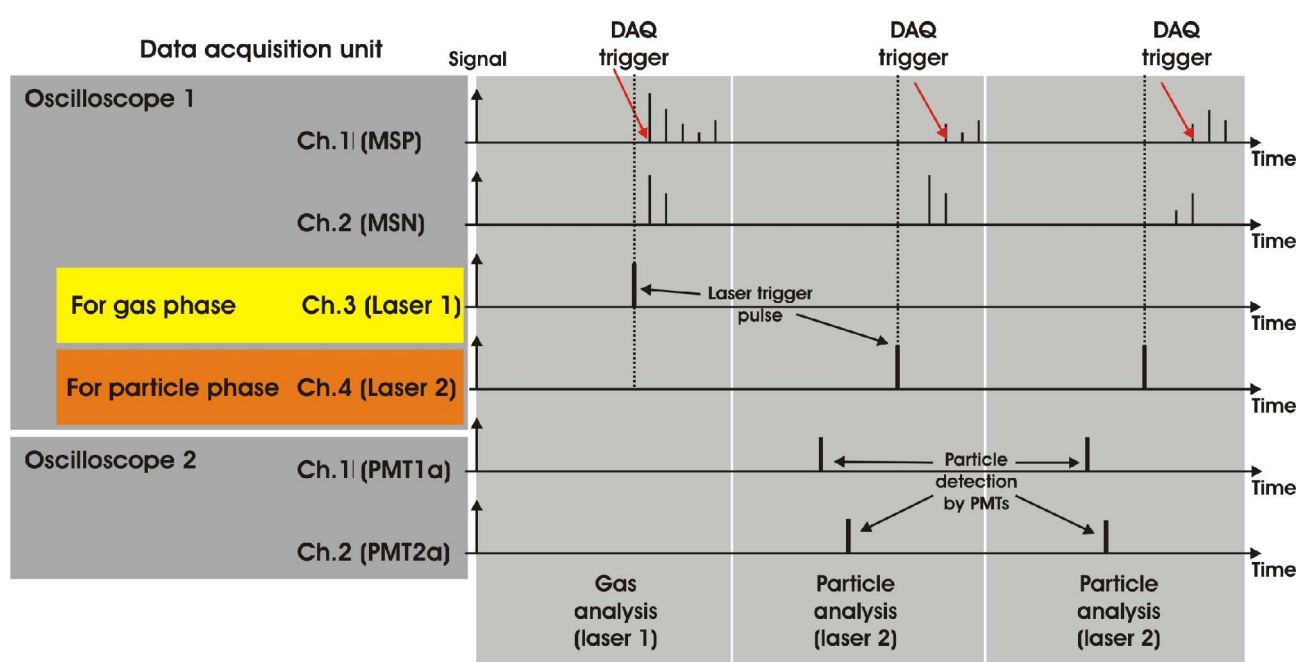


Figure. 81 : Simultaneous gas and particle phase aerosol analysis data acquisition scheme

Mass spectra of both polarities and trigger pulses of both ionization lasers are recorded on the same oscilloscope. Simultaneously a second oscilloscope records the photomultiplier signals. The data acquisition with both oscilloscopes is then triggered as the oscilloscope 1 detects a mass spectrum of a given polarity. The data are then off-line processed so that the mass spectra can be attributed to the right aerosol phase, gas or particle, by detecting the trigger pulse of one of the ionization laser. In case the particle phase is analyzed, the occurrence of peaks on the photomultiplier signals permits the confirmation that a particle is analyzed.

This method should work for moderate particles concentration and big enough particles to be detected. In the case of fine particles, both lasers should be triggered periodically in free running mode. The major problem raised here is what is the criteria to use to differentiate a mass spectra from a particle or from the gas. In the latter case, the gas phase mass spectra should vary much less with time than those from particles since the gas phase in a continuous medium.

If for the analysis of an aerosol, one has to focus on a high chemical analysis rate (CAR) to get representative data, the gas phase analysis can be performed at much lower rate that is adapted to the rate of change of the gas phase composition. It simply requires to operate the laser at a low rate,

14. To a better chemical characterization of the aerosol gas and particle phases

which is recommended, or to consider the recorded mass spectra at given time intervals.

It is here then necessary to evaluate the proper frequency to sample the gas phase so that changes from analysis to analysis are smooth enough to be considered negligible against the difference in particle to particle analysis.

The analysis frequency is constrained by the gas residence time in the SPALMS instrument. Indeed the wide volume of the instrument (inlet unit, ion source, mass spectrometer, pump tubings) and the gas residence time might simply physically average the gas phase composition if one consider that the gas phase expands quickly and is homogenized instantaneously in the ion source volume. The approximative volume of the ion source $V_{\text{ion source}}$ is estimated to be $\sim 2280 \text{ cm}^3$ and the volumic gas flow rate $Q_{v,\text{ionsource}}$ entering the ion source is estimated to be $4,13 \text{ m}^3/\text{s}$ (at 10^{-6} mbar and 295 K) by Eq. 6 what gives an approximated gas residence time $\tau_{\text{gas,ionsource}}$ in the ion source of $\sim 0,5 \text{ ms}$. As a result, any change in composition of the gas phase in a time longer than $\tau_{\text{gas,ionsource}}$ ($\sim 0,5 \text{ ms}$ here) can be detected. Moreover all mass spectra obtained showing an identical pattern over $\tau_{\text{gas,ionsource}}$ (here $\sim 0,5 \text{ ms}$) can reasonably be attributed with a high probability to the gas phase mass spectra.

To limit (if necessary) any averaging gas phase composition effect in the ion source, the gas phase can be sampled with an usual capillary system (similar to the one presented in Figure. 82) adapted to the SPALMS instrument that leads the gas directly to the ion source from the visiting trap of the ion source, face (3) or face (4), as presented in Figure. 8. The major problem at this stage is to eliminate the particles from the air before they enter the capillary since they might clogged it rapidly.

An alternative would be to recycle the air pumped away from the different inlet unit chambers by the vacuum pumps, which is particle poor, into the ion source. However the gas from the first inlet system chamber or the second one do still contain fine particles as demonstrated in Figure. 14 that are hardly removable from the gas phase. This makes this alternative unpractical so that it is easier to use a capillary inlet even if it will have to be regularly changed.

As a result, for practical reasons, the gas sampling from the particle inlet unit is preferred. If the particle analysis ability of the SPALMS instrument is characterized in this work previously, further studies are needed to investigate in precise details the sensitivity, the detection limit and the bias in the gas phase chemical composition obtained with this method.

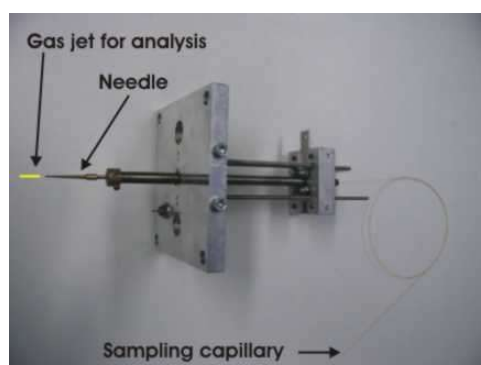


Figure. 82 : Usual gas inlet unit for laser time-of-flight mass spectrometers

14. To a better chemical characterization of the aerosol gas and particle phases

14.2 Toward a better single particle chemical characterization

The next section presents hardware setups and data analysis methods that should lead to gain more information about the chemical composition of the particle by better characterizing the extent of the desorption/ionization process and by using different laser system trigger schemes to operate the particle ablation.

14.2.1 Control of the laser desorption/ionization conditions

A major problem encountered in the field of laser based aerosol mass spectrometry is the uncontrolled one-step desorption/ionization process. This makes difficult the interpretation of the mass spectra to infer the chemical composition of the particle since it masks, fragments, rearranges the initial particle constituents as described in Chapter 2. To facilitate the mass spectra analysis, it is important to operate the desorption/ionization process in a controlled and/or known manner. Constraining the desorption/ionization process means that the laser power density experienced by the particle surface has to be known as well as the particle composition. Both of these information are not accessible since laser beams rarely have an homogeneous intensity distribution within the their cross-section and since the particle composition is indeed the object of the analysis. To better control the desorption/ionization process, in particular to better know the energy incident on the particle, two options can be proposed. The laser energy repartition can be made more uniform within the beam (i) or a test is to be developed to measure the power density experienced by the particle (ii).

Published attempts to control more the laser energy profiles in mass spectrometry concern the work of [Wenzel et Prather, 2004] or [Franck et al., 2005]. [Wenzel et Prather, 2004] showed the benefits of homogenizing the power density within the cross-section of the laser beam by conducting it through an optical fiber to the ion source. The authors report that the relative standard deviation of the total ion current measured for all mass spectra of a given particle type (2,4 dihydroxybenzoic acid, 2,4-DHB) dropped from 110% to 31% but also, more important, that for a given particle class, the sorting software based on an ART-2a algorithm neural network classifies all mass spectra in one class. The comparison of the mass spectra can therefore permit the differentiation of particles of various composition more reliably than before. On its side [Franck et al., 2005] obtains a homogeneous energy profile by firing the desorption/ionization laser at its maximum power, widening the beam with a lens and only selecting the central part of the laser beam for the desorption/ionization of the particle.

An other approach could be to validate the mass analysis only when the particle is vaporized and ionized in a specific zone of the desorption/ionization laser beam. This approach is commonly used for optical particle sizing to limit the influence of the trajectory ambiguity effects ([Baron and Willeke, 2001]) but it requires a pointing laser what render more complex the optical setup.

From another point of view, an imperfect laser beam energy profile can be considered as an opportunity to increase the range of power density that illuminates the particle. Indeed the imperfect power density distribution in the laser beam provides a wide range of power density levels. The particle is then irradiated by any of the energy level. Thus this provides different operating conditions that can be reflected in the mass spectrum pattern that can in turn inform further on the particle composition. In this case, one only needs to find a “power density tracer” that permits the attribution of the obtained mass spectra to a given desorption/ionization laser power level. This can be addressed in two manners. First the particle can be located within the laser beam by analyzing carefully the mass spectra. Secondly a chemical specie has to be found such that it shows a given

14. To a better chemical characterization of the aerosol gas and particle phases

mass spectrum pattern at a given laser power density level independently of the matrix used or of the aerosol composition.

The first solution requires the power density profile within the laser beam to be known and constant from shot-to-shot and to be well characterized before the measurement. If the mean laser pulse power is known, simply measured with a usual laser pulse sensor, one can access to the incident power density on the particle by locating it in the laser beam. The particle can be principally located in one direction (y-axis in Figure. 83) in the laser beam by observing the relative changes of the arrival time on the detectors of the mass spectrometer of specific cations and anions used as tracers of the particle position. The method principle is illustrated in Figure. 83.

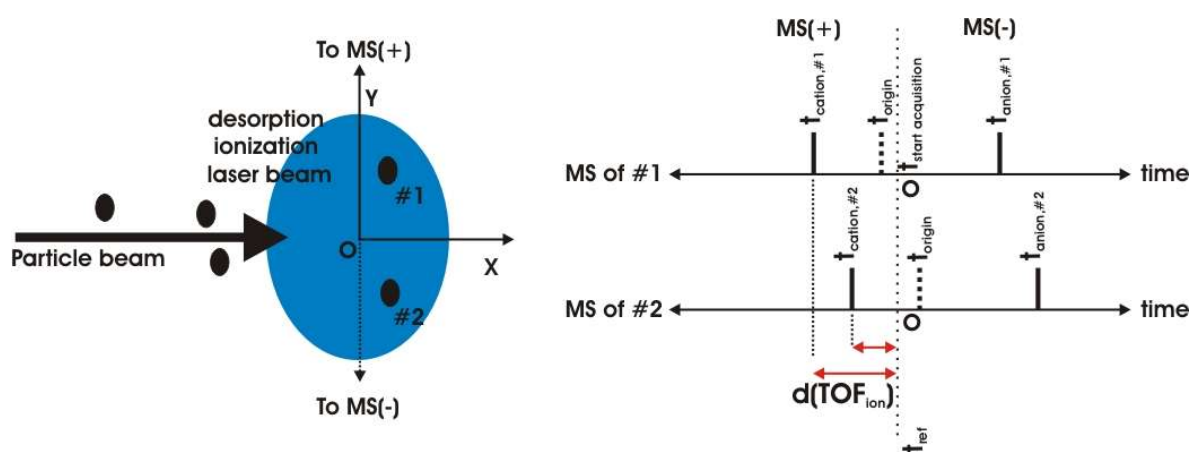


Figure. 83 : Particle location in the desorption/ionization laser inferred from the mass spectra

Unfortunately this method can not be used because the peak time measurement accuracy is limited by the shape/width of the peak. Besides the time difference $d(\text{TOF}_{\text{ion}})$ observed in the ion arrival time on the detector from particles located at both extremities of the laser beam are not big enough to be precisely measured. The carbon cluster C_2^- ($m/z = 24$) and sodium atom Na^+ ($m/z = 23$) are used for this purpose since they are present in almost every particle, their respective time-of-flight in the mass spectrometers of the SPALMS reaches $7,75 \mu\text{s}$ for a travel path of $\sim 1 \text{ m}$. The time-of-flight difference $d(\text{TOF}_{\text{ion}})$ of the tracer ions C^- and Na^+ measured for particles, #1 and particle #2 in Figure. 83, starting at opposite locations in the laser beam are roughly of $\sim 0,5$ and $7,7 \text{ ns}$ respectively for the nitrogen laser (beam diameter: $\text{Ø} = 60 \mu\text{m}$) and the excimer laser (beam diameter: $\text{Ø} = 1 \text{ mm}$). These time differences are measurable with the current hardware but are too small compared to the peak width of few ns. As a result, combined with the fact that the adjustments of the desorption/ionization laser relative to the particle beam might drift during the analysis, the method is not applicable to evaluate the power density incident of the particle surface.

It is therefore more interesting to find a tracer associated with the particle itself and independent of the experimental setup. Such a tracer could be a soot or organic compound since they are usual carbon material in particles which always produce cationic and anionic carbon/hydrogen clusters $\text{C}_n\text{H}_{m=1-4}$ if the power density exceeds a given threshold.

The power density level incident of the particle can be possibly inferred from the relative proportion of clusters of different sizes since the size of the carbon clusters in the mass spectrum decreases as the laser power increases ([Koo et al, 2002]). Logically, this method depends on the carbon speciation and on the amount of carbon material what makes it problematic to use. The alternative is

14. To a better chemical characterization of the aerosol gas and particle phases

here to consider the relative peak shape and dimension of negative carbon cluster ions C_2^- for example from particle to particle as will be illustrated later.

Figure. 84 shows a portion of a mass spectra from Palas Soot particles obtained at $\lambda = 248$ nm, $2,7$ $W/\mu m^2$ ((a), top panel) and at $\lambda = 337,1$ nm, $8,7$ $W/\mu m^2$ ((b), bottom panel). Two different patterns appear. For polydisperse particles, at similar maximum peak voltages, peaks are similar in width for both wavelengths. As the peak height increases the peak width increases and gets split into two peaks. Since all particles do have the same composition, similar shape, laser light absorption properties, the variation in the peak height and shape should be related to either the particle size or the laser light power density incident on the particle. This might be used as a “energy thermometer” for organic containing particles.

Due to the lack of data and the improper sizing unit, it was not possible to rigorously check this possibility. Mass spectra must be sorted after the particle size, the carbon cluster relative abundances and the mean laser power density to really evaluate the potential of this “energy thermometer”.

However, this observation can be used to qualitatively evaluate the quantity of the laser desorption/ionization process as will be discussed later.

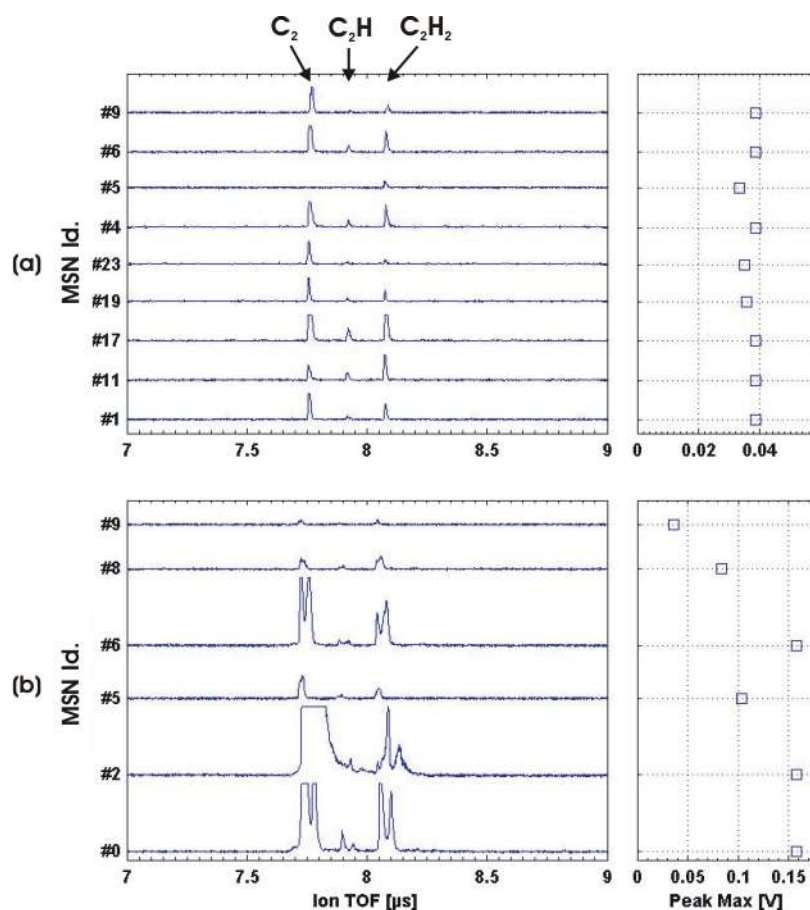


Figure. 84 : Double peak at a given m/z in negative mass spectra

Panel (a): Palas Soot particle, $\lambda = 248$ nm, $2,7$ $W/\mu m^2$. **Panel (a):** Palas Soot particle, $\lambda = 337,1$ nm, $8,7$ $W/\mu m^2$

14. To a better chemical characterization of the aerosol gas and particle phases

14.2.2 Surface and bulk particle analysis

A major question in single particle analysis by laser based mass spectrometry is the size of the fraction of the particle that is analyzed. Indeed as a function of the size and the laser power density, only the particle surface, a given depth or the total particle can be sampled. According to the laser shot-to-shot power density variation incident on the particle surface and to the variety of compositions and size of the aerosol, one can never know which fraction of the particle is analyzed. As a result, it is very important to attempt to qualify the kind of sampling that occurred as a single particle is analyzed.

For solid particles, the surface chemical composition is more relevant than the bulk composition to examine their effects on their environment. For example, adsorbed gas species might react preferentially on specific chemical species or water can crystallize more easily on given surface types. The bulk composition of solid particles is of interest mainly to locate the particle source in the environment. As for liquid particles, it is more difficult to state in which cases the knowledge of the surface composition is more pertinent than the bulk composition. The next section presents work directions that were tested or likely to be tested with the SPALMS instrument.

14.2.2.1 Published attempts

If many studies demonstrated the ability of aerosol mass spectrometry to probe the particle surface in known conditions as did [Carson et al., 1997], [Lazar et al., 1999] and [Woods et al., 2002], less studies were realized to evaluate, on a on-line and one-try basis, the extent of the single particle analysis. Indeed the above mentioned studies were made by investigating the same particle type for a given set of operating conditions and by deducing afterward by comparison which operating conditions merely sampled the particle surface or its bulk. A method that would permit for a on-line, one-try and single particle analysis to evaluate whether the particle analysis concerns mainly the particle surface or its bulk would be of great importance.

[Weiss et al., 1997] reports the possibility to detect the non-ablated rest of particles optically after the particle is hit by the desorption/ionization laser. A similar approach consists of detecting the rests of the particles with an electrometer placed after the desorption/ionization zone on the particle beam path. Such setups do exist but they are not operated for this purpose. Indeed such electrometers are essentially used to optimize the aerodynamic lens operating conditions (ATOFMS, TSI Inc. and [Mahadevan et al., 2002]).

Many authors prefer to evaluate the quantitativity of the desorption/ionization of the particle from the analysis of the mass spectrometer signals for given experimental situations. For example the influence of the relative position of the desorption/ionization laser compared to the mass spectrometer, the laser power density and the presence of multiply charged ions in the mass spectra can bring answers.

[Vera et al., 2005] investigated the influence of the relative position of the desorption/ionization laser beam and the bipolar mass spectrometer on the particle mass spectra. They observed some variations of the ion time-of-flight distribution that depend on the angle between the desorption/ionization laser beam and the mass spectrometer axis. They attribute these variations to the incomplete particle ablation in the case the desorption/ionization laser beam and the bipolar mass spectrometer are not exactly perpendicular.

[Reents et Ge, 2000] and [Park et al., 2005] consider the presence of doubly charged ions obtained at high laser power ($\sim 10^2$ W/ μm^2) in the positive mass spectra to evaluate the extent of the

14. To a better chemical characterization of the aerosol gas and particle phases

desorption/ionization of the particle made of pure material. The aim of their work was to relate the total ion current to the particle volume and further to the elemental particle composition. The relationship between the total ion current and the cube of the particle size appears to be linear in the case of [Reents et Ge, 2000] and to follow a power law in the case of [Park et al., 2005] which was attributed to an incomplete ion sampling by the mass spectrometer but not to an inefficient particle desorption/ionization.

The measured particle size by [Reents et Ge, 2000] as in [Park et al., 2005] are in good agreement with the other sizing methods used like SMPS and TEM with a better size resolution. From their studies, one can conclude that the comparison of the particle size inferred from the mass spectra and from another size measurement method can not be used to state about the quantitativity of the ablation process. Indeed in case of an incomplete ablation, the particle size inferred from the mass spectra must appear smaller than the size measured by the other sizing technique used. The uncertainties in the measurement process of the particle size combined to the need of calculating the particle size after the same equivalent size definition would make this approach difficult to work.

It exists some situations where the knowledge of the degree of ablation is not relevant to detect all present chemical constituents in the particle. [Neubauer et al., 1998] proposes a trick to have access in theory to all components of the aerosol particle if its constituents are soluble in water or another liquid. Indeed, the particle constituents can be dissolved and then freezed what leads the particle superficial layers to have the eutonic composition. The eutonic composition is the composition of the liquid that freezes the last and that contains a fraction of all constituents of the particle. This permits therefore the detection of all different chemicals independently of their relative proportions since the eutonic composition does not reflect quantitatively the bulk composition of the particle but only qualitatively. This is anyway not relevant since no aerosol mass spectrometer setups can analyze quantitatively an aerosol particle except for elemental composition as demonstrated by [Reents et Ge, 2000] and [Mahadevan et al., 2002]. This approach makes in particular more accessible the compounds of lower concentration in the particle.

14.2.2.2 Double desorption/ionization

If the problem can not be answered by the use of a single desorption/ionization laser, the problematic can potentially be addressed by performing the desorption and ionization of the particle constituents twice in a very close time with a moderated energetic laser. This imposes the ability to fire twice a laser and to perform twice the ion mass analysis within a short time. In the case of the SPALMS instrument, the extraction zone aperture of the mass spectrometer has a diameter of 4 mm that allows a time window for two successive laser shots and ion mass analysis of 20 μ s for a particle flying at 200 m/s, respectively 10 μ s at 400 m/s. Firing the same laser twice in 20 or 40 μ s is technically not feasible with the pulsed lasers available at the GSF-Forschungszentrum. This is nevertheless possible by using two laser systems where the first firing one triggers the second one shortly after. Considering the laser systems at the GSF-Forschungszentrum, the following laser combinations are possible as presented in Table 46 as well the proposed trigger methods.

Since this operation mode involves two successive desorption/ionization processes, the resulting ions have to be analyzed and sorted accordingly. A software solution and a hardware solution can be proposed to address this problematic. The software solution keeps the advantage of the simultaneous bipolar mass analysis but makes the mass spectra interpretation difficult if not impossible for complex aerosol particle compositions.

14. To a better chemical characterization of the aerosol gas and particle phases

The hardware approach makes the mass spectra analysis easier but it concerns only the cation analysis since one mass spectrometer tube is used for each desorption/ionization event.

<i>First laser</i>	<i>Second laser</i>	<i>Trigger mode</i>
Excimer laser	Nitrogen laser	Static or dynamic
Nd:YAG laser	Excimer laser	Free-running
Nd:YAG laser	Nitrogen laser	Free-running

Table 46 : Laser system combinations for on-line single particle depth profiling

- Software solution

In this case the mass spectrometer detector records the ion signal from both desorption/ionization events. The resulting cation and anion mass spectra correspond to the sum of the two mass spectra that are shifted in time. The time shift corresponds to the time delay between both laser shots in the case of the software solution or between each ion extractions in the hardware approach.

The method can theoretically work for the low mass range (up to $m/z \sim 300$) where the ion masses are discrete and have integer values so that both mass spectra can be separated from each other. It is however not successful if elements are very abundant what produces large peaks that can not permit the differentiation of peak of m/z to peak of $m/z+1$ as observed many times in the case of the ash sample.

Such a software method, if attracting, it not likely to be successful and is useless in case of a complex mixture as for example the case of the negative mass spectra #67 of the ash particle sample in Figure. 60 . An alternative to it is a hardware solution as presented below.

- Hardware solution

As previously presented in Chapter 8., the bipolar mass spectrometer has the feature to convert its anion mass spectrometer tube into a second mass spectrometer tube for the cation analysis if it is operated in pulsed mode. Indeed once the cations of the first desorption/ionization are extracted, the voltages of the second mass spectrometer tube are switched over after $\sim 5 \mu s$ so that a second cation mass analysis can occur. In this manner the ions resulting from each desorption/ionization event can be analyzed and give information about the radial composition of the particle.

The double desorption/ionization of the particle leads, if the laser energy of both laser pulses are energetic enough to produce mass spectra, to sample twice the particle at different depths or to sample the partially ablated particle and the gas phase species resulting from the first desorption/ionization event. Indeed the first laser pulse samples first a superficial part of the particle whereas the second a deeper part of the particle. However it does not inform if the whole particle is sampled.

14.2.2.3 Mass spectrum analysis

As explained in Chapter 8., the initial position and velocity of the ions have an influence on the mass spectra quality and the resolution $R = m/\Delta m$ in time-of-flight mass spectrometry. Indeed ions of identical mass m/z whose initial velocity is oriented toward the mass spectrometer arrive before

14. To a better chemical characterization of the aerosol gas and particle phases

the ions flying initially in the opposite direction. This makes the peak for a given m/z be split into two peaks as presented Figure. 85 and experimentally observed in Figure. 84(b).

On the example of [Vera et al., 2005], the mass spectrum analysis can inform about the quantitativity of the desorption/ionization process. Figure. 84(b) illustrates that peaks of a given m/z are split into two secondary peaks in certain circumstances. It leads to conclude here that the particle volatilization is rather complete than partial. Indeed the particle material is emitted uniformly in all space directions so that this symmetry is reproduced in the peak time detection of chemicals of given m/z in the mass spectra as illustrated in Figure. 85(b). On the other side, a strong signal would enlarge the peak and masks the eventual peak dedoubling features. The detection of the partial ablation of the particle is more difficult to detect since the mass spectra will appear to be displaced in one direction only (Figure. 85(c)). Such shift is difficult to detect since it appears in the same manner in mass spectra as when a particle is ablated at different locations within the laser beam as presented earlier in the chapter. Moreover it is difficult to define a reference ion time-of-flight for a given m/z to qualify this shift.

Nevertheless Figure. 84(b) indicates that ions of identical m/z emitted in opposite directions can arrive to the detector with a time interval of up to ~ 50 ns with the current mass spectrometer settings. Considering this, one might reasonably expect a shift of the mass spectra of up to 20 ns what is sensibly greater than the shift in time-of-flight induced by the undefined position of the particle within the desorption/ionization laser beam.

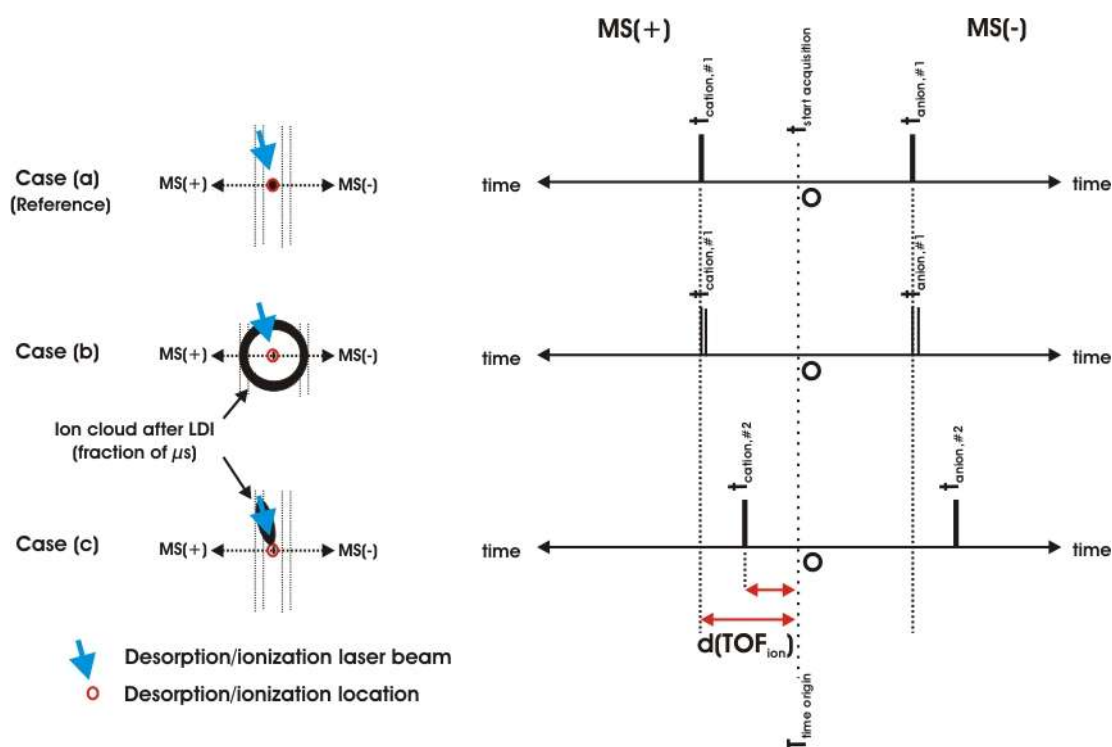


Figure. 85 : Influence of the ion cloud shape on mass spectra

Case (a): Ideal reference situation where the ion cloud does not expand. **Case(b):** Complete particle ablation. The mass peak is dedoubled. **Case(c):** Partial particle ablation

14. To a better chemical characterization of the aerosol gas and particle phases

However if the peak dedoubling feature at a given m/z seems to unambiguously support a complete ablation of the particle, an observed shift in one direction of the ion time-of-flight of the whole mass spectra can not reliably and conveniently support the occurrence of a partial vaporization of the particle. A better approach in this case would be to measure the ion current, and possibly the neutral species current as well, in different space directions. The detection of a higher ion current toward the desorption/ionization laser than in the other directions would better support the occurrence of a partial particle ablation. In practice, the ion current could be measured by the extraction electrodes themselves and by additional electrodes placed around the desorption/ionization zone so that most of the spatial directions can be sampled as illustrated in Figure. 86. Indeed the ion current can be measured on the extraction plates of the mass spectrometer on the example of the mass spectrometer adaptation of [Dessiaterik et al., 2003] who measured the ion current captured by the repeller of their mass spectrometer.

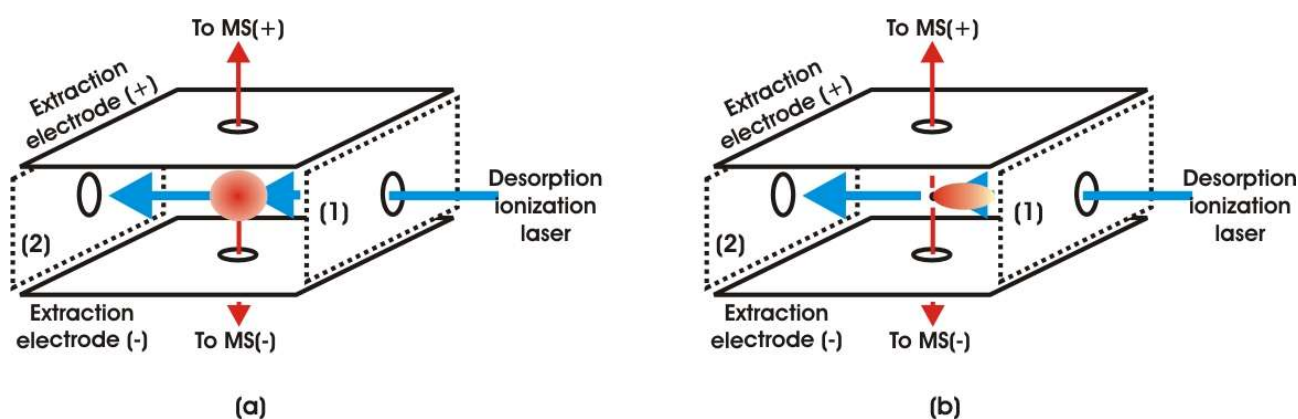


Figure. 86 : Multi-directional ion capture by the mass spectrometer extraction electrodes

Panel (a): Case of a complete particle ablation. **Panel (b):** Case of a partial particle ablation. The detection of the ion current in the different space direction should help to qualify the extent of the laser desorption/ionization better than the analysis of the mass spectra.

One should nevertheless point out that the particle homogeneity can significantly influence and bias the method presented above. Indeed [Zhigilei et al., 2003] investigated the material ejection patterns for different kind of aerosol particles. In particular, the figure of [Zhigilei et al., 2003] presented in this work in Figure. 47 let conclude that this approach is valid if the core of the particle only is absorbing the desorption/ionization laser light.

14.2.3 Comprehensive qualitative chemical analysis of the single particle

As described previously the addition of a second laser to perform a second analysis of the same aerosol particle by taking advantage of the specific mass spectrometer features of the SPALMS instrument has an interesting potential. The analysis scheme has simply to be adapted to the targeted aerosol particles.

14. To a better chemical characterization of the aerosol gas and particle phases

14.2.3.1 Qualitative chemical analysis with different desorption/ionization scheme

The interest of the two-step laser desorption/ionization approach is to perform the particle analysis once its constituents are in gas phase what eliminates uncharacterized matrix effects and simplifies the interpretation of the mass spectra. Since the mass spectrometer can sample both ion polarities at once or twice the same polarity from a particle within a few microseconds, many desorption-ionization-mass analysis combinations can be operated. They are denominated as presented in Table 47 and described in the rest of this section

<i>Name</i>	<i>Desorption laser</i>	<i>Ionization laser</i>	<i>Ion polarity analyzed in the MSP tube</i>	<i>Ion polarity analyzed in the MSN tube</i>	<i>Analyzed aerosol phase</i>
ODIMSB		UV	Cation	Anion	Particle
DIMSB	IR	UV	Cation	Anion (if any)	Neutrals cloud ⁽²⁾
DIMSB-P	IR	UV	Cation	Anion (if any)	Neutrals cloud ⁽²⁾ Particle rest
DI2MSB	IR	UV+PERCI	Cation	Anions	Neutral Cloud ⁽²⁾
DMSPIMSP	IR	UV	Cation Synchronized with desorption ⁽¹⁾	Cation Synchronized with ionization	Ion cloud Neutrals cloud ⁽²⁾
DI1MSPI2MSP	IR	UV(1) – UV(2)	Cation Synchronized with Ionization UV(1) ⁽¹⁾	Cation Synchronized with Ionization UV(2)	Neutrals cloud ⁽²⁾

Table 47 : Chemical analysis scheme nomenclature

⁽¹⁾ Indicate when the mass analysis is performed. ⁽²⁾ The neutral cloud is a cloud of neutral species produced by the desorption process Note: The different abbreviations refer to: **D**: desorption, **I**: ionization, **MSB**: bipolar mass analysis, **MSP**: cation mass analysis only, **P**: particle phase. The number indexes the process.

For example, DI1MSPI2MSP stands for desorption followed by two successive ionization and cation mass analyses.

The schemes ODIMSB and DIMSB are respectively the usual operation modes of aerosol laser based mass spectrometers. The scheme ODIMSB corresponds to the usual one-step laser desorption/ionization mode described in Chapter 6. whereas the scheme DIMSB stands for the “classic” two-step laser desorption/ionization mode. Since they were already extensively described before, they will not be addressed here.

14.2.3.1.1 Modified two-step laser desorption/ionization (Scheme DIMSB-P)

This scheme is a particular case of the usual two-step laser desorption/ionization mode described in Chapter 6. This is operated by [Zelenyuk et Imre, 2005] who operate their aerosol mass spectrometer in two modes. In the first mode, an infrared laser volatilizes the particle and a ultraviolet laser post-ionizes the resulting cloud of neutral species. In the second mode, the ionization laser is simply fired such that it ionizes the vapor from the previous desorption event and volatilizes and ionizes in one-step the eventual rest of the particle. According to the authors, this is a way to insure that the totality of the aerosol particle is chemically analyzed since they mention that

14. To a better chemical characterization of the aerosol gas and particle phases

the particle rests can be considered as refractory materials that are not vaporized by the desorption laser. The refractory nature of the particle rests is however still to be demonstrated since the desorption involves together thermal and mechanical processes.

14.2.3.1.2 Three-step desorption/ionization (Scheme DI2MSB)

The idea is here to keep a simple trigger scheme of the ionization step and an easy mean to attribute the mass spectra to the corresponding ionization event. Indeed, since ions from photoionization are mainly cations, it is to be found an ionization method that produces only anions in order to conserve the advantage of the bipolar mass spectrometer.

In this case the uncontrolled ionization step producing both anions and cations in the one-step laser desorption/ionization is replaced by the association of two monopolar ionization steps that are operated quasi simultaneously. The difficulty might be here to implement the negative ionization technique.

The PERCI ionization method presents in this regard many advantages. As presented by [LaFranchi et al., 2004], PERCI ionization is operated by the attachment of low energy electrons to molecules in a soft manner. The low energy electrons (<1eV) are generated by liberating them from a metal surface heated by a UV laser light ($\lambda = 235\text{-}300\text{ nm}$). The advantage of this method could be that the photoionization laser light for the positive ions production is also used to produce the photoelectrons needed for the PERCI ionization. Indeed, a beam splitter can split the laser beam in two beams: one is used for the usual photoionization whereas the other laser beam is lead to the metal surface that will produce photoelectrons. To be efficient the metal surface should be located close to the extraction zone center. Such trick would conserve the simple trigger scheme of the usual way of performing two-step laser ionization and fully use the bipolar mass spectrometer.

Other ionization methods producing negative ions can be used but they may not have the simplicity of the PERCI method presented here. Indeed, it might require to duplicate the ionization trigger signal and therefore complicate the general trigger scheme of the desorption/ionization and the data acquisition.

14.2.3.1.3 Successive cation mass analyses (Scheme DMSPIMSP and DI1MSPI2MSP)

As described in Chapter 8., the negative mass spectrometer tube can be used for a second cation mass analysis. The major difference with the former schemes is here that the mass analysis consists of two steps distant in time whereas in the previous one the ion analysis is performed simultaneously in both mass spectrometer tubes. Two approaches are possible where the approach 1 is the most convenient.

- Approach 1 (Scheme DMSPIMSP)

In this approach the objective is to take advantages of the eventual presence in the particle of compounds in their ionic form such as salts for example. Indeed these ionic species are liberated during the particle desorption by the IR laser pulse after the example of [Dessiaterik et al., 2003] who mass analyzed RbCl in ethylene glycol by only vaporizing the particle with an IR laser. The ion can be then immediately analyzed before the ionization laser is fired. Later the UV laser pulse

14. To a better chemical characterization of the aerosol gas and particle phases

ionizes the remaining neutral compounds as in classical two-step desorption/ionization.

One can then here differentiate the ionic species and neutral species in the particle. This scheme contains therefore already a “virtual separation” step. Such approach should be particularly interested for particles rich in ionic salts or water droplets rich in salts.

The first step could be replaced by a one-step desorption/ionization using the field-induced droplet ionization (FIDI) approach ([Grimm et Beauchamp, 2003]) to analyze first the soluble ionic material contained in a liquid droplet while the next UV laser will desorb and ionize the rest of the droplet constituents. It might also happen that this approach also ionizes softly the neutrals compounds of the particle since the electric field required to fragment the droplet is very high and might ionize the molecules as well. In this case, the extraction electrodes of the mass spectrometer should be pulsed while the data acquisition scheme should not modified compared to the previous methods.

- Approach 2 (DI1MSPI2MSP)

In this case the particle is volatilized with the IR laser but the mass spectrometer will analyze here the ions resulting from two successive ionization steps after the particle desorption. This requires here two different ionization methods and will lead to a better description of the particle composition if the used ionization methods are complementary like the combined use of REMPI and SPI ionization or REMPI and EI for example according to the work of [Mühlberger et al., 2004]. The major problem in this case is not the analysis with the mass spectrometer as presented before but how to implement two ionization methods to ionize the neutral cloud within a few microseconds in the ion source of the mass spectrometer. The introduction of a third laser is in principle possible but might be unpractical because of the room scarcity around the ion source and the complexity of trigger scheme of the different devices.

The approach 2 can be successfully performed if the particle is volatilized by thermodesorption. Indeed in this case, two lasers can only be used and the trigger scheme is simple.

For both approaches, one has to take into account the expansion of the particle material after the desorption process which dilutes the chemical species. This leads to a loss of sensitivity for the last ionization and mass analysis. To reduce this effect, the ionization and mass analysis should be performed as quick as possible in agreement with the speed of the mass spectrometer to perform the second mass analysis. Further studies are needed here to validate the concept on the practical point of view. Figure. 87 presents the different approaches.

The data acquisition is organized as presented in Figure. 88. Indeed the data acquisition is triggered by the obtention of a particle mass spectrum in the positive polarity. The laser output pulse signal from the laser itself or its trigger pulse is recorded for each laser shot that is intended to produce a mass spectrum. By an off-line data processing, the mass spectra can be attributed to their original ionization laser pulse.

14. To a better chemical characterization of the aerosol gas and particle phases

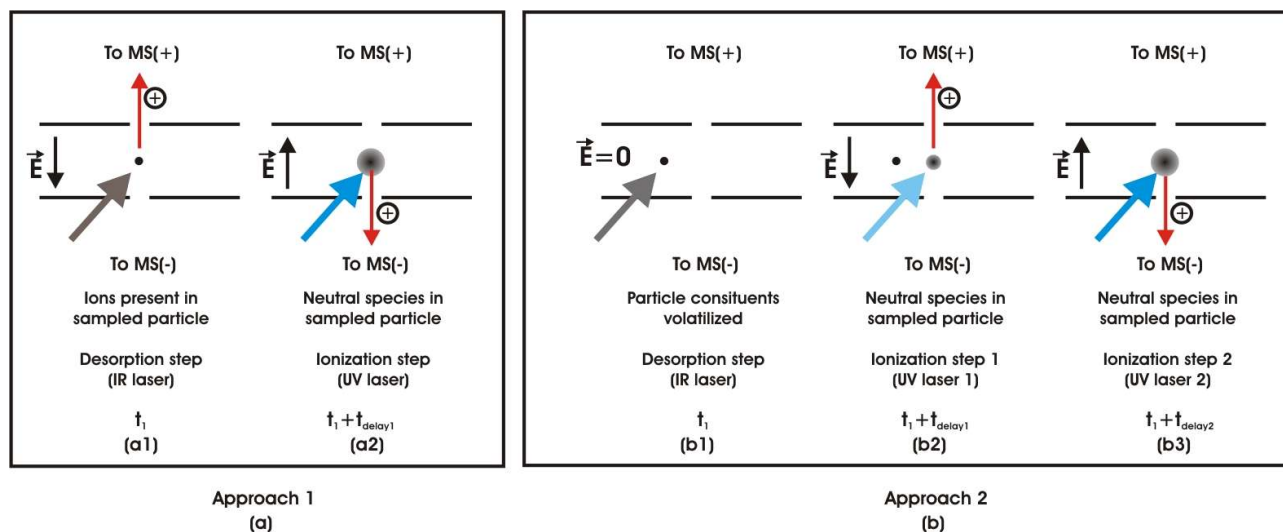


Figure. 87 : Principle of the 3-step desorption-ionization method for single particle analysis

Panel (a): The approach 1 permits the analysis of the cations initially present in the particle (step a1) which are vaporized by the desorption laser (an infrared laser) and directly analyzed in the cation mass spectrometer (MS(+)). A few microseconds later, the neutral species of the particle vaporized during the desorption step (step a1) are ionized (step a2) and the resulting cations analyzed. Between the step (a1) and (a2), the voltages of the anion mass spectrometer tube (MS(-)) are switched over to permit the second analysis of cations. **Panel (b):** The approach 2 permits the analysis of the vaporized molecules from the particle by the desorption laser (step b1) by ionizing them successively with different methods. First, molecules are ionized by a ionization method 1 (step b2) and analyzed in the cation mass spectrometer tube (MS(+)). A few microseconds later, the voltages of anion mass spectrometer tube (MS(+)) are switched over to perform the second cation mass analysis and the second ionization is triggered (step b3).

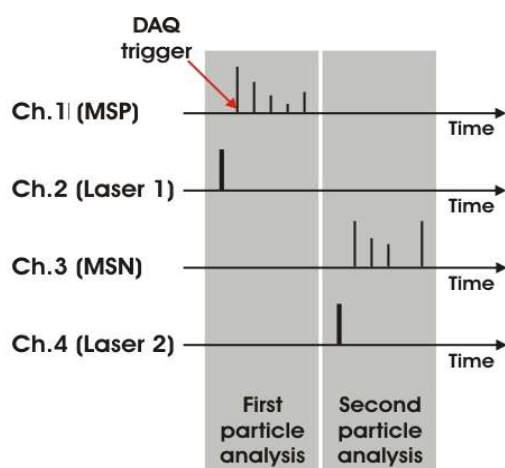


Figure. 88 : Data acquisition scheme for the 3-step desorption – two ionizations method

The mass spectra from each mass spectrometer tube (MSN and MSP) are recorded as well as the corresponding ionization laser trigger pulses on a 4-channels oscilloscope. The data acquisition is triggered by the obtention of a mass spectra at a given polarity. By a off-line data processing, one can identify which laser has been fired in order to relate the obtained mass spectra to the right ionization event.

14. To a better chemical characterization of the aerosol gas and particle phases

14.2.3.2 Qualitative analysis with an increased mass spectrum resolution

The accuracy of the measured ion mass-to-charge ratio m/z can bring additional information about the ions that are observed. However, this does not correct the bias induced by the chemical transformation of the particle during the laser desorption/ionization process. Indeed a better mass accuracy only permits a more reliable identification of the compounds with the same nominal mass since above a mass of 300, the nominal mass of an ion does not correspond to its exact mass. This can lead to false identification of ions due to its erroneous m/z value.

The difference between the nominal mass and the exact mass is called mass deficiency. It permits in particular the separation of different ions of similar nominal mass in different classes of compounds whose mass deficiency is characteristic of a group of chemicals as presented in [Hughey et al., 2001] and [Gross, 2004].

Such a method is only possible with a mass spectrometer that permits a high mass accuracy measurement. For aerosol mass spectrometers using time-of-flight mass spectrometry, the uncertainty in the determination of the ratio m/z is mainly attributed to the initial velocity of the ions in any directions rather than the initial position within the extraction source ([Vera et al., 2005]).

Performing a time-of-flight mass analysis that is independent of the initial velocity of the ions would improve the mass spectrum quality (resolution) and limit the errors due to the specific calibration of each mass spectrum. The idea is here to suppress the ion velocity component along the mass spectrometer axis and then to extract the ion into the mass spectrometer. This is the principle of the orthogonal acceleration time-of-flight mass spectrometry (oaTOFMS).

Ions are focused along an axis and then extracted perpendicularly what eliminates the effect of the initial velocity. The ions are then analyzed as in classical time-of-flight mass spectrometry. According to [Guilhaus et al., 2000], one can reach mass resolution up to 6000 with a MALDI-oaTOFMS. Indeed the interests of using an oaTOFMS appear only if it provides high mass accuracy measurements in order to get benefits of the mass deficiency.

It can be done in some manner in the case of a two-step desorption/ionization with the current setup of the bipolar mass spectrometer of the SPALMS instrument if the post-ionization laser beam diameter is “small”, the laser beam distant from the desorption laser and exactly coincident with the particle beam axis. In this case, only molecules whose velocity is parallel to the particle beam axis and almost orthogonal to the mass spectrometer axis are sampled. In this case the effects of the initial velocity and initial position of the ions are in principle reduced. Performed in the current setup, the particle analysis might lead to a low sensitivity since very few ions will then be sampled.

An other way to test this approach would be to displace the particle beam from the mass spectrometer axis and to extract the ions as they are produced by first an electric field orthogonal to the mass spectrometer axis to reduce initial velocity component along the mass spectrometer axis. Then the ions are transmitted in the mass spectrometer as in usual mode. The first extraction can be operated by applying an electric field between the electrode (1) and (2) presented in Figure. 86. If such a scheme is applied to the SPALMS instrument, this scheme can only work for one polarity and less ions will be analyzed due to the more complex extraction scheme. A better ion identification implies here a loss of information since only a fraction of ion from the laser desorption/ionization process will be analyzed.

Such a method is mainly attractive for all ion masses if the ionization process is soft, i.e. the aerosol is processed by a two-step laser desorption/ionization for example. The coupling of a two-step laser desorption/ionization and an orthogonal time-of-flight mass spectrometer instrument in this case is particularly powerful.

14. To a better chemical characterization of the aerosol gas and particle phases

This approach has been very recently operated by an Aerodyne aerosol mass spectrometer (Aerodyne AMS) equipped with an oaTOFMS (in V-, C- and W-version) with its usual desorption/ionization method, i.e., thermodesorption and electron impact ionization as reported in [Drewnick et al., 2005]. The replacement of the electron impact ionization step by a VUV photoionization step will greatly enhance the power of such an aerosol mass spectrometer.

15 My opinion about the future of aerosol mass spectrometry

This short chapter presents my opinion on the future of aerosol mass spectrometry based on the experience gained during this project over the last 3 years and my bibliographic compilation. It first summarizes in which directions immediate work has to be invested in such as in data analysis and a better control/comprehension of the one-step laser desorption/ionization. The last section presents the possible evolution of this field over the next decades during which efforts will be done to miniaturize and produce aerosol mass spectrometers at low cost in order to be operated in field and observation networks. Simultaneously aerosol mass spectrometry will become more modular so that particles can be analyzed in different manners before its final destructive chemical analysis by mass spectrometry.

15.1 Directions for immediate technical improvements and work

As mentioned early in this work, all the different aerosol mass spectrometer units as described in Chapter 2. are getting rather technically mature and exhaustive. The current major problems to face are the data collection from all data acquisition devices and their analysis/interpretation. The former is now real for this technique since each single particle analysis produces a huge amount of data that needs to be recorded, sorted and interpreted. Indeed data can not always be recorded as shown in this work and stressed by [Drewnick et al., 2005]. It requires therefore rapid data acquisition devices or/and the ability to process quickly the acquired data. If the high data acquisition speed is required in order to capture the information from the analysis of all sampled single particles, the huge amount of data should be analyzed and interpreted in terms of secondary information such as particle size, density, refractive index or chemical composition that can be used by anyone. If the data interpretation procedures are rather mature for some physical properties like particle size and density now, the access to the particle composition from the mass spectra is time consuming, case dependent and not straightforward. This requires in particular more laboratory work to better understand the mechanisms of the one-step desorption/ionization processes. These works should lead to define rules that can be used to better and quicker interpret the mass spectra to infer the particle composition. Future measurements but also previous measurements will benefit of it.

15.2 Evolution of aerosol mass spectrometry over the next decades

Aerosol mass spectrometry future developments will evolve in two main directions. One will lead to the miniaturization and cost reduction of selected aerosol mass spectrometer configurations while the other will lead to continue to develop more universal or specialized aerosol mass spectrometer instruments.

Indeed, aerosol mass spectrometers can analyze aerosol particles at only a given place. This is not compatible with the need to describe physically and chemically aerosols over a large geographic area for climate, atmospheric and health epidemiological studies. Since the aerosol characteristics are highly variable in time and place, good aerosol studies of the aerosol properties requires to operate a network of aerosol analyzers whose grid size is consistent with the aerosol particle property lifetime to be studied. To address this problematic and to increase the geographic area over which aerosols can be chemically analyzed on a single particle basis, it is necessary to operate cheap

15. My opinion about the future of aerosol mass spectrometry

and small size aerosol mass spectrometers. This approach is described by the concept of aerosol mass spectrometer in a “shoe-box” [Cziczo, 2005]. This is made possible by the constant tendency to the miniaturization of the different components. This trend already exists in the field of space exploration where many efforts are made to miniaturize similar quite sophisticated chemical analyzer devices as presented in [Brinckerhoff et al., 2003], [Rohner et al., 2004] and [Rohner et al., 2003].

The other approach concerns the improvement of the technique to make it approaches more the “ideal” aerosol chemical analyzer as defined by [Friedlander, 2000]. The idea is to make the aerosol mass spectrometer be a stand alone instrument that permits an exhaustive aerosol single particle chemical and physical analysis.

Recent developments in aerosol mass spectrometry made possible the access to the particle density, mass, and refraction index for particles that are big enough to be aerodynamically and optically sized with a good quality optical detection system as reported in [Moffet et Prather, 2005] and [Murphy et al., 2004]. This example illustrates the starting tendency of implementing measurement principles of standard aerosol analyzers in aerosol mass spectrometers since the particle beam allows their convenient implementation. However, it was made possible only when standard aerosol mass spectrometers fulfilled correctly their initial tasks and enough experience in their operation was gained. The example of [Moffet et Prather, 2005] and [Murphy et al., 2004] are interesting in the sense that it did not lead to a specific significant adaptation of their aerosol mass spectrometer. They just better use of the existing features of their instruments.

In a next future, aerosol mass spectrometers might consist of a series of remote sensing particle modules, mainly optical and electrical, mounted successively in line along the particle beam that sense the physical properties of the particle on its flight before it arrives to the desorption/ionization zone of the mass spectrometer. This way, shape, surface, mass, electric mobility diameter, surface composition or biological origin of particles can be then evaluated as operated by specific existing instruments (described in [Baron and Willeke, 2001]) before the chemical composition of the particle is obtained by the mass analysis that degrades the particle. Progresses in this area should be rapid since all these techniques are already commercially available in specialized instruments. This tendency is illustrated by the work of [Franck et al., 2005] who added some sensing modules between the inlet and the mass spectrometry unit to evaluate the particle shape and the particle coincidence events. It is also illustrated by the tandem use of a SMPS and AMS Aerodyne instrument to gain more information about the particle density and morphology by [Slowik et al., 2004].

The same tendency does exist also for the ionization and mass spectrometer unit which are modular once a standard inlet and detection unit are chosen. Indeed many mass spectrometer types and many ionization methods are being mounted on a Aerodyne AMS instrument that can be equipped either with a quadrupole, a C-time-of-flight, a W-time-of-flight or an ion trap mass spectrometer or with laser photoionization ([Ispra Meeting, 2005], this work). This technical option will permit a lot of progress in this field over the next years since aerosol particle sampling units are becoming well characterized and standardized. Most of the work is then to invest in the single particle chemical analysis.

The chemical analysis is a quite difficult step due to the variety of chemical composition of the particles and the low amount of material that is available for the chemical analysis. To date, only the ion mass can be used to infer the chemical composition of single particles. Even if high resolution mass spectrometry combined with soft desorption/ionization can permit the obtention of the elemental formula of molecular ion and sometimes its possible chemical functional group, a second

15. My opinion about the future of aerosol mass spectrometry

chemical analysis based on another principle would be necessary. For this task, many conventional techniques such as infra-red spectroscopy, Raman spectroscopy or UV-spectroscopy can be candidate. The challenge will here to make them as sensitive as mass spectrometry and to operate them rapidly on a flying particle at the same time of the mass analysis or before if they are non-destructive.

Combinations of different methods are proposed by [Beddows et Telle, 2005] for the case of Laser Induced Breakdown Spectroscopy (LIBS) and Raman Spectroscopy (RS) for the analysis of bioaerosols. The first experimental set-up that performs such an approach is proposed by [Van Wuijckhuijse, 2003] which first senses if the particle constituents fluoresce before analyzing the particle by mass spectrometry. The use of the particle fluorescence is not used to chemically analyze the particle *stricto sensu* but to trigger the analysis of the particle only if it is likely to have a biological origin. On the other hand, this setup would particularly be suited for the simultaneous use of LIBS and mass spectrometry as the particle is ablated. This should provide a better confidence in the elemental analysis of the particle and potentially an estimation of the extent of the particle ablation.

In the future, aerosol mass spectrometers will probably consist of a standard inlet unit, a standard detection/sizing unit and miscellaneous chemical analysis devices such as Infra-red, UV, Raman spectroscopy or LIBS in addition to the usual mass spectrometers.

16 Conclusion

The Single Particle Aerosol Laser Mass Spectrometer (SPALMS) developed in this study appears to be a powerful instrument that permits the physical and chemical analysis of aerosol particles. This instrument was designed based on the critical analysis of a bibliographic review of the current state of the technique. The SPALMS instrument samples the aerosol particles with a nozzle inlet unit, detects and sizes them respectively optically and aerodynamically. After the particle sizing step, the chemical analysis is operated by vaporizing and ionizing its chemical constituents by laser either in one or two steps before the resulting ions are transmitted to a bipolar mass spectrometer. The ion mass analysis provides then the chemical composition of the particle. The SPALMS instrument offers many data acquisition points (up to 12 channels) in order to record information at each measurement step and to merge them together. This should lead to additional properties of the single particle in comparison to the current usual use in aerosol mass spectrometry.

The nozzle inlet unit shows two interesting features that compensate the low chemical analysis rate of 7 Hz in the instrument current state. It permits first the sampling of particles by impaction on the last skimmer of the inlet and secondly, due to its higher carrier gas velocity, a better aerodynamic differentiation of the particles than can do an APS instrument or an aerodynamic lens inlet unit. The combination of the detection/sizing unit and the inlet unit permits the measurement of the aerosol particle size distribution in a reliable manner between 0,5 μm to 4 μm at a concentration of up to 800 particles per cm^3 . The detection/sizing unit permits in particular the measurement of the amount of scattered light as the particle crosses each sizing laser by four photomultipliers. With an adapted data analysis procedure, particles can not only be aerodynamically sized but also optically differentiated. Indeed, a data analysis method makes the interpretation of the scattered light possible by limiting the trajectory ambiguity effects. With a lower noise photomultiplier signal, one can potentially access to a shape index, defined as the deviation from sphericity, of the particle and to a method to treat coincidence events.

With a good quality particle detection signal, it is possible to evaluate how representative of the whole aerosol is the observed single particle chemical composition by comparing the aerodynamic-optical data set of the whole particle population to the similar data set of the only chemically analyzed particles. This permits in particular the evaluation of measurement errors due to the desorption/ionization laser trigger scheme or due to the size/composition of the particles.

Indeed, the desorption/ionization process that provides a “fingerprint” of the chemical composition of the particle does not always permit its detection if the laser power density is not high enough, the chemicals are difficult to ionize or chemical reactions proceed in the desorption plume. This is in particular illustrated by the case of the usual low occurrence of positive carbon clusters in mass spectra or by the apparent impossibility to detect ions from silica particles. This justifies the need of different desorption/ionization methods and their related trigger schemes and the need of a bipolar mass spectrometer.

Soot particles from Palas GmbH were extensively studied in this work since they are very convenient to test the SPALMS instrument. These soot particles were easily detected and the speciation of the carbon as elemental carbon was established in negative mass spectra. Similarly, negative mass spectra showed the presence of organic hydrogenated molecules in soot particles from wood combustion by the presence of hydrogenated carbon clusters C_nH_m ions. Positive mass spectra were found however to bring less chemical information since the relative high content of

sodium or potassium in the particle masks the signal due to other positive ions probably by either saturating the detector or by dramatically depleting the amount of positive ions by charge-transfer reactions because of the low ionization potential of sodium and potassium. The advantage of one-step desorption/ionization with a bipolar mass spectrometer is also fully demonstrated by the analysis of ash from the incineration in private fireplace of wood waste material. It suggests that the negative mass spectrometer brings a wealth of information about the speciation of some elements in the particle. Indeed, negative mass spectra indicate that iron, sodium, potassium, calcium and silicon are present in the ash particles respectively as oxides, sulfates and aluminosilicates. Moreover analyses confirmed that particles are to be considered individually.

Even if the one-step desorption/ionization is rich in information, the processes occurring in this step are complex and render difficult the mass spectra analysis because of the chemical ionization and fragmentation processes that take place. Indeed the two-step laser desorption/ionization analysis permitted the detection of PAHs in wood sample particles that were not detected before with a one-step approach. It points out that the better management and control of both the desorption and ionization steps lead to (i) limit the fragmentation of the molecules and (ii) to better resolve chemical mixtures. The chemical analyses presented here suggest that the comparison of mass spectra obtained in both conditions permits a better evaluation of the particle chemical composition by a better understanding the ionization processes.

These analyses lead particularly to develop other desorption/ionization schemes that should enhance the analytical potential of the SPALMS instrument. This is made possible by the unique feature of the mass spectrometer to perform either a simultaneous bipolar ion analysis or two successive cation mass analyses delayed by some microseconds. In this configuration, the same particle can be analyzed twice with different ionization methods and information about the radial composition can be accessible. In this case, each mass spectrometer tube is operated in pulse mode one after the other that permits the operation of a given ionization method for each mass analysis. For instance, possible schemes can address the analysis of initially present native cations in the particle and/or a better molecule identification capacity by first operating a soft photoionization followed by electron impact ionization to fragment the molecules. In addition, it exists the possibility to operate bipolar mass analysis with soft ionization methods producing cations (SPI, Single Photo Ionization) and anions (PERCI, Photo-Electron Resonance Capture Ionization).

Since the two or many steps laser desorption/ionization schemes are complex to operate, it is also important to better qualify the one-step approach. Indeed due to its simplicity, it should be in a next future commonly implemented in field instruments. The careful examination of the mass spectra signal obtained with a sufficiently good mass resolution should permit the evaluation of the extent of the particle ablation in certain circumstances by looking at the shape of the mass peaks at given low masses for usual ions observed in mass spectra such as the C_2 , C_2H and C_2H_2 negatively charged carbon clusters.

The operation of the SPALMS can be completed with the off-line analysis of particles sampled by impaction within the instrument in the inlet unit or after the desorption/ionization unit. Their analysis can address any low-volatile chemicals, confirm and lead to extrapolate the observed chemical composition of the single particles to the whole aerosol. In this work, an off-line analysis has been performed with PIXE (Proton Induced X-ray Emission) which gives the elemental composition even if it can also be easily operated by LMMS (Laser Microprobe Mass Spectrometry) or any conventional chromatographic methods. An Aerodynamic Particle Sizer (APS3321, TSI., Inc) was operated simultaneously in parallel to confirm the SPALMS measurements of the particle size distribution.

As a result, the SPALMS instrument design permits the analysis of single particle aerosol by providing the usual aerosol mass spectrometry information, “size and chemical fingerprint”, and offering additional data that complete the analysis. Indeed, its modular and flexible desorption/ionization methods and trigger scheme permit the adaptation of particle analysis to different aerosol types and to specific laboratory studies aimed at better understanding the desorption/ionization processes. These laboratory works would serve the aerosol mass spectrometry community by permitting a re-interpretation of the data and a better determination of the “real” chemical composition of the single particles.

As a result, from this study it appears that aerosol mass spectrometers will evolve to simple, robust, small and cheap instruments for their use in field measurement campaign and observation networks since their current basic features are well tested, rather mature, technically more reliable and sensitive than they were some years ago. On the other hand, these instruments will be further developed in a modular manner with the same inlet unit, detection/sizing unit but with different chemical analyzers that range from different mass spectrometers and different ionization methods to infrared, Raman spectroscopy and UV fluorescence. Finally various modules measuring, for example, the particle light scattering patterns or light depolarization should be inserted between the inlet unit and the chemical analyzer to complete the physical description of the single particle.

Annex A

A-1 Influence of sonic shock waves on the particle beam quality within the inlet unit

After the gas passes the sonic nozzle, its velocity increases until a shock wave occurs due to the friction of the moving gas with the quiet gas around. Across the shock wave, the gas velocity is reduced and its pressure equilibrates with the pressure of the “quiet” gas. The shock wave has a barrel shape as presented in Figure. 89. The dimensions of the barrel shock have to be known to position the next skimmer before the shock wave occurs in order not to influence the particle motion. Toward this purpose, the aim is to displace the shock wave exiting the nozzle or the skimmer orifice far enough, i.e. after the next skimmer orifice, so that the pressure drop across the shock wave can not influence any more the particle motion. Indeed the crossing of the shock waves might degrade the quality of the particle beam. The dimension of the barrel shock can be calculated within 5% by the following relationship (Eq. 30) reported by [Kievit, 1995], [Kievit et al., 1996], [Van Wuijckhuijse, 2003] and references therein.

$$\frac{L_C}{d_{nozzle}} = C_1 \cdot \left(\frac{P_{upstream}}{P_{downstream}} \right)^{C_2}$$

Eq. 30

where L_c is a characteristic length of the barrel shock as depicted in Figure. 89 and Table 48. D is the nozzle diameter d_{nozzle} , C_1 and C_2 are two specific constants of the characteristic length L_c . $P_{upstream}$ and $P_{downstream}$ are respectively the gas pressure before and after the nozzle.

For the design of inlet unit, it is important to locate the successive orifices such that their distance is smaller than the critical distance X_b . In the present case,

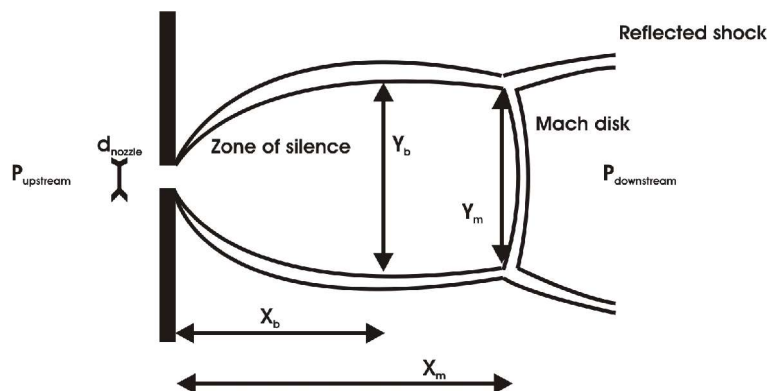


Figure. 89 : Sonic barrel shock after a nozzle

<i>Characteristic Length L_c</i>	<i>Constant C_1</i>	<i>Constant C_2</i>
X_B	0.47	0.49
X_M	0.74	0.49
Y_B	0.38	0.56
Y_M	0.31	0.56

Table 48 : Parameters for the calculation of the sonic barrel shock dimensions

<i>Location</i>	<i>Characteristics length of the barrel shock $X_b (X_m)$ [mm] (after Eq. 30)</i>	<i>Distance Inlet orifice to next orifice [mm]</i>	
		<i>Commercial Inlet</i>	<i>Home-made Inlet</i>
Chamber I	2,1 (3,4)	3	10
Chamber II	2,64 (4,16)	12	10
Ion source	20,1 (31,7)	54	58

Table 49 : Relative position of the nozzle-skimmer orifices in the home-made and commercial inlet unit

Both operated inlet units are such that particles cross a shock wave after each nozzle/skimmer orifice since the next skimmer that the particle passes is always located after the end of the shock wave generated by the previous orifice. Up to now, it was impossible to evaluate in the operating conditions of the SPALMS instrument in which extent, it degrades the quality of the generated particle beam. Considering the low pressure levels, one might expect a negligible influence. Considering the observation of Figure. 14, it might still have a significant impact since particles are still deviated by the gas flow stream in the chamber II where the pressure is roughly $\sim 5 \cdot 10^{-2}$ mbar.

A-2 Commercial inlet nozzle-skimmers unit

The commercial inlet unit was purchased from Bernhard Spengler and Klaus-Peter Hinz Scientific Instruments GBR. The technical data from the manufacturer are presented below and in Table 50 State 04/05. July 2001

- Nozzle orifice diameter: 500 μm
- Inverted skimmer orifice diameter: 400 μm
- plane skimmer orifice: 300 μm

<i>Location</i>	<i>Pressure level [mbar]</i>	<i>Pump system</i>
Chamber I	12 (open) 1,7 10^{-3} (closed)	Rotary pump (10m ³ /h)
Chamber II	4,8 10^{-2} (open) < 10^{-4} (closed)	Turbomolecular pump (60 l/s)
Ion source	6. 10^{-6} (open) 3,3 10^{-7} (closed)	Turbomolecular pump (330 l/s)

Table 50 : Pressure levels in the commercial nozzle system

A-3 Home-made nozzle-skimmer unit

The motivation of developing a home-made inlet unit was the possibility to use it not only as a conventional nozzle-skimmers assembly inlet unit but also as a housing for the aerodynamic lens which was designed and planed to be implemented. Such an extension was not possible with the current available commercial inlet unit. The home-made inlet unit was designed by T. Ferge in 2001 as an assembly of a nozzle, inverted skimmer and plane skimmer after the example of the nozzle systems presented in the literature by [Prather et al., 1994] and [Hinz et al., 1994]. The home-made inlet unit has the following characteristics.

<i>Characteristics^(*)</i>	<i>Home-made inlet unit</i>
Diameter $O_{atm,1}$	0,4 mm
Length $O_{atm,1}$	2 mm
Distance $O_{atm,1}-O_{1,2}$	10
Diameter $O_{1,2}$	0,3 mm
Length $O_{1,2}$	1,3 mm
Distance $O_{1,2} - O_{2,ion\ source}$	10
Diameter $O_{2,ion\ source}$	0,5 mm
Length $O_{2,ion\ source}$	2 mm
Distance $O_{2,ion\ source} - \text{Ionization volume}$	58
Nozzle angle (Half-Angle)	$\sim 17,4$
Inverted skimmer angle (Half-Angle)	$\sim 40^\circ$

Table 51 : Characteristic dimensions of the home-made inlet unit

(*) The quantities of this Table refer to Figure. 11

The home-made inlet unit was operated before using the commercial inlet unit. The commercial inlet unit has been finally exclusively used because the home-made one was not convenient to use in practice and because many parts were to be re-designed. The next section presents the reasons why the home-made inlet unit was not further used in this study.

In the home-made inlet, the alignment of the three successive orifices is very tricky to perform. Indeed each orifice is inserted within a housing-positioning cylinder that “precisely” define its position. Each orifice has a long length (1,3 to 2 mm) to limit the gas flow and control the particle flow direction. The improper fixation of the orifices in their housing cylinders frequently results in a imperfect orientation of the orifices. This makes the axes of the different orifices not match together what strongly negatively affects the inlet transmission efficiency. No means was found to check the correct relative adjustments of the successive orifices during the mounting of the inlet after its cleaning. The inlet unit can only be tested once it is totally mounted. Some attempts were made to check and improve the orifice alignments during the mounting by using a laser pointer going through the different orifices and by maximizing the transmitted light through the inlet when the position of the orifices is adjusted. This method is not reliable since the maximum light transmission does not mean the best aerodynamic adjustment of the orifices. The optical control is a first necessary test but remains not pertinent enough.

Moreover, if the cleaning of the nozzle is easy, the cleaning of the inverted skimmer is extremely

unpractical since it is needed to take apart half of the inlet unit and half of the vacuum tubings. This makes the inverted skimmer mounting, once cleaned, very tricky and very time-consuming. In spite of the prevision that the nozzle would be the weak part of the inlet unit, the home-made inlet always gets clogged on the inverted skimmer as it is by the current commercial inlet unit. This is in particular the case when submicrometer particles, such as soot particles, are sampled. This is mainly due to the fact that the top of the inverted skimmer has a non negligible flat surface (due to manufacturing constrains) on which particles easily impact and accumulate leading to the occlusion of the orifice.

These practical reasons make this inlet unit tricky and time-consuming to operate even if can produce, when perfectly mounted, a nice particle beam of similar characteristics as the commercial inlet does. Considering the orifice adjustment problems, the distance between each orifices (long compared to the literature data) and the thickness of orifices, the particle inlet transmission efficiency is expected to be, globally, worse than the commercial inlet unit. As a result, many parts were re-designed to improve it. The distance between the nozzle and inverted skimmer were made shorter, down to less than 10 mm, to increase the transmission efficiency. Furthermore, attempts to reduce the thickness of the orifices were made. The impact of these modifications were not evident to characterize so that it motivated us to use the commercial inlet unit which was much more friendly to use and much less time consuming to clean and exchange.

A-4 Home-made aerodynamic lens

The aerodynamic lens was designed based on the theoretical work of [Liu et al., 1995a], [Liu et al., 1995b] and [Zhang et al., 2002] that present the practical description and its scaling rules.

It was decided to dimension the aerodynamic lens such that particles focused by a single lens (a perforated disk) have a Stokes Number St_k ranging from 0,2 to 0,9. The ratio $d_{lens}/d_{lens\ aperture}$ (aperture lens diameter ratio to the internal housing diameter of the lens) was kept in the range of 4 to 5 and the distance between each lens was set to 5 cm.

The aerodynamic lens samples air from the atmosphere via a critical orifice of $\sim 150\ \mu\text{m}$ that reduces the pressure down to $\sim 10\ \text{mbar}$. A long and large tubing T-part (40 mm in diameter and 15 cm in length) is inserted between the critical orifice and the aerodynamic lens entrance to let the sampled particles slow down before they enter the series of five lenses spaced by 5 cm, whose aperture diameters range from 5 mm down to 3 mm with a thickness of 1 mm. The lenses are hold between two small spacing cylinders that press together on the lens and on an O-ring to avoid air leaks. The spacing cylinders (20 mm OD/14 mm ID) are inserted in a housing tube (ID of 20 mm and OD of 24 mm) that is inserted at the place of the nozzle tube of the home-made inlet unit. At the exit of the last lens, particles are then accelerated by a nozzle whose orifice has a diameter of 2 mm. After the nozzle, the particles fly successively through the inverted skimmer and the plane skimmer of the home-made inlet unit that reduces the pressure step by step to the level required to operate the mass spectrometer. The pressure levels before and after the aerodynamic lens are set and controlled by two rotary pumps DUO20 (Pfeiffer Vacuum GmbH, Asslar Germany) and butterfly valves (VAT Vakuumventile AG, Haag, Switzerland) whose aperture degree can be controlled to insure the gas flow to be in laminar regime. An ensemble [pump + valve] was connected on the T-part after the critical orifice and the second one after the exit of the aerodynamic lens nozzle. Due to scarcity of time, the aerodynamic lens was not tested in bench and with the inlet unit. A photo of the aerodynamic lens is presented in Figure. 34.

Bibliography

- Baron, P., A., Willeke, K., *Aerosol Measurement: Principles, Techniques, and Applications*, 2nd Edition, Wiley-Interscience, 2001
- Beddows, D. C. S., Telle, H. H., Prospects of real-time single particle biological aerosol analysis: A comparison between laser induced breakdown spectroscopy and aerosol time-of-flight mass spectrometry, *Spectrochimica Acta Part B*, xxx, xxx, 2005
- Bläsner, M., Wollny, A. G., Bormann, S., McKenna, D. S., Airborne mass spectrometer for measurements of single particle composition: Design and Instrument Characteristics, *Journal of Aerosol Science*, 31, S715-S716, 2000
- Boesl, U., Weinkauff, R., Weickhardt, C., Schlag, E. W., Laser ion sources for time-of-flight mass spectrometry, *International Journal of Mass Spectrometry and Ion*, 131, 87-124, 1994
- Brinckerhoff, W. B., Cornish, T. J., McEntire, R. W., Cheng, A. F., Benson, R. C., Miniature time-of-flight mass spectrometers for in situ composition studies, *Acta Astronautica*, 52, 397-404, 2003
- Cabalo, J., Zelenyuk, A., Baer, T., Miller, R. E., Two-color laser induced evaporation dynamics of liquid aerosols probed by Time-of-Flight Mass Spectrometry, *Aerosol Science and Technology*, 33, 3-19, 2000
- Card, J. B. A., Jones, A. R., A drop tube furnace study of coal combustion and unburned carbon content using optical techniques, *Combustion and Flame*, 101, 539-547, 1995
- Carranza, J. E., Fisher, B. T., Yoder, G. D., Hahn, D. W., On-line analysis of ambient air aerosols using laser-induced breakdown spectroscopy, *Spectrochimica Acta Part B*, 56, 851-864, 2001
- Carson, P. G., Johnston, M. V., Wexler, A. S., Real-time monitoring of the surface and total composition of aerosol particles, *Aerosol Science and Technology*, 26, 291-300, 1997
- Carson, P. G., Neubauer, K. R., Johnston, M. V., Wexler, A. S., On-line chemical analysis of aerosols by rapid single-particle mass spectrometry, *Journal of Aerosol Science*, 26, 535-545, 1995
- Chattopadhyay, S., Tobias, H. J., Ziemann, P. J., A Method for Measuring Vapor Pressures of Low-Volatility Organic Aerosol Compounds Using a Thermal Desorption Particle Beam Mass Spectrometer, *Analytical Chemistry*, 73, 3797-3803, 2001
- Cheng, Y. S., Barr, E. B., Marshall, I. A., Mitchell, J. P., Calibration and performance of an API aerosizer, *Journal of Aerosol Science*, 24, 501-514, 1993
- Cheng, Y. S., Dahneke, B. E., Properties of continuum source particle beams: II. beams generated in capillary expansions, *Journal of Aerosol Science*, 10, 363-368, 1979
- Cody, R. B., Laramée, J. A., Durst, H. D., Versatile New Ion Source for the Analysis of Materials in Open Air Under Ambient Conditions, *Analytical Chemistry*, 77, 2297-2302, 2005
- Cziczo, D. J., Personal communication, 2005
- Cziczo, D. J., DeMott, P. J., Brock, C., Hudson, P. K., Jesse, B., Kreidenweis, S. M., Prenni, A. J., Schreiner, J., Thomson, D. S., Murphy, D. M., A Method for Single Particle Mass Spectrometry of Ice Nuclei, *Aerosol Science and Technology*, 37, 460-470, 2003
- Dahneke, B. E., Cheng, Y. S., Properties of continuum source particle beams. I. Calculation methods and results, *Journal of Aerosol Science*, 10, 257-274, 1979
- Dalton, C. N., Jaoui, M., Kamens, R. M., Glish, G. L., Continuous Real-Time Analysis of Products from the Reaction of Some Monoterpenes with Ozone Using Atmospheric Sampling Glow Discharge Ionization Coupled to a Quadrupole Ion Trap Mass Spectrometer, *Analytical Chemistry*, 77, 3156-3163, 2005
- Davidson, C. I., Phalen, R. F., Solomon, P. A., Airborne particulate matter and human health: A review, *Aerosol Science and Technology*, 39, 737-749, 2005
- Davis, W.D., Continuous mass spectrometric of concentration of particulate impurities in air by use of surface ionization,

- Environment Science and Technology, 11, 593-596, 1977b
- Davis, W.D., Continuous mass spectrometric analysis of particulates by use of surface ionization, Environment Science and Technology, 11, 587-592, 1977a
- De Hoffmann, E., Stroobant, V., Mass Spectrometry, Principles and Applications, 2nd Edition, Wiley, 2003
- Dessiaterik, Y., Nguyen, T., Baer, T., Miller, R. E., IR vaporization mass spectrometry of aerosol particles with ionic solutions: The problem of ion-ion recombination, Journal of Physical Chemistry A, 107, 11245-11252, 2003
- Drewnick, F., Hings, S. S., DeCarlo, P., Jayne, J. T., Gonin, M., Fuhrer, K., Weimer, S., Jimenez, J. L., Demerjian, K. L., Borrmann, S., Worsnop, D. R., A New Time-of-Flight Aerosol Mass Spectrometer (TOF-AMS) - Instrument Description and First Field Deployment, Aerosol Science and Technology, 39, 637-658, 2005
- Drewnick, F., Schwab, J. J., Hogrefe, O., Peters, S., Husain, L., Diamond, D., Weber, R., Demerjian, K. L., Intercomparison and evaluation of four semi-continuous PM_{2.5} sulfate instruments, Atmospheric Environment, 37, 3335-3350, 2003
- European Conference on Aerosol Mass Spectrometry, JRC Ispra, Ispra, Italy, 2005
- Ferge, T., Karg, E., Schröppel, A., Coffee, K. R., Tobias, H. J., Frank, M., Gard, E. E., Zimmermann, R., Fast determination of the relative elemental and organic carbon content of aerosol samples by single-particle aerosol time-of-flight mass spectrometry, Environmental Science and Technology, xxx, in press, 2005a
- Ferge, T., Mühlberger, F., Zimmermann, R., Application of Infrared Laser Desorption Vacuum-UV Single-Photon Ionization Mass Spectrometry for Analysis of Organic Compounds from Particulate Matter Filter Samples, Analytical Chemistry, 77, 4528-4538, 2005
- Ferguson, D. P., Song, X.-H., Ramadan, Z., Allen, J. O., Hughes, L. S., Cass, G. R., Hopke, P. K., Prather, K. P., Quantification of ATOFMS data by multivariate methods, Analytical Chemistry, 73, 3535-3541, 2001
- Franck, M., Personal communication, 2005
- Friedlander, S. K., Smoke, Dust and Haze: Fundamentals of Aerosol Dynamics, 2nd Edition, Oxford University Press, 2000
- Gälli, M., Guazzoti, S. A., Prather, K. A., Improved lower particle size limit for aerosol time-of-flight mass spectrometry, Aerosol Science and Technology, 34, 381-385, 2001
- Gard, E., Mayer, J. E., Morrical, B. D., Dienes, T., Ferguson, D. P., Prather, K. A., Real-time analysis of individual atmospheric aerosol particles: design and performance of a portable ATOFMS, Analytical Chemistry, 69, 4083-4091, 1997
- Grantz, D. A., Garner, J. H. B., Johnson, D. W., Ecological effects of particulate matter, Environment International, 1006, 1-27, 2003
- Grehan, G., Gouesbet, G., Simultaneous measurements of velocities and sizes of particles in flows using a combined system incorporating a top-hat beam technique, Applied Optics, 25, 3527-3538, 1986
- Grimm, R. L., Beauchamp, J. L., Field-induced droplet ionization mass spectrometry, Journal of Physical Chemistry B, 107, 14161-14163, 2003
- Gross, D. S., Gälli, M. E., Silva, P. J., Prather, K. A., Relative Sensitivity Factors for Alkali Metal and Ammonium Cations in Single-Particle Aerosol Time-Of-Flight Mass Spectra, Analytical Chemistry, 72, 416-422, 2000
- Gross, J. H., Mass Spectrometry, A textbook, Springer, 2004
- Guilhaus, M., Principles and Instrumentation in Time-of-Flight Mass Spectrometry, Journal of Mass Spectrometry, 30, 1519-1532, 1995
- Guilhaus, M., Selby, D., Mlynski, V., Orthogonal acceleration time-of-flight mass spectrometry, Mass Spectrometry Reviews, 19, 65-107, 2000
- Hauler, T. E., Boesl, U., Kaesdorf, S., Zimmermann, R., Mobile resonance enhanced multiphoton ionisation-time-of-

- flight mass spectrometer with a novel hybrid laser desorption/molecular beam ion source for rapid detection of aromatic trace compounds from gas phase and solid samples, *Journal of Chromatography A*, 1058, 39-49, 2004
- He, L., Murray, K. K., 337 nm matrix-assisted laser desorption ionization of single aerosol particles, *Journal of Mass Spectrometry*, 34, 909-914, 1999
- Hinds, W. C., *Aerosol technology : Properties, Behavior and Measurement of Airborne Particle*, 2nd, Wiley-Interscience, 1999
- Hinz, K.-P., Kaufmann, R., Spengler, B., Laser-induced mass analysis of single particles in the airborne state, *Analytical Chemistry*, 66, 2071-2076, 1994
- Hinz, K.-P., Kaufmann, R., Spengler, B., Simultaneous detection of positive and negative ions from single airborne particles by real-time laser mass spectrometry, *Aerosol Science and Technology*, 24, 233-242, 1996
- Hinz, K.-P., Trimborn, A., Weingartner, E., Henning, S., Baltensperger, U., Spengler, B., Aerosol single particle composition at the Jungfraujoch, *Journal of Aerosol Science*, 36, 123-145, 2005
- Hughey, C. A., Hendrickson, C. L., Rodgers, R. P., Marshall, A. G., Qian, L., Kendrick Mass Defect Spectrum: A compact Visual Analysis for Ultrahigh-resolution Broadband Mass Spectra, *Analytical Chemistry*, 73, 4676-4681, 2001
- Jacob, D. J., Heterogeneous chemistry and tropospheric ozone, *Atmospheric Environment*, 34, 2131-2159, 2000
- Jayne, J. T., Leard, D. C., Zhang, X., Davidovits, P., Smith, K. A., Kolb, C. E., Worsnop, D. R., Development of an aerosol mass spectrometer for size and composition analysis of submicron particles, *Aerosol Science and Technology*, 33, 49-70, 2000
- Jimenez, J. J., <http://cires.colorado.edu/~jjose/ams.html>, 2005
- Johnston, M. V., Sampling and analysis of individual particles by aerosol mass spectrometry, *Journal of Mass Spectrometry*, 35, 585-595, 2000
- Jones, A. R., Light scattering for particle characterization, *Progress in Energy and Combustion Science*, 25, 1-53, 1999
- Kalberer, M., Paulsen, D., Sax, M., Steinbacher, M., Dommen, J., Prevot, A. S. H., Fisseha, R., Weingartner, E., Frankevich, V., Zenobi, R., Baltensperger, U., Identification of Polymers as Major Components of Atmospheric Organic Aerosols, *Science*, 303, 1659-1662, 2004
- Kane, D. B., Johnston, M. V., Size and composition biases on the detection of Individual ultrafine particles by aerosol mass spectrometry, *Environment Science and Technology*, 34, 4887-4893, 2000
- Kane, D. B., Oktem, B., Johnston, M. V., An Electrostatic Lens for Focusing Charged Particles in a Mass Spectrometer, *Aerosol Science and Technology*, 35, 990-997, 2001
- Karas, M., Krüger, R., Ion Formation in MALDI: The Cluster Ionization Mechanism, *Chemical Reviews*, 103, 427-439, 2003
- Kievit, O., Development of a laser mass spectrometer for aerosols, Delft University Of Technology, The Netherlands, 1995
- Kievit, O., Weiss, M., Verheijen, P. J. T., Marijnissen, J. C. M., Scarlett, The on-line chemical analysis of single particles using aerosol beams and time-of-flight mass spectrometry, *Chemical Engineering Communications*, 151, 79-100, 1996
- Knochenmuss, R., A quantitative Model of Ultraviolet Matrix-Assisted Laser Desorption/ionization Including Analyte Ion Generation, *Analytical Chemistry*, 75, 2199-2207, 2003
- Knochenmuss, R., Photionization Pathways and Free Electrons in UV-MALDI, *Analytical Chemistry*, 76, 3179-3184, 2004
- Knochenmuss, R., Zenobi, R., MALDI Ionization: The Role of In-Plume Processes, *Chemical Review*, 103, 441-452, 2003
- Koo, Y.-M., Choi, Y.-K., Lee, K. H., Jung, K.-W., Mass spectrometric Study of Carbon Cluster Formation in Laser

- Ablation of Graphite at 355 nm, *Bulletin of the Korean Chemical Society*, 23, 309-314, 2002
- Kückelmann, U., Warscheid, B., Hoffmann, T., On-line characterization of organic aerosols formed from biogenic precursors using atmospheric pressure chemical ionization mass spectrometry, *Analytical Chemistry*, 72, 1905-1912, 2000
- LaFranchi, B. W., Zahardis, J., Petrucci, G. A., Photoelectron resonance capture ionization mass spectrometry: A soft ionization source for mass spectrometry of particle-phase organic compounds, *Rapid Communications in Mass Spectrometry*, 18, 2517-2521, 2004
- Laven, Philip, <http://www.philiplaven.com/mieplot.htm>, January 2006
- Lazar, A. C., Reilly, P. T. A., Whitten, W. B., Ramsey, J. M., Real-time surface analysis of individual airborne environmental particles, *Environment Science and Technology*, 33, 3993-4001, 1999
- Lazar, A. C., Reilly, P. T. A., Whitten, W. B., Ramsey, J. M., Laser Desorption/In Situ Chemical Ionization Aerosol Mass Spectrometry for Monitoring Tributyl Phosphate on the Surface of Environmental Particles, *Analytical Chemistry*, 72, 2142-2147, 2000
- Lee, D., Park, K., Zachariah, M. R., Determination of the Size Distribution of Polydisperse Nanoparticles with Single-Particle Mass Spectrometry: The Role of Ion Kinetic Energy, *Aerosol Science and Technology*, 39, 162-169, 2005
- Lee, S.-H., Murphy, D. M., Thomson, D. S., Middlebrook, A. M., Chemical components of single particles measured with Particle Analysis by Laser Mass Spectrometry (PALMS) during the Atlanta SuperSite Project: Focus on organic/sulfate, lead, soot, and mineral particles, *Journal of Geophysical research*, 107, doi:10.1029/2000JD000011, 2002
- Liu, P., Ziemann, P. J., Kittelson, D. B., McMurry, P. H., Generating particle beams of controlled dimensions and divergence: II. Experimental evaluation of particle motion in aerodynamic lenses and nozzle expansions, *Aerosol Science and Technology*, 22, 314-324, 1995
- Liu, P., Ziemann, P. J., Kittelson, D. B., McMurry, P. H., Generating particle beams of controlled dimensions and divergence: I. Theory of motion in aerodynamic lenses and nozzle expansions, *Aerosol Science and Technology*, 22, 293-313, 1995
- Lohmann, U., Feichter, J., Global indirect aerosol effects: a review, *Atmospheric Chemistry and Physics*, 5, 715-737, 2005
- Mahadevan, R., Lee, D., Sakurai, H., Zachariah, M. R., Measurement of Condensed-Phase reaction Kinetics in the Aerosol Phase Using Single Particle Mass Spectrometry, *Journal of Physical Chemistry*, 106, 11083-11092, 2002
- Mallina, R. V., Wexler, A. S., Rhoads, K. P., Johnston, M. V., High Speed Particle Beam Generation: A Dynamic focusing Mechanism for Selecting Ultrafine Particles, *Aerosol Science and Technology*, 33, 87-104, 2000
- Mamyrin, B. A., Laser assisted reflectron time-of-flight mass spectrometry, *International Journal of Mass Spectrometry and Ion*, 131, 1-19, 1994
- Marijnissen, J., Scarlett, B., Verheijen, P., Proposed on-line aerosol analysis combining size determination. laser-induced fragmentation and time-of-flight mass spectrometry, *Journal of Aerosol Science*, 19, 1307-1310, 1988
- Matthias-Maser, S., Jaenicke, R., The size distribution of primary biological aerosol particles with radii > 0.2 μm in an urban/rural influenced region, *Atmospheric Research*, 39, 279-286, 1995
- McKeown, P. J., Johnston, M. V., Murphy, D. M., On-Line Single Particle Analysis by Laser Desorption Mass Spectrometry, *Analytical Chemistry*, 63, 2069-2073, 1991
- Middha, P., Wexler, A. S., Particle Focusing Characteristics of Sonic Jets, *Aerosol Science and Technology*, 37, 907-915, 2003
- Middha, P., Wexler, A. S., Particle-Focusing Characteristics of Matched Aerodynamic Lenses, *Aerosol Science and Technology*, 39, 222-230, 2005
- Middlebrook, A. M., Murphy, D. M., Lee, S.-H., Thomson, D. S., Prather, K. A., Wenzel, R. J., Liu, D.-Y., Phares, D. J., Rhoads, K. P., Wexler, A. S., Johnston, M. V., Jimenez, J. L., Jayne, J. T., Worsnop D. R., Yourshaw, I., Seinfeld, J.

- H., Flagan, R. C., A comparison of mass spectrometers during the 1999 Atlanta Supersite Project, *Journal of Geophysical Research*, 108, doi:10.1029/2001JD000660, 2003
- Middlebrook, A. M., Thomson, D. S., Murphy, D. M., On the purity of laboratory generated sulfuric acid droplets and ambient particles studied by laser mass spectrometry, *Aerosol Science and Technology*, 27, 293-307, 1997
- Moffet, R. C., Prather, K. A., Extending ATOFMS measurements To Include Refractive Index and Density, *Analytical Chemistry*, ASAP Article, xxx, 2005
- Morriscal, B. D., Fergenson, D. P., Prather, K. A., Coupling two-step laser desorption/ionization with aerosol time-of-flight mass spectrometry for the analysis of individual organic particles, *Journal of American Mass Spectrometry Society*, 9, 1068-1073, 1998
- Mühlberger, F., Hafner, K., Kaesdorf, S., Ferge, T., Zimmermann, R., Comprehensive on-line characterization of complex gas mixtures by quasi-simultaneous resonance-enhanced multiphoton ionization, vacuum-UV single photon ionization, and electron impact ionization in a time-of-flight mass spectrometer: setup and instrument characterization, *Analytical Chemistry*, 76, 6753-6764, 2004
- Mühlberger, F., Wieser, J., Ulrich, A., Zimmermann, R., Coupling of a novel Electron Beam Pumped Rare Gas-Excimer VUV-Light Source for Single Photon Ionization (SPI) to a Mobile Time-of-Flight Mass Spectrometer: A New Concept for a Robust and Compact On-Line Real-Time Industrial Process Gas Analyzer, *Analytical Chemistry*, 74, 3790-3801, 2002
- Murphy, D. M., Cziczo, D. J., Hudson, P. K., Schein, M. E., Thomson, D. S., Particle density inferred from simultaneous optical and aerodynamic diameters sorted by composition, *Journal of Aerosol Science*, 35, 135-139, 2004
- Murphy, D. M., Thomson, D. S., Chemical composition of single aerosol particles at Idaho Hill: Negative ion measurements, *Journal of Geophysical Research*, 102, 6353-6368, 1997
- Murphy, D. M., Thomson, D. S., Chemical composition of single aerosol particles at Idaho Hill: Positive ion measurements, *Journal of Geophysical Science*, 102, 6341-6352, 1997
- Murphy, D. M., Thomson, D. S., Laser ionization mass spectroscopy of single aerosol particles, *Aerosol Science and Technology*, 22, 237-249, 1995
- Murphy, D. M., Thomson, D. S., Middlebrook, A. M., Schein, M. E., In situ single-particle characterization at Cape Grim, *Journal of Geophysical Research*, 103(D13), 16485-16491, 1998
- Nash, D. G., Frank Liu, X., Mysak, E. R., Baer, T., Aerosol particle mass spectrometry with low photon energy laser ionization, *International Journal of Mass Spectrometry*, 241, 89-97, 2005
- National Institute of Standards and Technology, <http://webbook.nist.gov/chemistry>, 2005
- Neubauer, K. R., Johnston, M. V., Wexler, A. S., Chromium speciation in aerosols by rapid single-particle mass spectrometry, *International Journal of Mass Spectrometry and Ion Processes*, 151, 77-87, 1995
- Neubauer, K., R., Johnston, M., V., Wexler, A. S., Humidity effects on the mass spectra of single aerosol particles, *Atmospheric Environment*, 32, 2521-2529, 1998
- Noble, C. A., Prather, K. A., Real-Time Measurement of Correlated Size and Composition Profiles of Individual Atmospheric Aerosol Particles, *Environment Science and Technology*, 30, 2667-2680, 1996
- Noble, C. A., Prather, K. A., Real-time single particle mass spectrometry: a historical review of a quarter century of the chemical analysis of aerosols, *Mass Spectrometry Reviews*, 19, 248-274, 2000
- Öktem, B., Tolocka, M. P., Johnston, M. V., On-line analysis of organic components in fine and ultrafine particles by photoionization aerosol mass spectrometry, *Analytical Chemistry*, 76, 253-261, 2004
- Oskouie, A., K., Noll, K., E., Wang, H.-C., Determination of particle diameter and lumped density and shape factor using a three-beam time-of-flight (TOF) instrument, *Journal of Aerosol Science*, 33, 1125-1138, 2002
- Palthauf, G., Dyer, P. E., Photochemical Processes and Effects in Ablation, *Chemical Reviews*, 103, 487-518, 2003
- Park, K., Lee, D., Rai, A., Mukherjee, D., Zachariah, M. R., Size-Resolved Kinetic Measurements of Aluminium

- Nanoparticle Oxidation with Single Particle Mass Spectrometry, *Journal of Physical Chemistry B*, 109, 7290-7299, 2005
- Phares, D. J., Rhoads, K. P., Wexler, A. S., Kane, D. B., Johnston, M. V., Application of the ART-2a Algorithm to Laser Ablation Aerosol Mass Spectrometry of Particle Standards, *Analytical Chemistry*, 73, 2338-2344, 2001
- Prather, A. K., Nordmeyer, T., Salt, K., Real-time characterization of individual aerosol particles using time-of-flight mass spectrometry, *Analytical Chemistry*, 66, 1403-1407, 1994
- Ravishankara, A. R. , Atmospheric chemistry: long-term issues, *Chemical Reviews*, 103, No 12 (special issue), 2003
- Reents, D. W., Schabel, M., Measurement of individual particle atomic composition by aerosol mass spectrometry, *Analytical Chemistry*, 73, 5403-5414, 2001
- Reents, W. D., Downey, S. W., Emerson, A. B., Majsce, A. M., Muller, A. J., Siconolfi, D. J., Sinclair, J. D., Swanson, A. G., Single Particle Characterization by Time-of-Flight Mass Spectrometry, *Aerosol Science and Technology*, 23, 263-270, 1995
- Reents, W. D., Ge, Z., Simultaneous elemental composition and size distributions of submicron particles in real time using laser atomization/ionization mass spectrometry, *Aerosol Science and Technology*, 33, 122-134, 2000
- Reilly, P. T. A., Gieray, R. A., Yang, M., Whitten, W. B., Ramsey, J. M., Tandem mass spectrometry of individual airborne microparticles, *Analytical Chemistry*, 69, 36-39, 1997
- Reilly, P. T. A., Lazar, A. C., Gieray, R. A., Whitten, W. B., Ramsey, J. M, Elucidation of charge-transfer-induced matrix effects in environmental aerosols via real-time aerosol mass spectral analysis of individual airborne particles, *Aerosol Science and Technology*, 33, 135-152, 2000
- Rodgers, R. P., Lazar, A. C., Reilly, P. T. A., Whitten, W. B., Ramsey, J., Direct determination of soil surface-bound polycyclic aromatic hydrocarbons in petroleum-contaminated soils by real-time aerosol mass spectrometry, *Analytical Chemistry*, 72, 5040-5046, 2000
- Rodgers, R. P., Reilly, P. T. A., Whitten, W. B., Ramsey, J. M., Real-time observation of metastable polymeric species formed from precursor, *Chemical Physics Letters*, 397, 324-328, 2004
- Rohner, U., Whitby, J. A., Wurz, P. , A miniature laser ablation time-of-flight mass spectrometer for in situ planetary exploration, *Measurement Science and Technology*, 14, 2159-2164, 2003
- Rohner, U., Whitby, J. A., Wurz, P., Barbarash, S., Highly miniaturized laser ablation time-of-flight mass spectrometer for a planetary rover, *Review of Scientific Instruments*, 75, 1314-1322, 2004
- Salt, K., Noble, C. A., Prather, K. A., Aerodynamic particle sizing versus light scattering intensity measurement as methods for real-time particle sizing coupled with time-of-flight mass spectrometry, *Analytical Chemistry*, 68, 230-234, 1996
- Schreiner, J., Voigt, C., Mauersberger, K., McMurry, P., Ziemann, P., Aerodynamic Lens System for Producing Particle Beams at Stratospheric Pressures , *Aerosol Science and Technology*, 29, 50-56, 1998
- Shapiro, A. H., *The Dynamic and Thermodynamics of compressible fluid flow, Volume I.* , The Ronald Press Company, 1953
- Shibagaki, K., Kawashima, Sasaki, K., Kadota, K., Formation of Positive and Negative Carbon Cluster Ions in the initial Phase of Laser Ablation in Vacuum, *Japanese Journal of Applied Physics*, 39, 4959-4963, 2000
- Silva, P. J., Prather, K. A., Interpretation of Mass Spectra from Organic Compounds in Aerosol Time-Of-Flight Mass Spectrometry, *Analytical Chemistry*, 72, 3553-3562, 2000
- Simon, P. K., Dasgupta, P. K., Continuous automated measurement of the soluble fraction of atmospheric particulate matter, *Analytical Chemistry*, 67, 71-78, 1995
- Sinha, M. P., Laser-induced volatilization and ionization of microparticles, *Review of Scientific Instrumentation*, 55, 886-891, 1984
- Slowik, J. G., Stainken, K., Davidovits, P., Williams, L. R., Jayne, J. T., Kolb, C. E., Worsnop, D. R., Rudich, Y.,

- DeCarlo, P. F., Jimenez, J. L., Particle Morphology and Density Characterization by Combined Mobility and Aerodynamical Diameter Measurements. Part 2: Application to Combustion-Generated Soot Aerosols as a Function of Fuel Equivalence Ratio, *Aerosol Science and Technology*, 38, 1206-1222, 2004
- Sokolik, I. N., Toon, O. B., Incorporation of mineralogical composition into models of the radiative properties of mineral aerosol from UV to IR wavelengths, *Journal of Geophysical Research*, 104, 9423-9444, 1999
- Stolzenburg, M. R., Hering, S. V., Method for the automated measurement of fine particle nitrate in the atmosphere, *Environment Science and Technology*, 34, 907-914, 2000
- Stowers, M. A., van Wuijckhuijse, A. L., Marijnissen, J. C. M., Kientz, Ch. E., Ciach, T., Fluorescence pre-selection of bioaerosol for single particle mass spectrometry, *Applied Optics*, xxx, submitted for publication, 2004
- Suess, D. T., Prather, K. A., Mass Spectrometry of Aerosols, *Chemical reviews*, 99, 3007-3035, 1999
- Sullivan, R. C., Prather, K. A., Recent Advances in Our Understanding of Atmospheric Chemistry and Climate Made Possible by On-Line Aerosol Analysis Instrumentation, *Analytical Chemistry*, 77, 3861-3886, 2005
- Svane, M., Hagström, M., Pettersson, J. B. C., Chemical analysis of individual alkali-containing aerosol particles: design, *Aerosol Science and Technology*, 38, 655-663, 2004
- Sykes, D. C., Woods E., III, Smith, G. D., Baer, T., Miller, R. E. , Thermal Vaporization-Vacuum Ultraviolet Laser Ionization Time-of-Flight Mass Spectrometry of Single Aerosol Particles, *Analytical Chemistry*, 74, 2048-2052, 2002
- Takats, Z., Wiseman, J. M., Gologan, B., Cooks, R. G., Mass Spectrometry Sampling Under Ambient Conditions with Desorption Electrospray Ionization, *Science*, 306, 471-473, 2004
- Tan, P. V., Malpica, O., Evans, G., Owega, S., Fila, M. S., Chemically-assigned classification of aerosol mass spectra, *Journal of the American Society for Mass Spectrometry*, 13, 826-838, 2002
- Thomson, D. S., Middlebrook, A. M., Murphy, D. M., Thresholds for laser-induced ion formation from aerosols in a vacuum using ultraviolet and vacuum-ultraviolet laser wavelengths, *Aerosol Science and Technology*, 26, 544-559, 1997
- Thomson, D. S., Murphy, D. M., Laser-induced ion formation thresholds of aerosol particles in vacuum, *Applied Optics*, 32, 6818-6826, 1993
- Tobias, H. J., Ziemann, P. J., Compound identification in organic aerosols using temperature-programmed thermal desorption particle beam mass spectrometry, *Analytical Chemistry*, 71, 3428-3435, 1999
- Trimborn, A., Hinz, K.-P., Spengler, B., Online analysis of atmospheric particles with a transportable laser mass spectrometer, *Aerosol Science and Technology*, 33, 191-201, 2000
- Tsai, C. J., Chein, H. M., Chang, S. T., Kuo, J. Y., Performance evaluation of an API aerosizer, *Journal of Aerosol Science*, 29, 839-853, 1998
- Tsai, C.-J., Chen, S.-C., Huang, C.-H., Chen, D.-R., A Universal Calibration Curve for the TSI Aerodynamic Particle Sizer, *Aerosol Science and Technology*, 38, 467-474, 2004
- Van Orden, A., Saykally, R. J., Small Carbon Clusters: Spectroscopy, Structure, and Energetics, *Chemical Reviews*, 98, 2313-2357, 1998
- Van Wuijckhuijse, A., L., Aerosol Time-Of-Flight Mass Spectrometry: An approach to detect, select and identify bioaerosols, Technical University Delft, The Netherlands, 2003
- Van Wuijckhuijse, A. L., Stowers, M. A., Kleefsman, W. A., van Baar, B. L. M., Kientz, Ch. E., Marijnissen, J. C. M., Matrix-assisted laser desorption/ionisation aerosol time-of-flight mass spectrometry for the analysis of bioaerosols: development of a fast detector for airborne biological pathogens, *Journal of Aerosol Science*, 36, 677-687, 2005
- Vera, C. C., Trimborn, A., Hinz, K.-P., Spengler, B., Initial velocity distributions of ions generated by in-flight laser desorption/ionization of individual polystyrene latex microparticles as studied by the delayed ion extraction method, *Rapid Communications in Mass Spectrometry*, 19, 133-146, 2005
- Vera, C. C., Zubarev, R., Ehring, H., Hakansson, P., Sunqvist, B. U. R., A Three-point Calibration Procedure for

- Matrix-assisted Laser Desorption/Ionization Mass Spectrometry Utilizing Multiply Charged Ions and Their Mean Initial Velocities, *Rapid Communications in Mass Spectrometry*, 10, 1429-1432, 1996
- Vestal, M. L., *Methods of Ion Generation*, *Chemical Reviews*, 101, 361-375, 2001
- Voisin, D., Smith, J. N., Sakurai, H., McMurry, P. H., Eisele, F. L., *Thermal Desorption Chemical Ionization Mass Spectrometer for Ultrafine Particle Chemical Composition*, *Aerosol Science and Technology*, 37, 471-475, 2003
- Walsh, J. J., Steidinger, K. A., *Saharan dust and Florida red tides: The cyanophyte connection*, *Journal of Geophysical Research*, 106, 11597-11612, 2001
- Weiss, M., Verheijen, P., J., T., Marijnissen, J., C., M., Scarlett, B., *On the performance of an on-line time-of-flight mass spectrometer for aerosols*, *Journal of Aerosol Science*, 28, 159-171, 1997
- Wenzel, R. J., Prather, K. A., *Improvements in ion signal reproducibility obtained using a homogeneous laser beam for on-line laser desorption/ionization of single particles*, *Rapid Communications in Mass Spectrometry*, 18, 1525-1533, 2004
- Wexler, A., Prather, K. A., *Online Single Particle Analysis*, *Aerosol Science and Technology*, 33 (1-2), special issue, 2000
- Whiteaker, J. R., Prather, K. A., *Hydroxymethanesulfonate as a tracer for fog processing of individual aerosol particles*, *Atmospheric Environment*, 37, 1033-1043, 2003
- Wilson, J. C., Liu, B. Y., *Aerodynamic particle size measurement by laser-doppler velocimetry*, *Journal of Aerosol Science*, 11, 139-150, 1980
- Woods, E. III, Smith, G. D., Miller, R. E., Baer, T., *Depth profiling of heterogeneously mixed aerosol particles using single-particle mass spectrometry*, *Analytical Chemistry*, 74, 1642-1649, 2002
- Woods, E., III, Smith, G. D., Dessiaterik, Y., Baer, T., Miller, R. E., *Quantitative detection of aromatic compounds in single aerosol particle mass spectrometry*, *Analytical Chemistry*, 73, 2317-2322, 2001
- Zelenyuk, A., Imre, D., *Single Particle Laser Ablation Time-of-Flight Mass Spectrometer: An introduction to SPLAT*, *Aerosol Science and Technology*, 39, 554-568, 2005
- Zhang, X., Smith, K. A., Worsnop, D. R., Jimenez, J., Jayne, J. T., Kolb, C. E., *A numerical Characterization of particle beam collimation by an aerodynamic lens-nozzle system: Part.I An individual lens or nozzle*, *Aerosol Science and Technology*, 36, 617-631, 2002
- Zhang, X., Smith, K. A., Worsnop, D. R., Jimenez, J., Jayne, J. T., Kolb, C. E., Morris, J., Davidovits, P., *A numerical Characterization of particle beam collimation: Part. II Integrated aerodynamic-lens-nozzle system*, *Aerosol Science and Technology*, 38, 619-638, 2004
- Zhao, W., Hopke, P. K., Qin, X., Prather, K. A., *Predicting bulk ambient aerosol compositions from ATOFMS data with ART-2a and multivariate analysis*, *Analytica Chimica Acta*, 549, 179-187, 2005
- Zhigilei, L. V., Yingling, Y. G., Itina, T. E., Schoolcraft, T. A., Garrison, B. J., *Molecular dynamics simulations of matrix-assisted laser desorption-connections to experiment*, *International Journal of Mass Spectrometry*, 226, 85-106, 2003
- Zhigilei, L., V., Garrison, B. J., *Computer simulation study of damage and ablation of submicron particles from short-pulse laser irradiation*, *Applied Surface Science*, 127-129, 142-150, 1998
- Zimmermann, R., *Personal communication*, 2005
- Zimmermann, R., Ferge, T., Gälli, M., Karlsson, R., *Application of single-particle laser desorption/ionization time-of-flight mass spectrometry for detection of polycyclic aromatic hydrocarbons from soot particles originating from an industrial combustion process*, *Rapid Communications in Mass Spectrometry*, 17, 851-859, 2003
- Zimmermann, R., Van Vaeck, L., Davidovic, M., Beckmann, M., Adams, F., *Analysis of Polycyclic Aromatic Hydrocarbons (PAH) Adsorbed on Soot Particles by Fourier Transform Laser Microprobe Mass Spectrometry (FT-LMMS): Variation of the PAH Patterns at Different Positions in the combustion Chamber of an Incineration Plant*, *Environment Science and Technology*, 34, 4780-4788, 2000

Curriculum Vitae

Stéphane Gallavardin

birth date: 31 January 1974

Aerosol Scientist

Work experience in Switzerland, Germany, United-States and France

Juli 2005 – present **Swiss Federal Institute of Technology, Zürich, Switzerland**

- Research Scientist (Post-Doc) at the Institute for Climate and Atmospheric Science
- Analysis of mineral dusts by aerosol mass spectrometry

Dec 2001 – June 2005 **GSF-Forschungszentrum, Munich, Germany**

- PhD student at the Institute for Ecological Chemistry
- Development, construction and operation of an aerosol mass spectrometer for the real-time chemical analysis of aerosol single particle
- Development of related analysis concepts and strategies

Oct. 1999 – Jan. 2001 **Harvard University, Cambridge, MA, USA**

- Research Assistant at the Atmospheric Chemistry Modeling Group
- Modeling of the night chemistry of the peroxyacetyl nitrate (PAN) with a 0D- and 1D-Model
- Bibliographic synthesis on the physical and chemical fate of the methanol in the atmosphere

Feb. 1999 – June 1999 **CNRS, Grenoble, France**

- Diploma thesis at the Laboratory of Glaciology and Geophysics of the Environment
- Reconstitution of the atmospheric concentration and evaluation of the sources of CFCs, HFCs and HCFCs over the last century from their concentration in the air trapped in firn snow

Feb. 1998 – July 1998 **Metaleurop Recherche SA., Trappes, France**

- Diploma thesis at the Department of Hydrometallurgy
- Development of a liquid-liquid extraction process of iron and zinc from a nickel chloride solution

Sept. 1996 – Aug. 1997 **Linde AG, Industrial Gases, Munich, Germany**

- Placement (sandwich year) at the Department of Special Gases
- Development of a process for the identification of gases in gas cylinder by ultrasounds

Educational

1998 – 1999 **University Joseph Fourier, Grenoble, France**

- Master of Physics and Chemistry of the Atmosphere
- Majors: Atmospheric Chemistry, Climatology and Glaciology

1992-1998 **Technical University of Chemistry Physics and Electronics of Lyon, France)**

- Master of Chemistry and Chemical Engineering (French title “Ingénieur Chimiste CPE Lyon”)
- Majors: Chemical Engineering and Analytical Chemistry

Extra-curricula

- Hiking, Trekking, Swimming, Cycling
- Photography, Public speaking (Toastmasters International - TMI)
- Boy scout group leader (1994 – 2003)
- Synergie, junior-company (Project manager) (1994 – 1996)
- Active Board Member of AEGEE-Grenoble (European Student Association) (1998 - 1999)

Competences

Languages

- French (native), English (fluent), German (fluent), Spanish (beginner)

Informatics

- Windows, Unix/Linux, Mac, Fortran 77, Labview, MATLAB
- OpenOffice, Scilab

Aerosol science

- On-line aerosol mass spectrometry
- Aerosol size measurement (APS, SMPS, ELPI)
- Theory: particle transport, particle optical properties, particle desorption, particle chemistry

Publication list

Combined operation of a laser based single particle mass spectrometer with an aerodynamic particle sizer, S. Gallavardin, T. Ferge and R. Zimmermann, *Journal of Aerosol Science*, Vol. 35, Suppl.1, S.847, 2004

A mobile and modular single particle laser desorption ionization time-of-flight mass spectrometer for the analysis of combustion aerosols at incineration plants, S. Gallavardin, T. Ferge and R. Zimmermann, *Journal of Aerosol Science*, Vol. 34, Suppl.2, S.945, 2003

A new mobile Aerosol time-of-flight mass spectrometer (ATOFMS) for analysis of combustion aerosols at industrial scale incinerators, T. Ferge, S. Gallavardin, A. Kettrup and R. Zimmermann, *Abstract International Aerosol Conference*, Taipei, Taiwan, 2002, Poster Presentation Poster ThPI39

Analysis of soot samples from an incineration plant: Observation of adsorbed polycyclic aromatic hydrocarbons by single particle mass spectrometry, T. Ferge, S. Gallavardin, A. Kettrup, R. Zimmermann, *Proceedings International Conference on Laser Probing Conference*, Leuven, Belgium, 2002